iScience

CellPress

Article

Photoredox-Catalyzed Enantioselective α-Deuteration of Azaarenes with D_2O

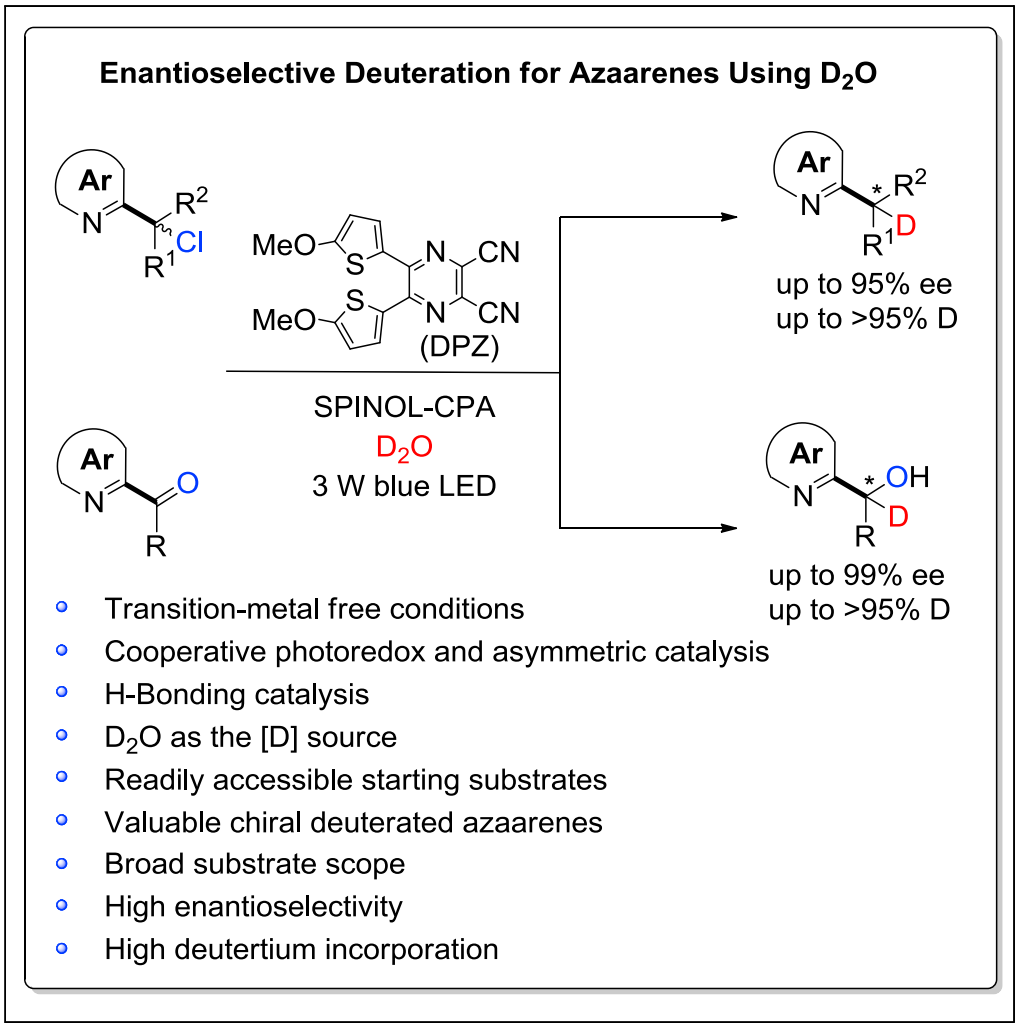

Tianju Shao, Yajuan Li, Nana Ma, ..., Xiaowei Zhao, Baokun Qiao, Zhiyong Jiang

qiaobaok@163.com (B.Q.)
chmjzy@henu.edu.cn (Z.J.)

HIGHLIGHTS

Enantioselective deuteration enabled by photoredox asymmetric catalysis

D_2O as the deuterium source

Azaarenes with a deuterated stereocenter

Transition-metal-free catalyst system

DATA AND SOFTWARE AVAILABILITY

www.ccdc.cam.ac.uk/getstructures

Shao et al., iScience 16, 410–419
June 28, 2019
https://doi.org/10.1016/j.isci.2019.06.007

iScience

CellPress

Article

Photoredox-Catalyzed Enantioselective α-Deuteration of Azaarenes with D_2O

Tianju Shao,[1,4] Yajuan Li,[1,4] Nana Ma,[2,4] Chunyang Li,[1] Guobi Chai,[3] Xiaowei Zhao,[1] Baokun Qiao,[1,*] and Zhiyong Jiang[1,2,5,*]

SUMMARY

The site-specific incorporation of deuterium (D) into small molecules is frequently used to access isotopically labeled compounds with broad utility in many research areas, such as drug development, mechanistic studies, and NMR analyses. Nevertheless, the deuteration of a stereocenter in an enantioselective manner, which could slow the metabolism and improve the bioavailability of bioactive molecules, remains challenging owing to the lack of established catalytic methods. Here, we report an asymmetric α-deuteration strategy for azaarenes with inexpensive D_2O as the deuterium source. A cooperative visible light-driven photoredox and chiral Brønsted acid–catalyzed system using a Hantzsch ester as the terminal reductant has been developed, which enables racemic α-chloro-azaarenes and prochiral azaarene-substituted ketones to experience a single-electron reduction–enantioselective deuteration process. The transition metal-free method provides important chiral α-deuterated azaarenes in satisfactory yields with good to excellent enantioselectivities (up to 99% ee) and substantial deuterium incorporation.

INTRODUCTION

Deuterium (^{2}H, D), an economical nonradioactive isotope, has been widely used in drug development, mechanistic studies, and NMR analyses (Elmore, 2009; Elmore and Bragg, 2015; Hall and Hanzlik, 1990; Nelson and Trager, 2003; MacDonald and Lu, 2002; Meanwell, 2011). A number of efficient deuterium-labeling techniques have been established through the increasing attention and contributions from various scientists (Alonso et al., 2002; Atzrodt et al., 2007; Loh et al., 2017; Zhang et al., 2019). The enantioselective incorporation of a deuterium atom on a stereocenter of a bioactive molecule could potentially slow its metabolism and improve its bioavailability (Maltais et al., 2009), but such processes remain underdeveloped (Hammadi et al., 1997; Lethu et al., 2018; Curran and Abraham, 1993; Curran and Ramamoorthy, 1993; Mohrig et al., 2011; Taglang et al., 2015; Hale and Szymczak, 2016; Palmer and Chirik, 2017; Zhao et al., 2012; Sakamoto et al., 2012; Sandoval et al., 2017). To date, few catalytic manifolds have been developed to accomplish this task (Taglang et al., 2015; Hale and Szymczak, 2016; Palmer and Chirik, 2017; Zhao et al., 2012; Sakamoto et al., 2012; Sandoval et al., 2017), and the existing systems of using the readily accessible racemic or prochiral feedstocks require prefabricated and expensive deuterium sources to attain excellent enantiofacial selectivity (Sakamoto et al., 2012; Sandoval et al., 2017). Azaarenes are ubiquitous in natural products and pharmaceuticals; however, to date, construction of their deuterated variants in enantioselective manner has not been reported.

Delivering a deuterium ion from inexpensive D_2O to a prochiral tertiary carbanion in a chiral environment would be a promising strategy. Currently, H–D exchange reactions are among the main protocols for the preparation of deuterium-labeled compounds to meet the high demands (Atzrodt et al., 2007). The energy difference between de-protonation and de-deuteration that results in accumulation of deuterated species is subtle; therefore, achieving satisfactory enantioselectivity will be difficult using this strategy (Zhao et al., 2012). Recently, we reported the asymmetric construction of α-tertiary carbon stereocenters of electron-deficient azaarenes by developing a photoredox radical conjugate addition–enantioselective protonation reaction from vinylazaarenes (Yin et al., 2018). This study provided an important indication that single-electron reduction of the α-radical species is an irreversible strategy to generate α-carbanions of azaarenes. In photoredox catalysis (Yin et al., 2018; Prier et al., 2013; Shaw et al., 2016), the reductive dehalogenation of alkyl halides through a single-electron transfer (SET) fragmentation process enables the traceless formation of alkyl radicals (Hironaka et al., 1984; Staveness et al., 2016; Fukuzumi et al., 1990; Narayanam et al., 2009; Neumann et al., 2011; Tahara and Hisaeda, 2011; Maji et al., 2010; Li et al., 2018). Following our discovery, we explored the possibility of using this powerful strategy to generate α-radicals of azaarenes from

[1]Key Laboratory of Natural Medicine and Immuno-Engineering of Henan Province, Henan University, Kaifeng, Henan 475004, P. R. China

[2]Henan Key Laboratory of Organic Functional Molecules and Drug Innovation, School of Chemistry and Chemical Engineering, Henan Normal University, Xinxiang, Henan 453007, P. R. China

[3]Zhengzhou Tobacco Research of CNTC, Zhengzhou, Henan 450001, P. R. China

[4]These authors contributed equally

[5]Lead Contact

*Correspondence: qiaobaok@163.com (B.Q.), chmjzy@henu.edu.cn (Z.J.)

https://doi.org/10.1016/j.isci.2019.06.007

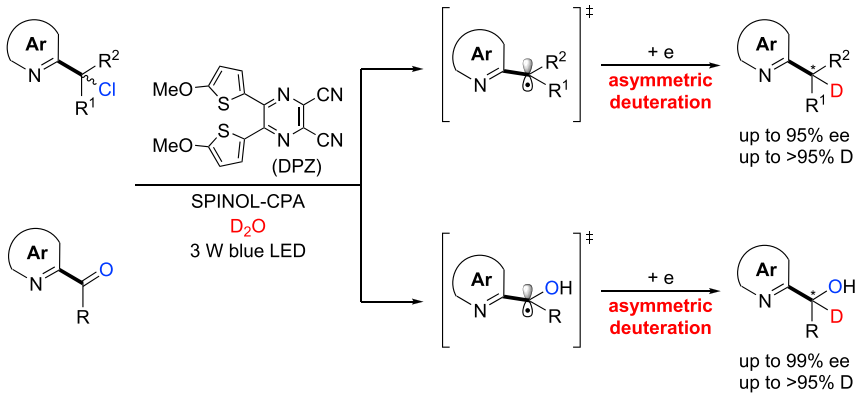

Figure 1. Outline of This Work

α-halo-azaarenes. Notably, the ability of the subsequent process to cause protonation-like deuteration with D_2O (Maji et al., 2010; Fan et al., 2018; Ju et al., 2018; Liao et al., 2018) but not hydrogen atom transfer (HAT) (Hironaka et al., 1984; Narayanam et al., 2009; Neumann et al., 2011) is crucial in the production of deuterated stereocenters. Meanwhile, to achieve high D incorporation, excess D_2O might be utilized to compete with the H^+ from the sacrificial reductant and reaction environment, but this excess reagent would pose a formidable challenge for chiral Brønsted acid catalysis, a promising platform for derivatizing azaarene-based substrates (Yin et al., 2018; Hepburn and Melchiorre, 2016; Proctor et al., 2018; Xu et al., 2018).

Herein, we demonstrate proof of this concept and report the first enantioselective reductive dechlorination–deuteration of α-chloro-azaarenes under the visible-light-driven cooperative photoredox asymmetric catalysis (Brimioulle et al., 2015; Skubi et al., 2016; Rono et al., 2013) of a dicyanopyrazine-derived chromophore (DPZ) as a photosensitizer and a 1,1′-spirobiindane-7,7′-diol (SPINOL)-based chiral phosphoric acid (CPA) with D_2O as the deuterium source (Figure 1). A variety of valuable chiral α-deuterated azaarenes featuring various substituents on the stereocenters were obtained in high yields, with excellent D incorporation and with good to excellent enantioselectivities. More importantly, this catalytic system is very versatile showing compatibility with asymmetric reduction–deuteration of azaarene-substituted ketones, leading to important α-deuterated azaarene-based secondary alcohols with satisfactory results.

RESULTS AND DISCUSSION

Reaction Optimization

Recognizing the paucity in viable catalytic methods to access the enantioenriched derivatives of α-aryl-α-branched alkyl-substituted quinolines, which possess significant bioactive potential (Kaila et al., 2008; Huang et al., 2010), we began our investigation using 2-(1-chloro-2-methyl-1-phenylpropyl)quinoline (**1a**) as the model substrate. The reduction potential of **1a** (*E*red 1/2 = − 0.639 V vs. SCE in CH_3CN) indicated that our developed metal-free DPZ (*E*red 1/2 = −1.07 V vs SCE in CH_3CN and −1.45 V vs SCE in CH_2Cl_2) will be able to reduce it through a reductive quenching cycle. Hence, we performed the initial study using 0.5 mol% DPZ, 1.5 equiv. of Hantzsch ester (HE) **HE-1** as the terminal reductant and 10 equiv. of D_2O as the deuterium source. Desired α-deuterated quinoline **2a** was obtained in a 58% yield within 30 min (see entry 1, Table S1 in the Supplemental Information). The moderate D incorporation (53%) confirmed that the developed transformation might include a dechlorination-deuteration process. Subsequently, we evaluated a range of chiral H-bonding catalysts, reductants, and reaction parameters (see Tables S1, S2 and S3). The reaction performed in mesitylene at 25°C for 20 min in the presence of 1.0 mol% DPZ, 20 mol% SPINOL-CPA **C1**, 1.5 equiv. of **HE-1**, 1.0 equiv. of $NaHCO_3$, and 150 equiv. of D_2O afforded enantioenriched product **2a** in a 75% yield with 93% ee and >95% D incorporation (entry 1, Table 1). Catalysts **C2** and **C3** provided **2a** in 22% ee and 28% ee, respectively (entries 2–3), indicating that the substituents at the 6,6′-positions of SPINOL had a substantial influence on the enantioselectivity of the transformation. **HE-2**, with a *tert*-butyl ester, provided a slightly lower enantioselectivity (entry 4). When the reductant was changed from an HE to a tertiary amine, i.e., iPr_2EtN, the reaction became sluggish, leading to **2a** in 25% yield with 39% ee (entry 5). Other photoredox catalysts such as $[Ir(ppy)_2(dtbpy)]PF_6$ and 1,3-dicyano-2,4,5,6-tetrakis(*N*,*N*-diphenylamino)benzene (4DPAIPN) (Luo and Zhang, 2016) were

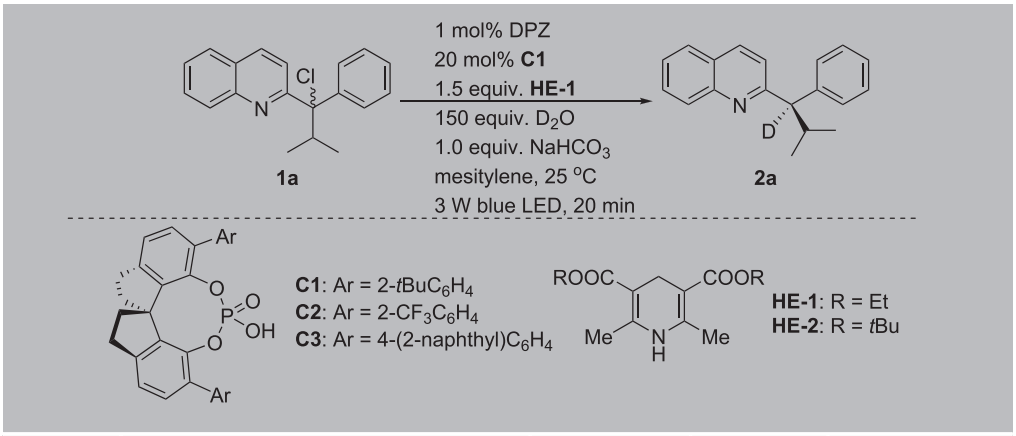

Entry	Variation from Standard Conditions	Yield (%)[a]	ee (%)[b]	D Incorp. (%)[c]
1	None	75	93	>95
2	**C2** instead of **C1**	52	22	>95
3	**C3** instead of **C1**	69	28	>95
4	**HE-2** instead of **HE-1**	76	91	93
5	iPr_2EtN instead of **HE-1**	25	39	86
6	Ir(III)[d] instead of DPZ	52	76	88
7	4DPAIPN instead of DPZ	43	73	90
8	Na_2CO_3 instead of $NaHCO_3$	51	61	89
9	No **C1**	73	NA	>95
10	No DPZ	0	NA	NA
11	No light	0	NA	NA
12	Under air	0	NA	NA

Table 1. Optimization of the Reaction Conditions

NA, not available; 4DPAIPN, 1,3-dicyano-2,4,5,6-tetrakis(*N*,*N*-diphenylamino)benzene.

Also see Tables S1, S2, and S3.

The reaction was performed on a 0.05 mmol scale. The wavelength of the 3 W blue LED was 410–510 nm.

[a]Yield of isolated product.

[b]Determined by HPLC analysis on a chiral stationary phase.

[c]Determined by ^1H NMR spectroscopy.

[d]Ir(III) = $[Ir(ppy)_2(dtbpy)]PF_6$.

tested, but no improvements in the yield and enantioselectivity were observed (entries 6–7). Using a stronger inorganic base, Na_2CO_3 instead of $NaHCO_3$, as the acid-binding agent also deteriorated the reaction outcome (entry 8). Of note, the reaction conducted in the absence of catalyst **C1** generated **2a** in a similar yield and D incorporation, suggesting that a considerable competitive racemic background transformation is active (entry 9). The subsequent control experiments confirmed that DPZ, visible light, and the oxygen-free environment are indispensable to this deuteration reaction (entries 10–12).

Substrate Scope with Respect to α-Chloro Azaarenes

With the optimum reaction conditions in hand, the scope of this asymmetric α-deuteration of azaarenes was examined (Figure 2). A wide range of α-chloro-2-quinolines containing both aryl and alkyl groups on the sp^3–C were evaluated. The transformations proceeded rapidly and smoothly, furnishing chiral products **2a-cc** in 58%–89% yields with 80%–95% ee and high levels of D incorporation within 20–40 min. The introduction of distinct electron-withdrawing or electron-donating substituents at the *para*- and *meta*-positions (**2b-f** and **2i-l**) of the α-aryl ring did not affect the excellent enantioselectivity. Methyl group at

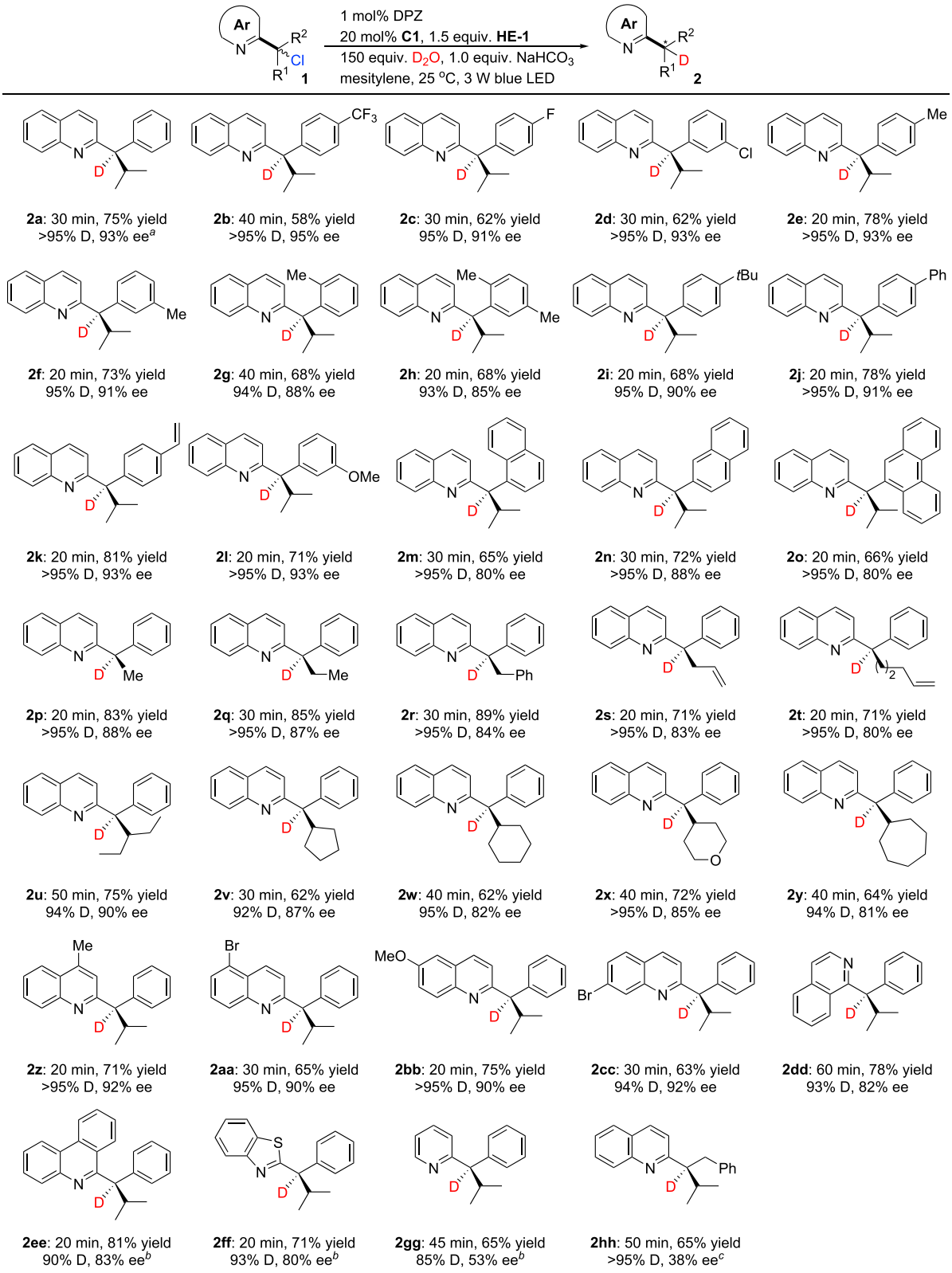

Figure 2. Enantioselective Dehalogenative Deuteration (0.1 mmol scale)

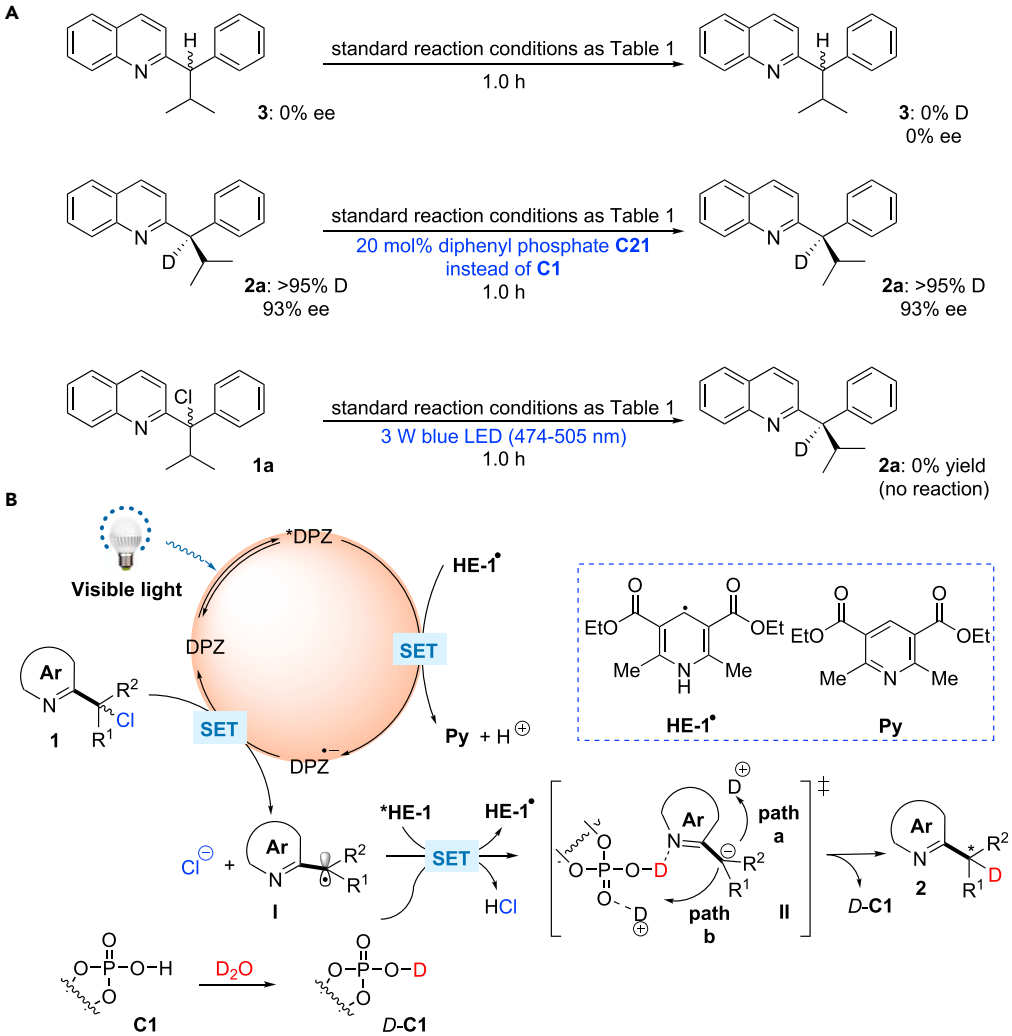

Figure 3. Control Experiments and the Proposed Mechanism

(A) Control experiments for the H–D exchange of reduction product and the conversion of **1a** with an excitation wavelength from 474 to 505 nm.

(B) The possible mechanism for the photoredox-catalyzed enantioselective α-deuteration of Azaarenes.

the ortho-position (**2g-h**) decreased the enantioselectivity slightly to 90% ee probably owing to steric hindrance. A similar steric effect was observed when bulkier fused aromatic rings, such as 1-naphthyl (**2m**), 2-naphthyl (**2n**), and 9-phenanthryl (**2o**), were in the α-position of the 2-quinolines. The catalytic system was also compatible with α-chloro-2-quinolines with diverse linear (**2p-t**), bulky branched (**2u**), and cyclic (**2v-y**) α-alkyl groups, based on the good to excellent enantioselectivities obtained with these substrates. With respect to the quinoline moiety, the installation of substituents on its 4-, 5-, and 6-positions resulted in the corresponding products **2z-cc** with excellent enantioselectivities. Other such α-chloro-azaarenes were also tested. Chiral α-deuterated 1-isoquinoline (**2dd**), 6-phenanthridine (**2ee**), and 2-benzothiazole (**2ff**) were obtained in 71%–81% yields with 80%–83% ee and excellent D incorporation, which highlights the generality of this catalysis platform. As an exception, when the azaarene was 2-pyridine, the corresponding product **2gg** was obtained with only moderate enantioselectivity. Noticeably, 4DPAIPN was used as the photoredox catalyst to furnish **2ee**, **2ff**, and **2gg** as DPZ could not promote the transformation. To define the substrate scope, the phenyl group of **1a** was changed as benzyl group; however, product **2hh** was achieved in 65% yield with >95% D incorporation but only 38% ee, which thus still represents a challenging task. The reaction to access **2a** on a 5.0 mmol scale gave a similar yield, enantioselectivity, and D incorporation (footnote *a*), suggesting the potential scalability of this method.

Mechanistic Studies

To probe the mechanism, compound **3**, i.e., non-deuterated racemic **2a**, was evaluated under the standard reaction conditions (Figure 3A). After 1 h, the ee value of **3** remained 0% and no deuterated product **2a** was observed. Similarly, chiral **2a** with 93% ee was examined using 20 mol% diphenyl phosphate **C21** instead of **C1**, and no changes in the enantiomeric purity or D incorporation were found. Consequently, the effects of H–D exchange for product **2** on the enantioselectivity and D incorporation could be excluded.

On the account of the excitation spectra of DPZ and **HE-1**, Stern-Volmer experiments were first conducted using an excitation wavelength of 415 nm (see Supplemental Information). Luminescence quenching of *DPZ ($E^t(S^*/S^{\bullet-})$ = +1.42 V vs. SCE in CH_3CN and +0.91 V vs. SCE in CH_2Cl_2) by **HE-1** (*E*red 1/2 = +0.97 V vs. SCE in CH_3CN) and ***HE-1** ($E^t(S^*/S^{\bullet-}) \approx$ –2.28 V vs. SCE in CH_3CN) (Jung et al., 2016) by **1a** (*E*red 1/2 = –0.639 V vs. SCE in CH_3CN) was observed. Meanwhile, no measurement of *DPZ by **1a** in the absence and presence of **C1** was revealed. Since the excitation of **HE-1** to ***HE-1** is impossible at $\lambda > 445$ nm according to its excitation spectrum, such experiments were performed with an excitation wavelength of 448 nm, indicating no measurable luminescence quenching of *DPZ by **HE-1** or **1a** and ***HE-1** by **1a**. We also tested the transformation of **1a** with a laser line filter (CWL = 488 $\pm$ 2 nm, FWHM = 10 $\pm$ 2 nm, emission wavelengths from 474 to 505 nm, Figure 3A), and no reaction was found. The results suggest the indispensable role of ***HE-1** in the reaction. Therefore, the catalytic cycle likely begins from the SET of *DPZ with trace **HE-1**$^{\bullet}$ (*E*red 1/2 $\approx$ –0.76 V vs. SCE), which is generated from ***HE-1** and α-chloro-azaarenes **1** under irradiation with visible light (Figure 3B) (Cao et al., 2019). The success of 4DPAIPN (*E*red 1/2 = –1.52 V vs. SCE in CH_3CN) (Luo and Zhang, 2016) but failure of DPZ in the transformations of 6-phenanthridine-derived (**1ee**, *E*red 1/2 = –0.963 V vs. SCE in CH_3CN) and 2-benzothiazole-derived (**1ff**, *E*red 1/2 = –1.227 V vs. SCE in CH_3CN) substrates demonstrates that $DPZ^{\bullet-}$ should engage in the SET reduction of **1** to furnish radical species **I**. It is also noteworthy that no transformation of **1a** was observed in the absence of DPZ (entry 10, Table 1). Accordingly, a HAT (Lee et al., 2017) or a reduction–protonation/deuteration process between **HE-1**$^{\bullet}$ and radical **I** seems unfavorable. To provide **HE-1**$^{\bullet}$ to propagate the photocatalytic cycle, the reduction of **I** by ***HE-1** with a stronger reductive ability than **HE-1**$^{\bullet}$ thus represents the most likely approach. Owing to the free proton from catalyst **C1** and high concentration of D_2O, deuterated **C1**, i.e., *D*-**C1**, would serve as a more stable hydrogen-bond donor to interact with the nitrogen atom in the azaarene, providing the enantiocontrolling environment for the deuteration of prochiral carbanion intermediate **II** to give chiral products **2** in high enantioselectivities. With respect to the enantioselective deuteration process, the intermediate **II** could directly abstract deuterium ion from the reaction system through the **pathway a**. However, the ability of P=O of CPA as Lewis base to grab a deuterium also leads to an alternative **pathway b** to deliver deuterium ion. To better understand the mechanism, DFT calculations were carried out (for computational details see Supplemental Information), and the calculated ΔG values are shown in Figure 4. The data suggest that the formation of (*R*)-**2a** through **TSA** only requires 2.0 kcal/mol, but affording (*S*)-**2a** through the proton from H_2O (D_2O) attacked by the α-anion of quinoline has to overcome high energy barriers (39.7 and 35.2 kcal/mol). This result is consistent with the experimental results. In this context, although chiral catalyst CPA cannot accelerate the transformations, it will act as a deuterium transfer interchange to enable the elusive enantioselective manifold with high enantioselectivity.

Extension of the Method to Azaarene-Based Ketones

Azaarene-substituted secondary alcohols, as another kind of α-tertiary carbon-based azaarene derivative, are also important building blocks of numerous pharmaceuticals and biologically active compounds (Rennison et al., 2007). The chiral transition metal-catalyzed asymmetric transfer hydrogenation of aryl *N*-heteroaryl ketones with sodium formate as a hydrogen source has been developed to access the chiral variants (Liu et al., 2018). However, this strategy is only suitable for aryl *N*-heteroaryl ketones and is likely not compatible to introduce deuterium on the stereocenters with D_2O as the deuterium reagent. Given that azaarene-substituted ketones are readily accessible and abundant, we anticipated evaluating the possibility of this double single-electron reduction–enantioselective deuteration method for these feedstocks, to directly provide the enantioenriched α-deuterated azaarene-substituted secondary alcohols. Literature investigation showed that azaarene rings are more liable to reduction than carbonyls in azaarene-substituted ketone derivatives in the presence of CPA catalyst and HE reductant (Rueping and Antonchick, 2007). Thus, the chemoselectivity with enantioselectivity and D incorporation would constitute formidable challenges in the desired transformations. Phenyl(quinolin-2-yl)methanone (**4a**, E_p^1 = –0.905 V, E_p^2 = –1.434 V vs. SCE in CH_3CN) was first selected to be examined under the standard reaction conditions (see Table 1). Although the desired product **5a** was obtained with moderate enantioselectivity (61% ee), the

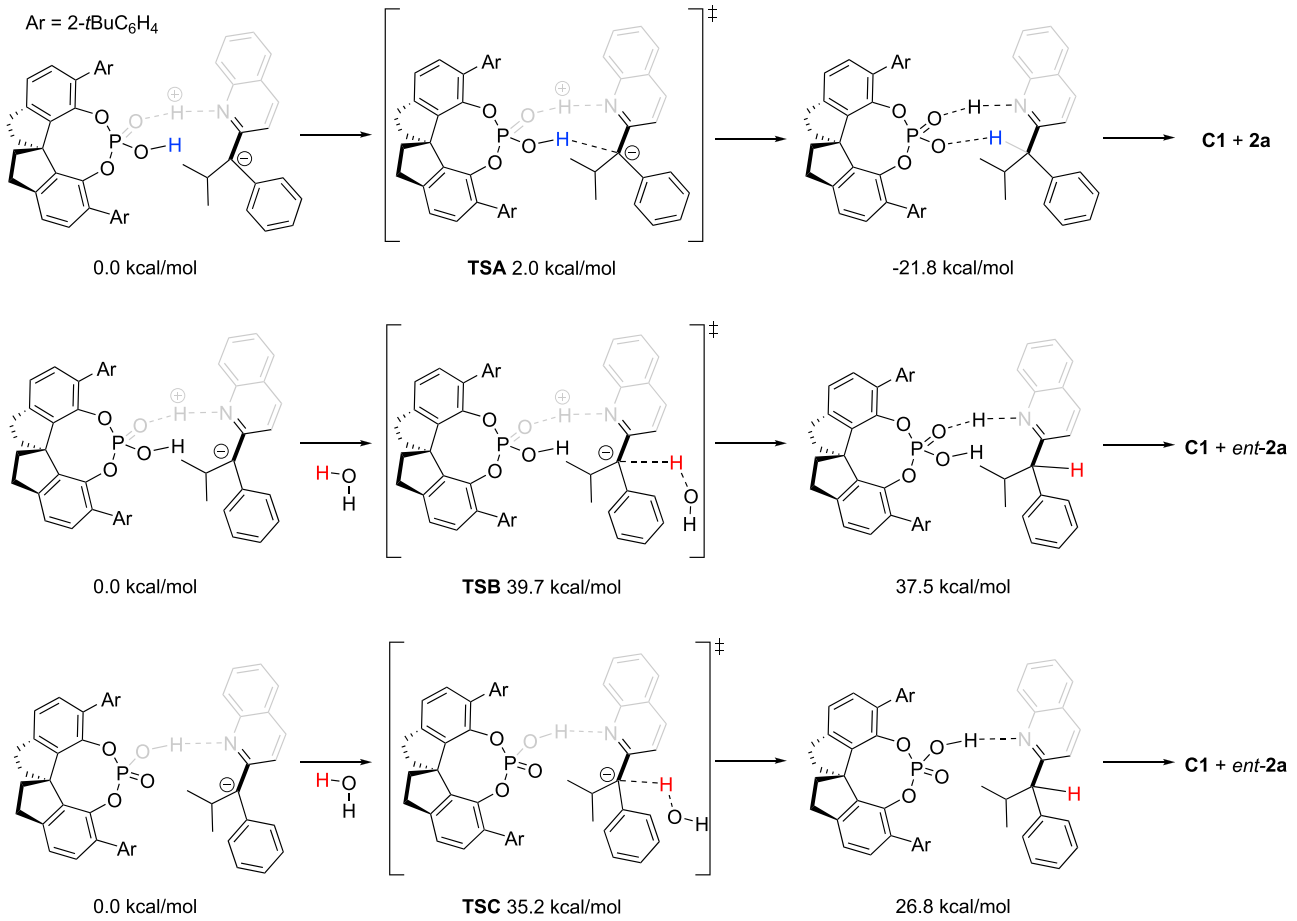

Figure 4. Calculated ΔG Values of Possible Pathways for the Formation of 2a or *ent*-2a

high yield (80%) and moderate D incorporation (72%) prompted us to explore a series of chiral CPAs and the reaction parameters (see Table S4). To our delight, when 0.5 mol% DPZ, 10 mol% CPA **C2**, 1.5 equiv. of **HE-1**, 200 equiv. of D_2O, 0.2 equiv. of NaCl as an additive, and CMPE as the solvent were used, at −5°C, **5a** was achieved in 96% yield with 91% ee and 91% D incorporation (Figure 5). A series of 2-quinoline-substituted ketones were next examined, leading to chiral products **5b-m** in 65%–99% yields with 80%–99% ee and excellent D incorporation. Satisfactory results were achieved with fused aromatic (**5g**) and heteroaromatic (**5h-i**) rings as well as alkyls (**5l-m**) as the substituents of ketones underscore the generality of this catalytic system. Furthermore, ketones substituted with other azaarenes such as 6-phenanthridine (**5n**), *N*-Boc-2-benzimidazole (**5o**), and 2-benzothiazole (**5p**) were also compatible. It is worth mentioning that, although 2-(α-hydroxybenzyl)-benzimidazole (HBB) is a highly selective and potent inhibitor of picornavirus multiplication in cell culture, no catalytic method to access its optical pure isomer has been established (Tamm and Eggers, 1963; Kadin et al., 1964; Akihama et al., 1968; Tamm et al., 1969). The success in the synthesis of its chiral variant featuring a deuterium on the stereocenter, i.e., **5o**, highlights the significance of this methodology.

Conclusion

In summary, we have developed the first catalytic asymmetric α-deuteration of azaarenes. Through cooperative, visible-light-driven photoredox and chiral H-bonding catalysis, both racemic α-chloro-azaarenes and prochiral azaarene-substituted ketones can undergo a double single-electron reduction–enantioselective deuteration process with a Hantzsch ester as the terminal reductant and inexpensive D_2O as the deuterium source. The developed reaction can furnish a variety of important enantioenriched α-deuterated azaarenes in satisfactory yields with high D incorporation. Although excess D_2O is used and a

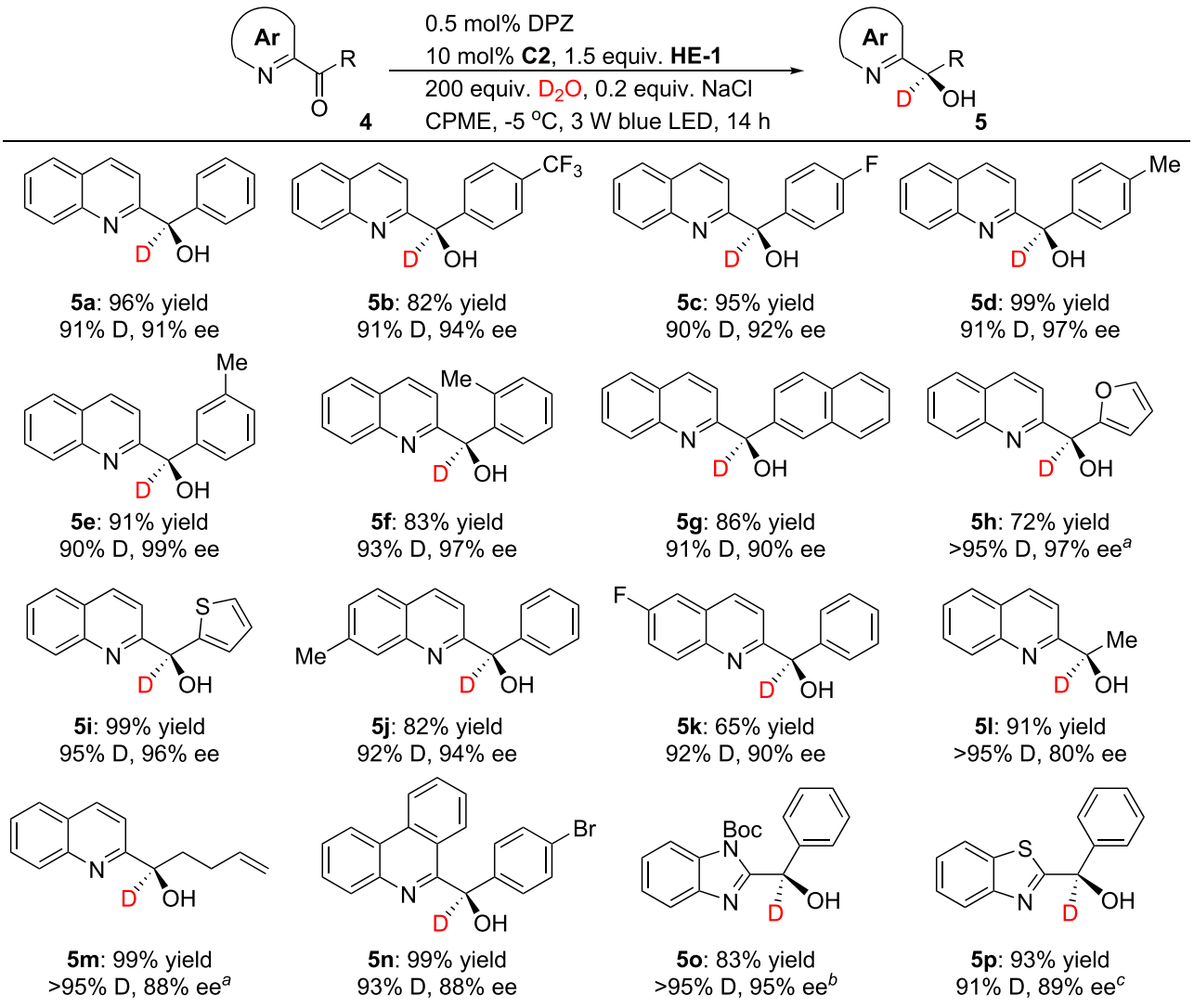

Figure 5. Enantioselective Reductive Deuteration (0.1 mmol scale)

strong racemic background process occurs directly through the intrinsic redox catalytic cycle, good to excellent enantioselectivities were obtained, which confirms the efficacy of the catalytic system. Therefore, we anticipate that this work will inspire the pursuit of the D_2O-enabled asymmetric construction of C–D bonds in various valuable molecules through this highly reactive radical-based dual catalysis platform.

Limitations of the Study

In both reaction systems, pyridine-based substrates were not applicable given the unsatisfactory enantioselectivity. With respect to the dehalogenative deuteration, poor enantioselectivity of mono-azaarene-substituted alkyl chlorides represents another important limitation.

METHODS

All methods can be found in the accompanying Transparent Methods supplemental file.

DATA AND SOFTWARE AVAILABILITY

The crystallography data have been deposited at the Cambridge Crystallographic Data Center (CCDC) under accession number CCDC: 1893142 (**8**) and 1902192 (**5n**) and can be obtained free of charge from www.ccdc.cam.ac.uk/getstructures.

SUPPLEMENTAL INFORMATION

Supplemental Information can be found online at https://doi.org/10.1016/j.isci.2019.06.007.

ACKNOWLEDGMENTS

Grants from the National Natural Science Foundation of China (21672052, 21603062), Young Elite Scientists Sponsorship Program by CAST (2017QNRC001), and Henan University are gratefully acknowledged. The calculations are supported by the High Performance Computing (HPC) Center of Henan Normal University.

AUTHOR CONTRIBUTIONS

Z.J. conceived and designed the study and wrote the paper. T.S., Y.L., C.L., and B.Q. performed the experiments and analyzed the data. B.Q. prepared the Supplemental Information. N.M. conducted DFT calculations. G.C. collected HRMS data. X.Z. synthesized some of the substrates. All authors discussed the results and commented on the manuscript.

DECLARATION OF INTERESTS

The authors declare no competing financial interests.

Received: April 22, 2019
Revised: June 2, 2019
Accepted: June 5, 2019
Published: June 28, 2019

REFERENCES

Akihama, S., Okude, M., Sato, K., and Iwabuchi, S. (1968). Inhibitory effect of 1,2-bis(2-benzimidazolyl)1,2-ethanediol derivatives on poliovirus. Nature *217*, 562–563.

Alonso, F., Beletskaya, I.P., and Yus, M. (2002). Metal-mediated reductive hydrodehalogenation of organic halides. Chem. Rev. *102*, 4009–4091.

Atzrodt, J., Derdau, V., Fey, T., and Zimmermann, J. (2007). The renaissance of H/D exchange. Angew. Chem. Int. Ed. *46*, 7744–7765.

Brimioulle, R., Lenhart, D., Maturi, M.M., and Bach, T. (2015). Enantioselective catalysis of photochemical reactions. Angew. Chem. Int. Ed. *54*, 3872–3890.

Cao, K., Tan, S.M., Lee, R., Yang, S., Jia, H., Zhao, X., Qiao, B., and Jiang, Z. (2019). Catalytic enantioselective addition of prochiral radicals to vinylpyridines. J. Am. Chem. Soc. *141*, 5437–5443.

Curran, D.P., and Abraham, A.C. (1993). 1,2-Asymmetric induction in radical reactions. Deuteration and allylation reactions of β-oxy-o-iodoanilides. Tetrahedron *49*, 4821–4840.

Curran, D.P., and Ramamoorthy, P.S. (1993). 1,2-Asymmetric induction in radical reactions. Deuteration and allylation reactions of β-oxy-α-bromo esters. Tetrahedron *49*, 4841–4858.

Elmore, C.S. (2009). The use of isotopically labeled compounds in drug discovery. Annu. Rep. Med. Chem. *44*, 515–534.

Elmore, C.S., and Bragg, R.A. (2015). Isotope chemistry; a useful tool in the drug discovery arsenal. Bioorg. Med. Chem. Lett. *25*, 167–171.

Fan, X., Gong, X., Ma, M., Wang, R., and Walsh, P.J. (2018). Visible light-promoted CO_2 fixation with imines to synthesize diaryl α-amino acids. Nat. Commun. *9*, 4936.

Fukuzumi, S., Mochizuki, S., and Tanaka, T. (1990). Photocatalytic reduction of phenacyl halides by 9,10-dihydro-10-methylacridine: control between the reductive and oxidative quenching pathways of tris(bipyridine) ruthenium complex utilizing an acid catalysis. J. Phys. Chem. *94*, 722–726.

Hale, L.V.A., and Szymczak, N.K. (2016). Stereoretentive deuteration of α-chiral amines with D_2O. J. Am. Chem. Soc. *138*, 13489–13492.

Hall, L.R., and Hanzlik, R.P. (1990). Kinetic deuterium isotope effects on the *N*-demethylation of tertiary amides by cytochrome P-450. J. Biol. Chem. *265*, 12349–12355.

Hammadi, A., Ménez, A., and Genet, R. (1997). Asymmetric deuteration of *N*-acetyl-(*Z*)-α,β-dehydrotryptophan-(*L*)-phenylalanine methyl ester produced by (*L*)-tryptophan 2′,3′-oxidase from chromobacterium vioaceum. A new route for stereospecific labelling of peptides. Tetrahedron *53*, 16115–16122.

Hepburn, H.B., and Melchiorre, P. (2016). Brønsted acid-catalysed conjugate addition of photochemically generated α-amino radicals to alkenylpyridines. Chem. Commun. (Camb.) *52*, 3520–3523.

Hironaka, K., Fukuzumi, S., and Tanaka, T. (1984). Tris(bipyridyl) ruthenium (II)-photosensitized reaction of 1-benzyl-1,4-dihydronicotinamide with benzyl bromide. J. Chem. Soc. Perkin Trans. *2*, 1705–1709.

Huang, A., Moretto, A., Janz, K., Lowe, M., Bedard, P.W., Tam, S., Di, L., Clerin, V., Sushkova, N., Tchernychev, B., et al. (2010). Discovery of 2-[1-(4-chlorophenyl)cyclopropyl]-3-hydroxy-8-(trifluoromethyl)quinoline-4-carboxylic acid (PSI-421), a P-selectin inhibitor with improved pharmacokinetic properties and oral efficacy in models of vascular injury. J. Med. Chem. *53*, 6003–6017.

Ju, T., Fu, Q., Ye, J.H., Zhang, Z., Liao, L.L., Yan, S.S., Tian, X.Y., Luo, S.P., Li, J., and Yu, D.G. (2018). Selective and catalytic hydrocarboxylation of enamides and imines with CO_2 to generate α,α-disubstituted α-amino acids. Angew. Chem. Int. Ed. *57*, 13897–13901.

Jung, J., Kim, J., Park, G., You, Y., and Cho, E.J. (2016). Selective debromination and α-hydroxylation of α-bromo ketones using Hantzsch esters as photoreductants. Adv. Synth. Catal. *358*, 74–80.

Kadin, S.B., Eggers, H.J., and Tamm, I. (1964). Synthesis and virus-inhibitory activity of *D*- and *L*-isomers of 2-(α-hydroxybenzyl)-benzimidazole. Nature *201*, 639–640.

Kaila, N., Janz, K.M., Huang, A., Moretto, A.F., and Bedard, P.W. (2008). Preparation of quinoline compounds as selectin inhibitors for disease treatment. PCT Int. Appl., 121817 A3.

Lee, K.N., Lei, Z., and Ngai, M.-Y. (2017). β-Selective reductive coupling of alkenylpyridines with aldehydes and imines via synergistic Lewis acid/photoredox catalysis. J. Am. Chem. Soc. *139*, 5003–5006.

Lethu, S., Ano, H., Murata, M., and Matsuoka, S. (2018). Enantioselective deuteration of β-substituted α,β-unsaturated esters by rhodium-1,2-bis(2,5-diphenylphospholano)ethane. Eur. J. Org. Chem. *2018*, 235–239.

Li, J., Kong, M., Qiao, B., Lee, R., Zhao, X., and Jiang, Z. (2018). Formal enantioconvergent substitution of alkyl halides via catalytic

asymmetric photoredox radical coupling. Nat. Commun. *9*, 2445.

Liao, L.-L., Cao, G.-M., Ye, J.-H., Sun, G.-Q., Zhou, W.-J., Gui, Y.-Y., Yan, S.-S., Shen, G., and Yu, D.-G. (2018). Visible-light-driven external-reductant-free cross-electrophile couplings of tetraalkyl ammonium salts. J. Am. Chem. Soc. *140*, 17338–17342.

Liu, Q., Wang, C., Zhou, H., Wang, B., Lv, J., Cao, L., and Fu, Y. (2018). Iridium-catalyzed highly enantioselective transfer hydrogenation of aryl *N*-heteroaryl ketones with *N*-oxide as a removable *ortho*-substituent. Org. Lett. *20*, 971–974.

Loh, Y.Y., Nagao, K., Hoover, A.J., Hesk, D., Rivera, N.R., Colletti, S.L., Davies, I.W., and MacMillan, D.W.C. (2017). Photoredox-catalyzed deuteration and tritiation of pharmaceutical compounds. Science *358*, 1182–1187.

Luo, J., and Zhang, J. (2016). Donor–acceptor fluorophores for visible–light-promoted organic synthesis: photoredox/Ni dual catalytic $C(sp^3)$–$C(sp^2)$ cross-coupling. ACS Catal. *6*, 873–877.

MacDonald, D., and Lu, P. (2002). Determination of DNA structure in solution: enzymatic deuteration of the ribose 2′carbon. J. Am. Chem. Soc. *124*, 9722–9723.

Maji, T., Karmakar, A., and Reiser, O. (2010). Visible-light photoredox catalysis: dehalogenation of vicinal dibromo-, α-halo-, and α,α-dibromocarbonyl compounds. J. Org. Chem. *76*, 736–739.

Maltais, F., Jung, Y.C., Chen, M., Tanoury, J., Perni, R.B., Mani, N., Laitinen, L., Huang, H., Liao, S., Gao, H., et al. (2009). In vitro and in vivo isotope effects with hepatitis C protease inhibitors: enhanced plasma exposure of deuterated telaprevir versus telaprevir in rats. J. Med. Chem. *52*, 7993–8001.

Meanwell, N.A. (2011). Synopsis of some recent tactical application of bioisosteres in drug design. J. Med. Chem. *54*, 2529–2591.

Mohrig, J.R., Reiter, N.J., Kirk, R., Zawadski, M.R., and Lamarre-Vincent, N. (2011). Effect of buffer general acid–base catalysis on the stereoselectivity of ester and thioester H/D exchange in D_2O. J. Am. Chem. Soc. *133*, 5124–5128.

Narayanam, J.M.R., Tucker, J.W., and Stephenson, C.R.J. (2009). Electron-transfer photoredox catalysis: development of a tin-free reductive dehalogenation reaction. J. Am. Chem. Soc. *131*, 8756–8757.

Nelson, S.D., and Trager, W.F. (2003). The use of deuterium isotope effects to probe the active site properties, mechanism of cytochrome P450-catalyzed reactions, and mechanisms of metabolically dependent toxicity. Drug Metab. Dispos. *31*, 1481–1489.

Neumann, M., Füldner, S., König, B., and Zeitler, K. (2011). Metal–free, cooperative asymmetric organophotoredox catalysis with visible light. Angew. Chem. Int. Ed. *50*, 951–954.

Palmer, W.N., and Chirik, P.J. (2017). Cobalt-catalyzed stereoretentive hydrogen isotope exchange of $C(sp^3)$–H bonds. ACS Catal. *7*, 5674–5678.

Prier, C.K., Rankic, D.A., and MacMillan, D.W.C. (2013). Visible light photoredox catalysis with transition metal complexes: applications in organic synthesis. Chem. Rev. *113*, 5322–5363.

Proctor, R.S.J., Davis, H.J., and Phipps, R.J. (2018). Catalytic enantioselective Minisci-type addition to heteroarenes. Science *360*, 419–422.

Rennison, D., Bova, S., Cavalli, M., Ricchelli, F., Zulian, A., Hopkins, B., and Brimble, M.A. (2007). Synthesis and activity studies of analogues of the rat selective toxicant norbormide. Bioorg. Med. Chem. *15*, 2963–2974.

Rono, L.J., Yayla, H.G., Wang, D.Y., Armstrong, M.F., and Knowles, R.R. (2013). Enantioselective photoredox catalysis enabled by proton-coupled electron transfer: development of an asymmetric aza-Pinacol cyclization. J. Am. Chem. Soc. *135*, 17735–17738.

Rueping, M., and Antonchick, A.P. (2007). Organocatalytic enantioselective reduction of pyridines. Angew. Chem. Int. Ed. *46*, 4562–4565.

Sakamoto, T., Mori, K., and Akiyama, T. (2012). Chiral phosphoric acid catalyzed enantioselective transfer deuteration of ketimines by use of benzothiazoline as a deuterium donor: synthesis of optically active deuterated amines. Org. Lett. *14*, 3312–3315.

Sandoval, B.A., Meichan, A.J., and Hyster, T.K. (2017). Enantioselective hydrogen atom transfer: discovery of catalytic promiscuity in flavin-dependent 'ene'-reductases. J. Am. Chem. Soc. *139*, 11313–11316.

Shaw, M.H., Twilton, J., and MacMillan, D.W.C. (2016). Photoredox catalysis in organic chemistry. J. Org. Chem. *81*, 6898–6926.

Skubi, K.L., Blum, T.R., and Yoon, T.P. (2016). Dual catalysis strategies in photochemical synthesis. Chem. Rev. *116*, 10035–10074.

Staveness, D., Bosque, I., and Stephenson, C.R.J. (2016). Free radical chemistry enabled by visible light-induced electron transfer. Acc. Chem. Res. *49*, 2295–2306.

Taglang, C., Martínez-Prieto, L.M., del Rosal, I., Maron, L., Poteau, R., Philippot, K., Chaudret, B., Perato, S., Lone, S.A., Puente, C., et al. (2015). Enantiospecific C–H activation using ruthenium nanocatalysts. Angew. Chem. Int. Ed. *54*, 10474–10477.

Tahara, K., and Hisaeda, Y. (2011). Eco-friendly molecular transformations catalyzed by a vitamin B12 derivative with a visible-light-driven system. Green Chem. *13*, 558–561.

Tamm, I., and Eggers, H.J. (1963). Specific Inhibition of replication of animal viruses. Science *142*, 24–33.

Tamm, I., Eggers, H.J., and Bablanian, R. (1969). Structural requirements of selective inhibition of enteroviruses by 2-(α-hydroxybenzyl)-benzimidazole and related compounds. Nature *223*, 785–788.

Xu, C., Muir, C.W., Leach, A.G., Kennedy, A.R., and Watson, A.J.B. (2018). Catalytic enantioselective synthesis of α-chiral azaheteroaryl ethylamines by asymmetric protonation. Angew. Chem. Int. Ed. *57*, 11374–11377.

Yin, Y., Dai, Y., Jia, H., Li, J., Bu, L., Qiao, B., Zhao, X., and Jiang, Z. (2018). Conjugate addition–enantioselective protonation of *N*-aryl glycines to α-branched 2-vinylazaarenes via cooperative photoredox and asymmetric catalysis. J. Am. Chem. Soc. *140*, 6083–6087.

Zhang, M., Yuan, X.-A., Zhu, C., and Xie, J. (2019). Deoxygenative deuteration of carboxylic acids with D_2O. Angew. Chem. Int. Ed. *58*, 312–316.

Zhao, Y., Lim, X., Pan, Y., Zong, L., Feng, W., Tan, C.-H., and Huang, K.-W. (2012). Asymmetric H–D exchange reactions of fluorinated aromatic ketones. Chem. Commun. (Camb.) *48*, 5479–5481.

ISCI, Volume *16*

Supplemental Information

Photoredox-Catalyzed Enantioselective α-Deuteration of Azaarenes with D_2O

Tianju Shao, Yajuan Li, Nana Ma, Chunyang Li, Guobi Chai, Xiaowei Zhao, Baokun Qiao, and Zhiyong Jiang

Supplemental Figures for ^{1}H and ^{13}C NMR Spectra and HPLC Spectra

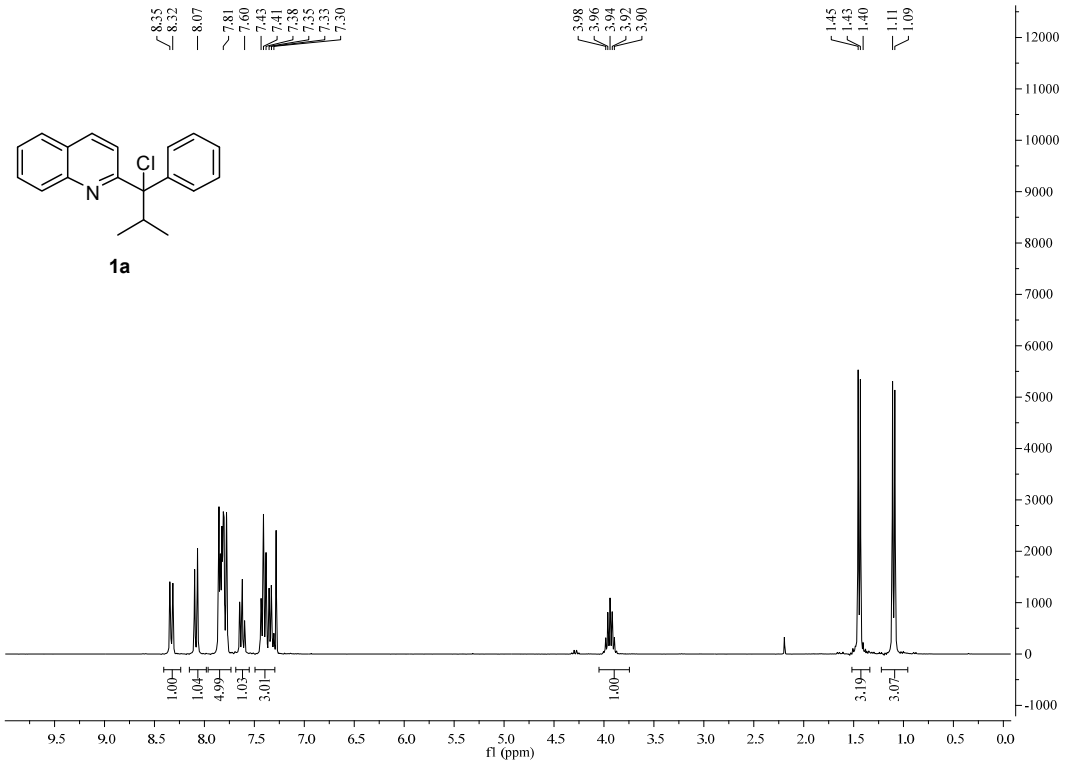

Figure S1. ^{1}H NMR spectrum for **1a**, related to **Figure 2**.

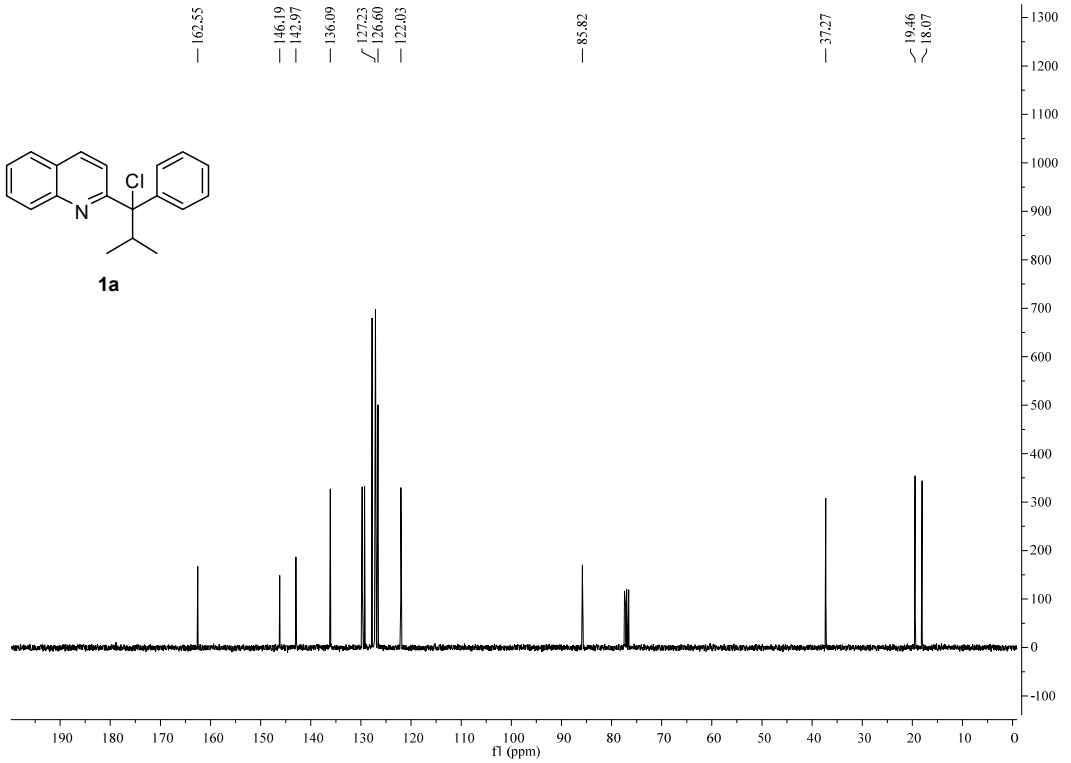

Figure S2. ^{13}C NMR spectrum for **1a**, related to **Figure 2**.

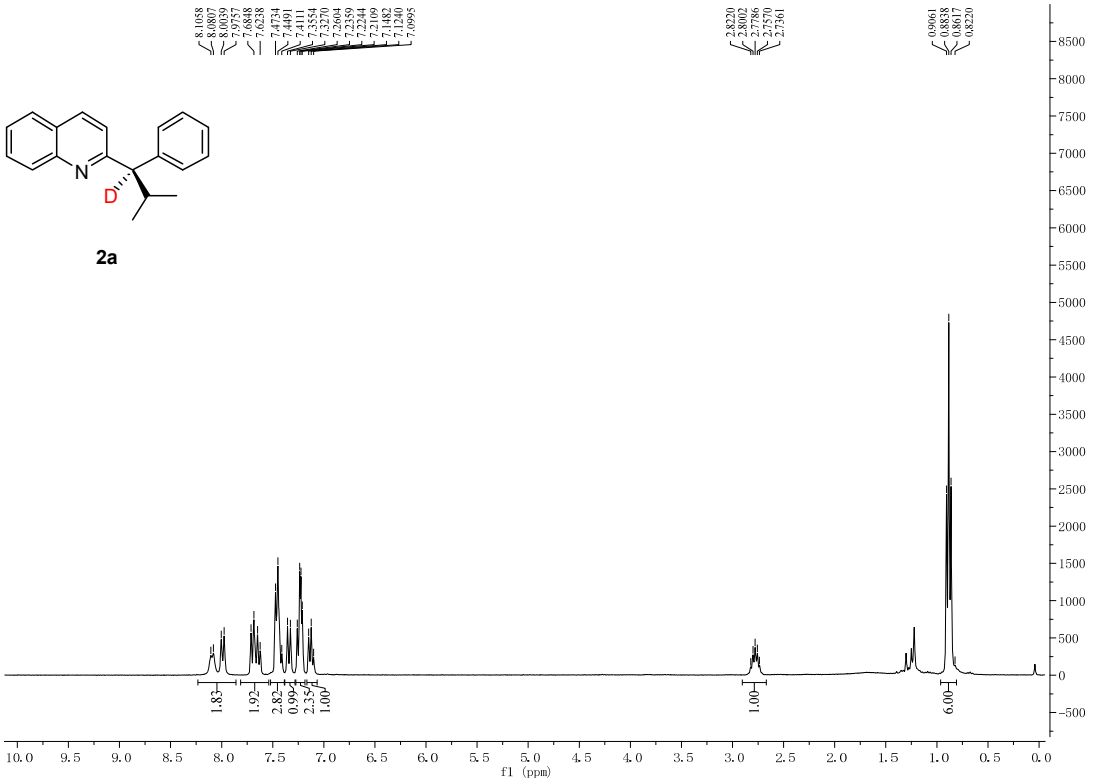

Figure S3. ^{1}H NMR spectrum for **2a**, related to **Figure 2**.

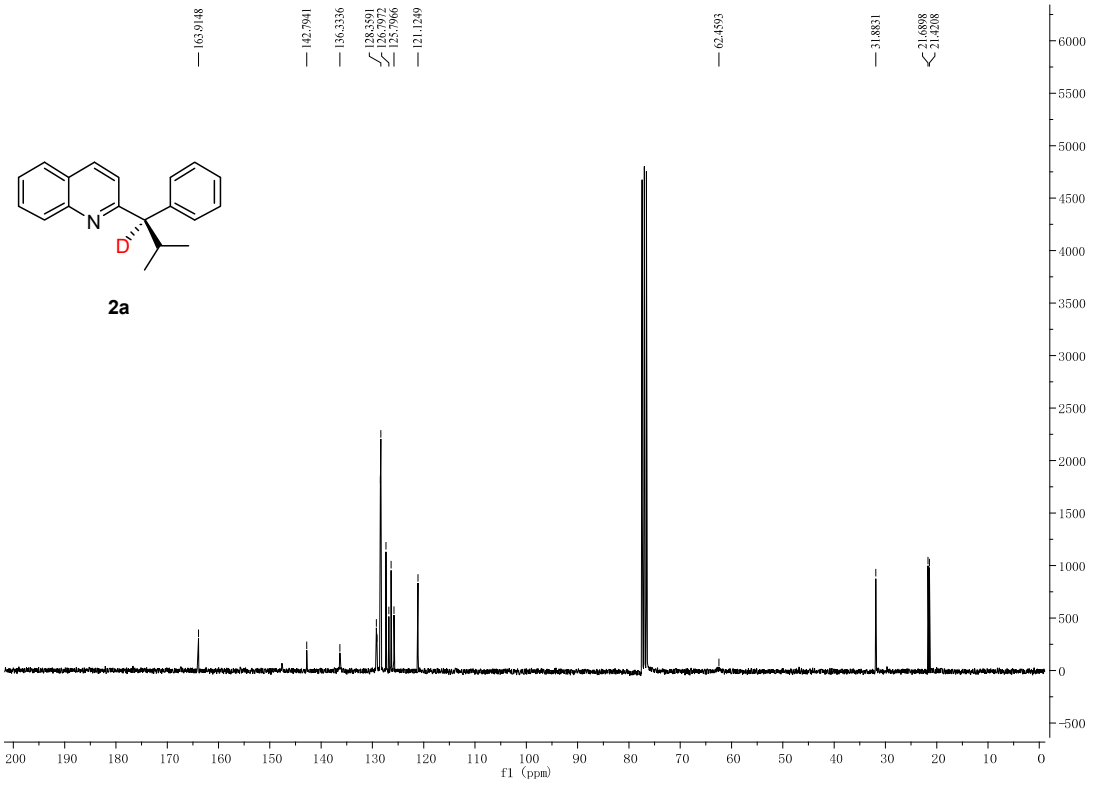

Figure S4. ^{13}C NMR spectrum for **2a**, related to **Figure 2**.

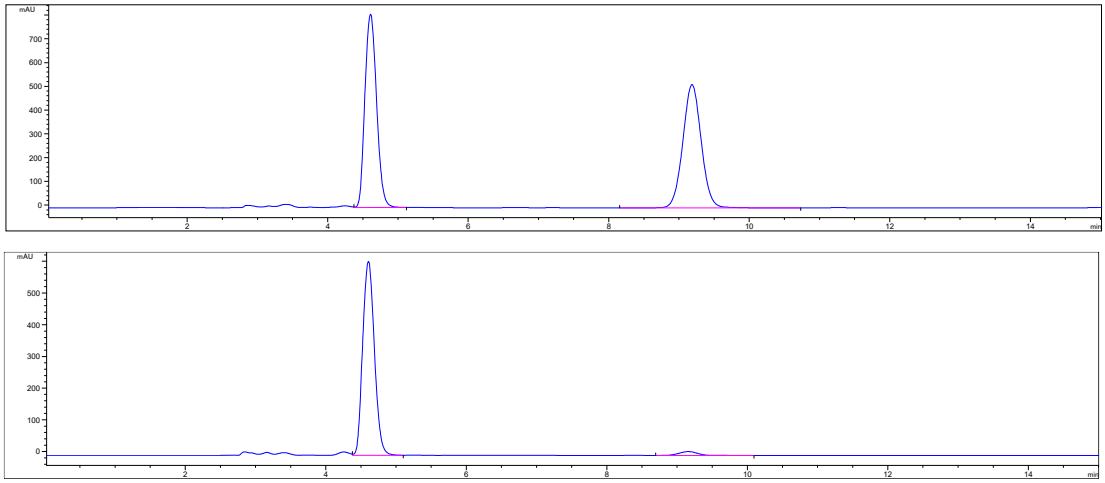

Figure S5. HPLC spectrum for **2a**, related to **Figure 2**.

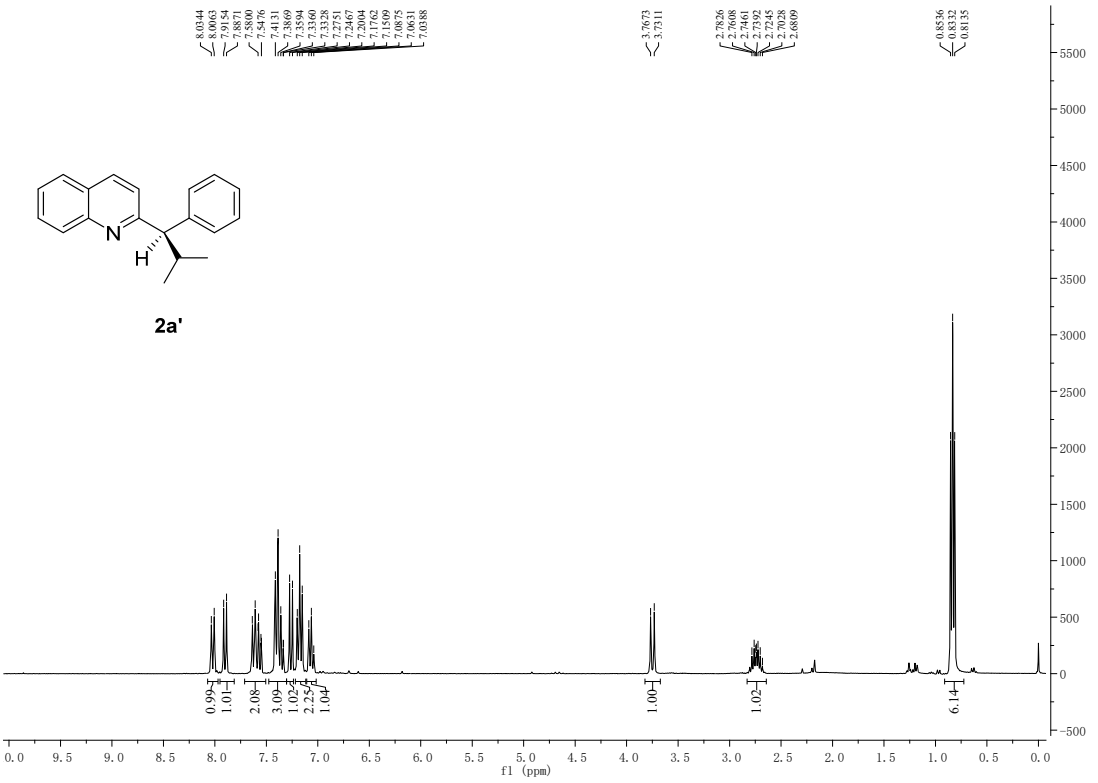

Figure S6. ^{1}H NMR spectrum for **2a'**, related to **Figure 2**.

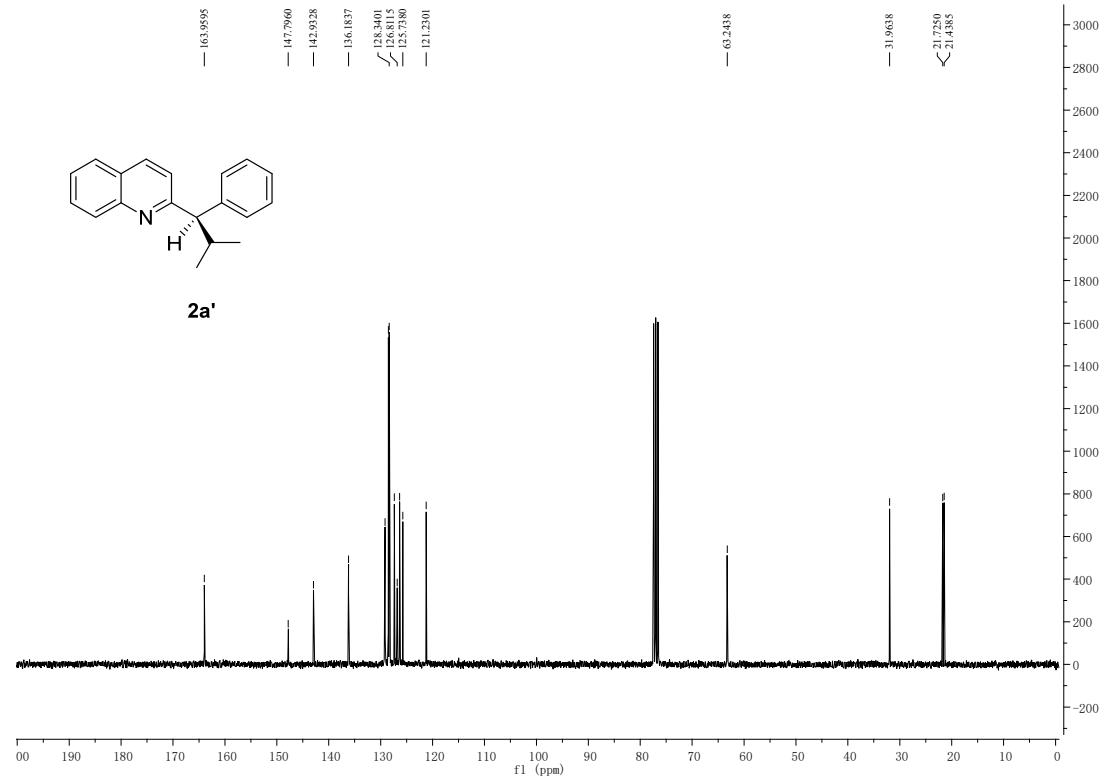

Figure S7. ^{13}C NMR spectrum for **2a'**, related to **Figure 2**.

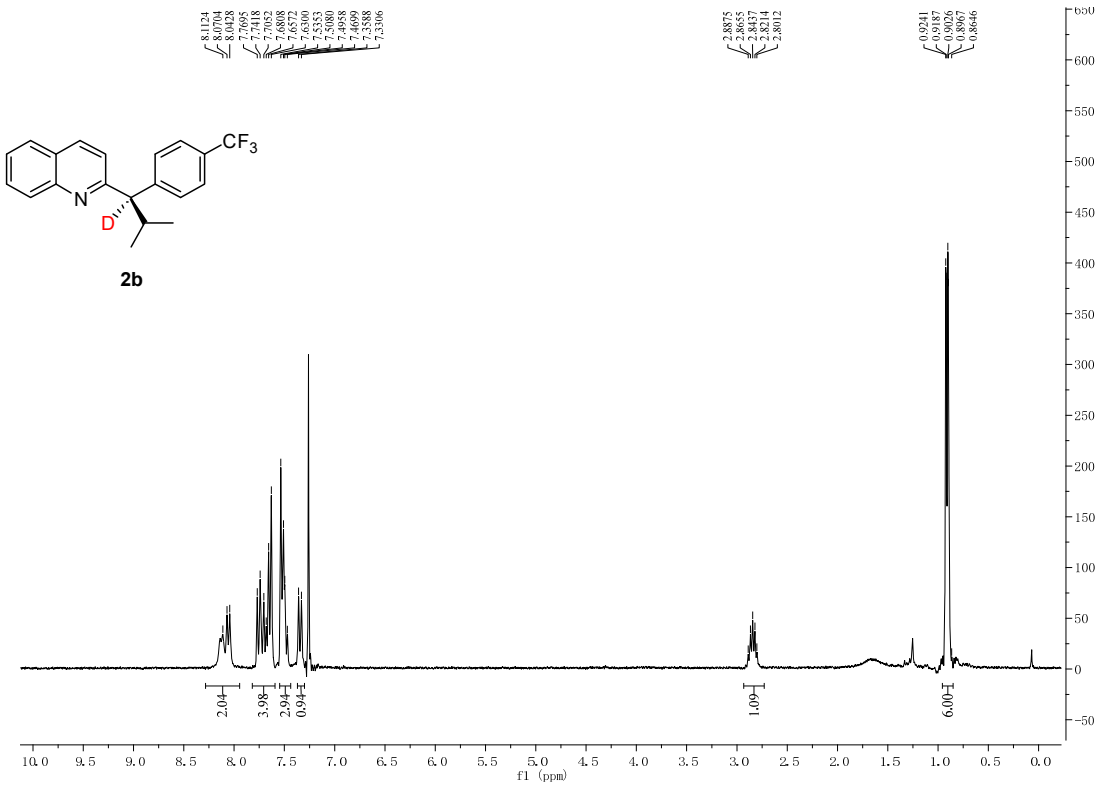

Figure S8. ^{1}H NMR spectrum for **2b**, related to **Figure 2**.

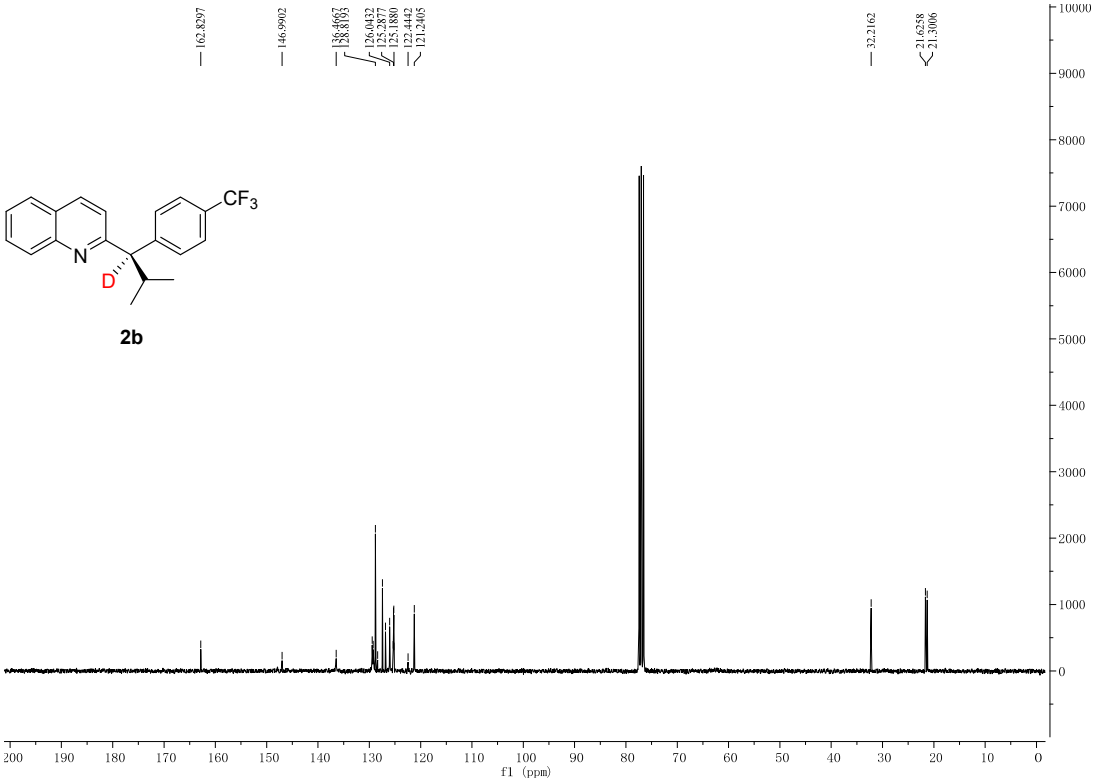

Figure S9. ^{13}C NMR spectrum for **2b**, related to **Figure 2**.

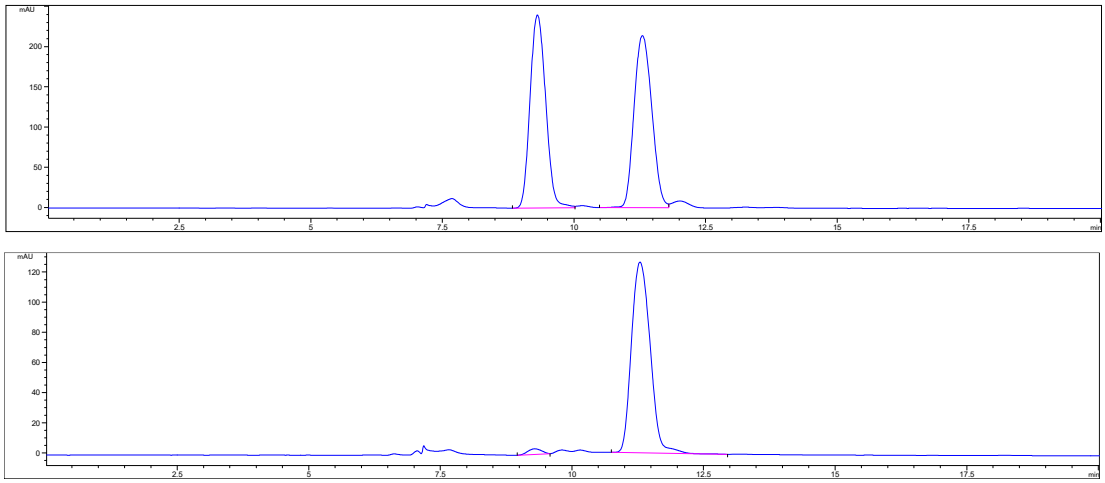

Figure S10. HPLC spectrum for **2b**, related to **Figure 2**.

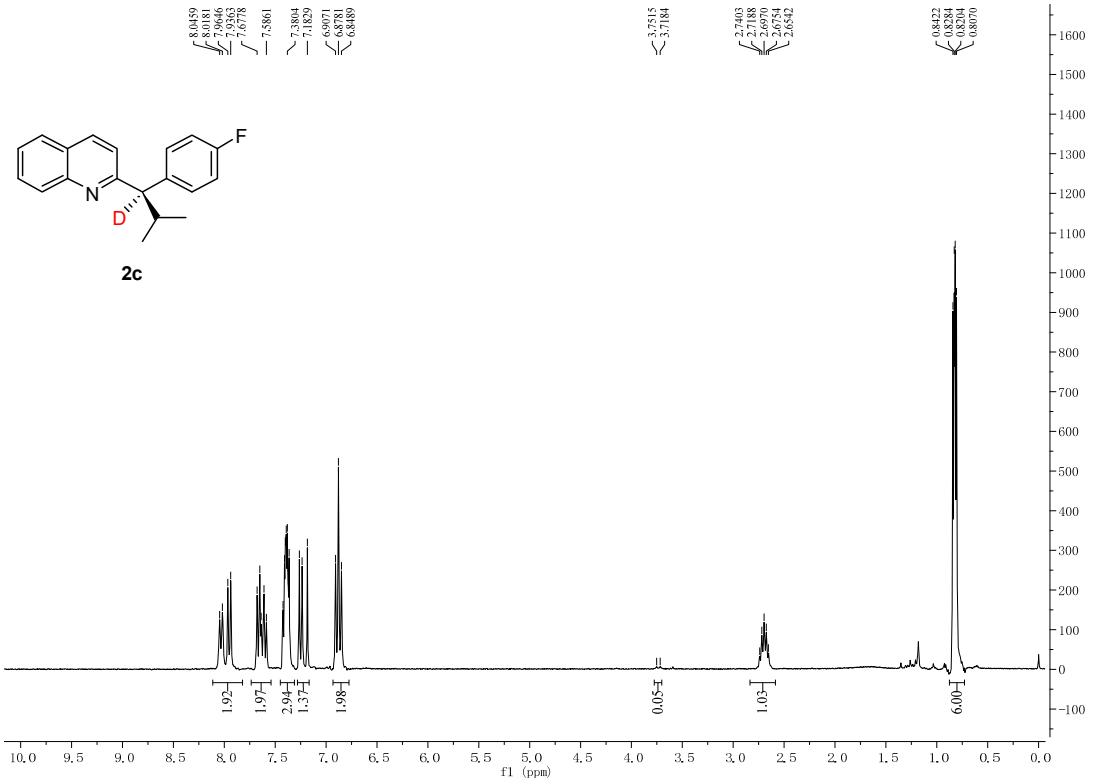

Figure S11. [1]H NMR spectrum for **2c**, related to **Figure 2**.

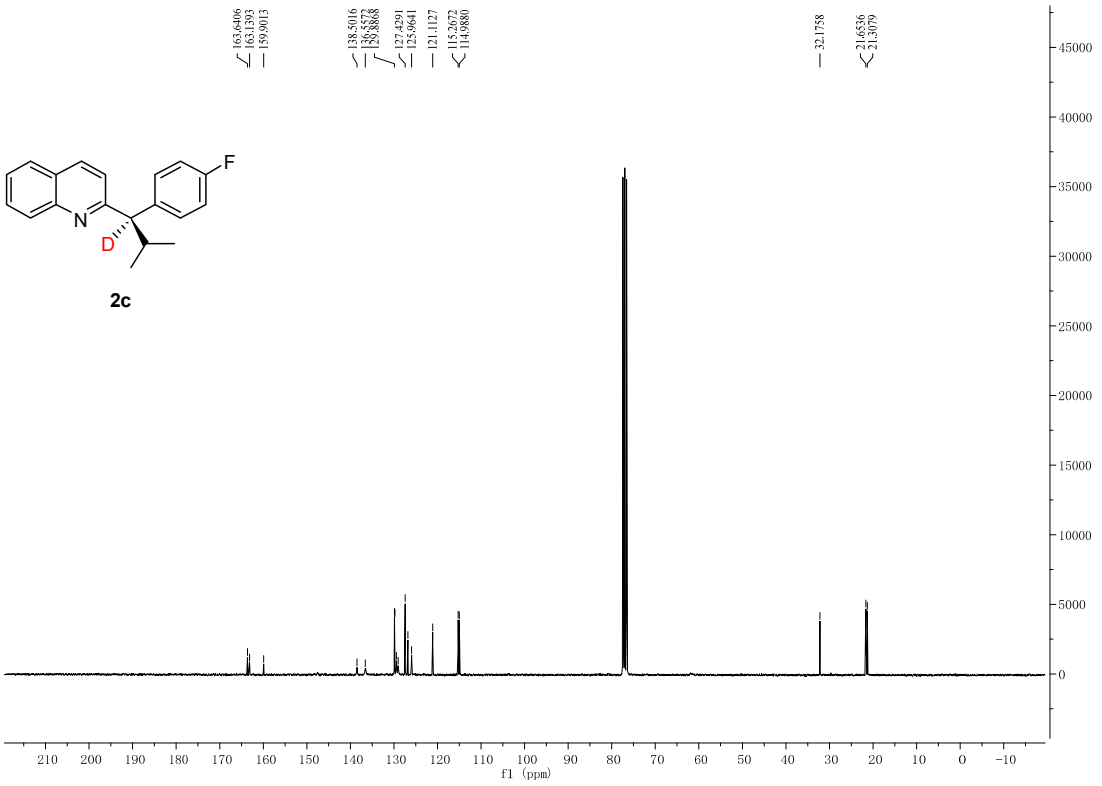

Figure S12. [13]C NMR spectrum for **2c**, related to **Figure 2**.

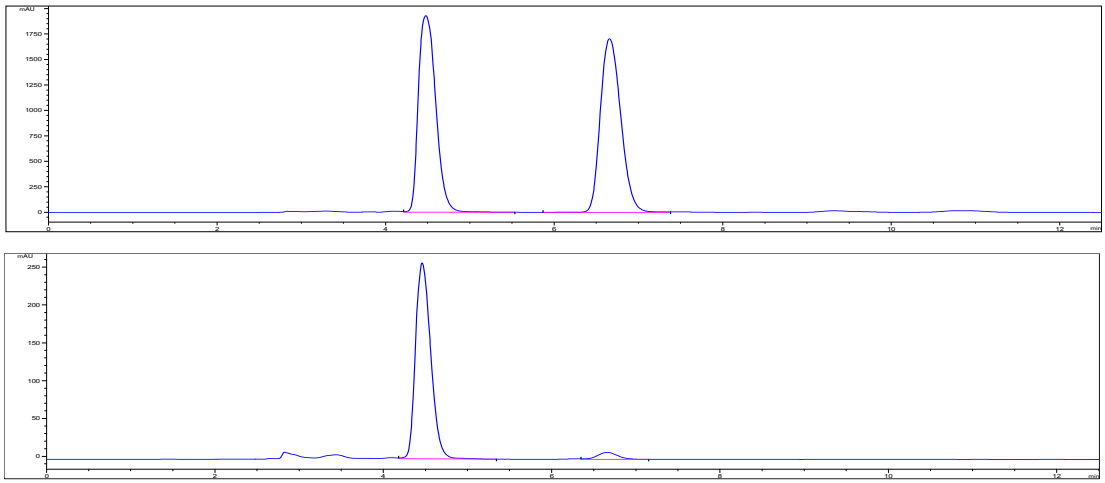

Figure S13. HPLC spectrum for **2c**, related to **Figure 2**.

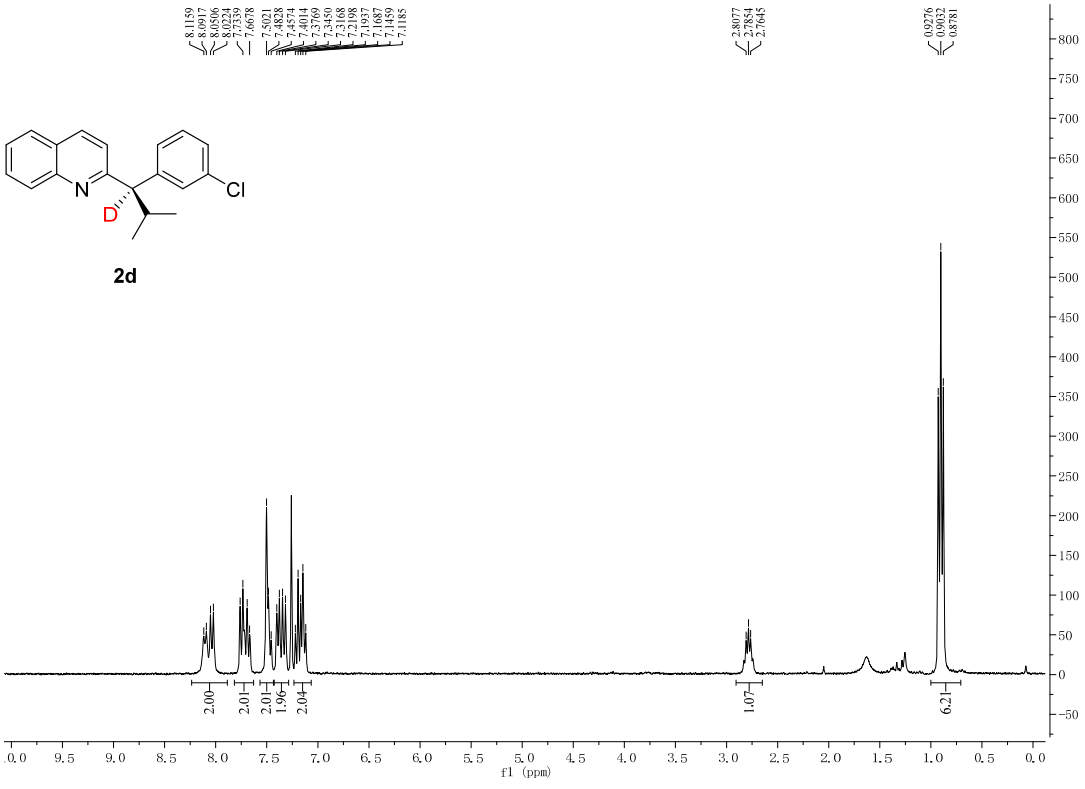

Figure S14. ^{1}H NMR spectrum for **2d**, related to **Figure 2**.

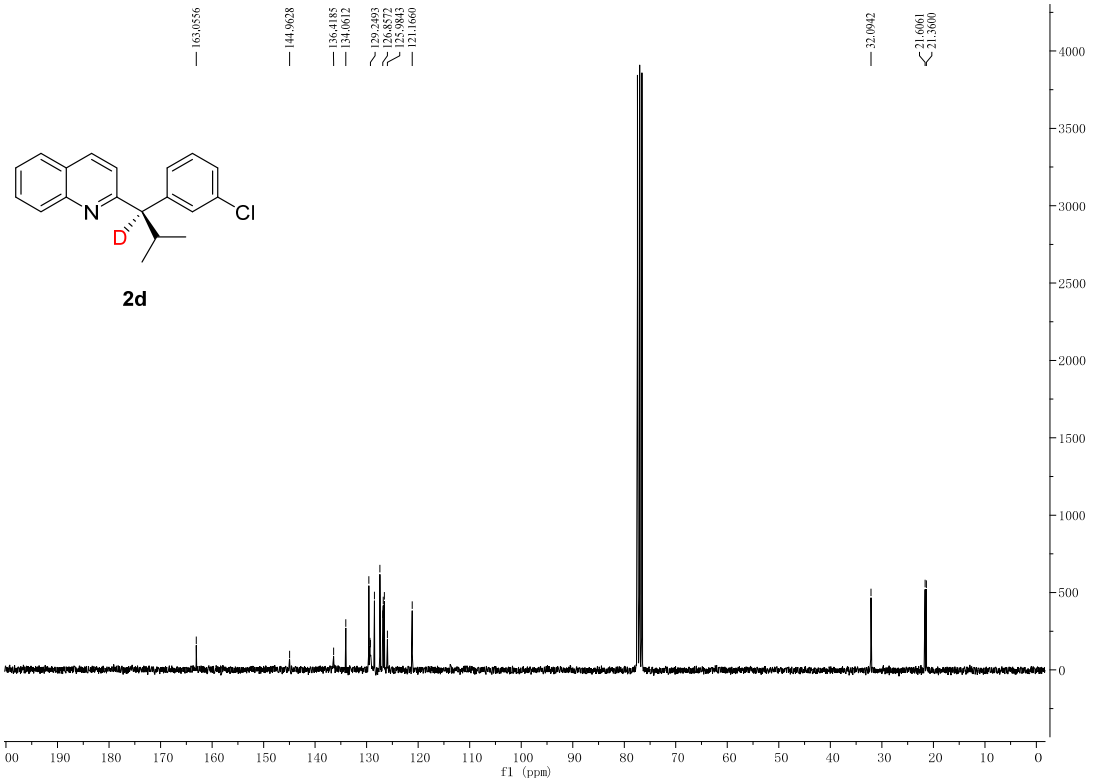

Figure S15. ^{13}C NMR spectrum for **2d**, related to **Figure 2**.

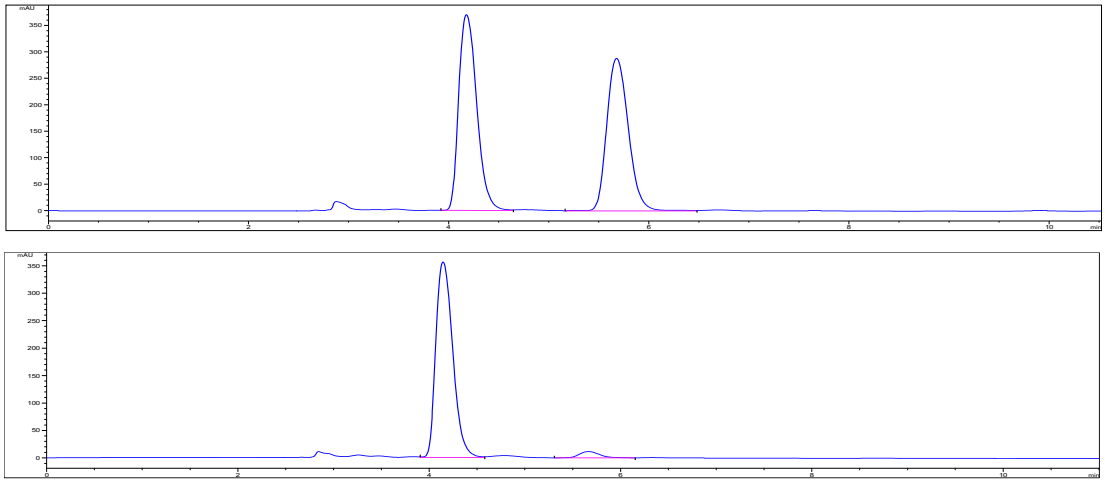

Figure S16. HPLC spectrum for **2d**, related to **Figure 2**.

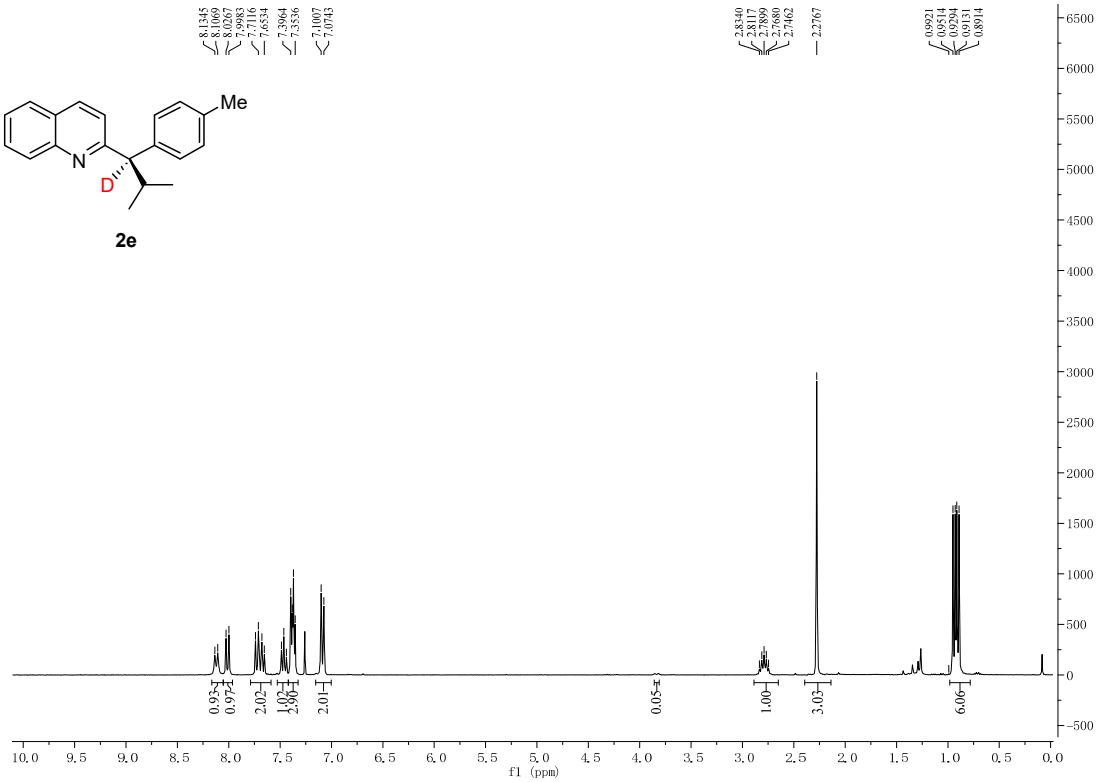

Figure S17. [1]H NMR spectrum for **2e**, related to **Figure 2**.

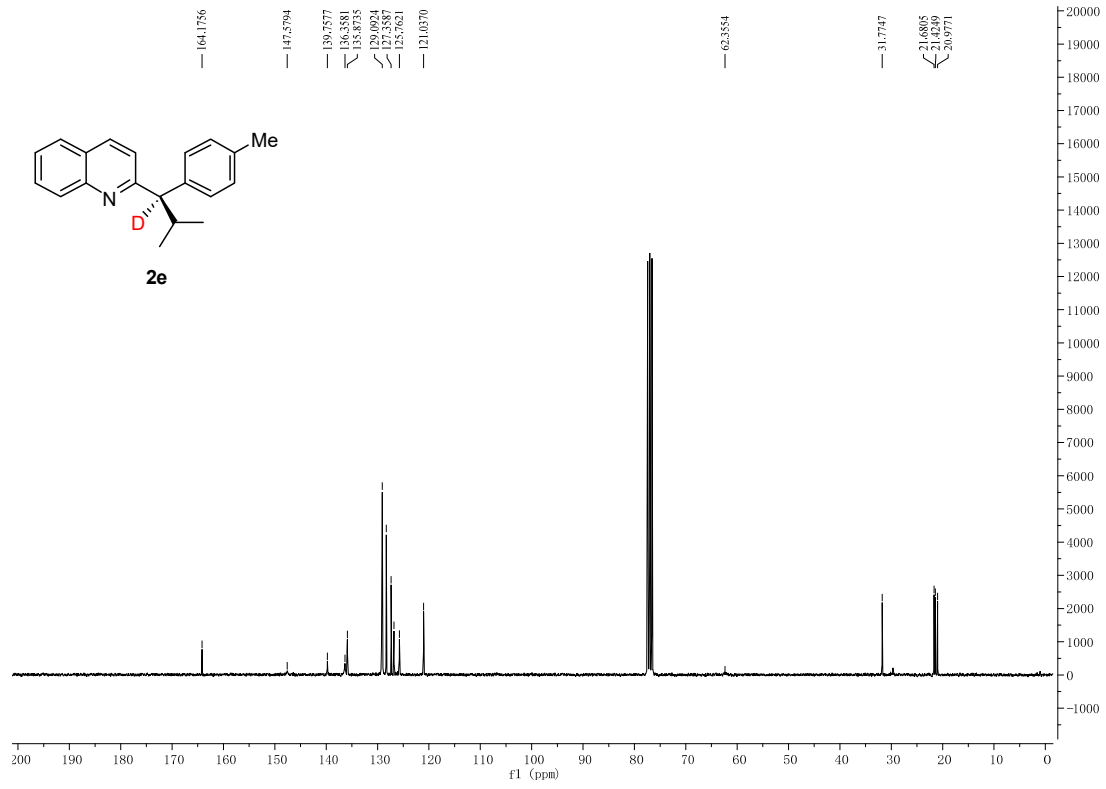

Figure S18. [13]C NMR spectrum for **2e**, related to **Figure 2**.

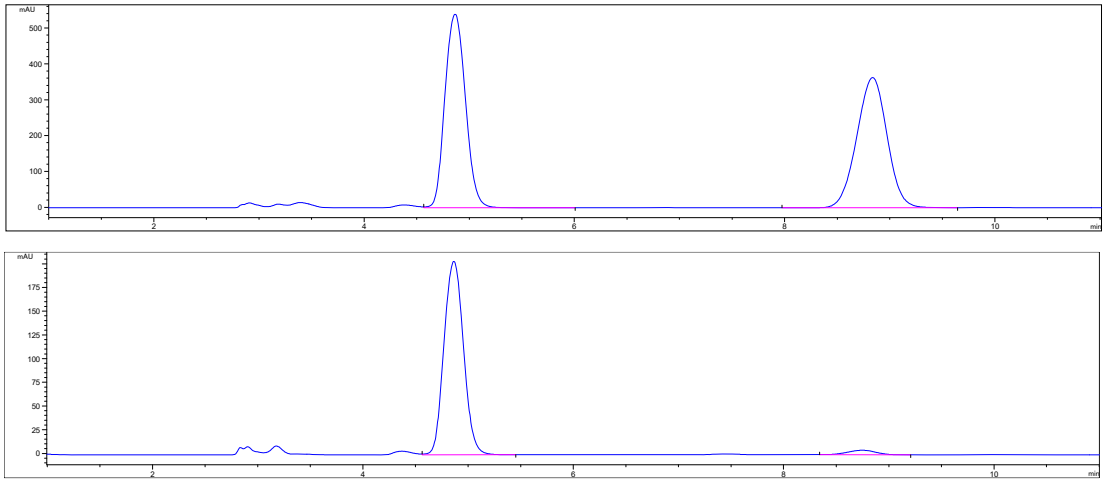

Figure S19. HPLC spectrum for **2e**, related to **Figure 2**.

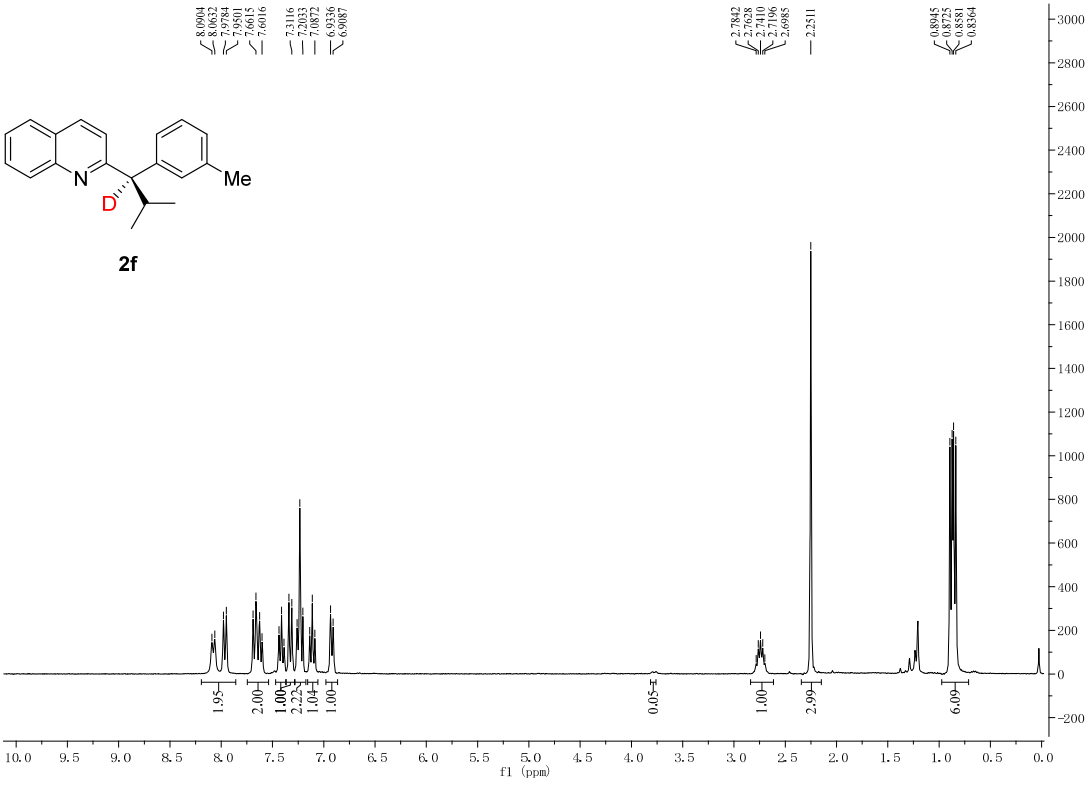

Figure S20. ^{1}H NMR spectrum for **2f**, related to **Figure 2**.

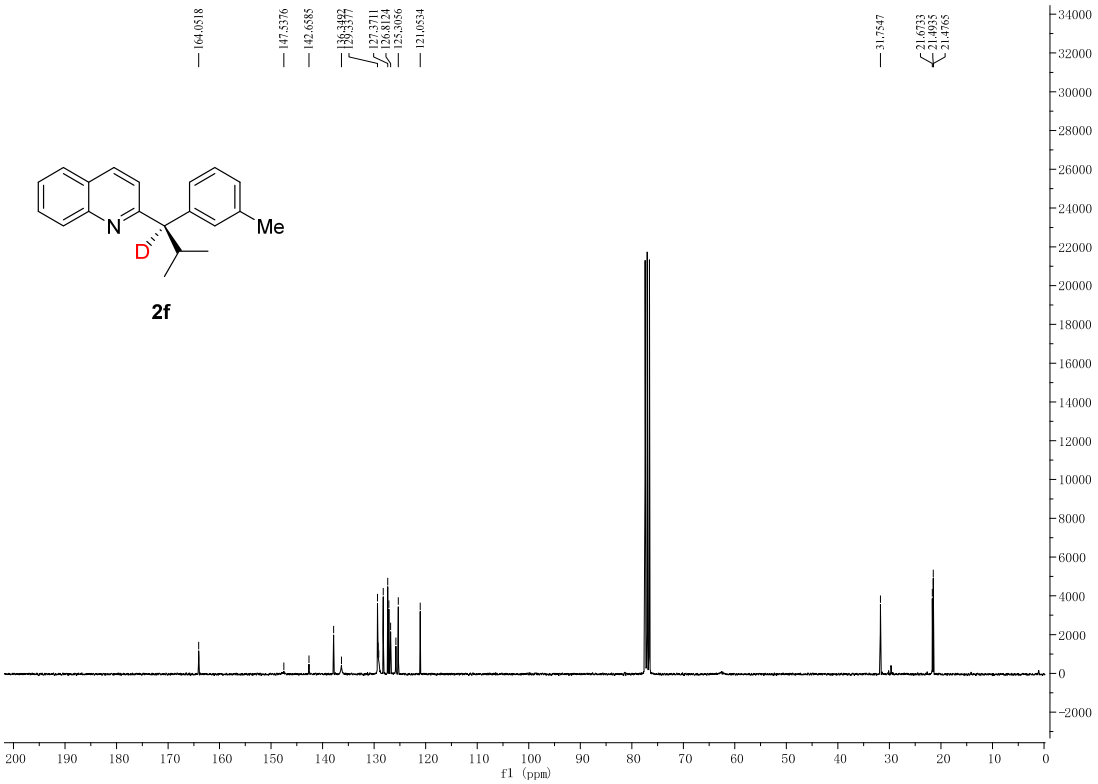

Figure S21. ^{13}C NMR spectrum for **2f**, related to **Figure 2**.

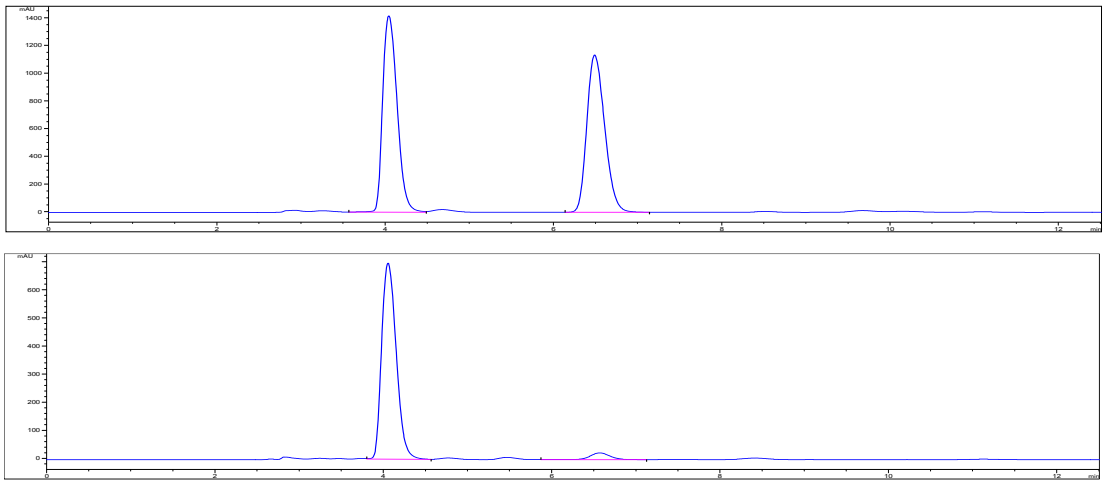

Figure S22. HPLC spectrum for **2f**, related to **Figure 2**.

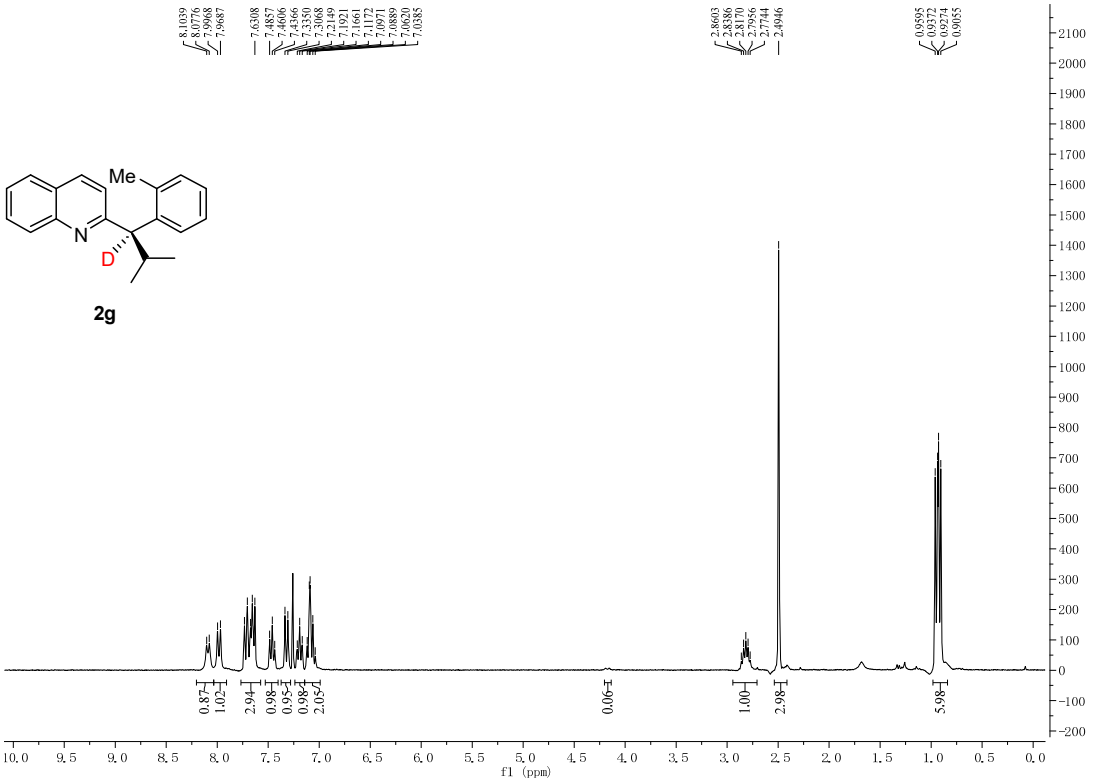

Figure S23. [1]H NMR spectrum for **2g**, related to **Figure 2**.

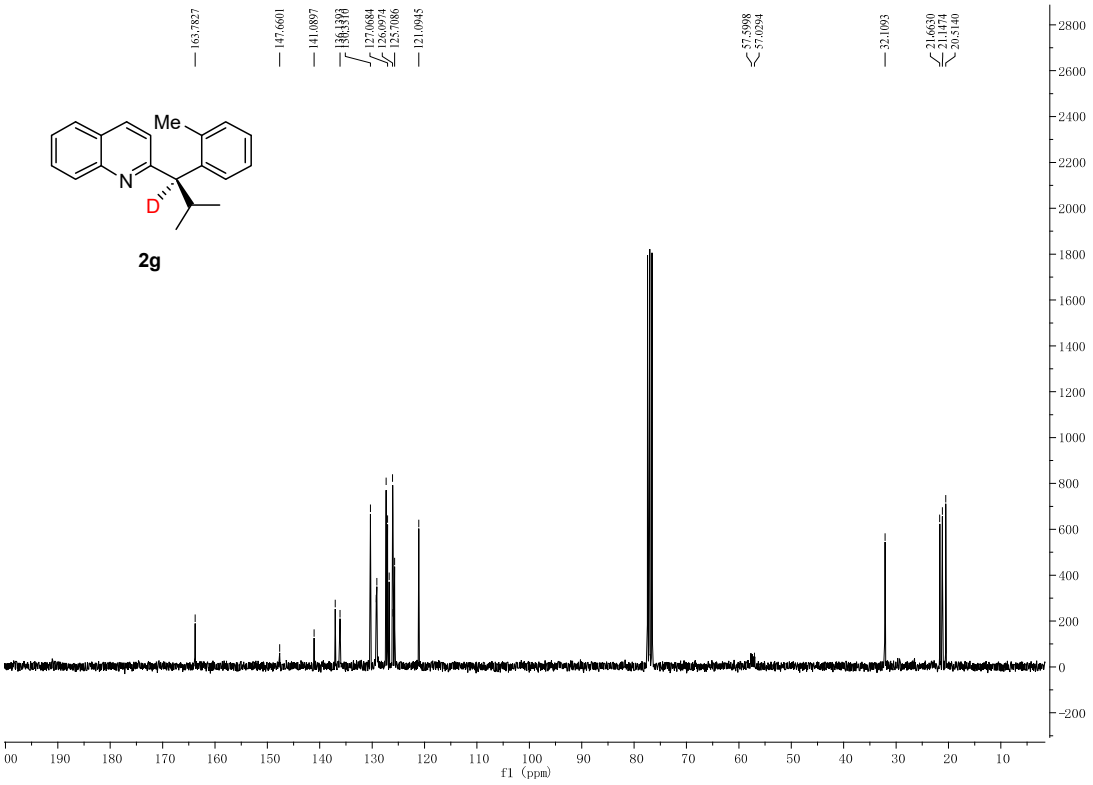

Figure S24. [13]C NMR spectrum for **2g**, related to **Figure 2**.

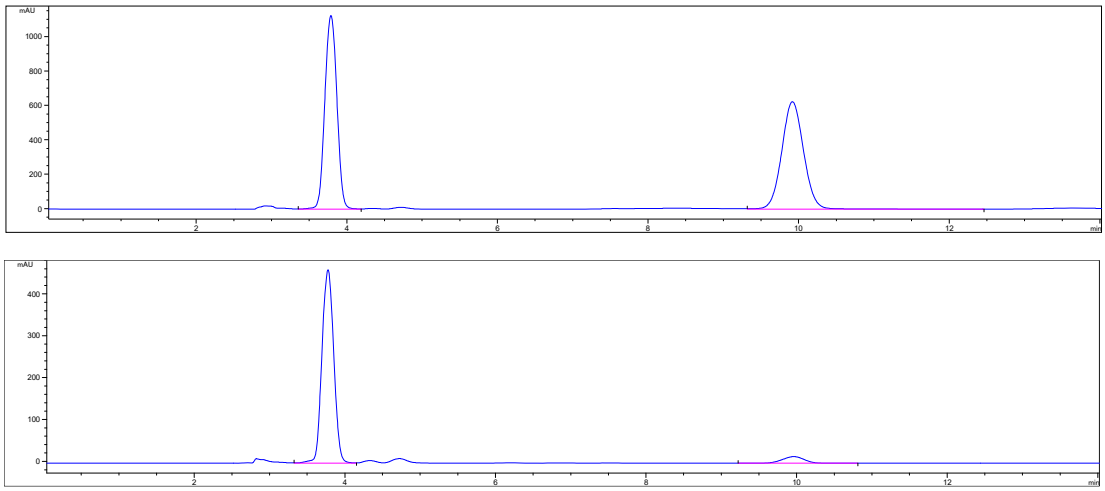

Figure S25. HPLC spectrum for **2g**, related to **Figure 2**.

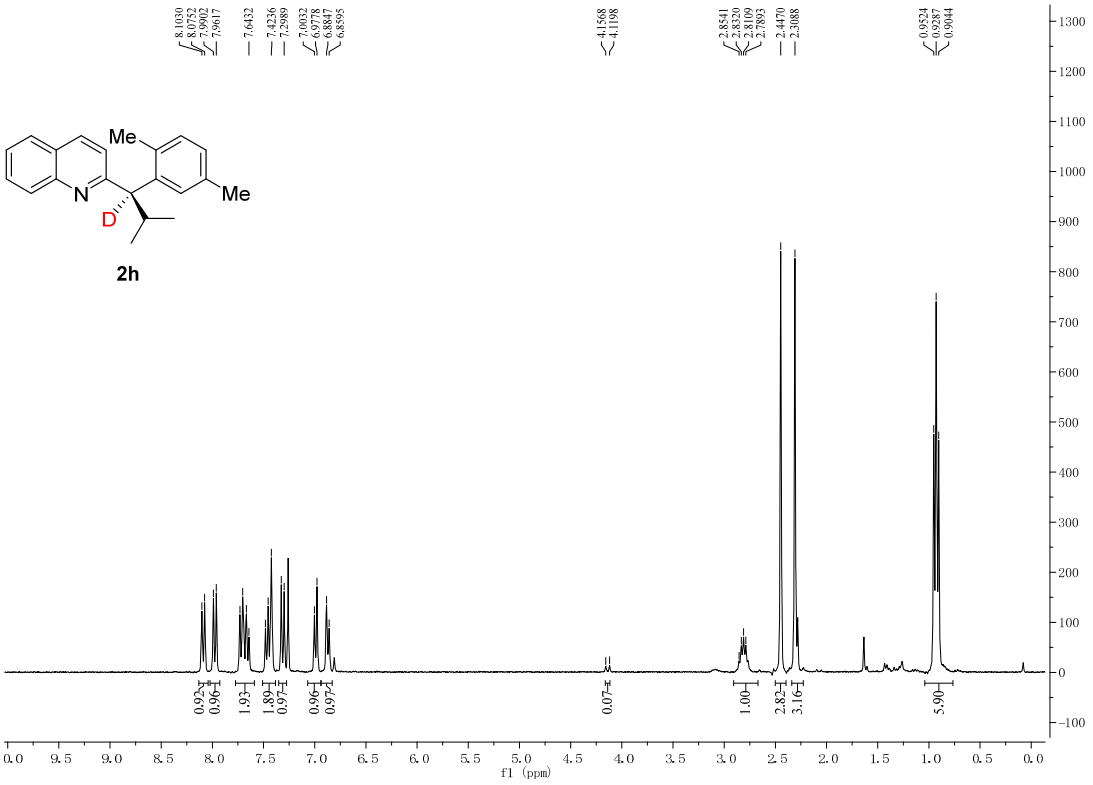

Figure S26. ^{1}H NMR spectrum for **2h**, related to **Figure 2**.

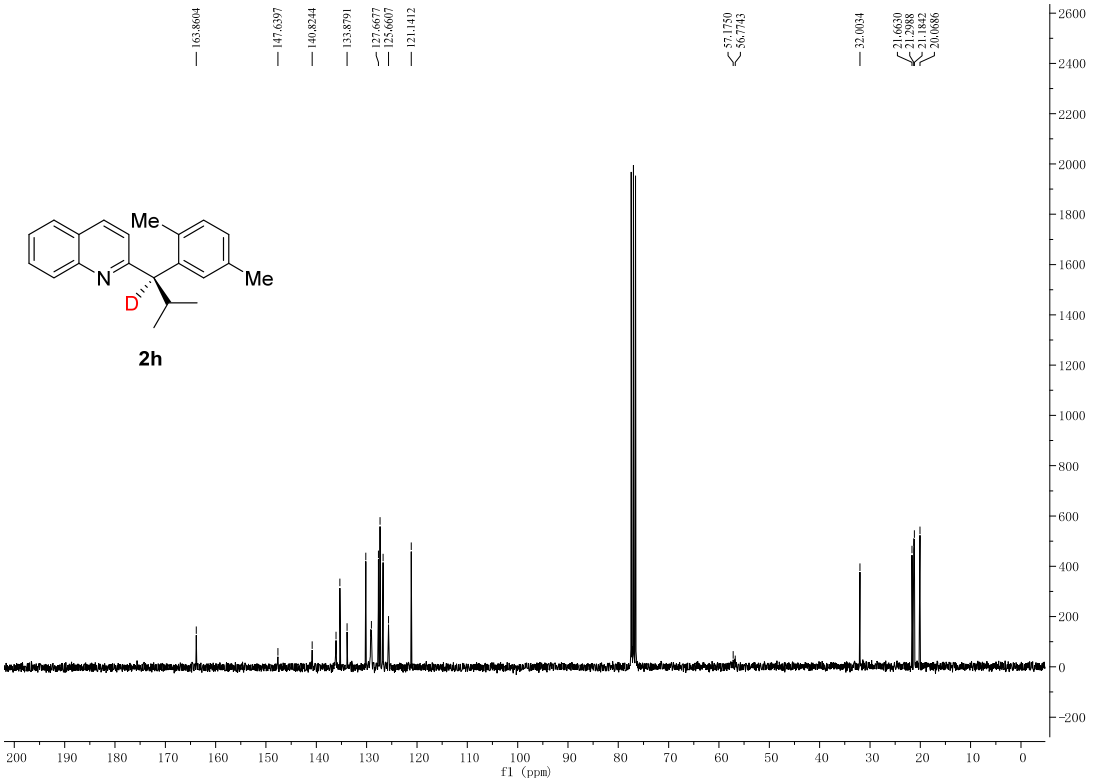

Figure S27. ^{13}C NMR spectrum for **2h**, related to **Figure 2**.

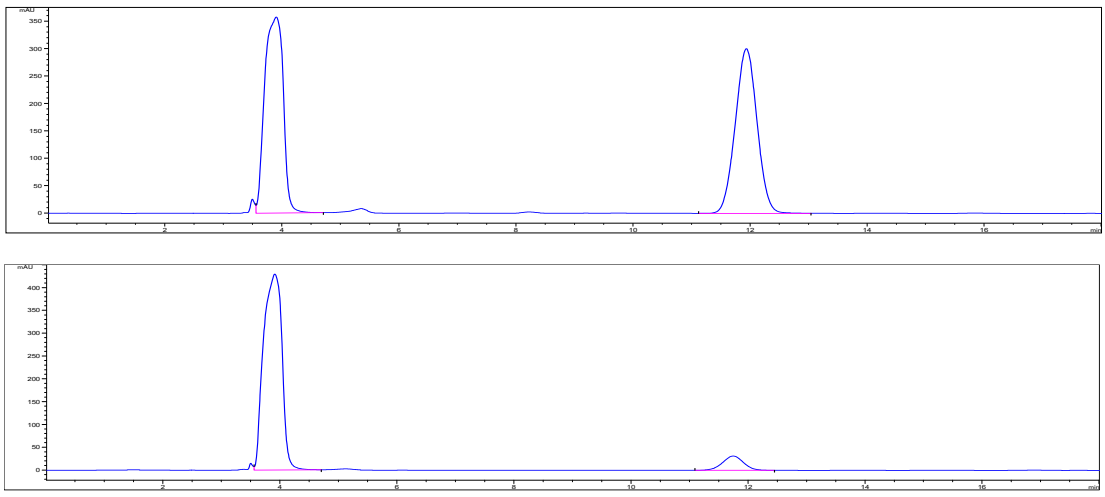

Figure S28. HPLC spectrum for **2h**, related to **Figure 2**.

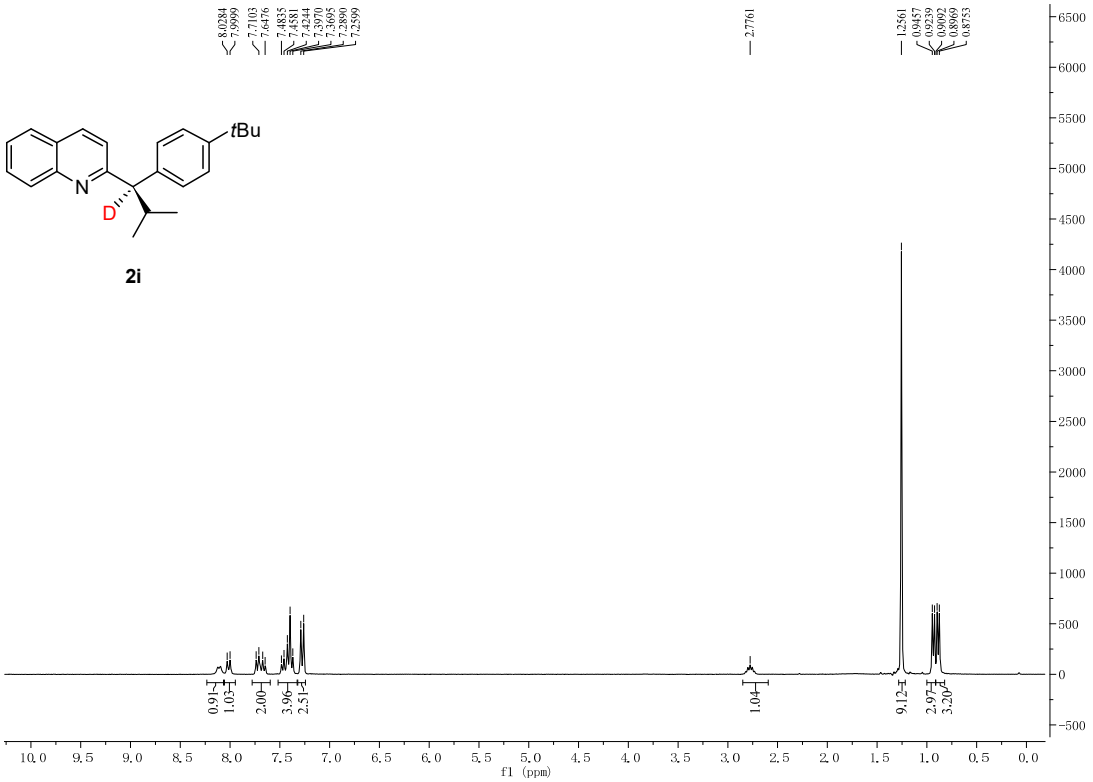

Figure S29. ^{1}H NMR spectrum for **2i**, related to **Figure 2**.

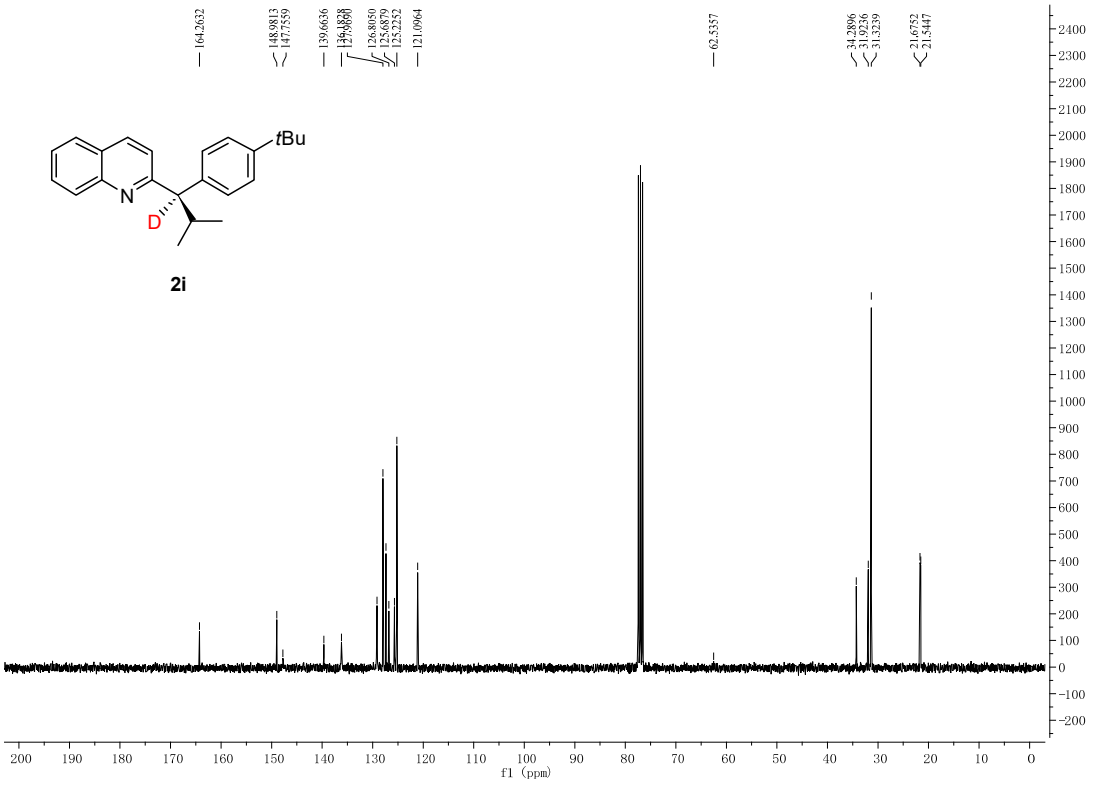

Figure S30. ^{13}C NMR spectrum for **2i**, related to **Figure 2**.

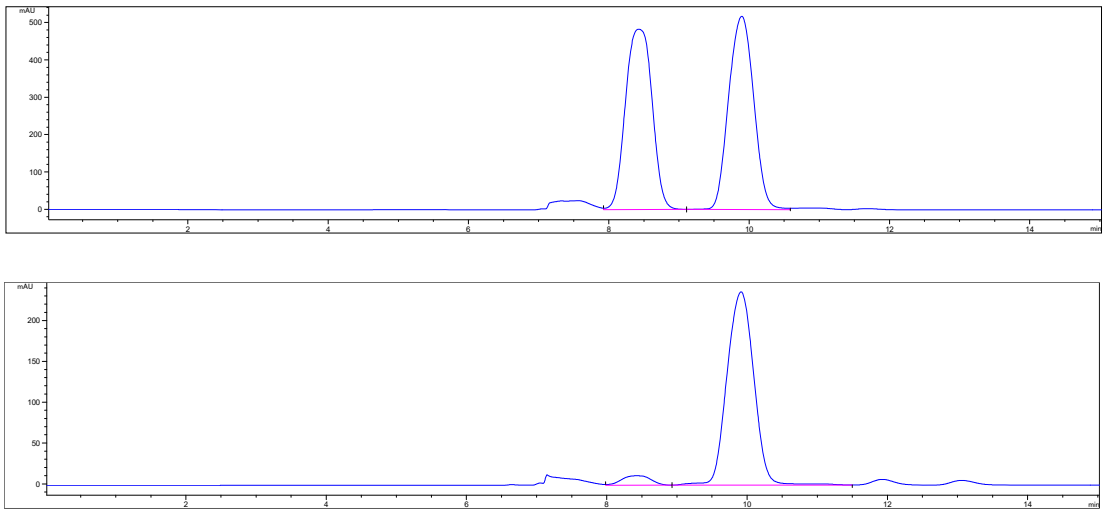

Figure S31. HPLC spectrum for **2i**, related to **Figure 2**.

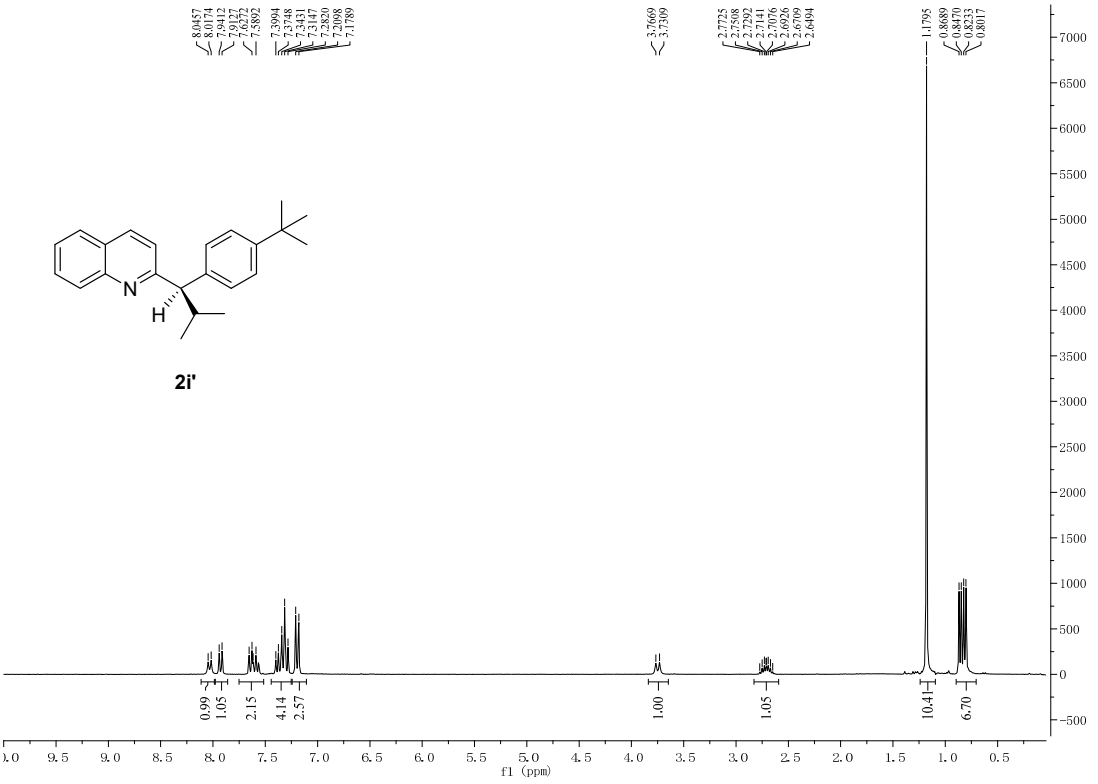

2i'

Figure S32. ^{1}H NMR spectrum for **2i'**, related to **Figure 2**.

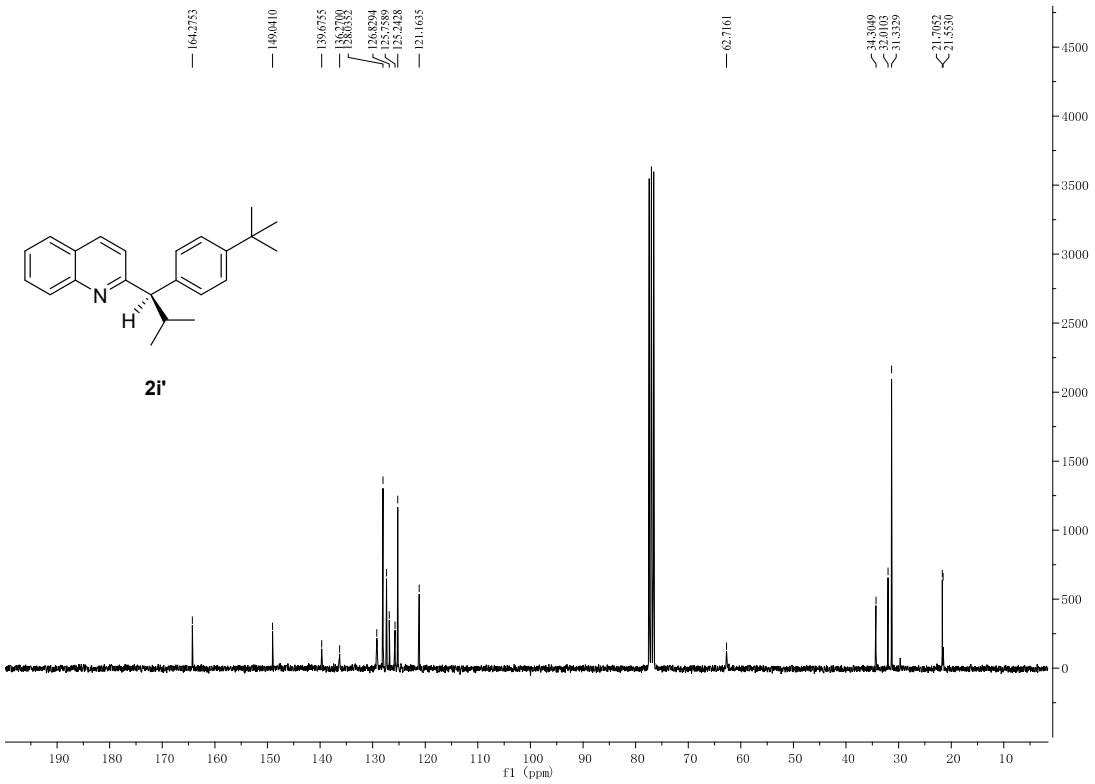

Figure S33. ^{13}C NMR spectrum for **2i'**, related to **Figure 2**.

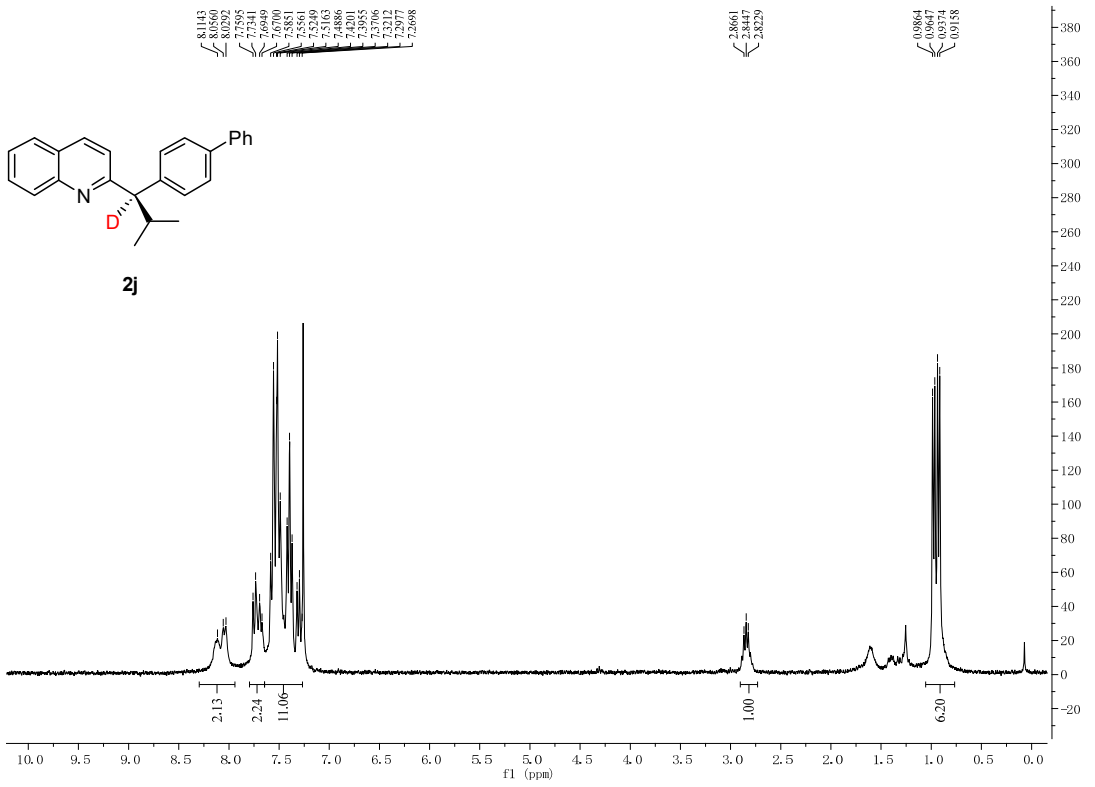

Figure S34. ^{1}H NMR spectrum for **2j**, related to **Figure 2**.

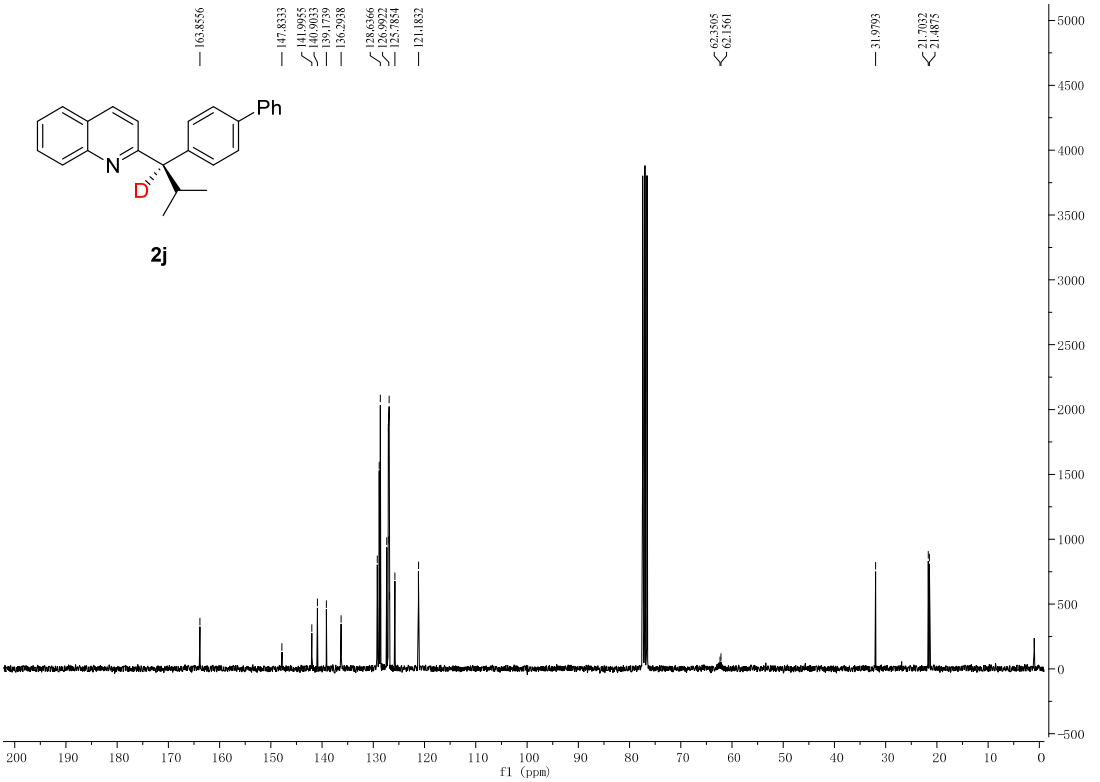

Figure S35. ^{13}C NMR spectrum for **2j**, related to **Figure 2**.

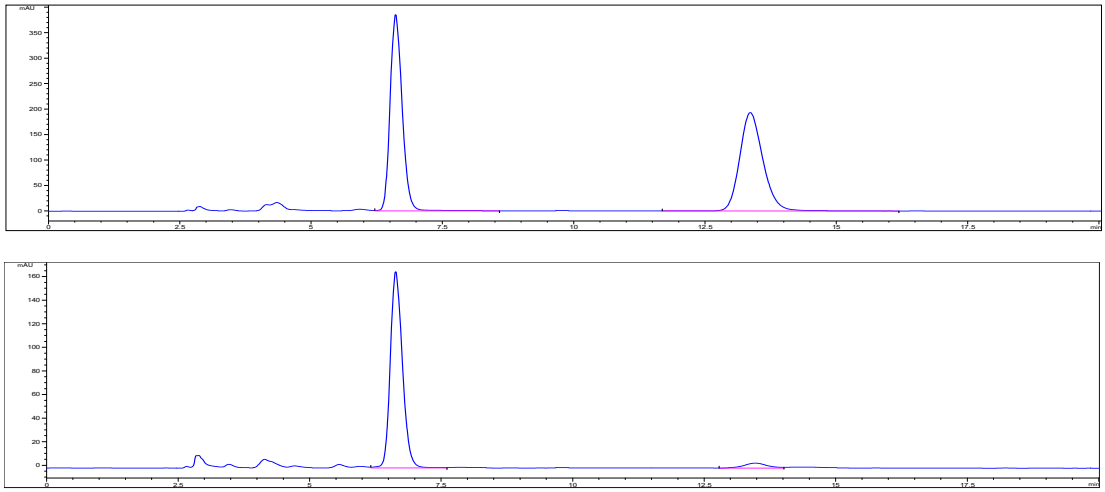

Figure S36. HPLC spectrum for **2j**, related to **Figure 2**.

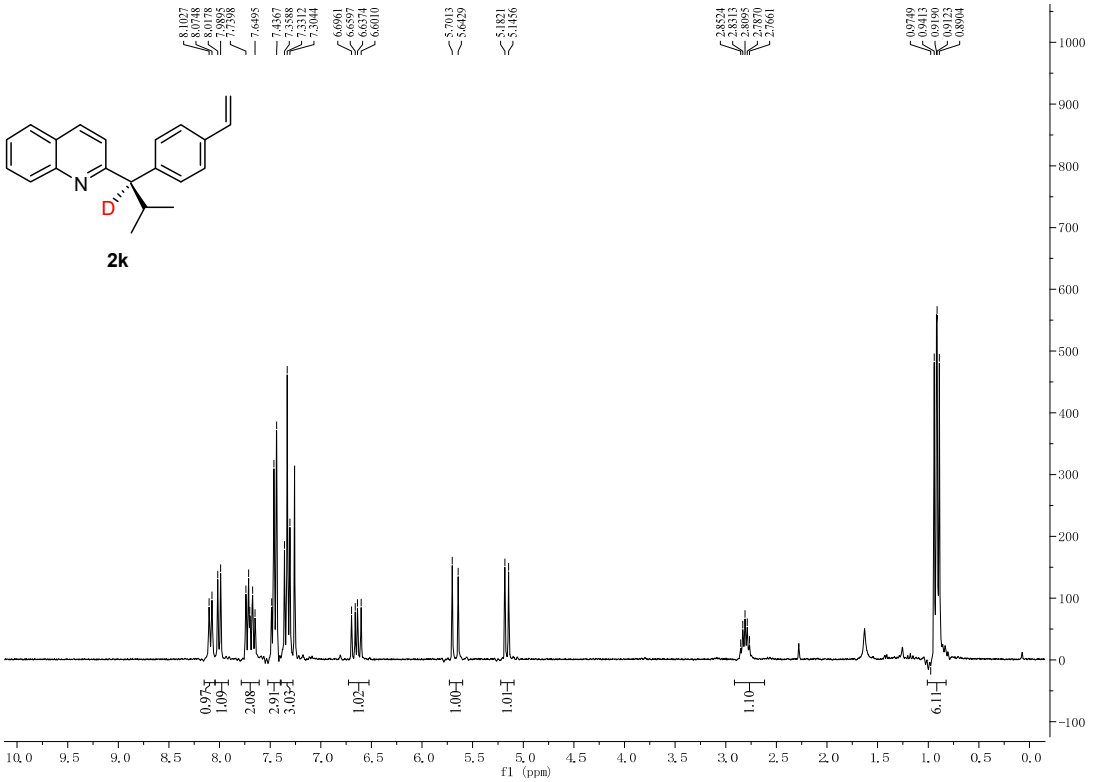

Figure S37. ^{1}H NMR spectrum for **2k**, related to **Figure 2**.

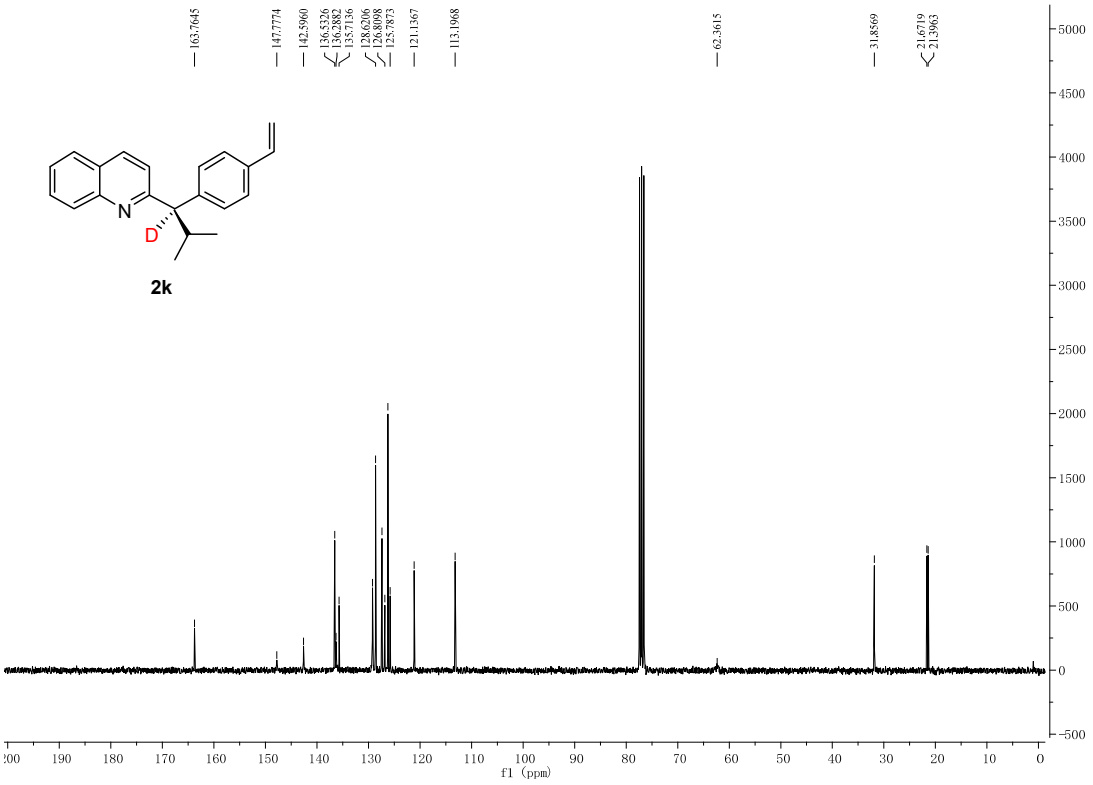

Figure S38. ^{13}C NMR spectrum for **2k**, related to **Figure 2**.

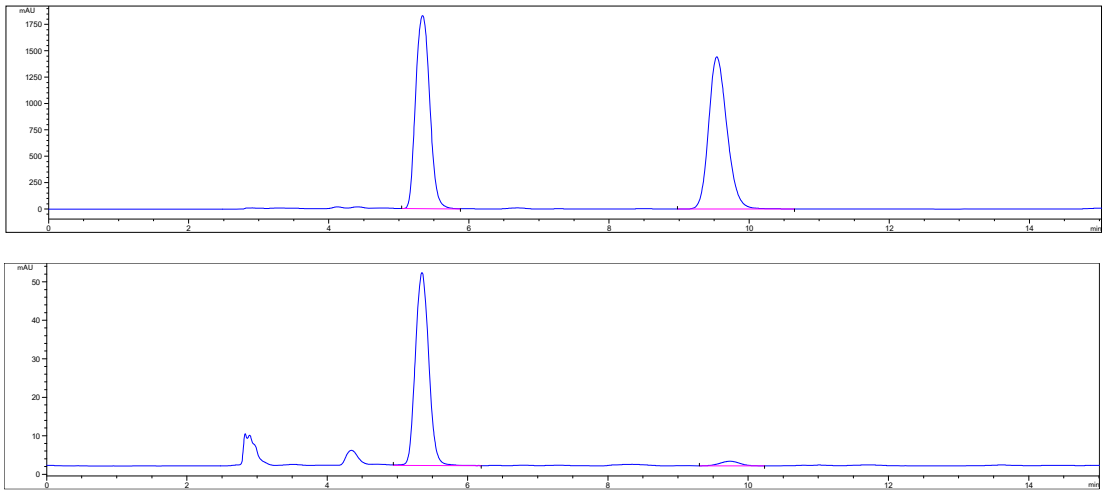

Figure S39. HPLC spectrum for **2k**, related to **Figure 2**.

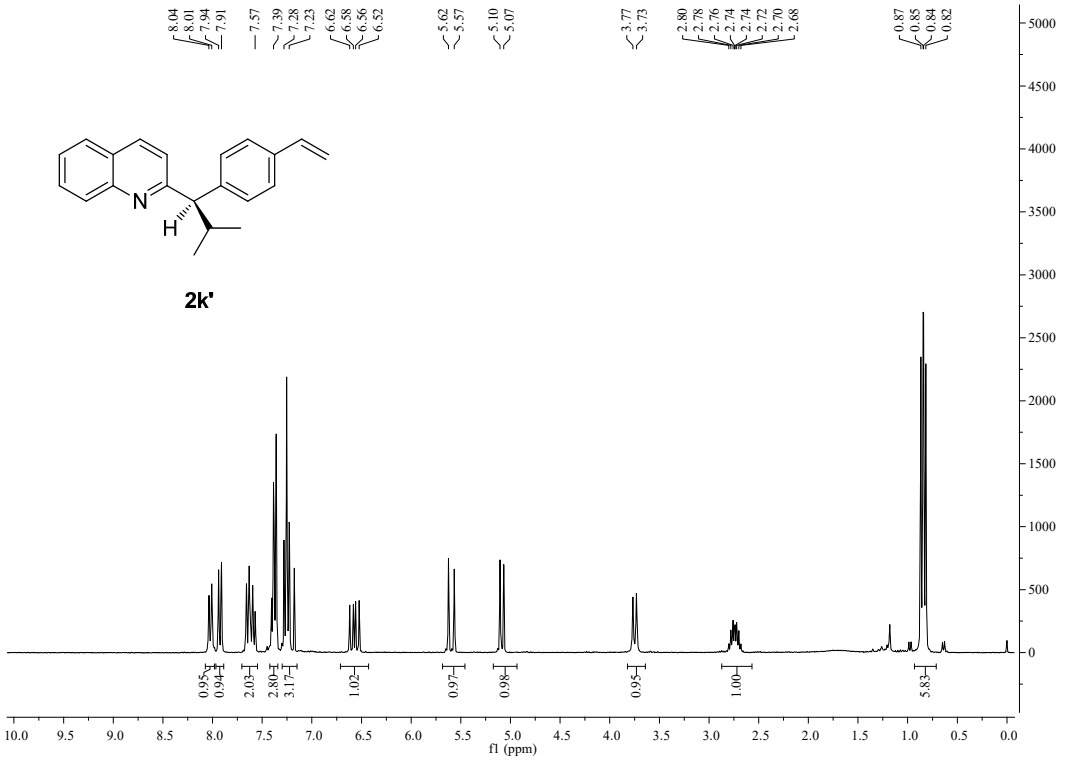

Figure S40. ^{1}H NMR spectrum for **2k'**, related to **Figure 2**.

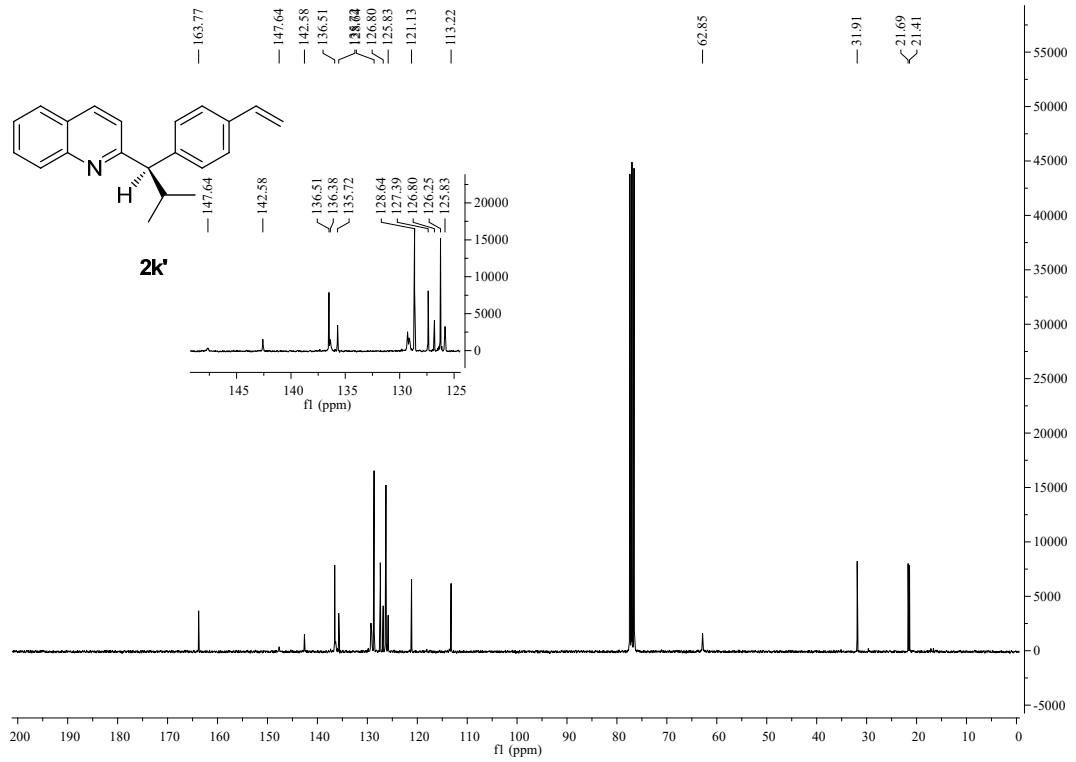

Figure S41. ^{13}C NMR spectrum for **2k'**, related to **Figure 2**.

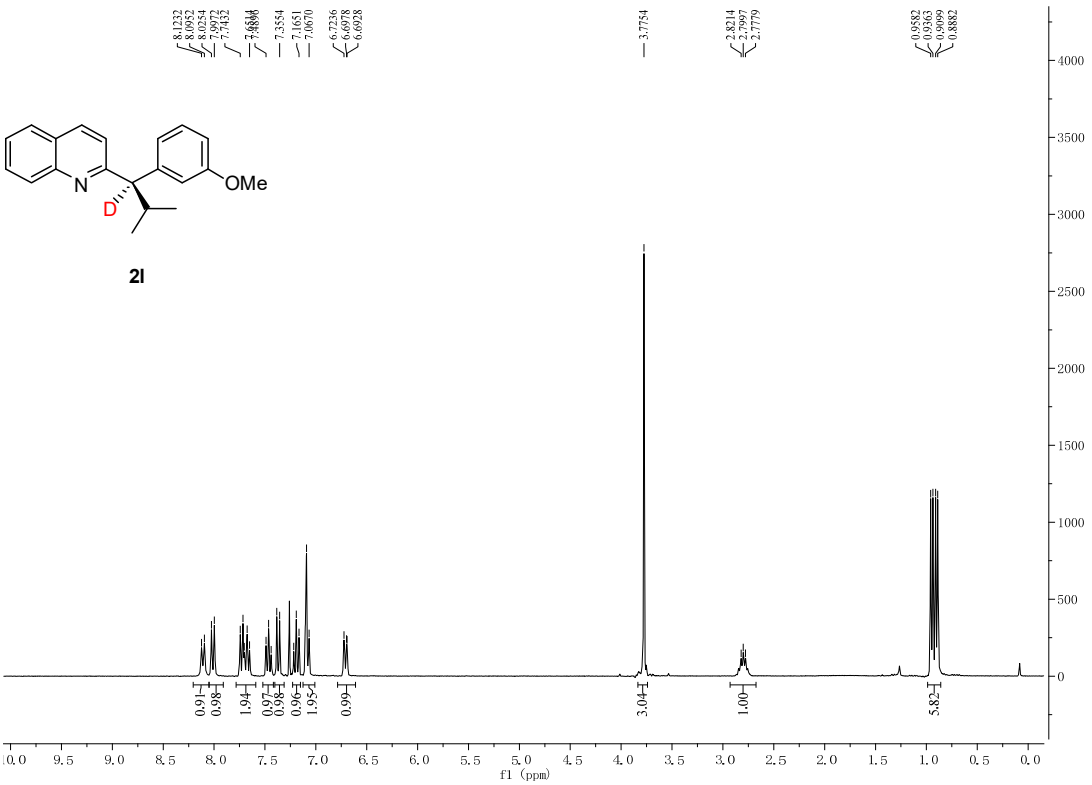

Figure S42. ^{1}H NMR spectrum for **2l**, related to **Figure 2**.

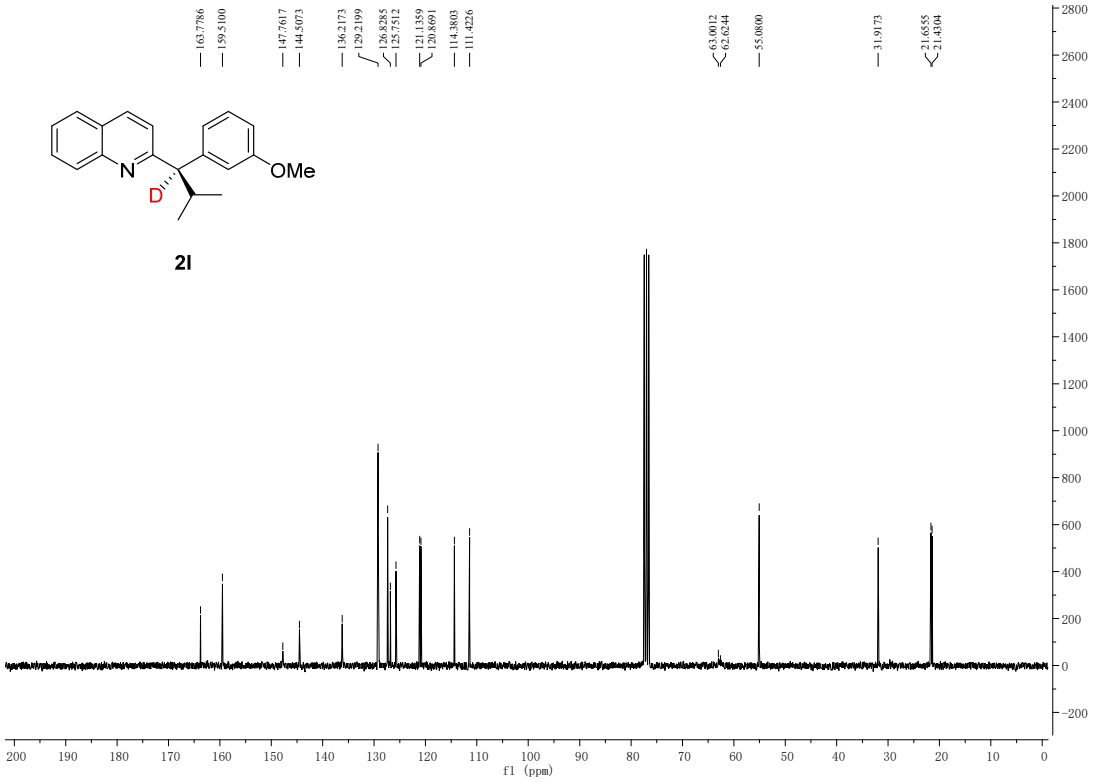

Figure S43. ^{13}C NMR spectrum for **2l**, related to **Figure 2**.

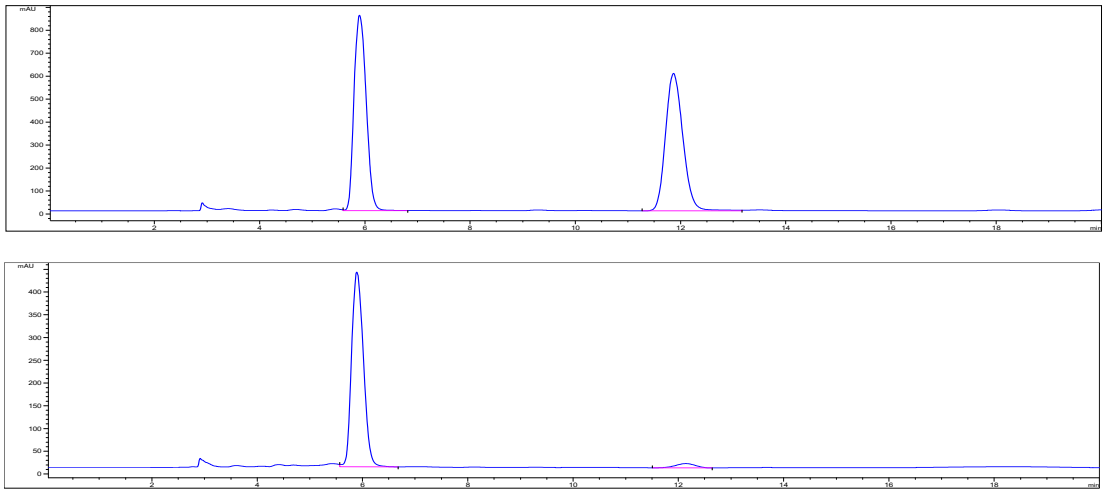

Figure S44. HPLC spectrum for **2l**, related to **Figure 2**.

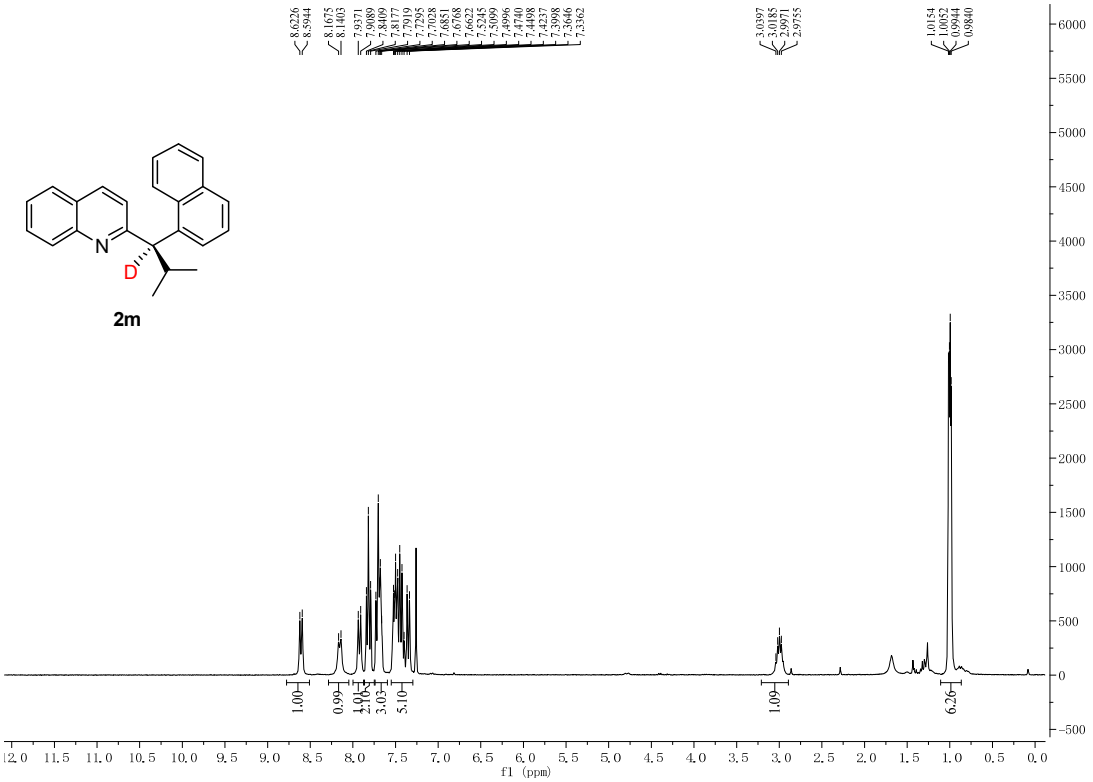

Figure S45. ^{1}H NMR spectrum for **2m**, related to **Figure 2**.

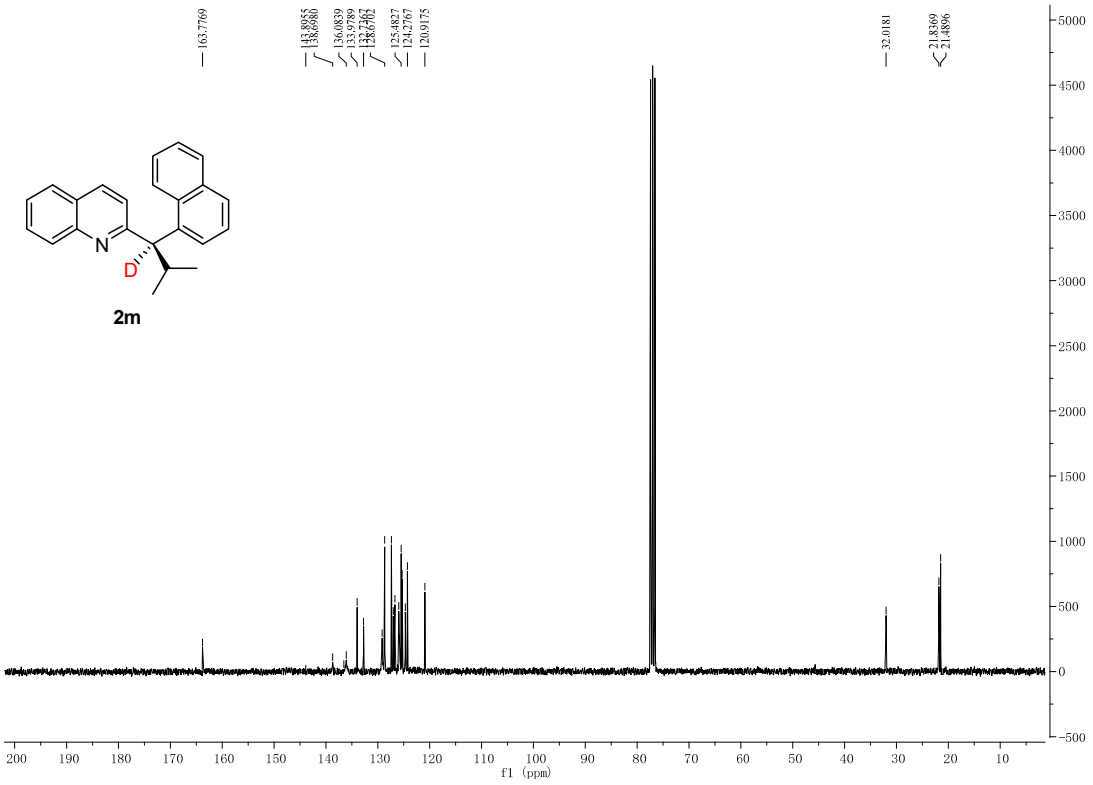

Figure S46. ^{13}C NMR spectrum for **2m**, related to **Figure 2**.

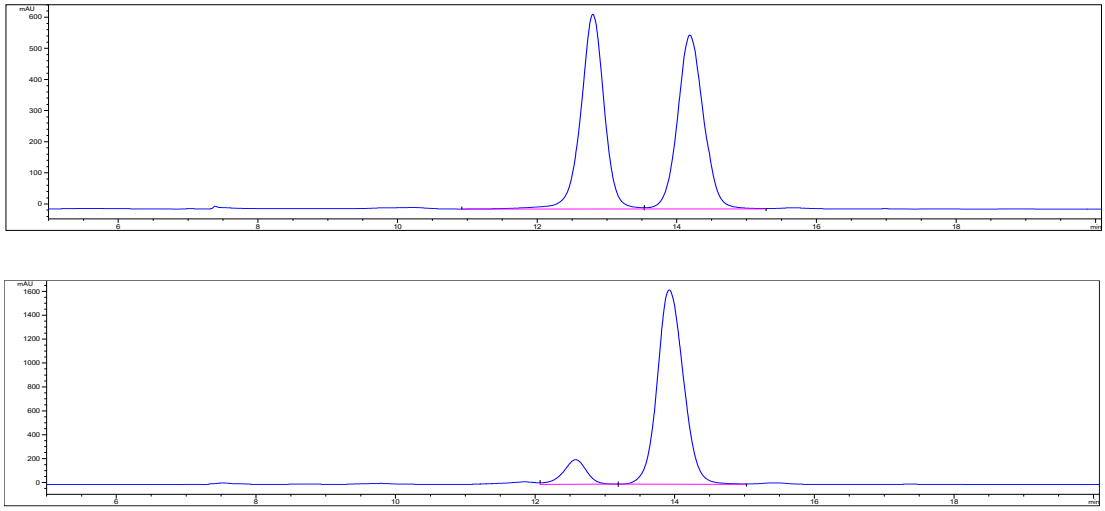

Figure S47. HPLC spectrum for **2m**, related to **Figure 2**.

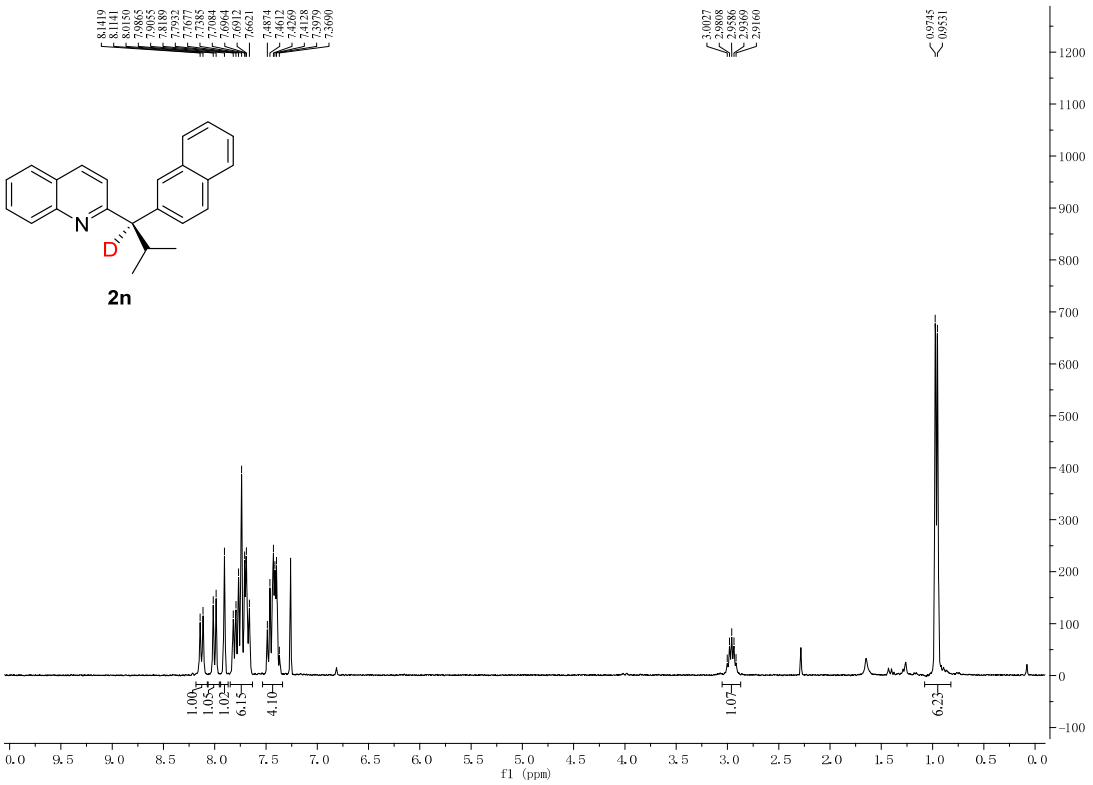

Figure S48. ^{1}H NMR spectrum for **2n**, related to **Figure 2**.

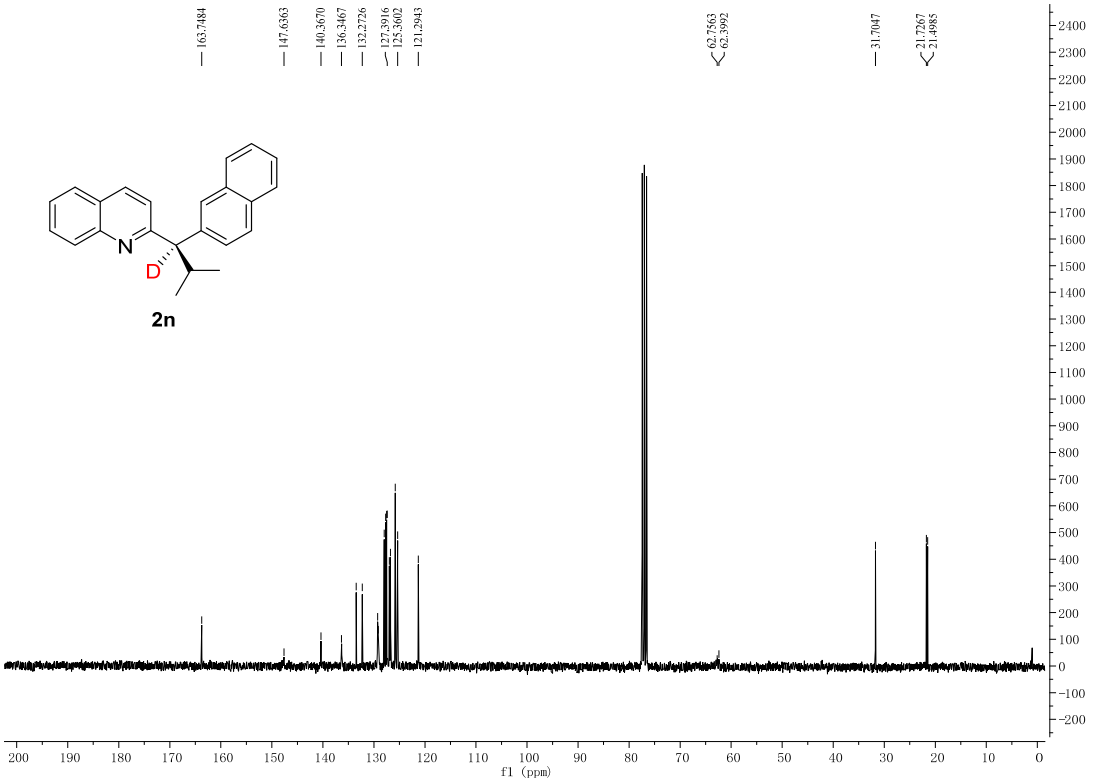

Figure S49. ^{13}C NMR spectrum for **2n**, related to **Figure 2**.

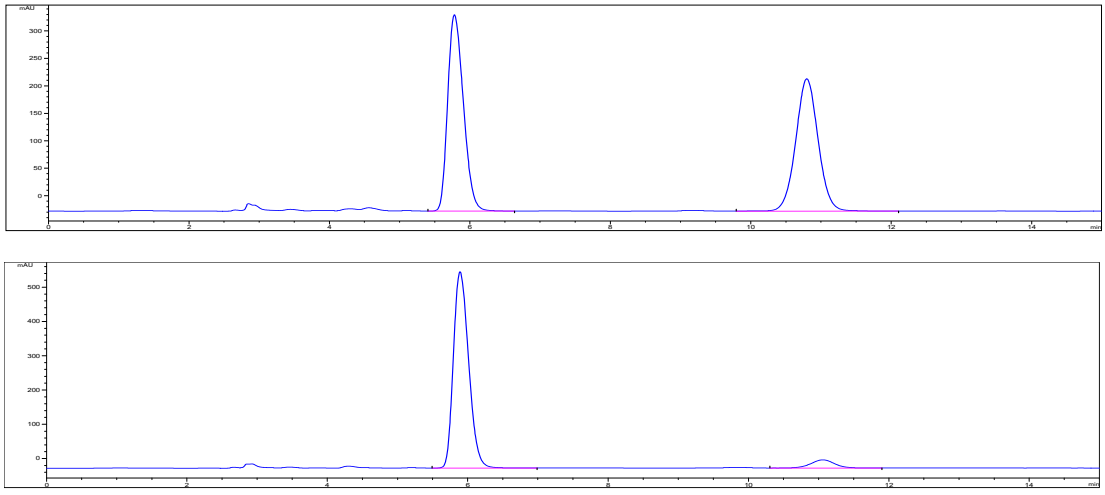

Figure S50. HPLC spectrum for **2n**, related to **Figure 2**.

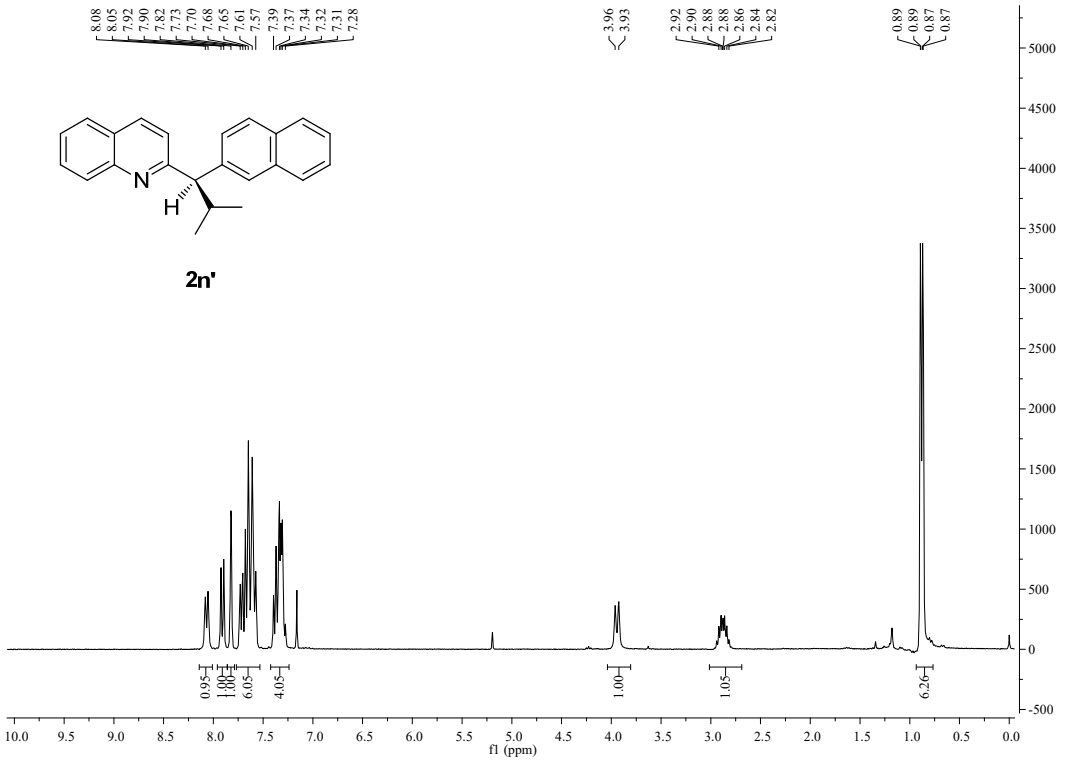

Figure S51. ^{1}H NMR spectrum for **2n'**, related to **Figure 2**.

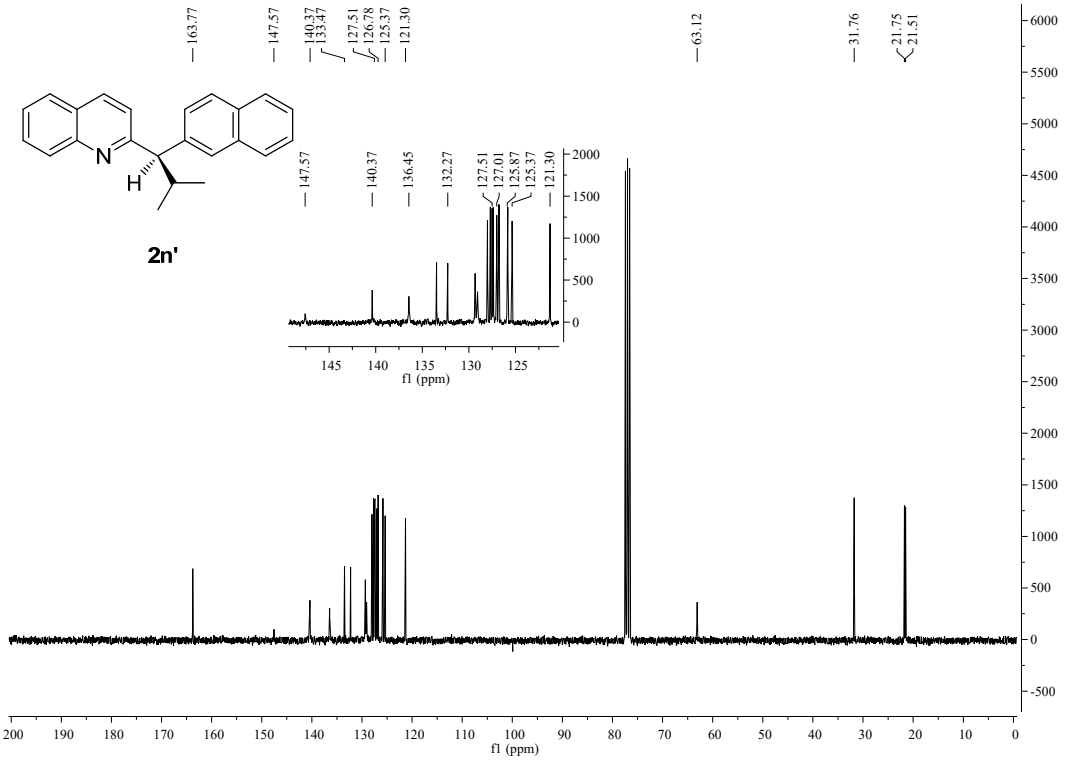

Figure S52. ^{13}C NMR spectrum for **2n'**, related to **Figure 2**.

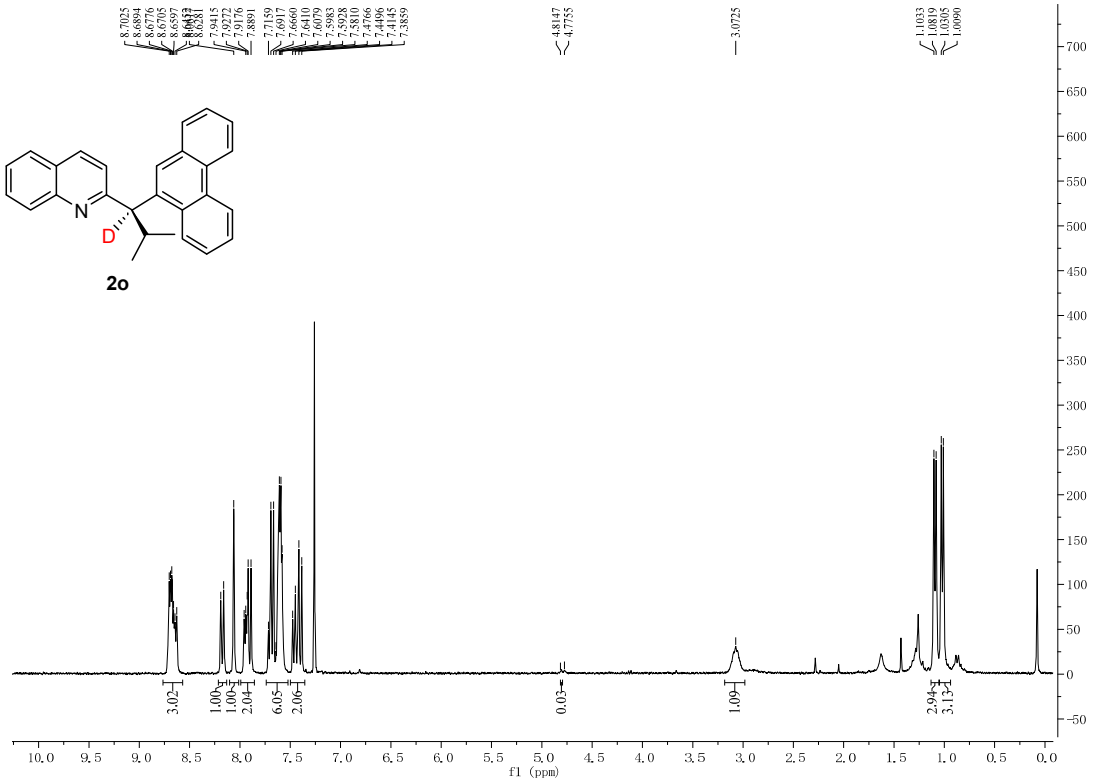

Figure S53. [1]H NMR spectrum for **2o**, related to **Figure 2**.

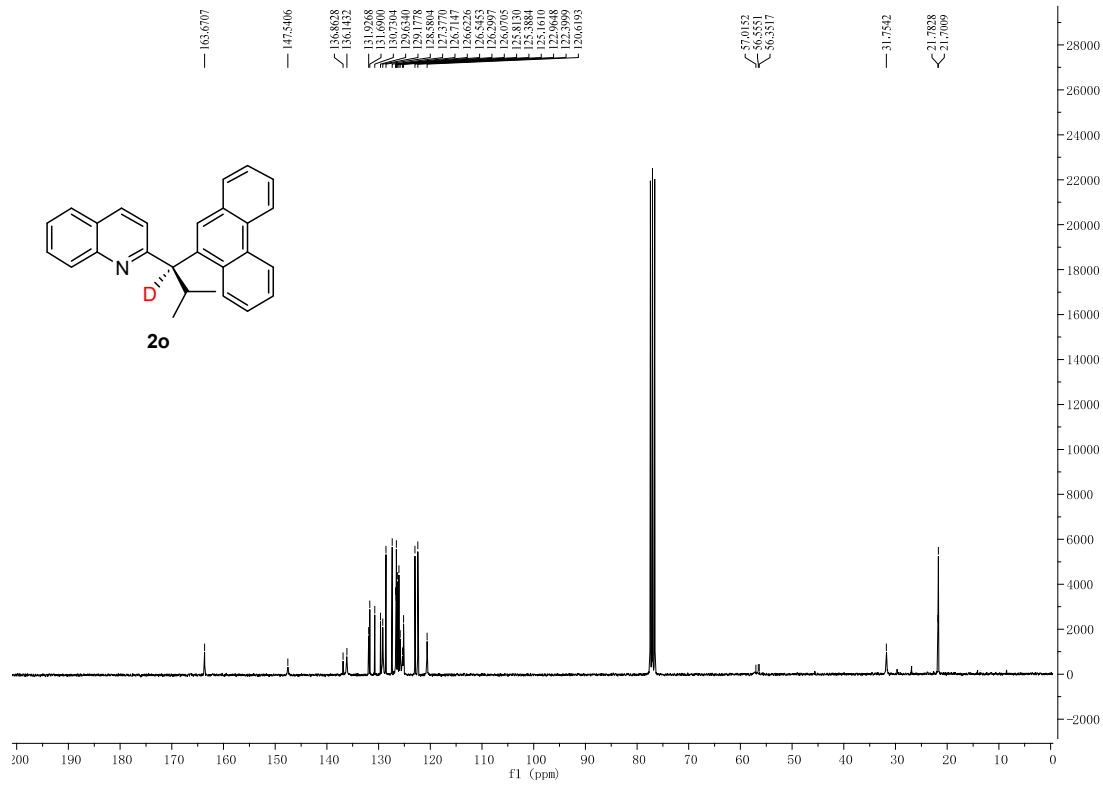

Figure S54. [13]C NMR spectrum for **2o**, related to **Figure 2**.

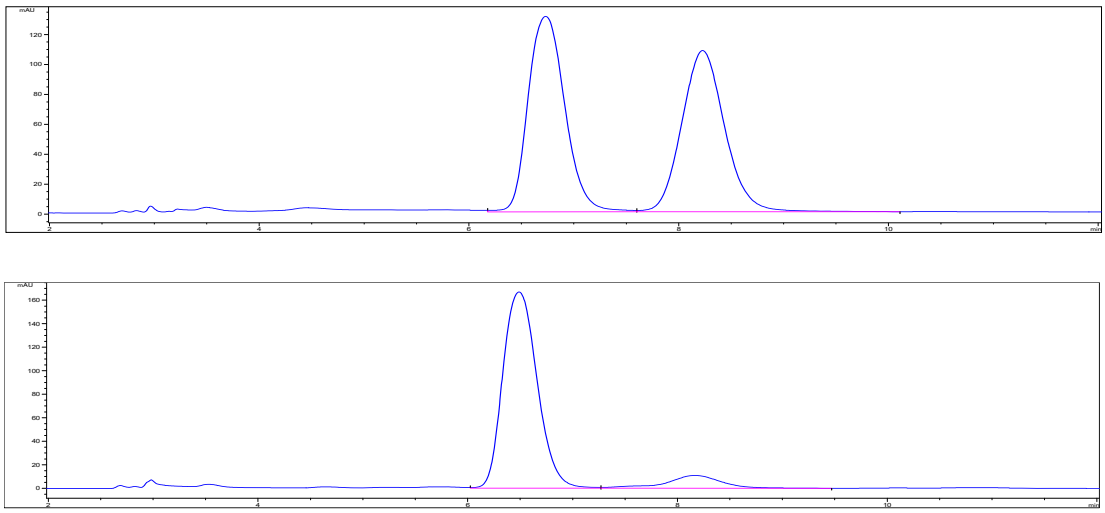

Figure S55. HPLC spectrum for **2o**, related to **Figure 2**.

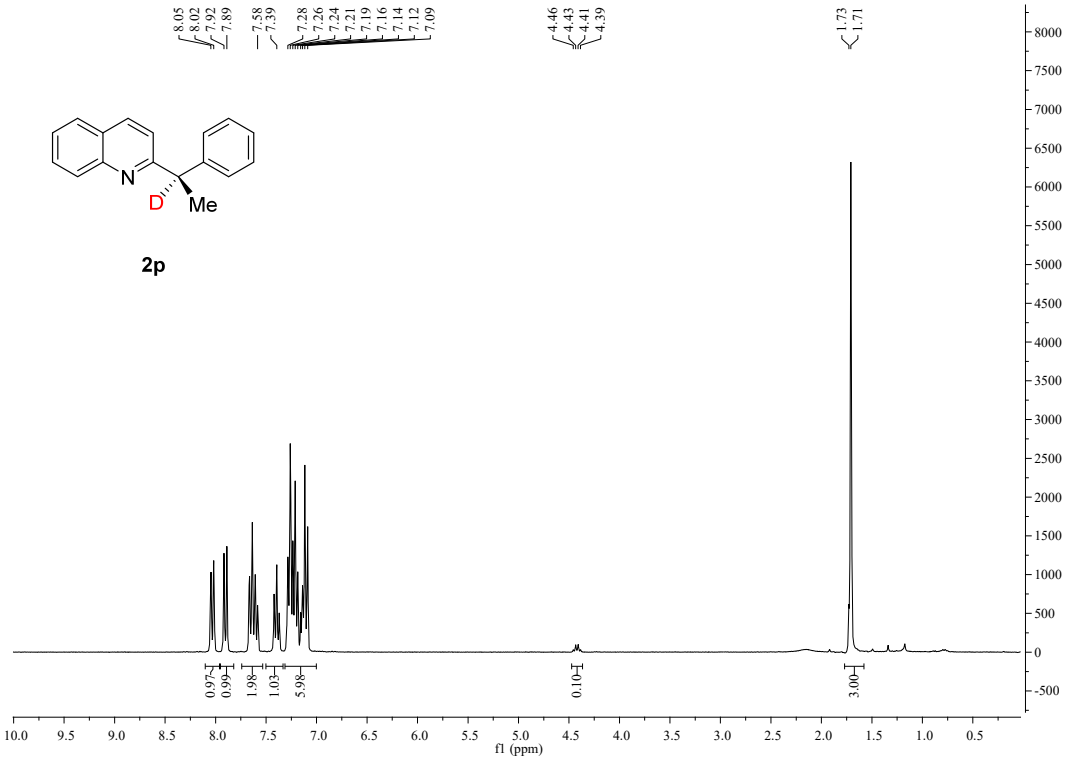

Figure S56. ^{1}H NMR spectrum for **2p**, related to **Figure 2**.

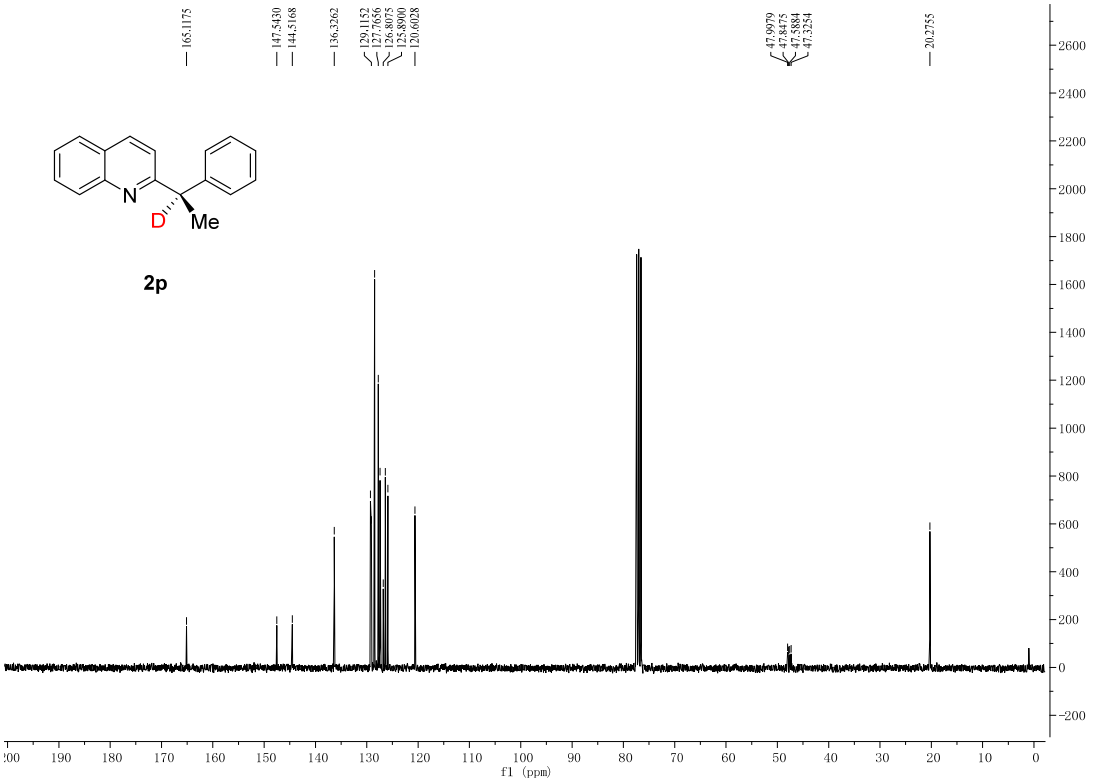

Figure S57. ^{13}C NMR spectrum for **2p**, related to **Figure 2**.

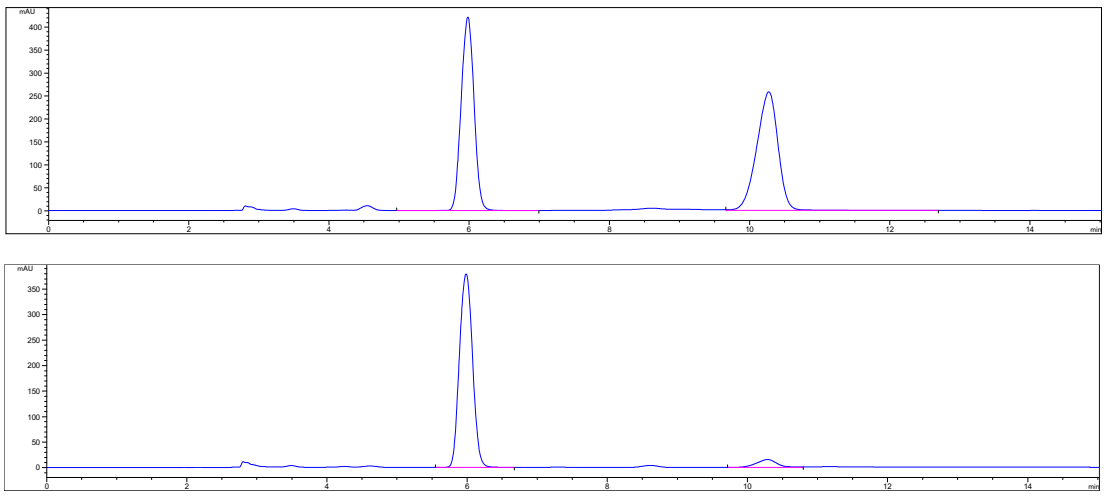

Figure S58. HPLC spectrum for **2p**, related to **Figure 2**.

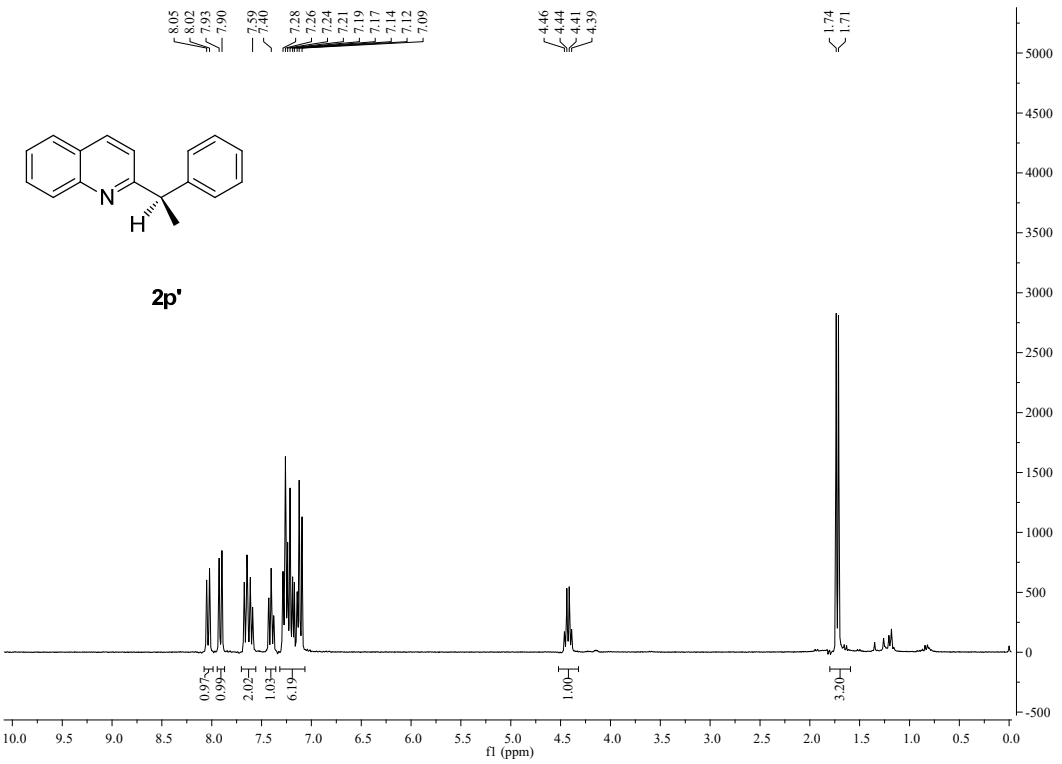

Figure S59. ^{1}H NMR spectrum for **2p'**, related to **Figure 2**.

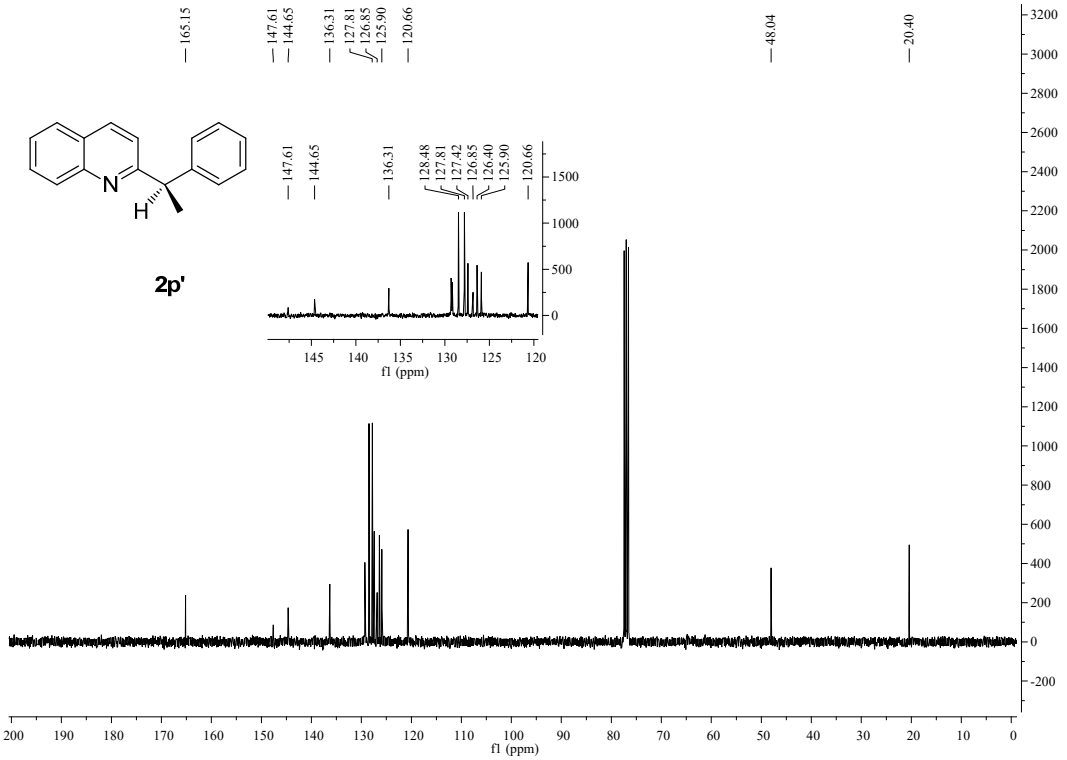

Figure S60. ^{13}C NMR spectrum for **2p'**, related to **Figure 2**.

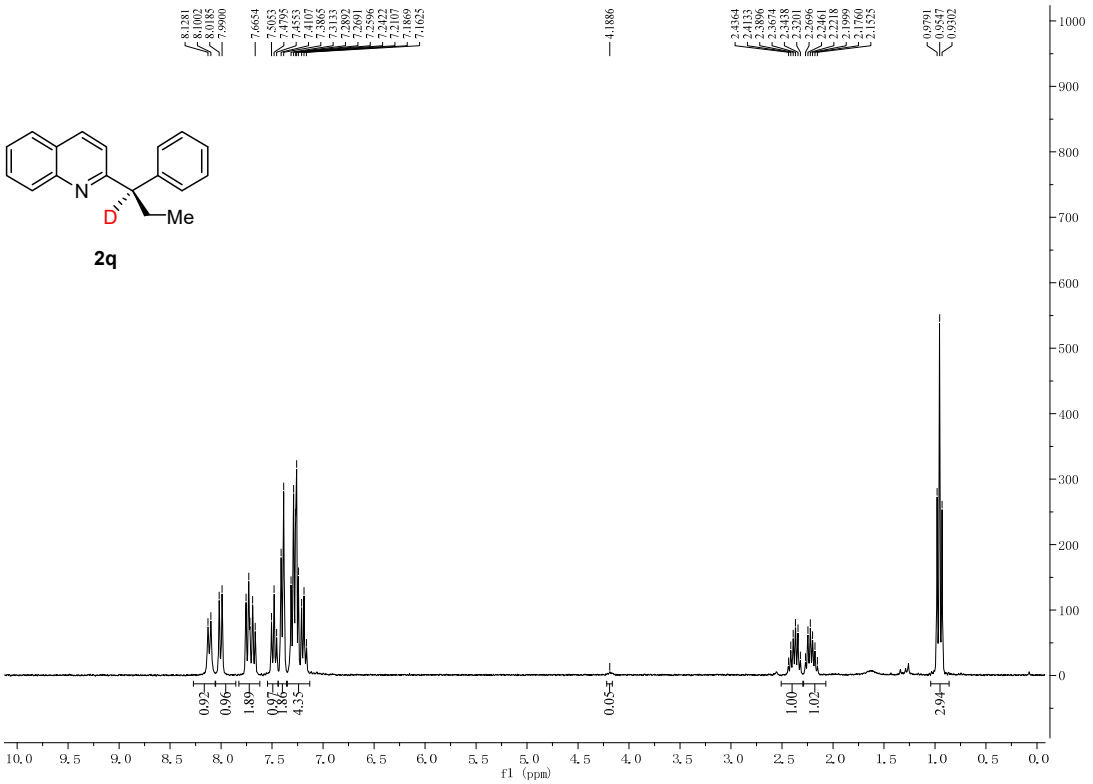

Figure S61. ^{1}H NMR spectrum for **2q**, related to **Figure 2**.

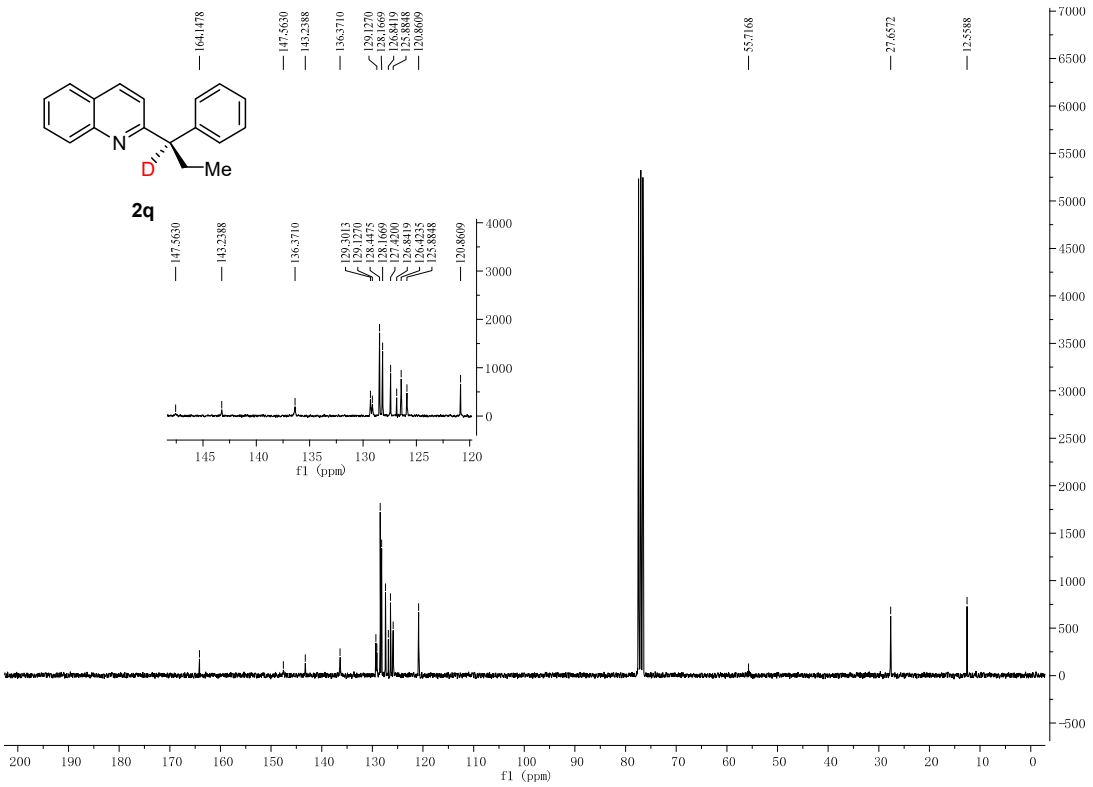

Figure S62. ^{13}C NMR spectrum for **2q**, related to **Figure 2**.

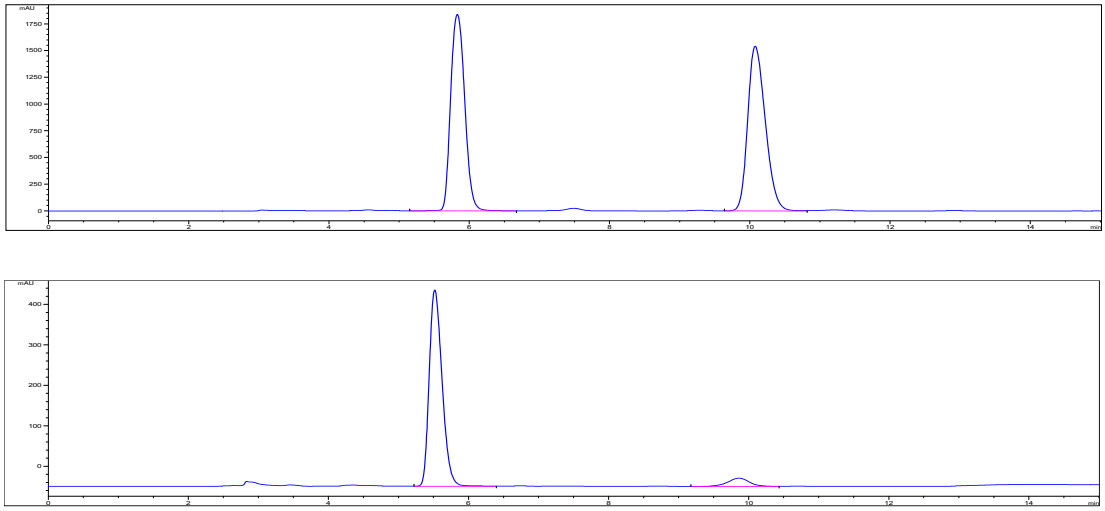

Figure S63. HPLC spectrum for **2q**, related to **Figure 2**.

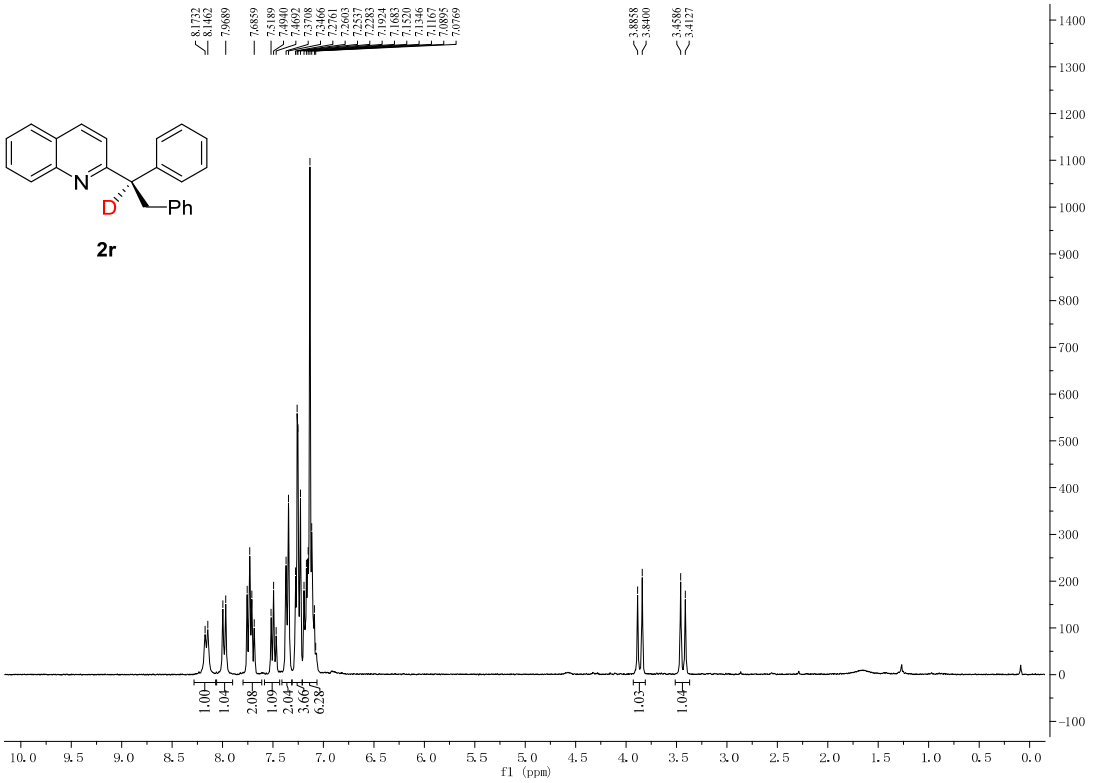

Figure S64. ^{1}H NMR spectrum for **2r**, related to **Figure 2**.

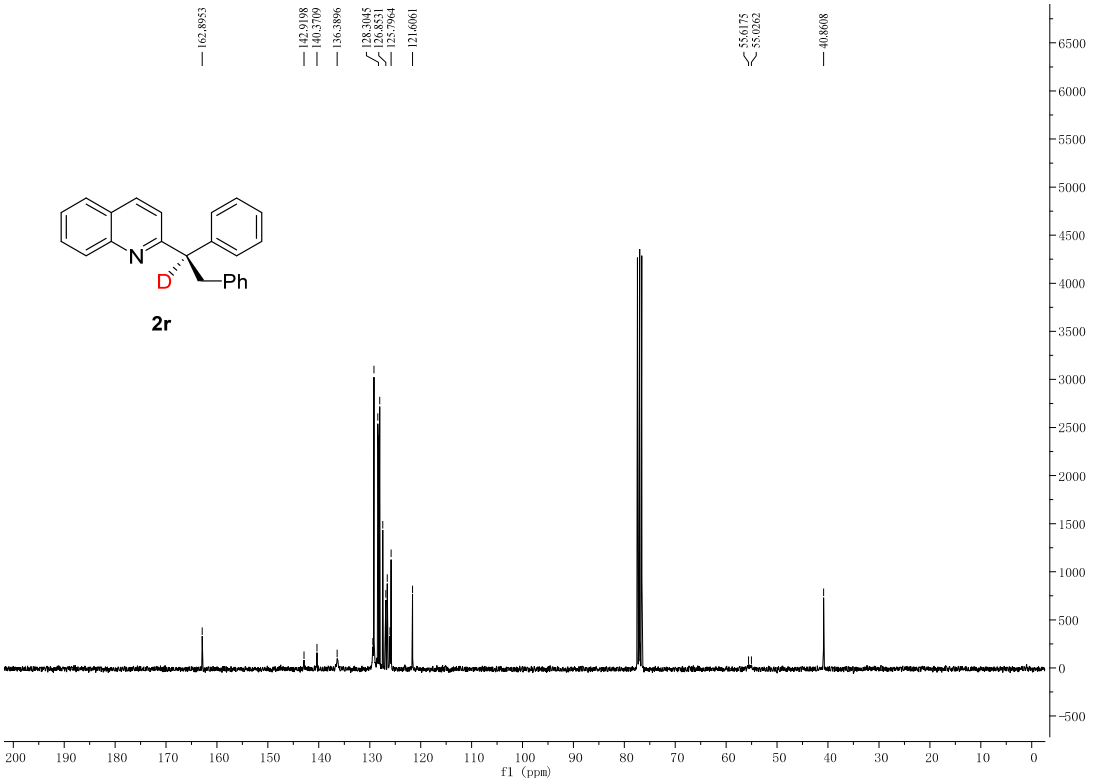

Figure S65. ^{13}C NMR spectrum for **2r**, related to **Figure 2**.

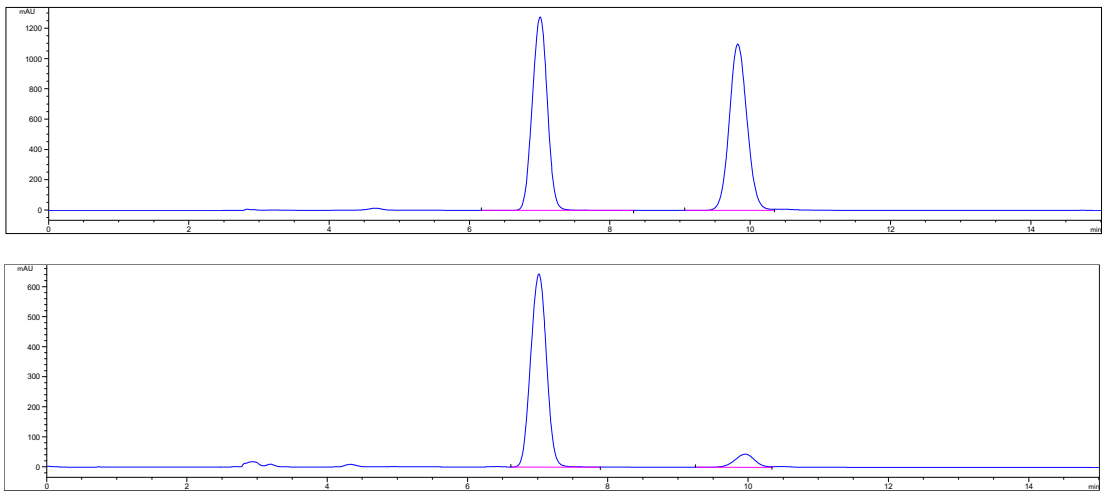

Figure S66. HPLC spectrum for **2r**, related to **Figure 2**.

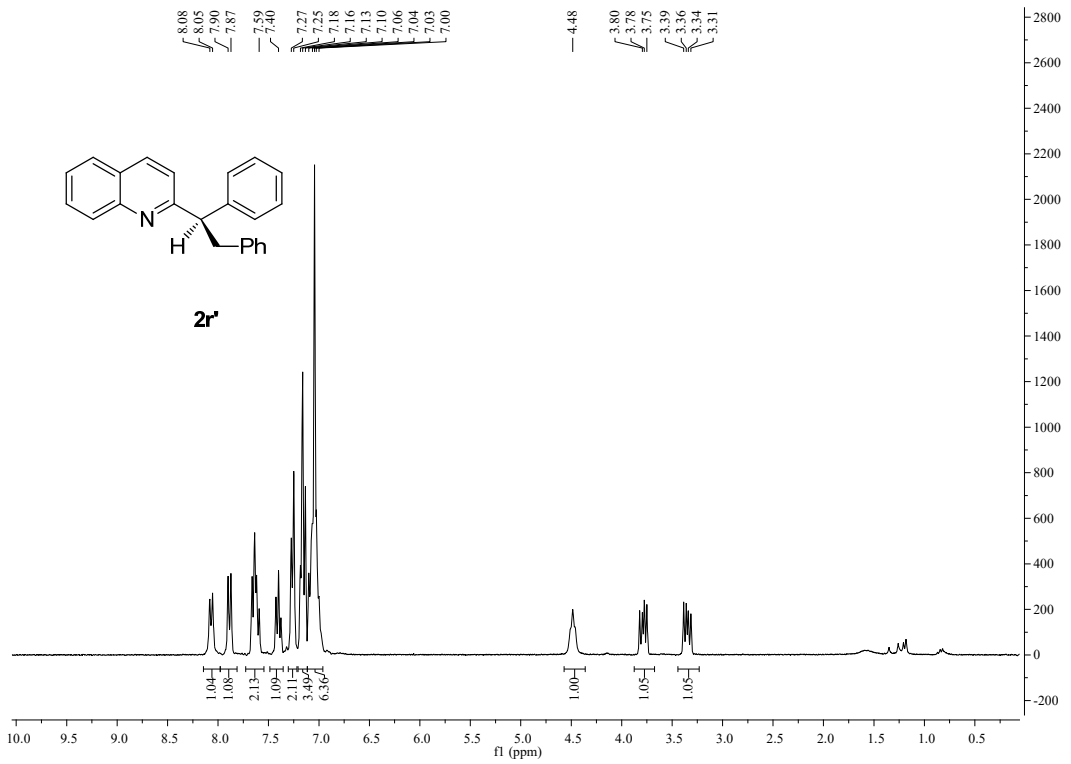

Figure S67. ^{1}H NMR spectrum for **2r'**, related to **Figure 2**.

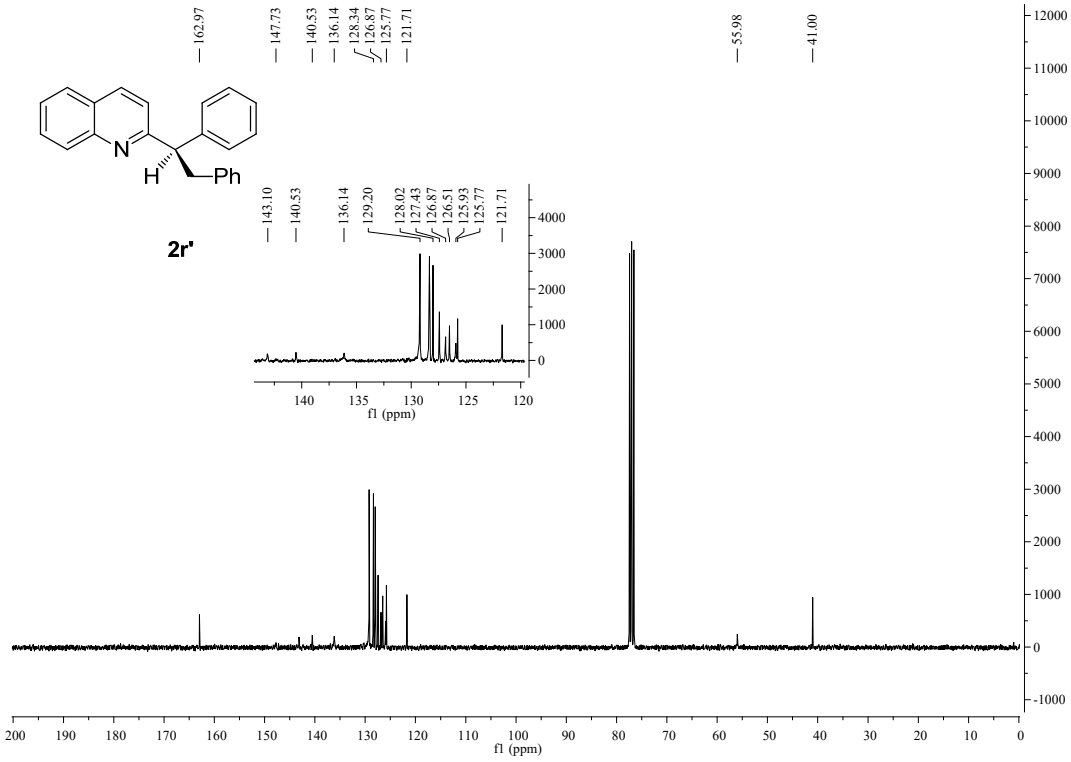

Figure S68. ^{13}C NMR spectrum for **2r'**, related to **Figure 2**.

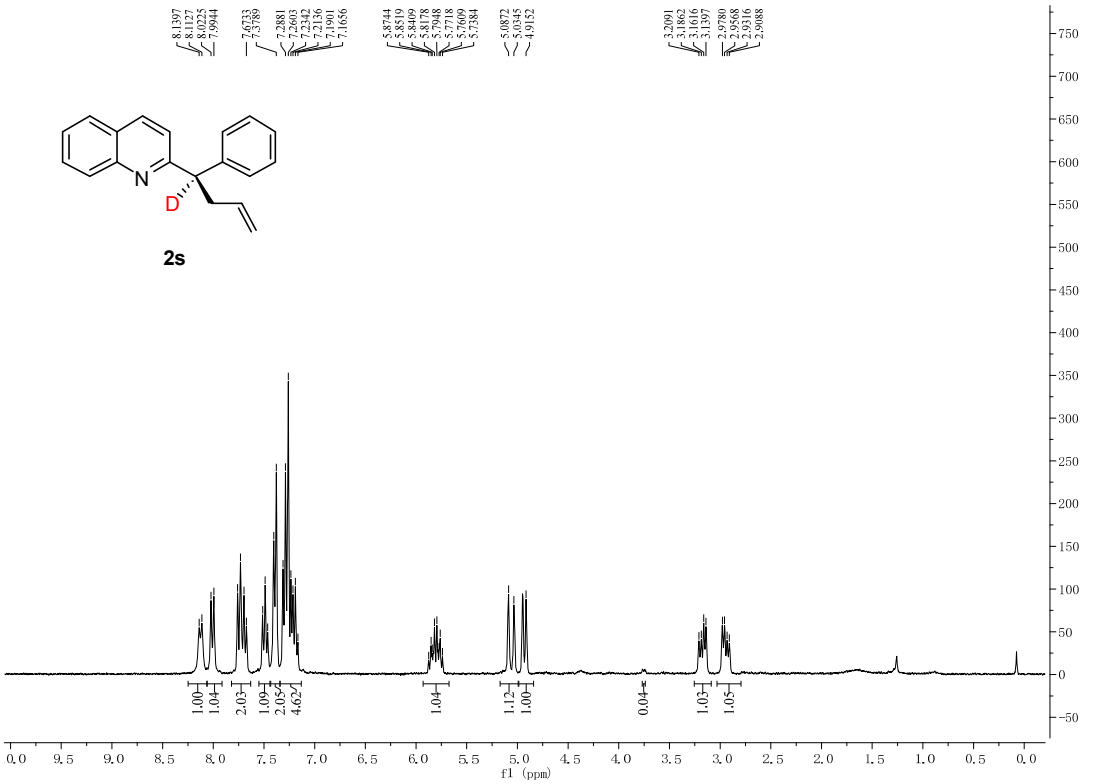

Figure S69. ^{1}H NMR spectrum for **2s**, related to **Figure 2**.

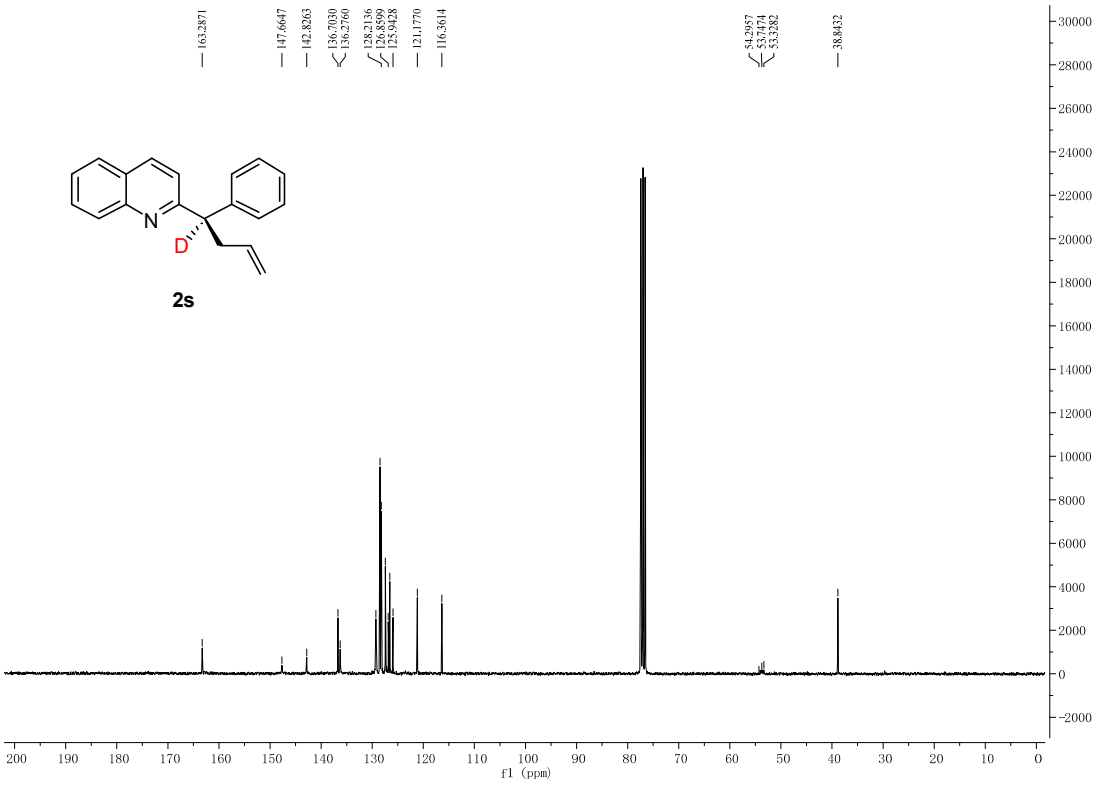

Figure S70. ^{13}C NMR spectrum for **2s**, related to **Figure 2**.

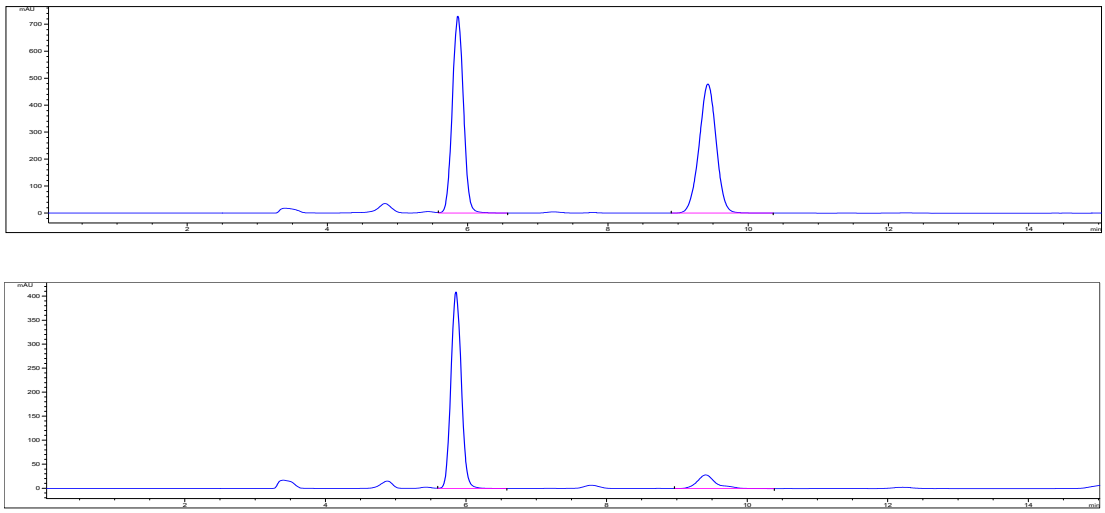

Figure S71. HPLC spectrum for **2s**, related to **Figure 2**.

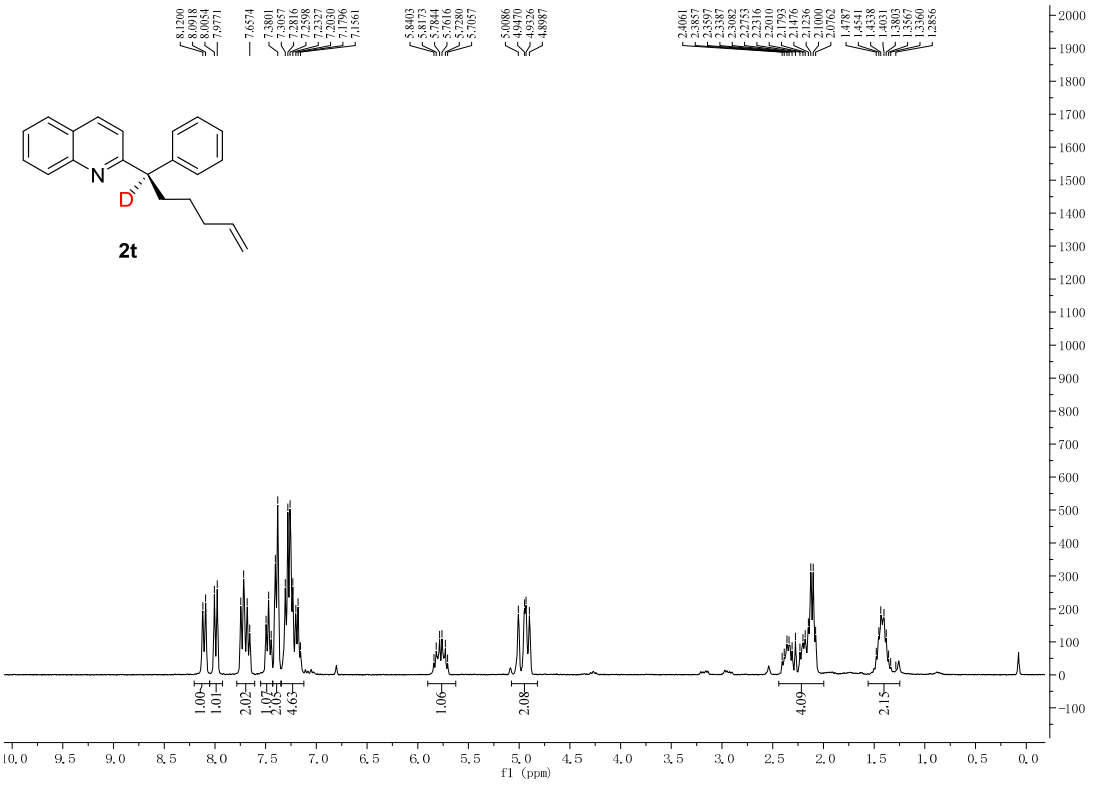

Figure S72. ^{1}H NMR spectrum for **2t**, related to **Figure 2**.

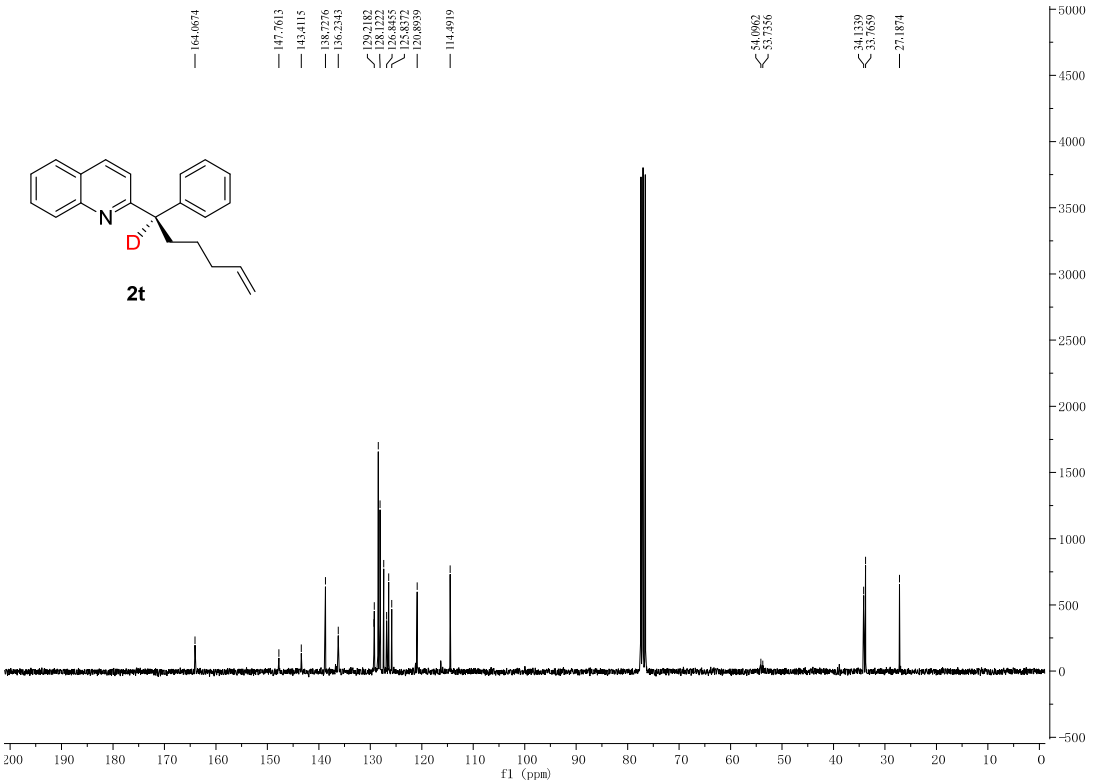

Figure S73. ^{13}C NMR spectrum for **2t**, related to **Figure 2**.

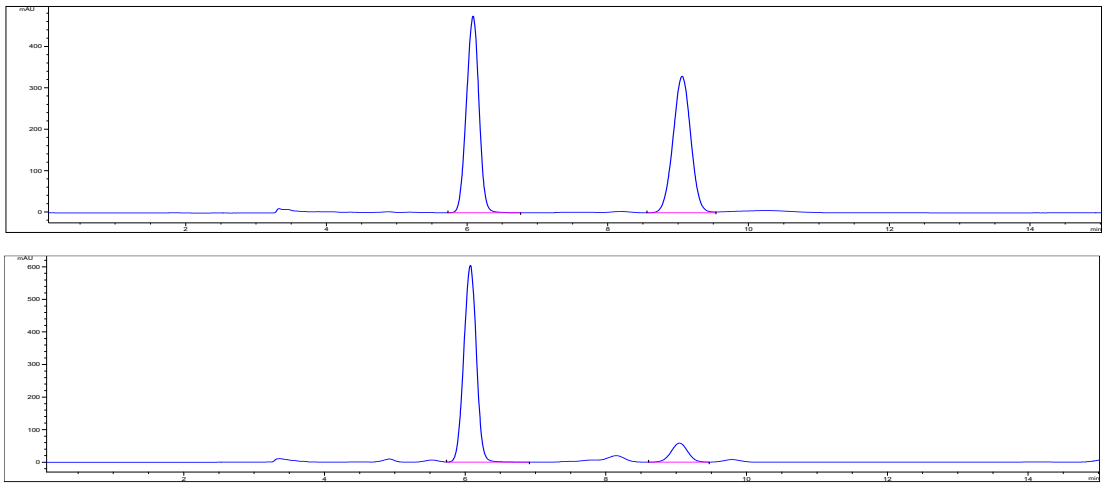

Figure S74. HPLC spectrum for **2t**, related to **Figure 2**.

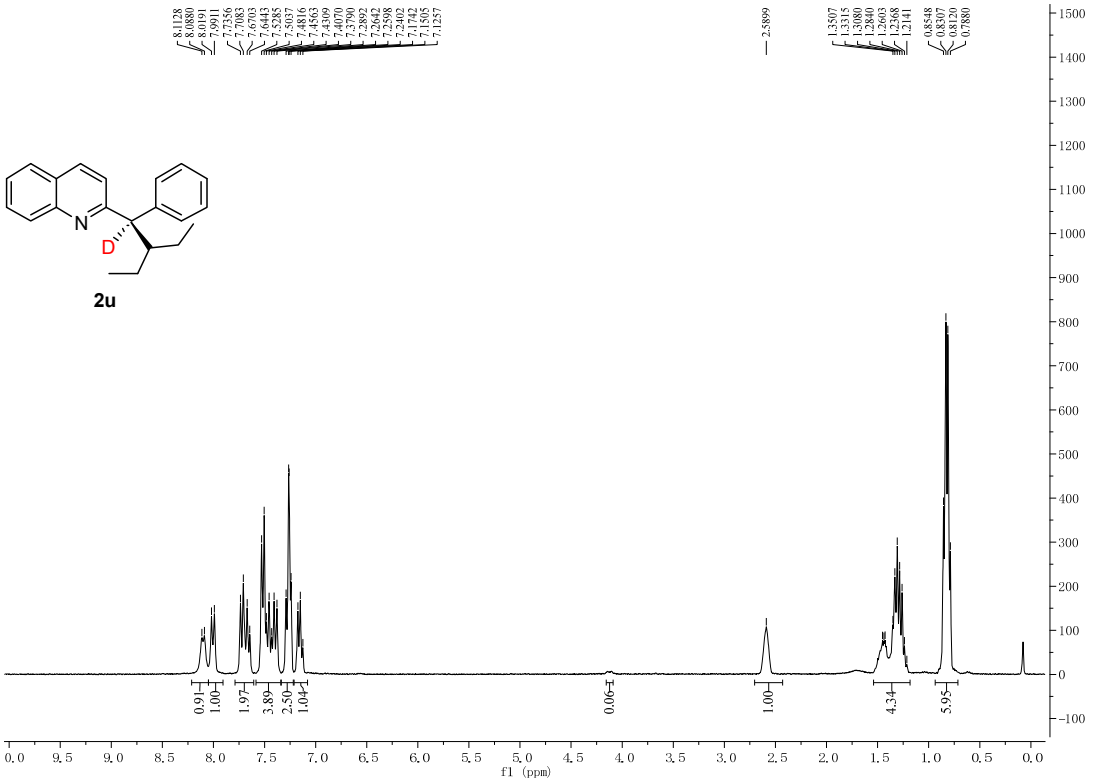

Figure S75. ^{1}H NMR spectrum for **2u**, related to **Figure 2**.

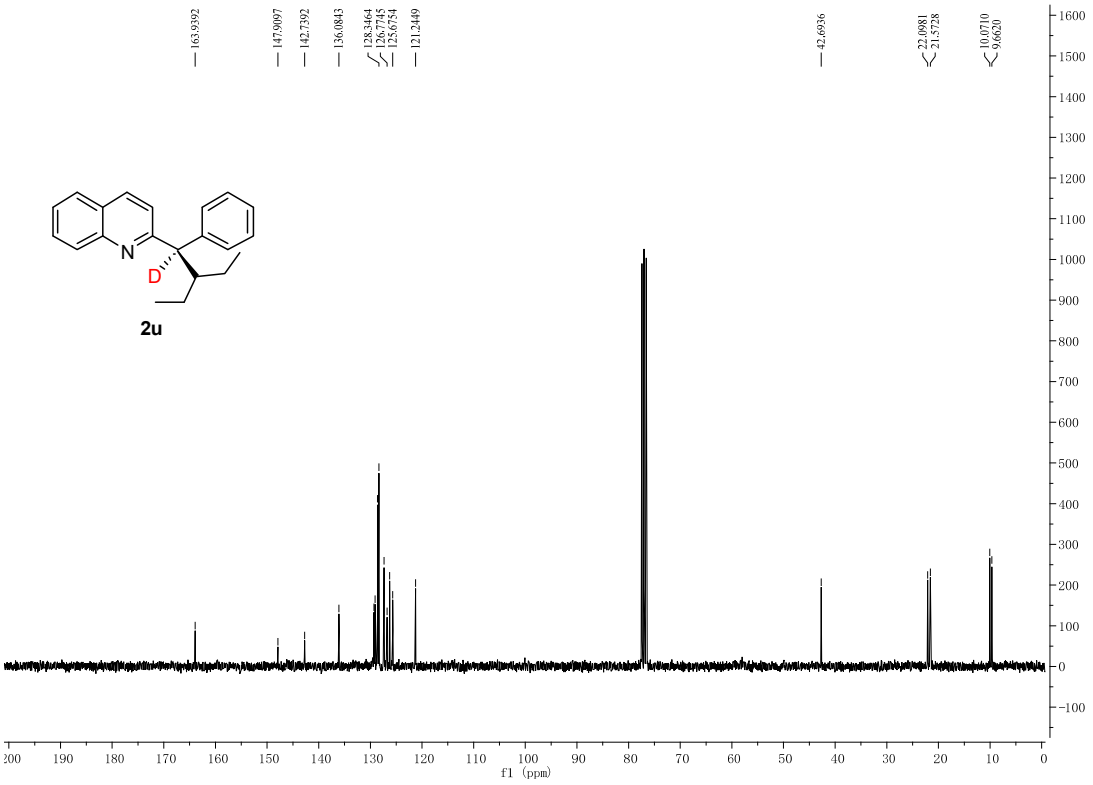

Figure S76. ^{13}C NMR spectrum for **2u**, related to **Figure 2**.

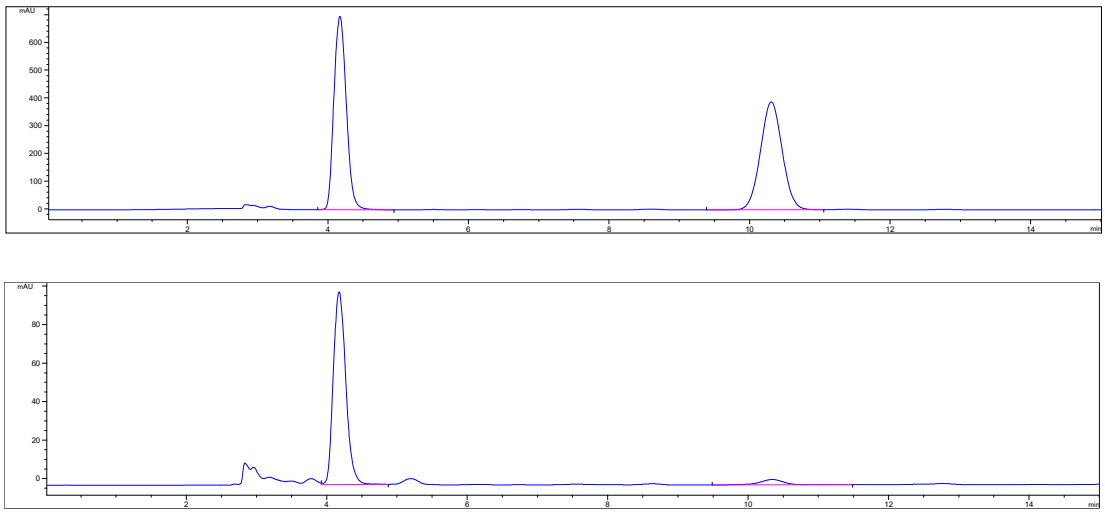

Figure S77. HPLC spectrum for **2u**, related to **Figure 2**.

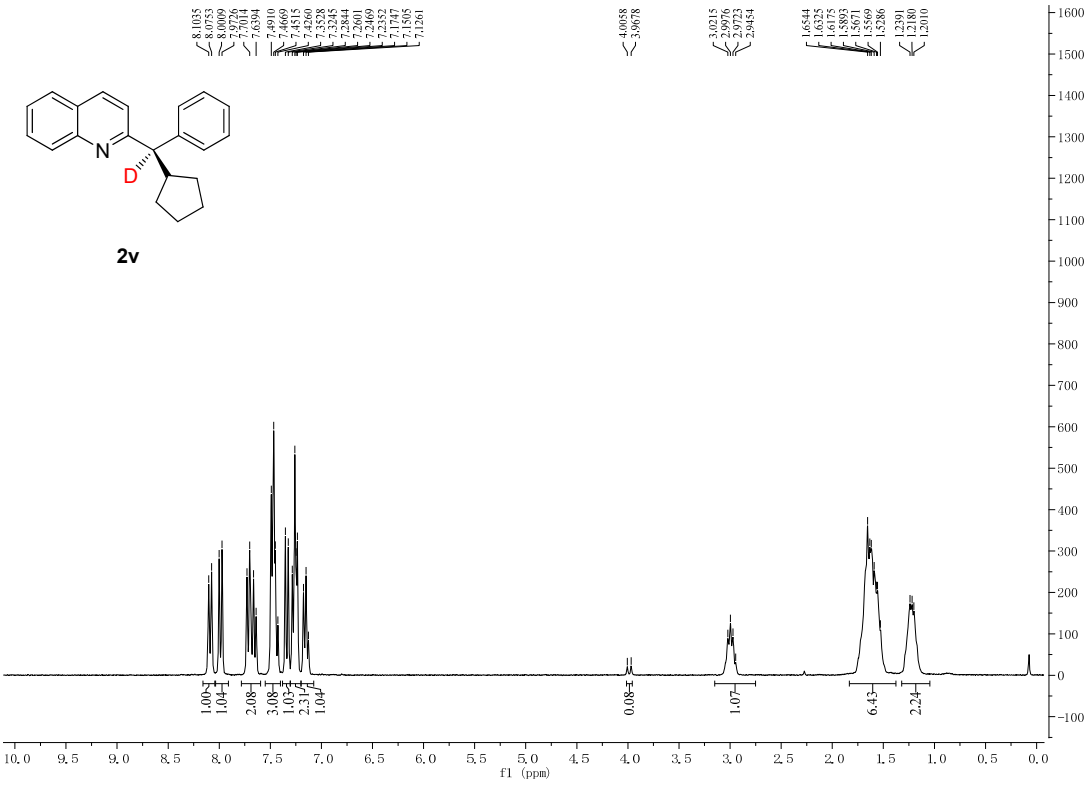

Figure S78. ^{1}H NMR spectrum for **2v**, related to **Figure 2**.

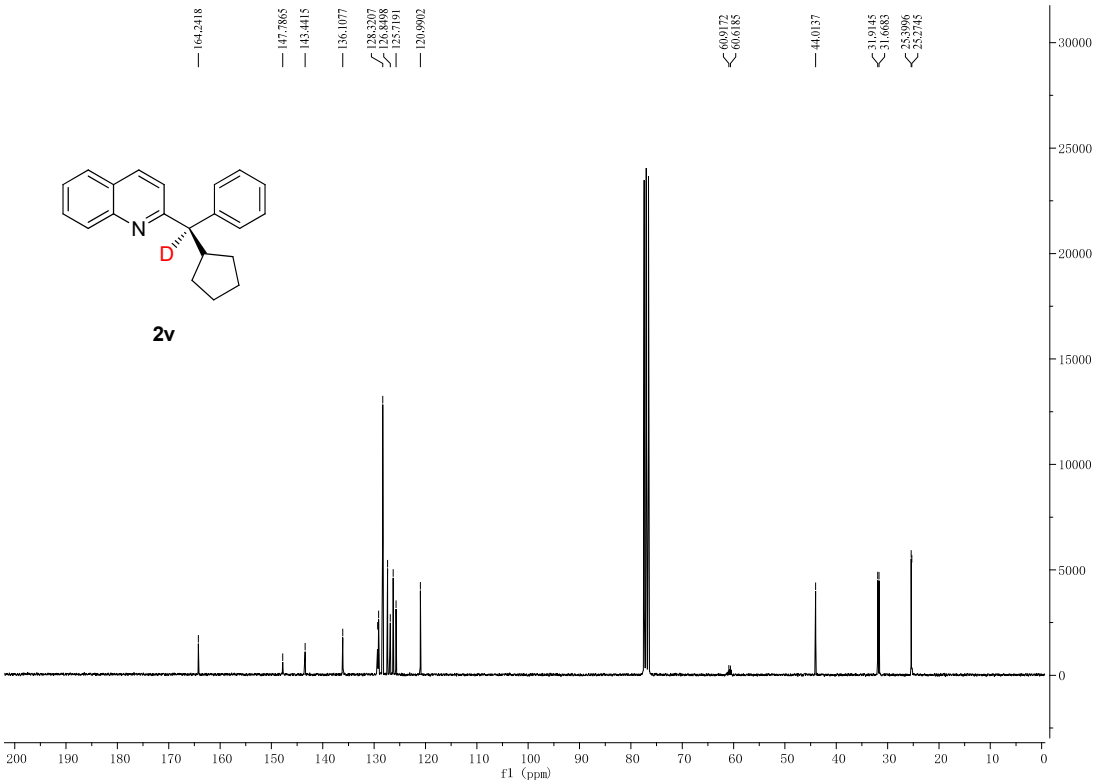

Figure S79. ^{13}C NMR spectrum for **2v**, related to **Figure 2**.

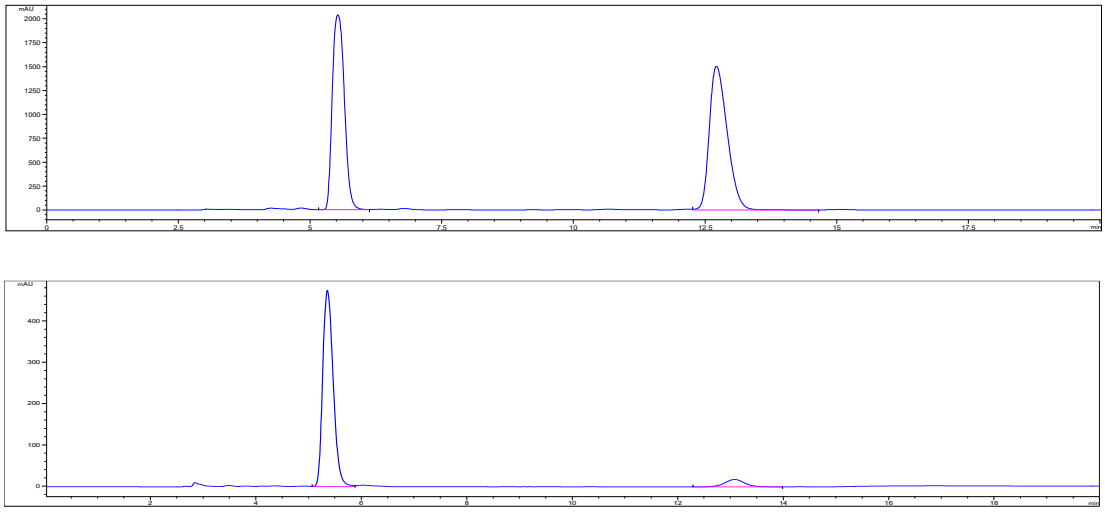

Figure S80. HPLC spectrum for **2v**, related to **Figure 2**.

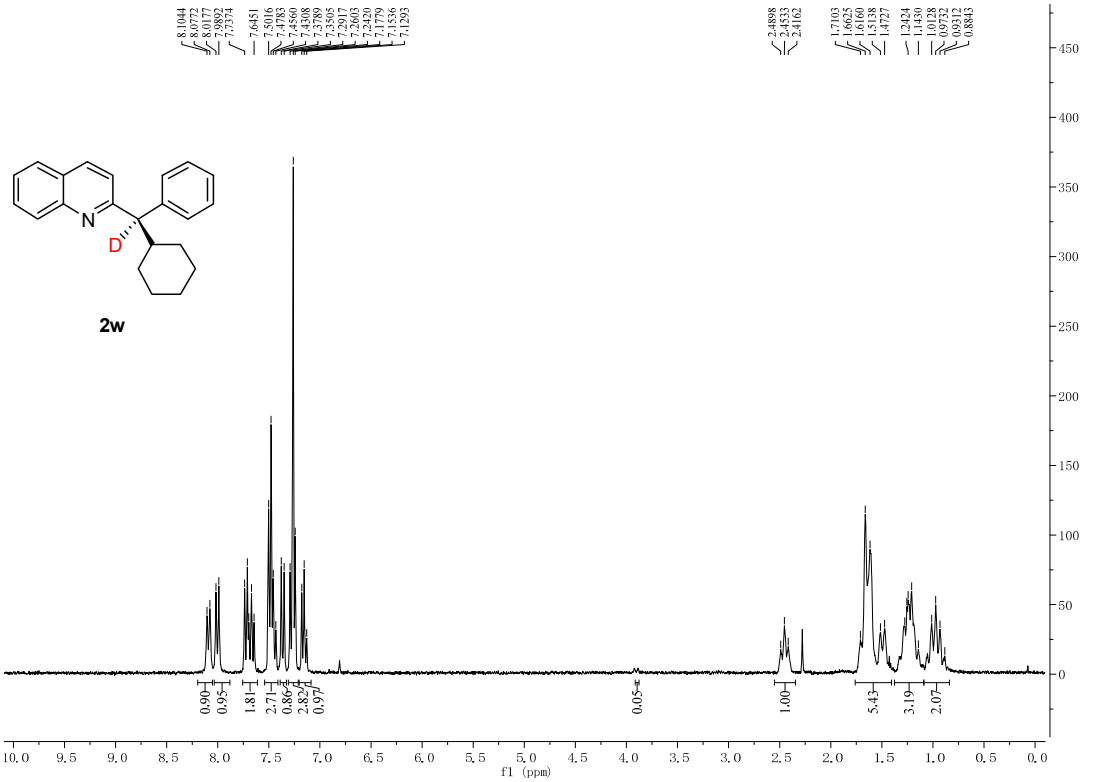

Figure S81. ^{1}H NMR spectrum for **2w**, related to **Figure 2**.

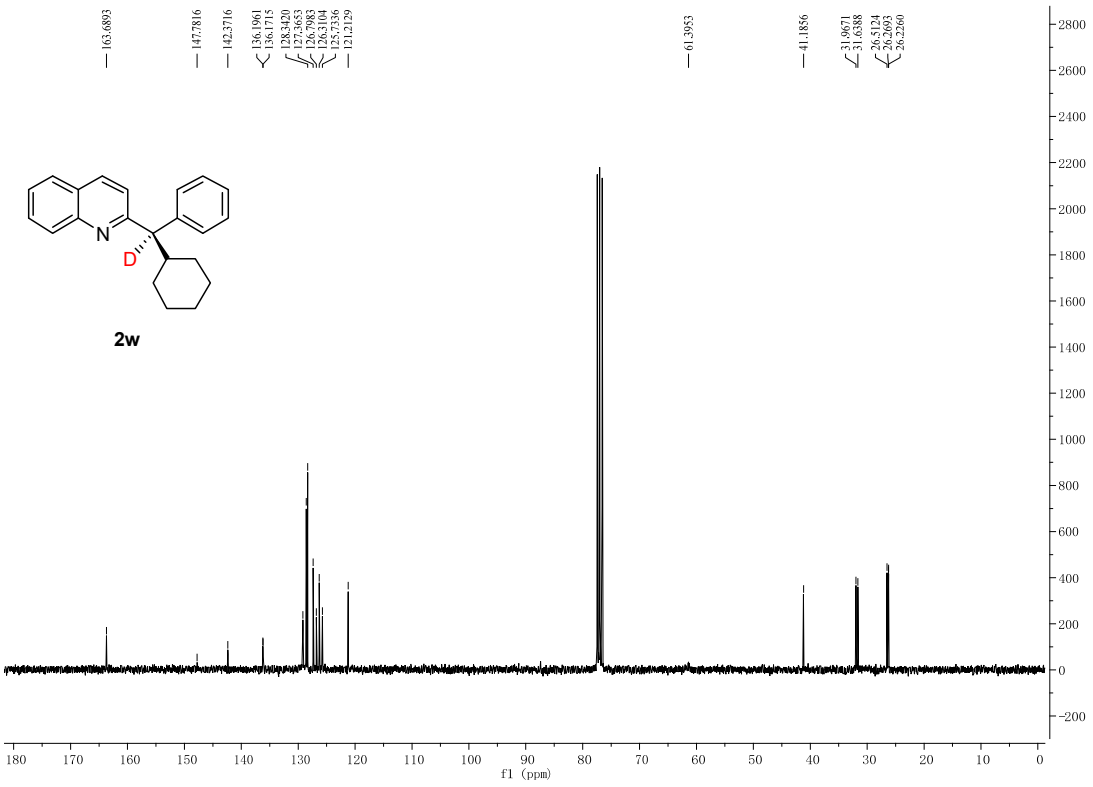

Figure S82. ^{13}C NMR spectrum for **2w**, related to **Figure 2**.

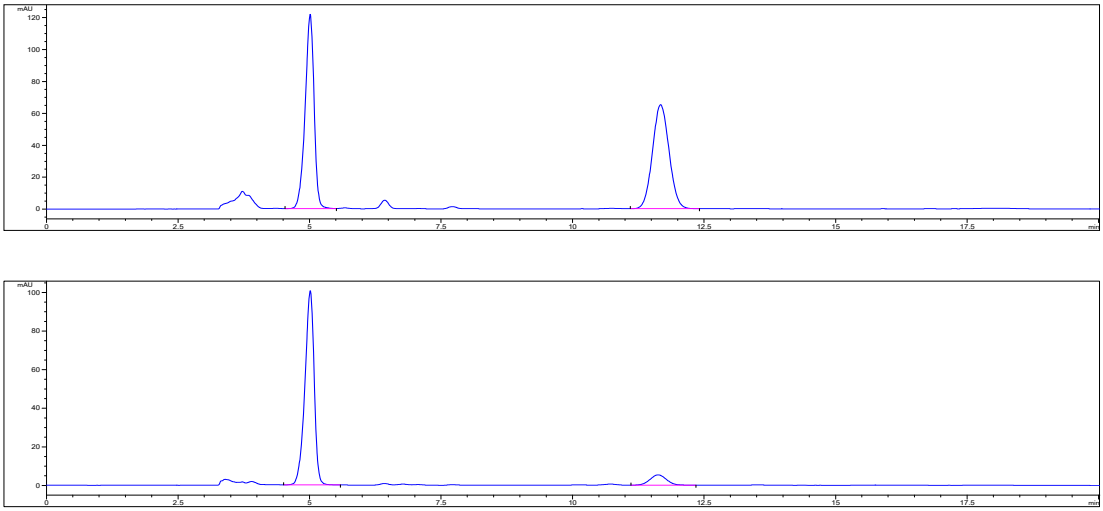

Figure S83. HPLC spectrum for **2w**, related to **Figure 2**.

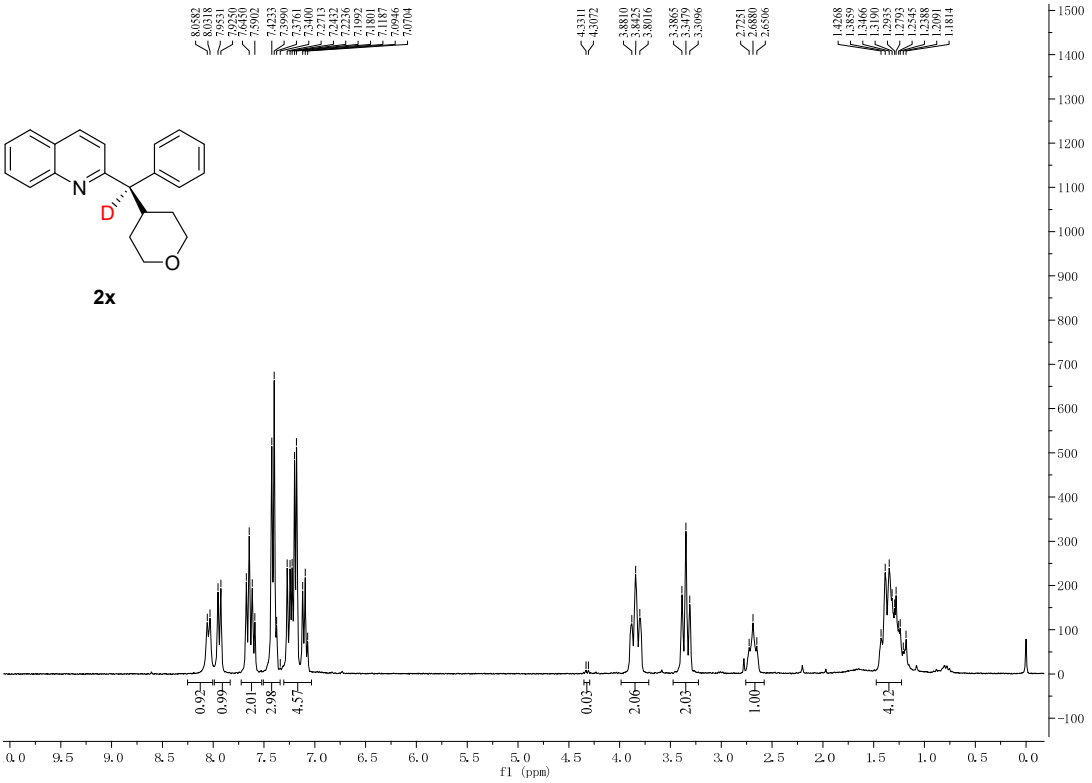

Figure S84. ^{1}H NMR spectrum for **2x**, related to **Figure 2**.

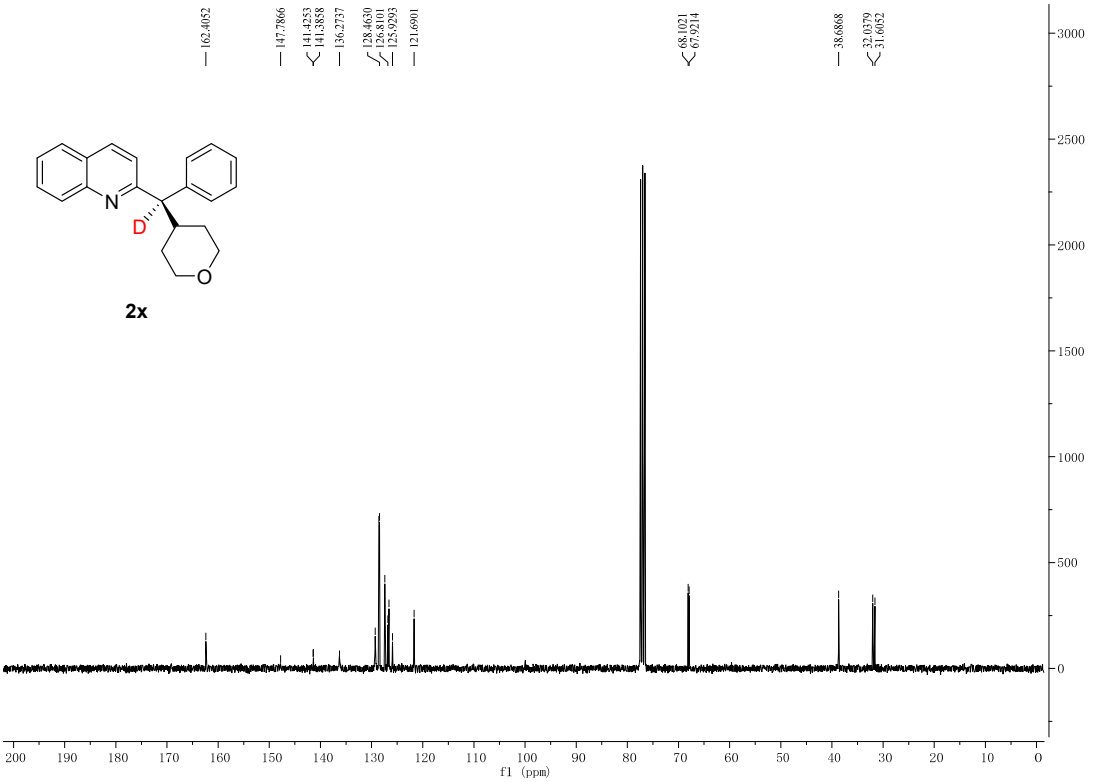

Figure S85. ^{13}C NMR spectrum for **2x**, related to **Figure 2**.

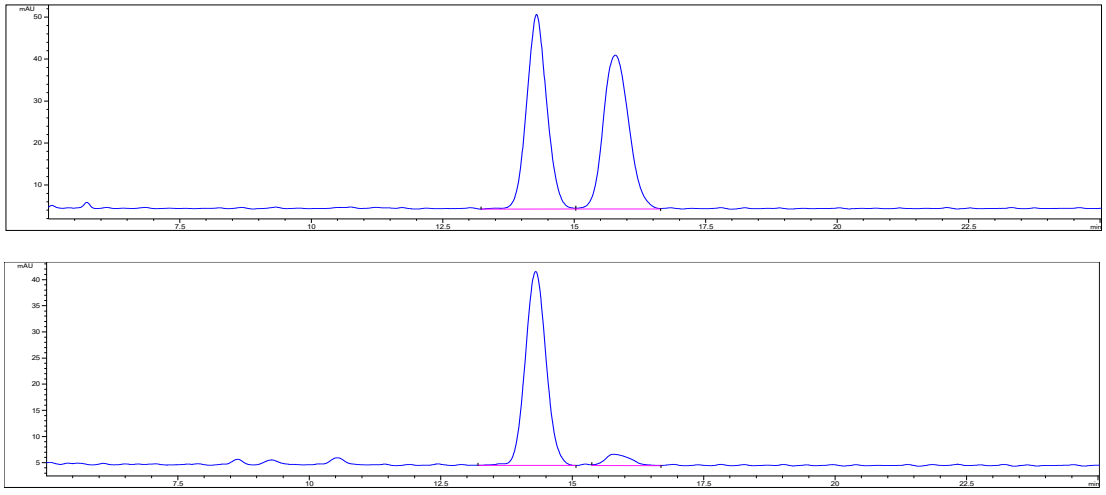

Figure S86. HPLC spectrum for **2x**, related to **Figure 2**.

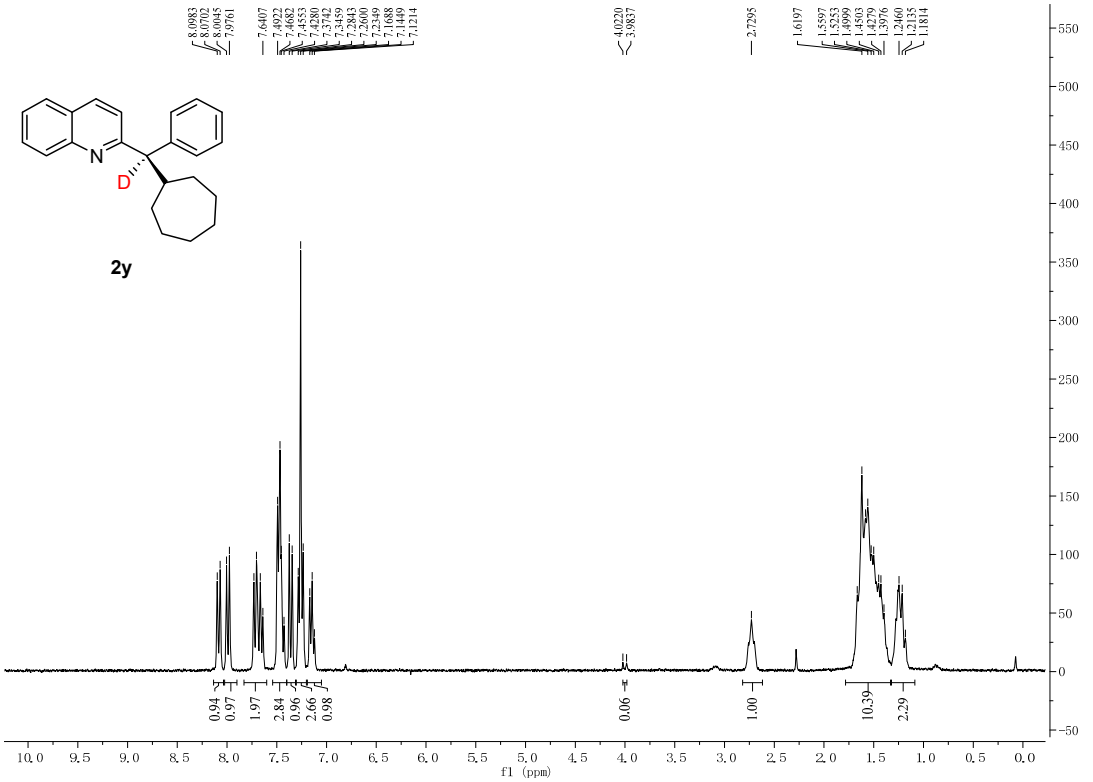

Figure S87. ^{1}H NMR spectrum for **2y**, related to **Figure 2**.

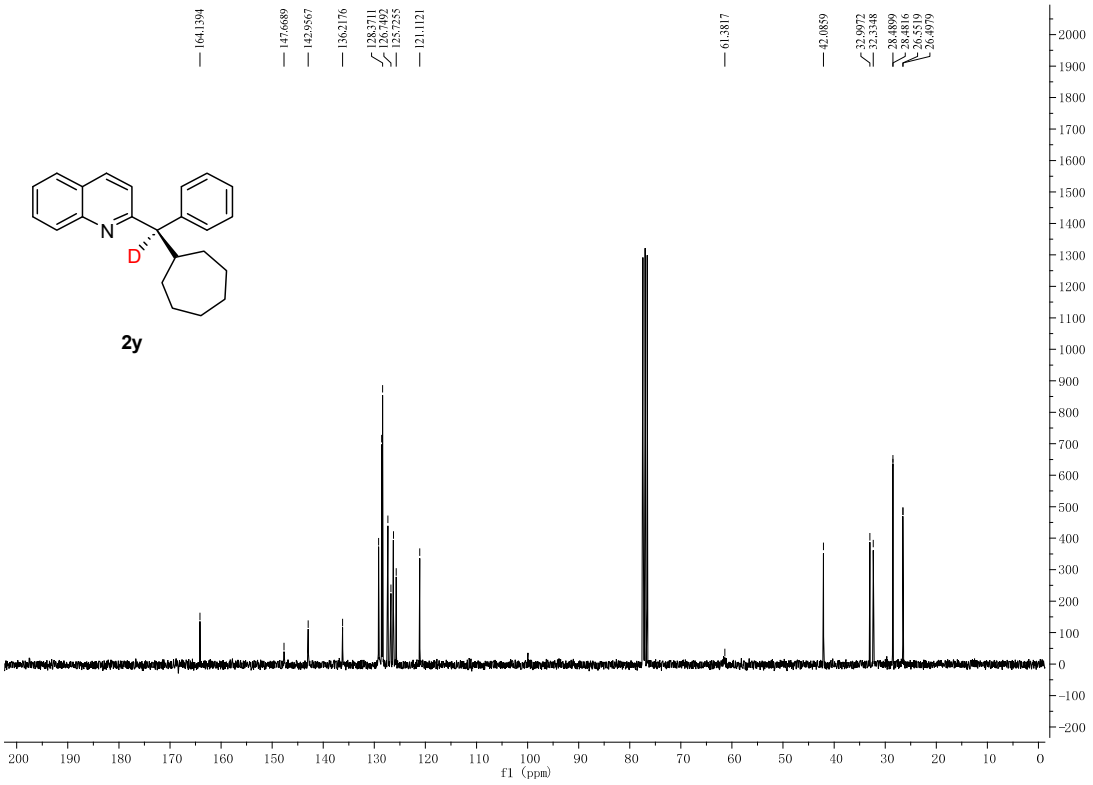

Figure S88. ^{13}C NMR spectrum for **2y**, related to **Figure 2**.

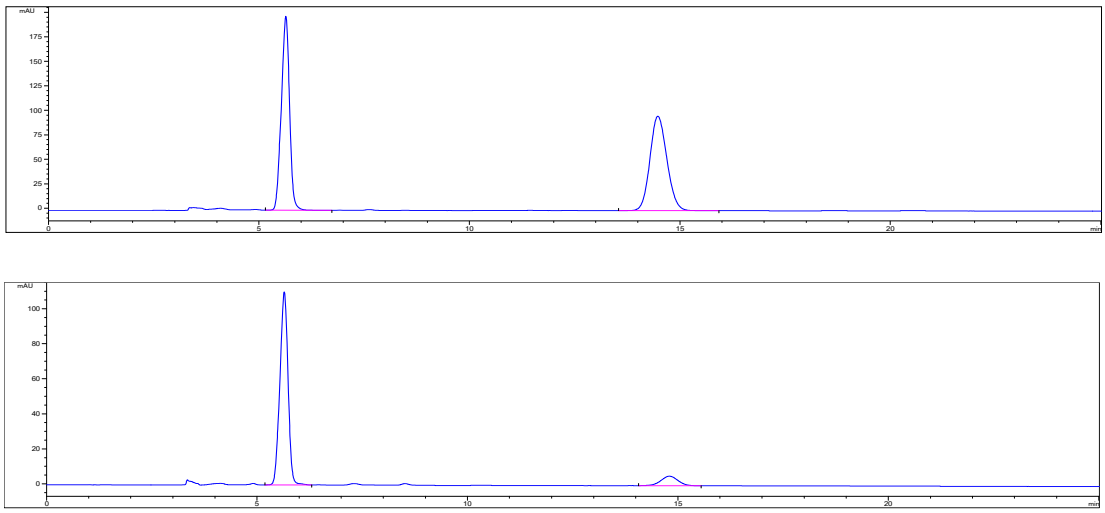

Figure S89. HPLC spectrum for **2y**, related to **Figure 2**.

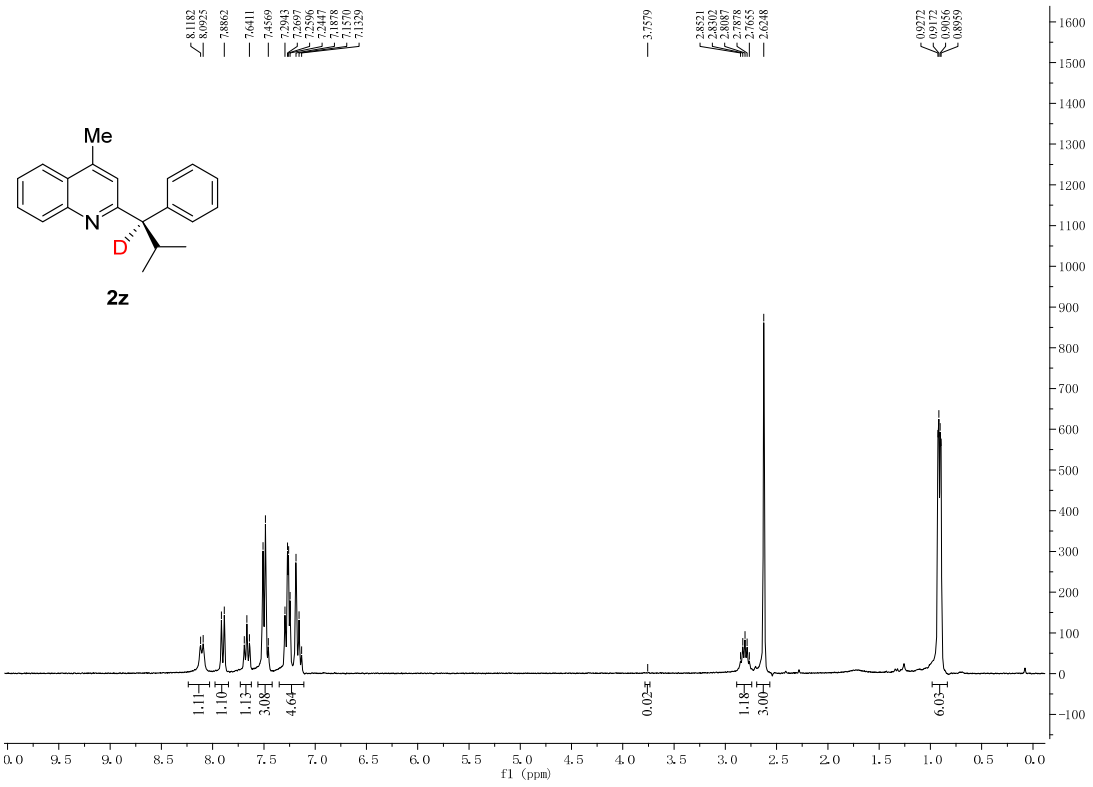

Figure S90. ^{1}H NMR spectrum for **2z**, related to **Figure 2**.

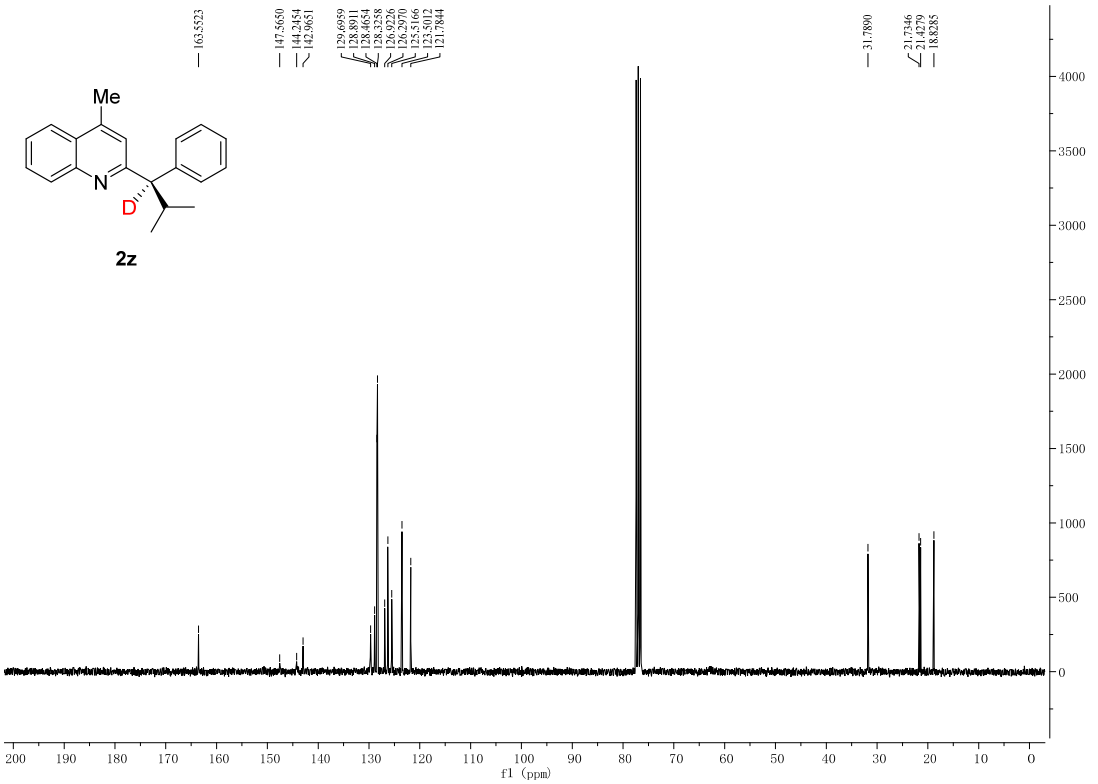

Figure S91. ^{13}C NMR spectrum for **2z**, related to **Figure 2**.

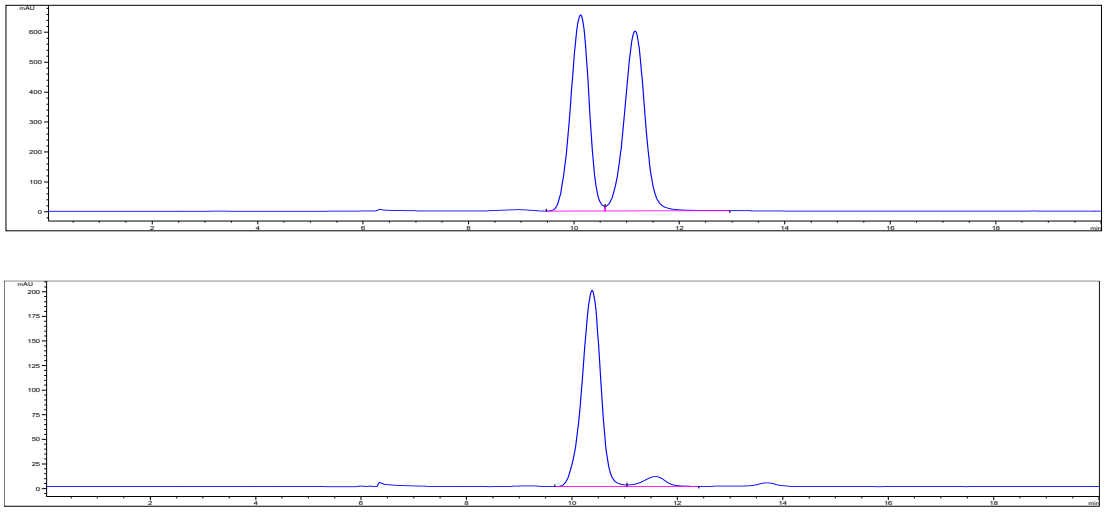

Figure S92. HPLC spectrum for **2z**, related to **Figure 2**.

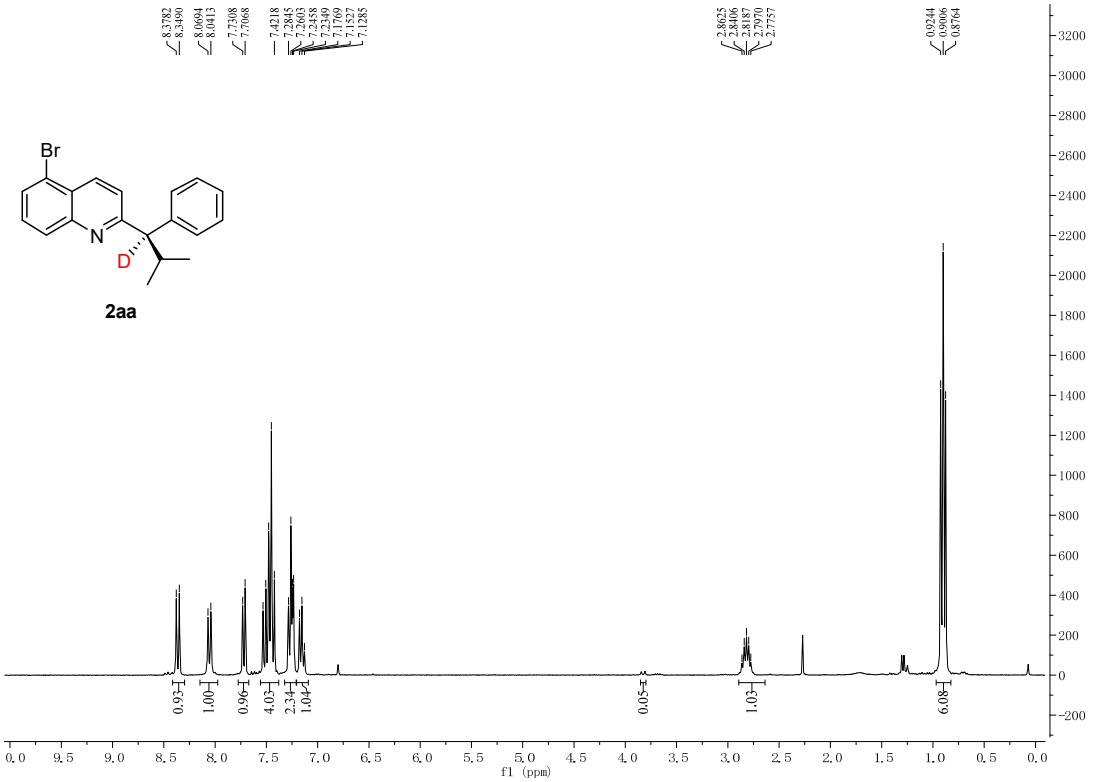

Figure S93. ^{1}H NMR spectrum for **2aa**, related to **Figure 2**.

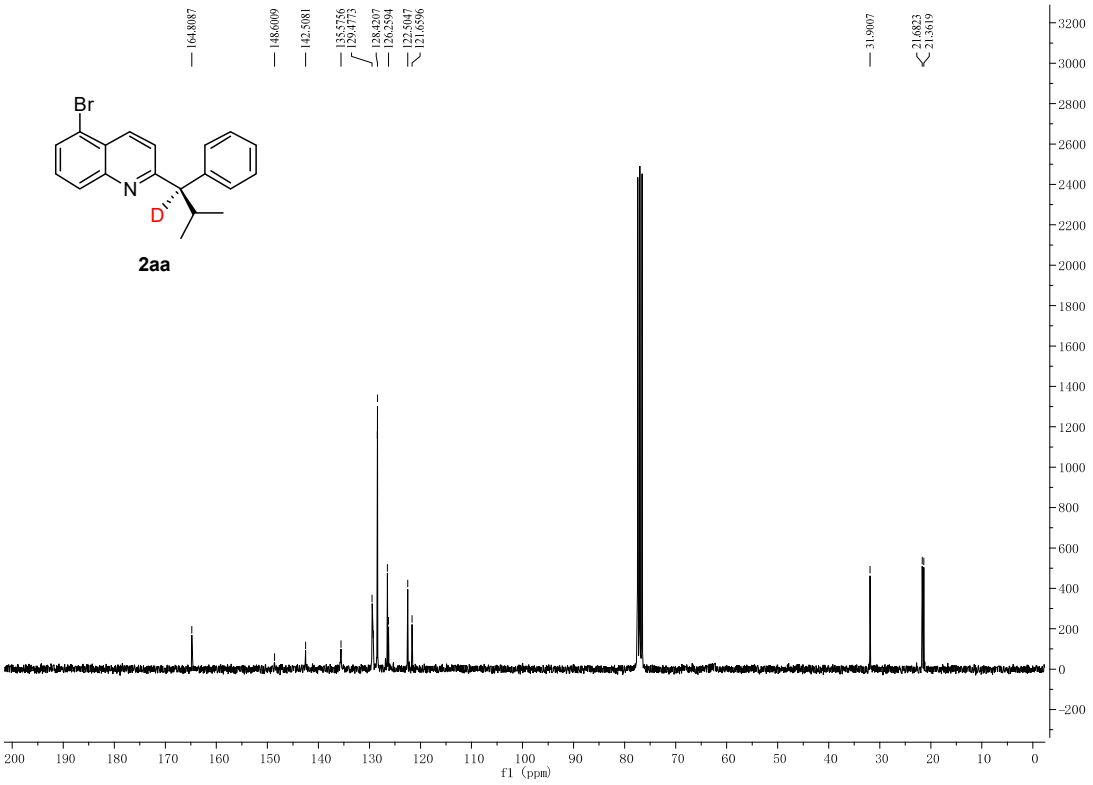

Figure S94. ^{13}C NMR spectrum for **2aa**, related to **Figure 2**.

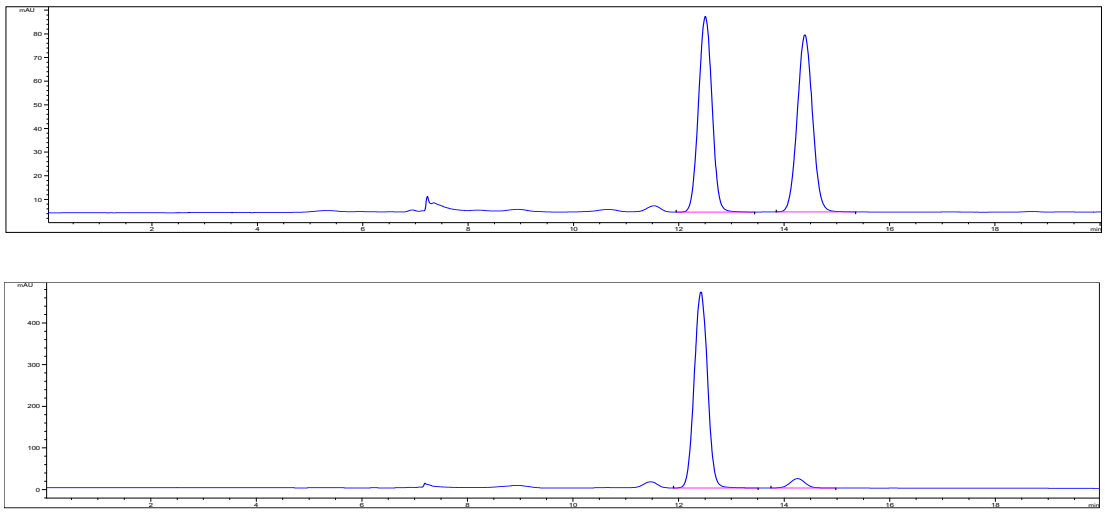

Figure S95. HPLC spectrum for **2aa**, related to **Figure 2**.

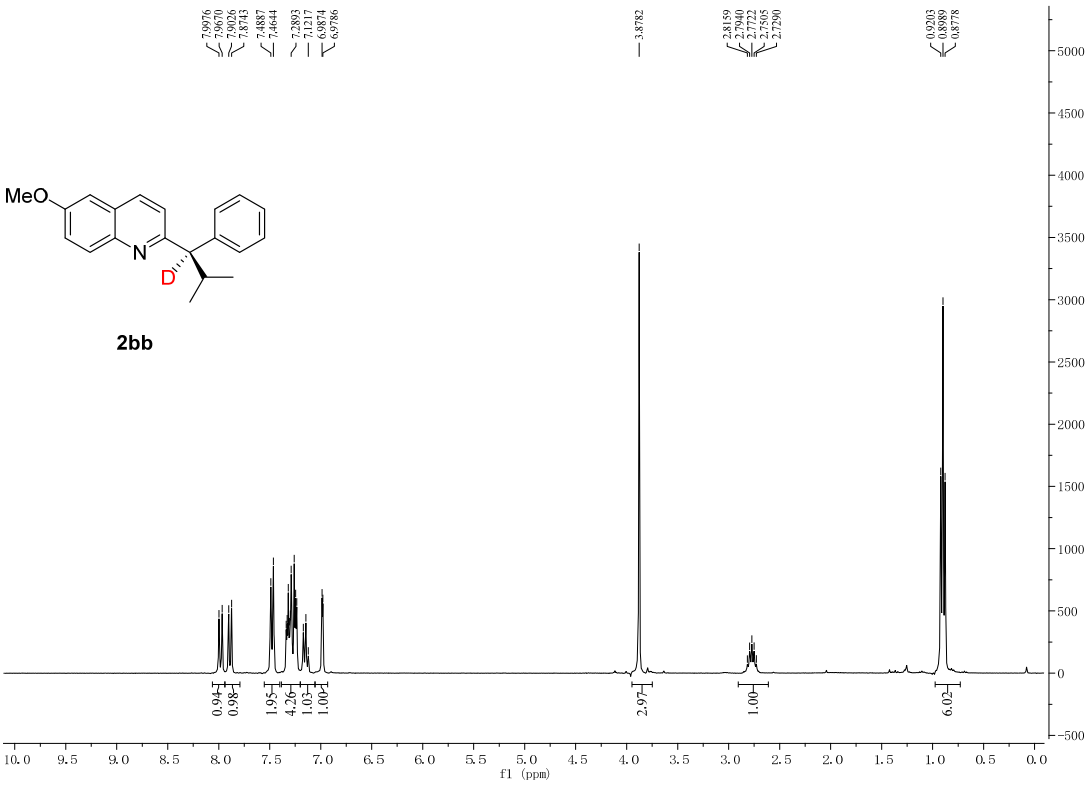

Figure S96. ^{1}H NMR spectrum for **2bb**, related to **Figure 2**.

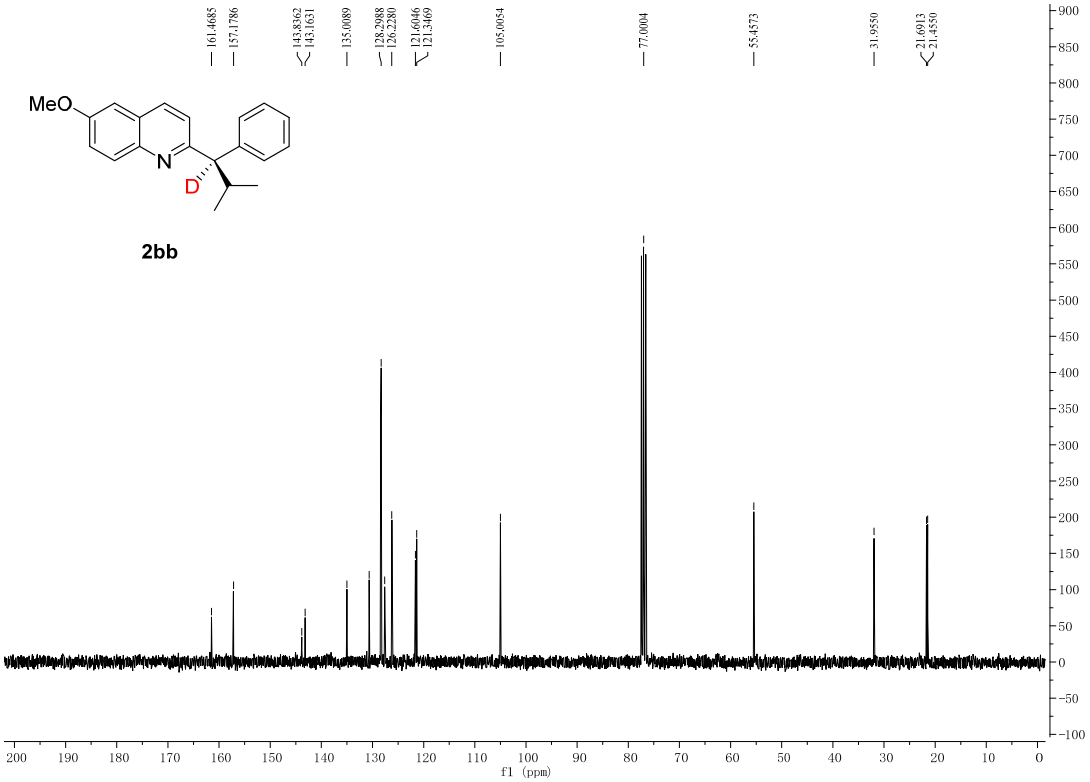

Figure S97. ^{13}C NMR spectrum for **2bb**, related to **Figure 2**.

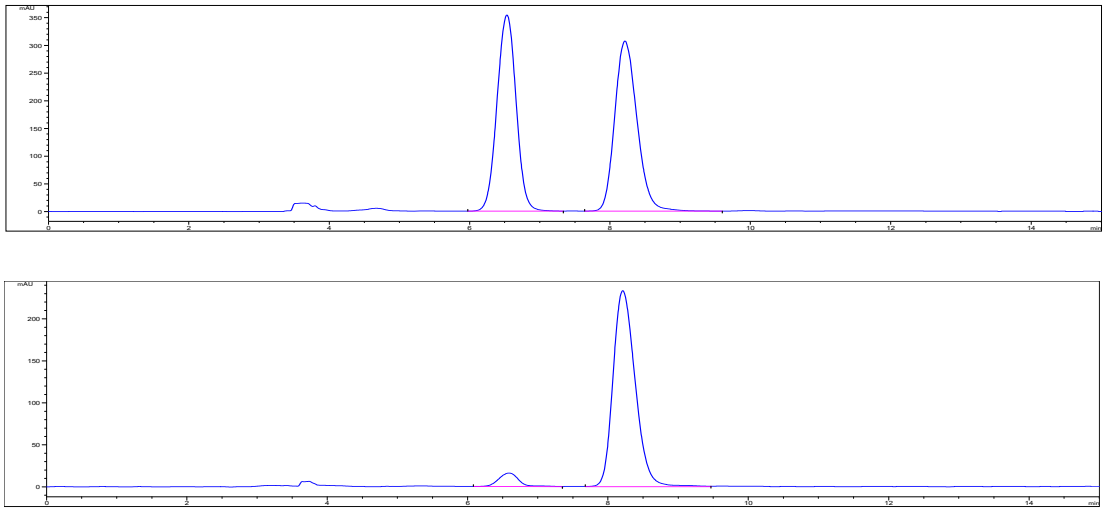

Figure S98. HPLC spectrum for **2bb**, related to **Figure 2**.

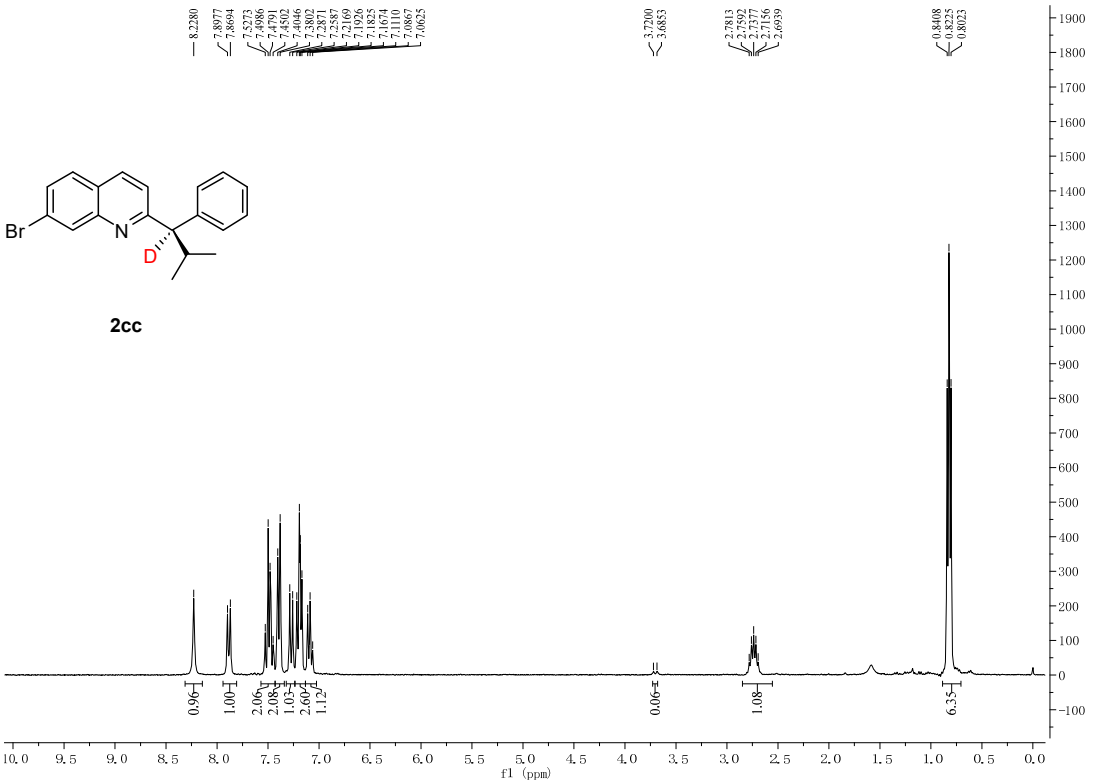

Figure S99. ^{1}H NMR spectrum for **2cc**, related to **Figure 2**.

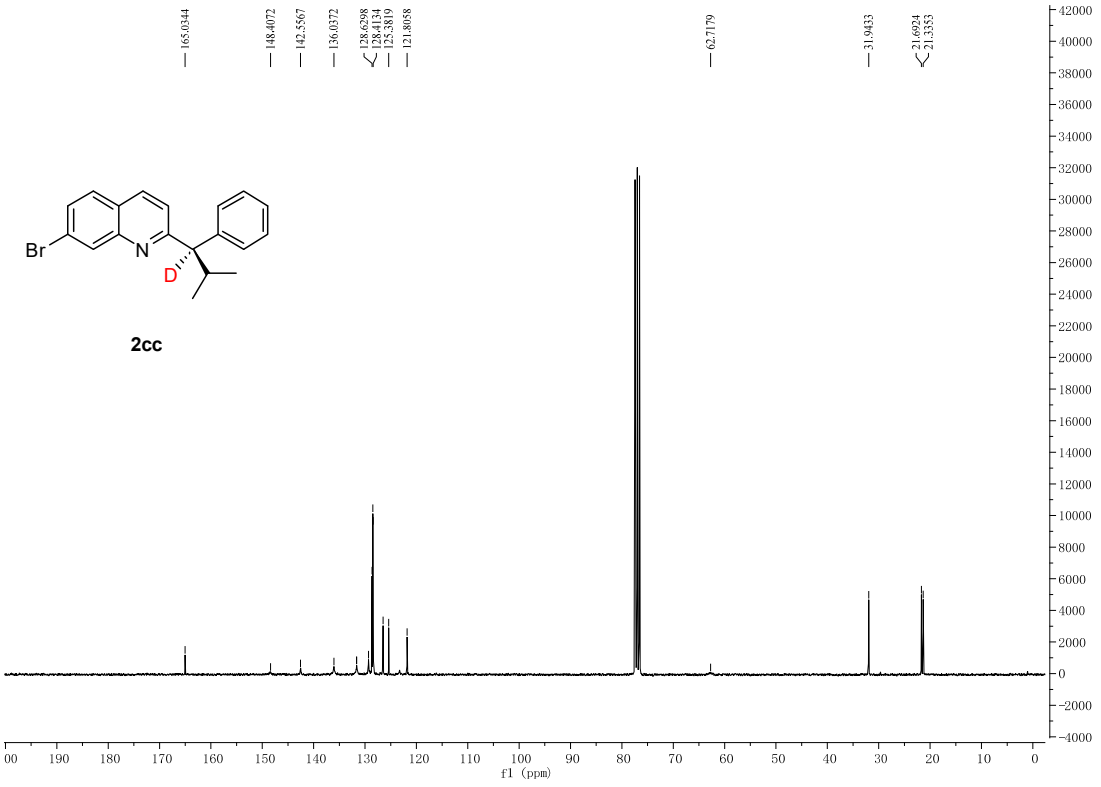

Figure S100. ^{13}C NMR spectrum for **2cc**, related to **Figure 2**.

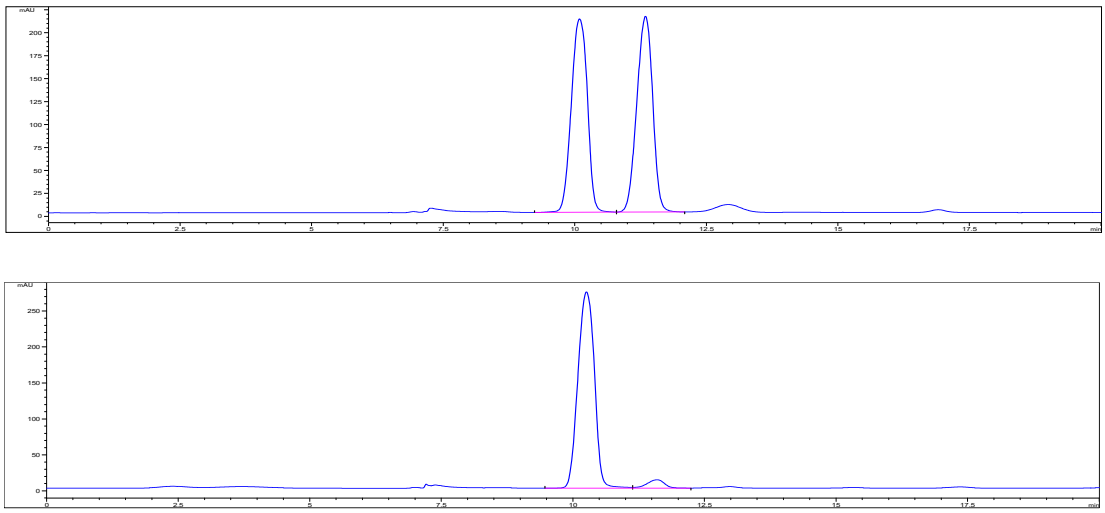

Figure S101. HPLC spectrum for **2cc**, related to **Figure 2**.

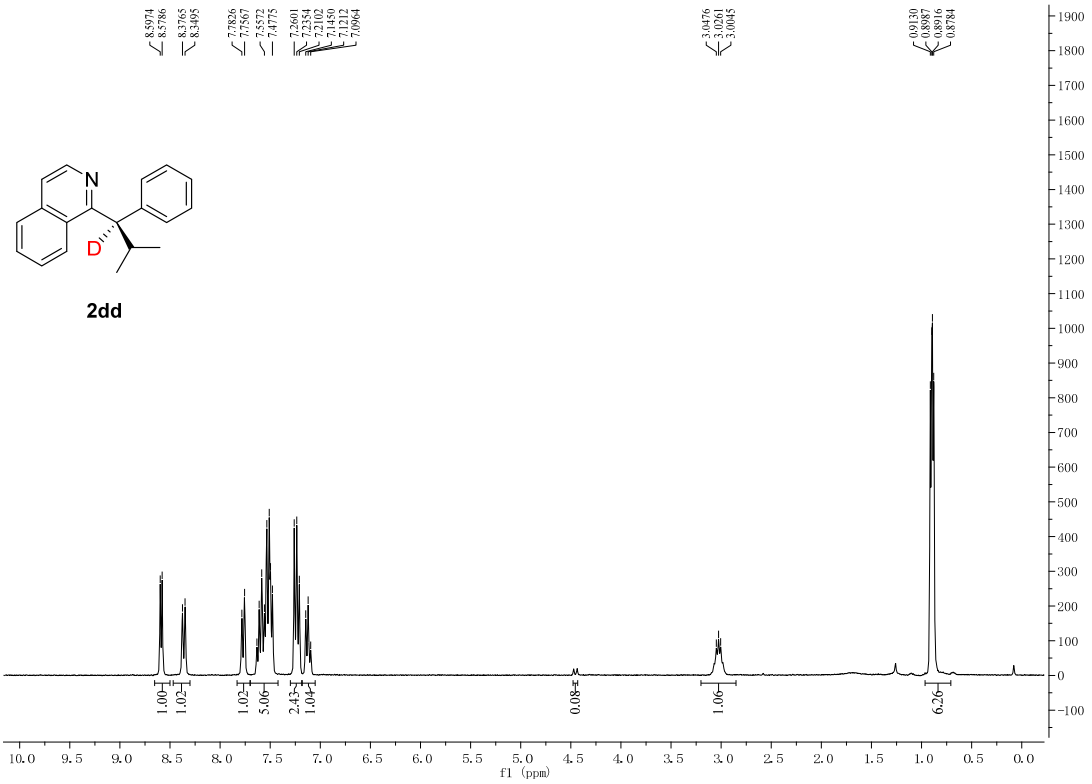

Figure S102. ^{1}H NMR spectrum for **2dd**, related to **Figure 2**.

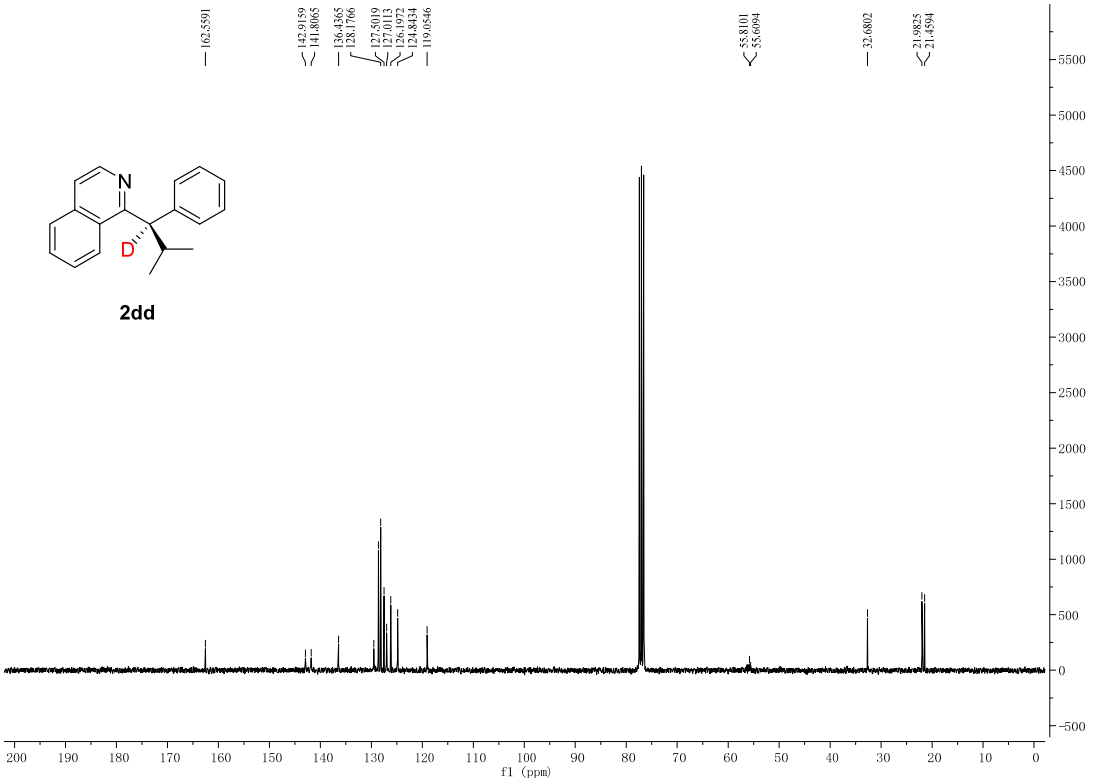

Figure S103. ^{13}C NMR spectrum for **2dd**, related to **Figure 2**.

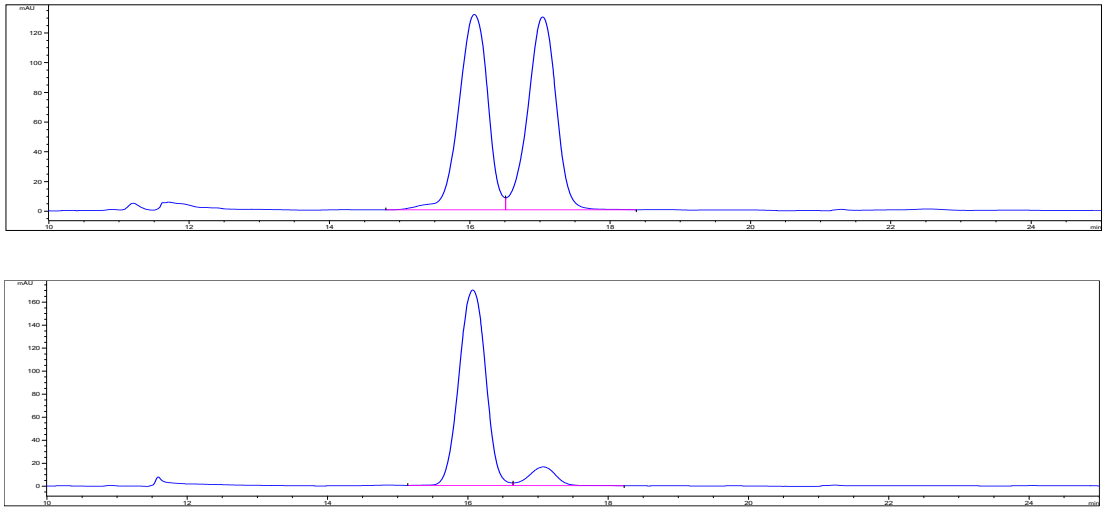

Figure S104. HPLC spectrum for **2dd**, related to **Figure 2**.

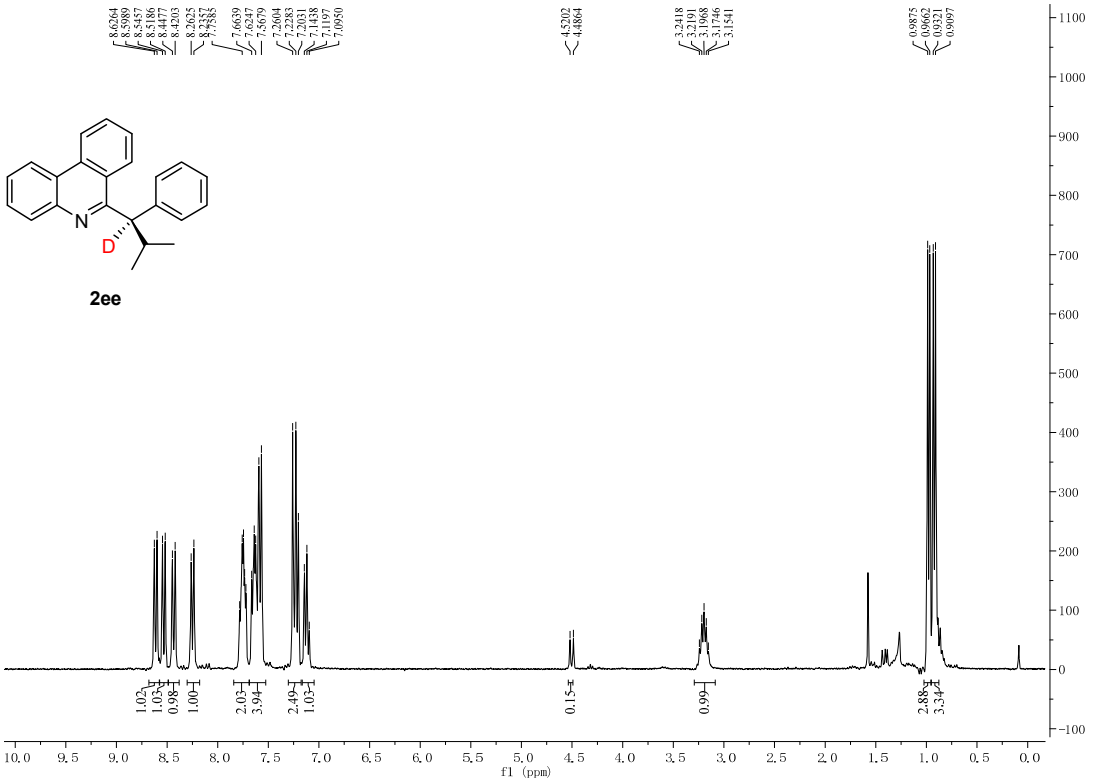

Figure S105. ^{1}H NMR spectrum for **2ee**, related to **Figure 2**.

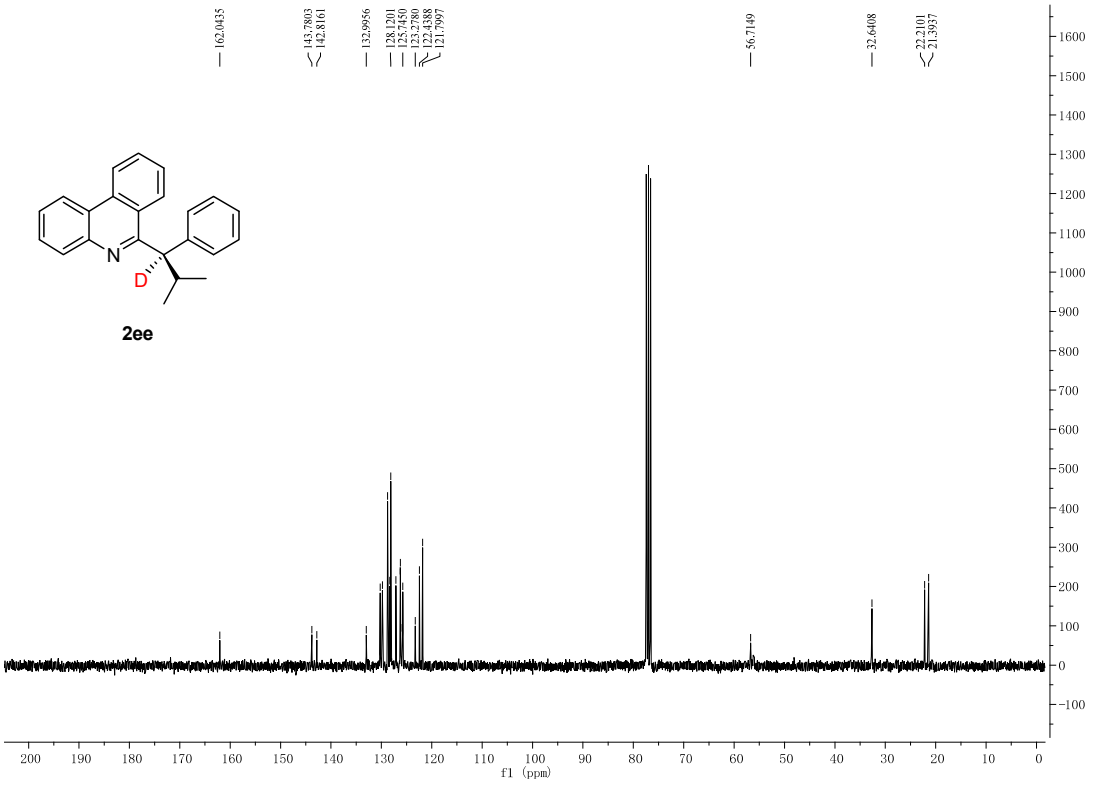

Figure S106. ^{13}C NMR spectrum for **2ee**, related to **Figure 2**.

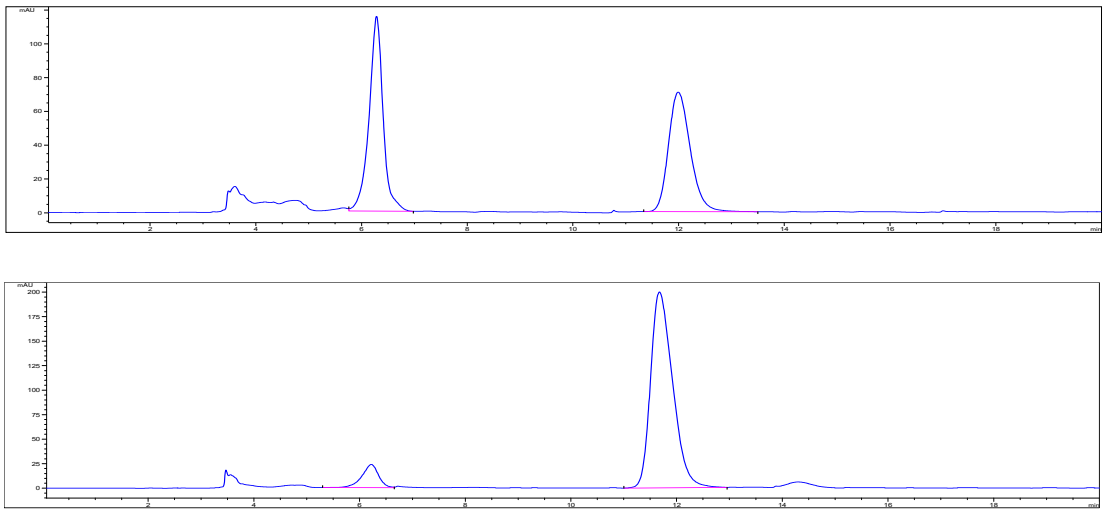

Figure S107. HPLC spectrum for **2ee**, related to **Figure 2**.

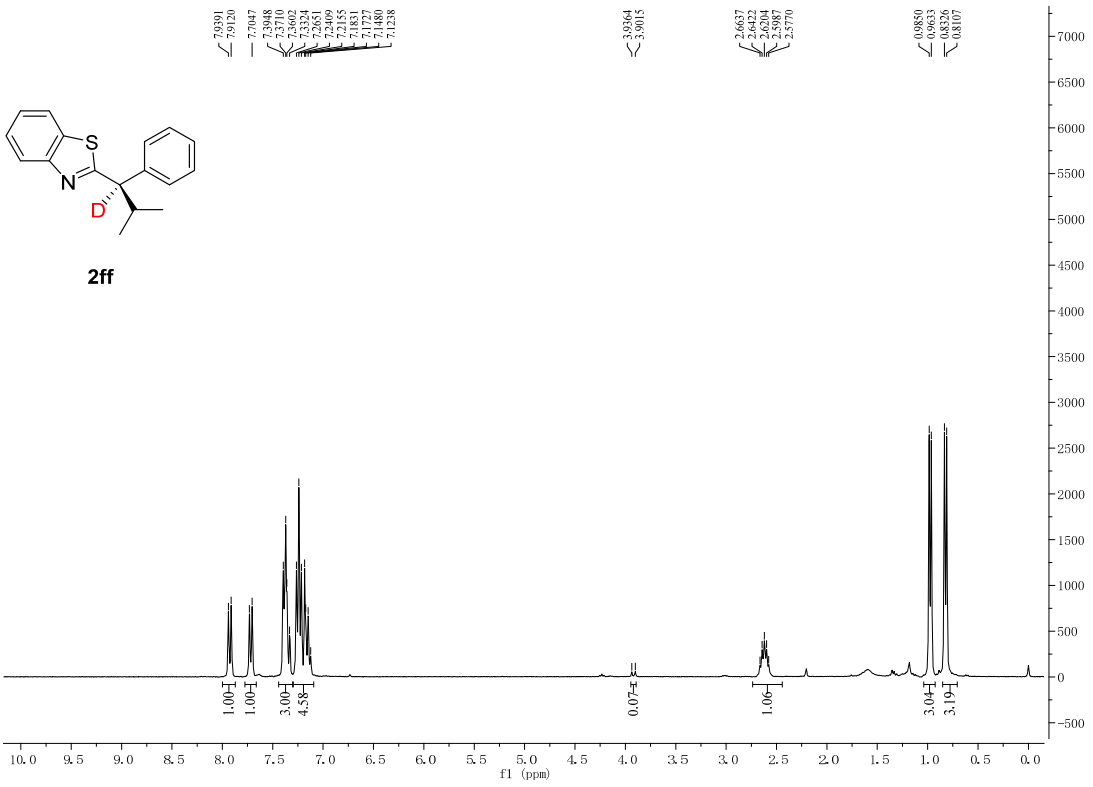

Figure S108. ^{1}H NMR spectrum for **2ff**, related to **Figure 2**.

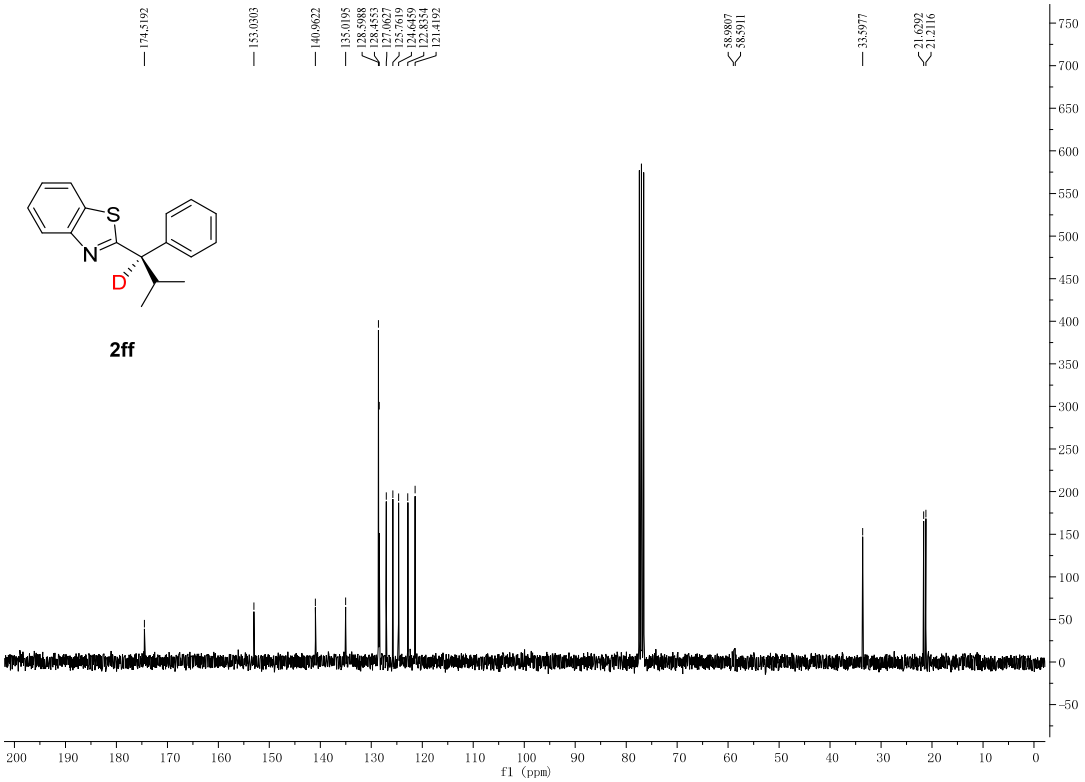

Figure S109. ^{13}C NMR spectrum for **2ff**, related to **Figure 2**.

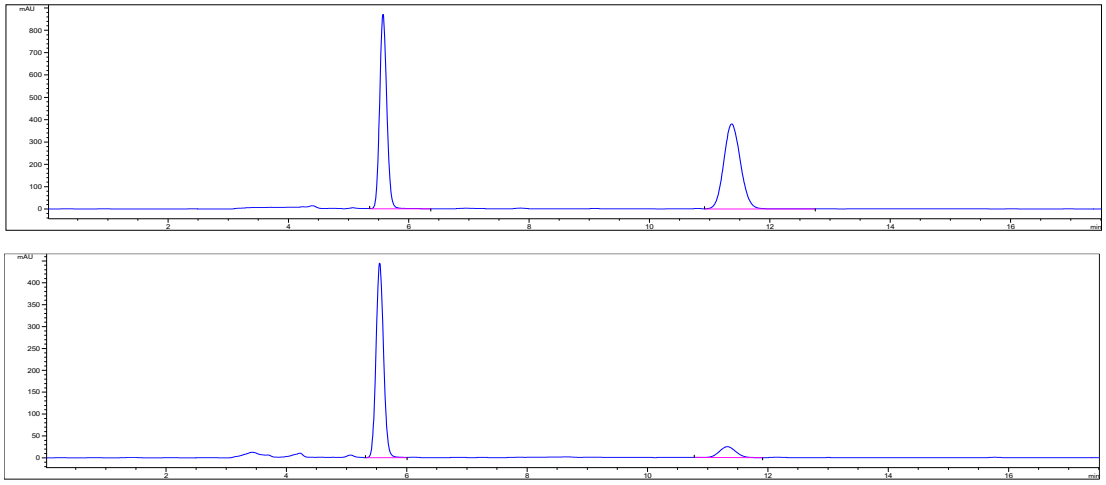

Figure S110. HPLC spectrum for **2ff**, related to **Figure 2**.

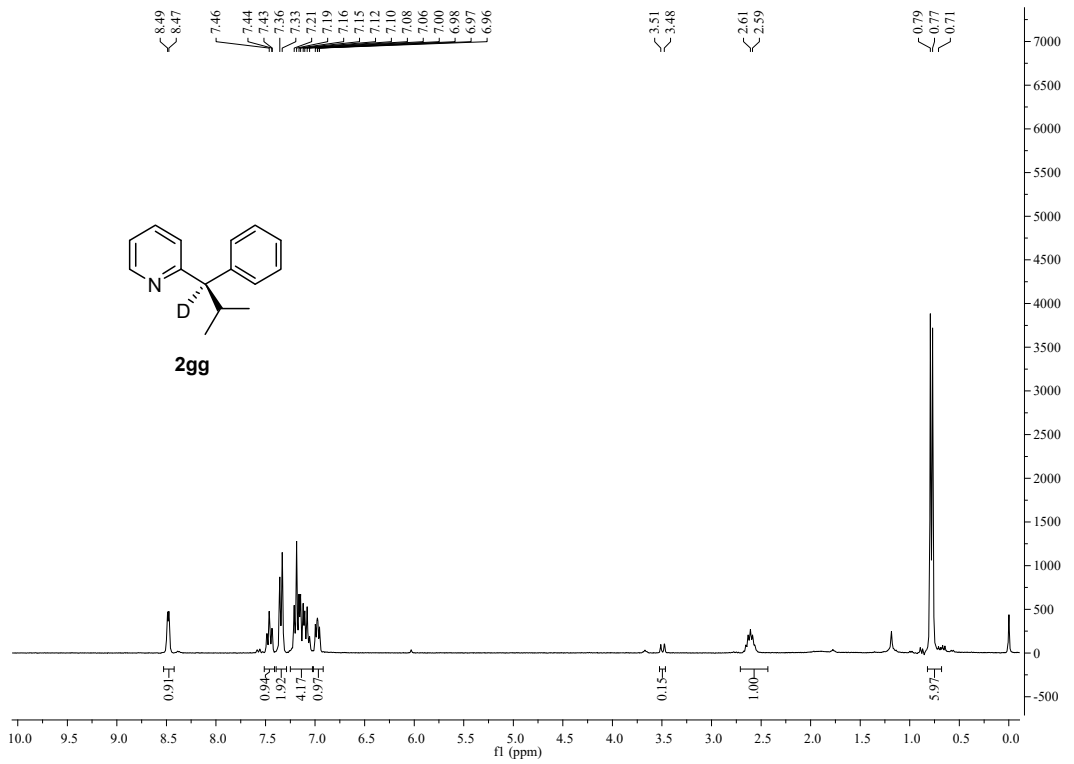

Figure S111. ^{1}H NMR spectrum for **2gg**, related to **Figure 2**.

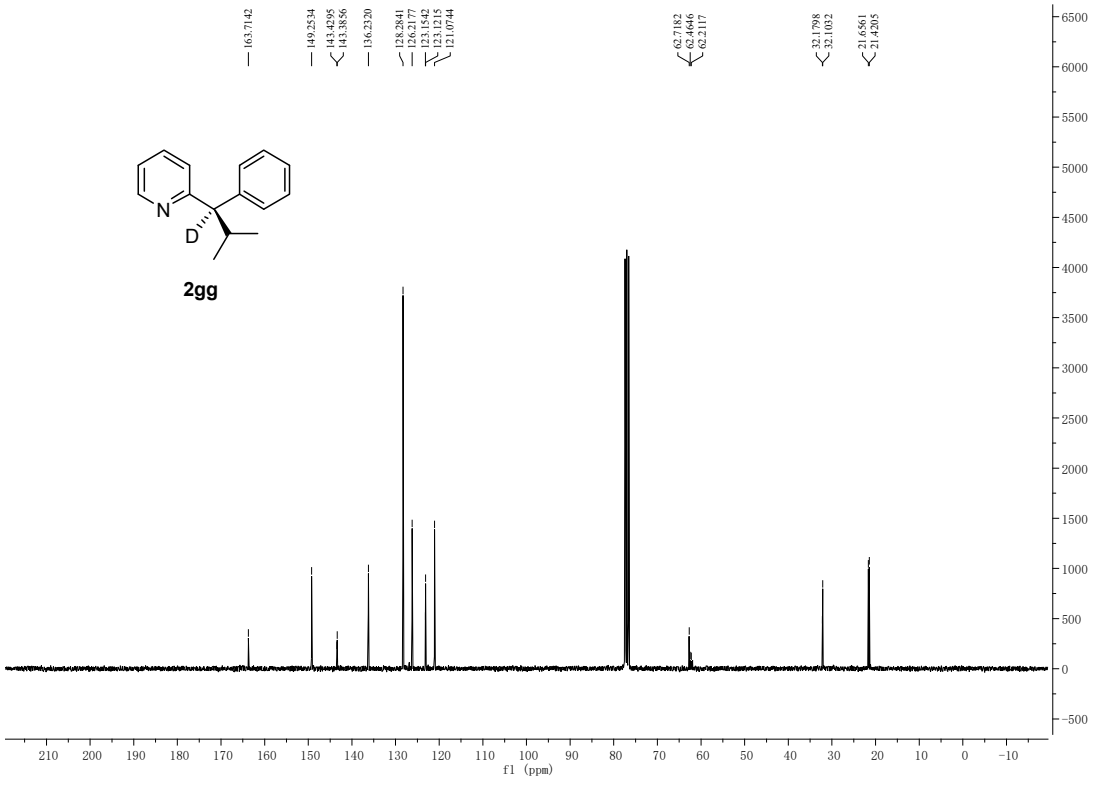

Figure S112. ^{13}C NMR spectrum for **2gg**, related to **Figure 2**.

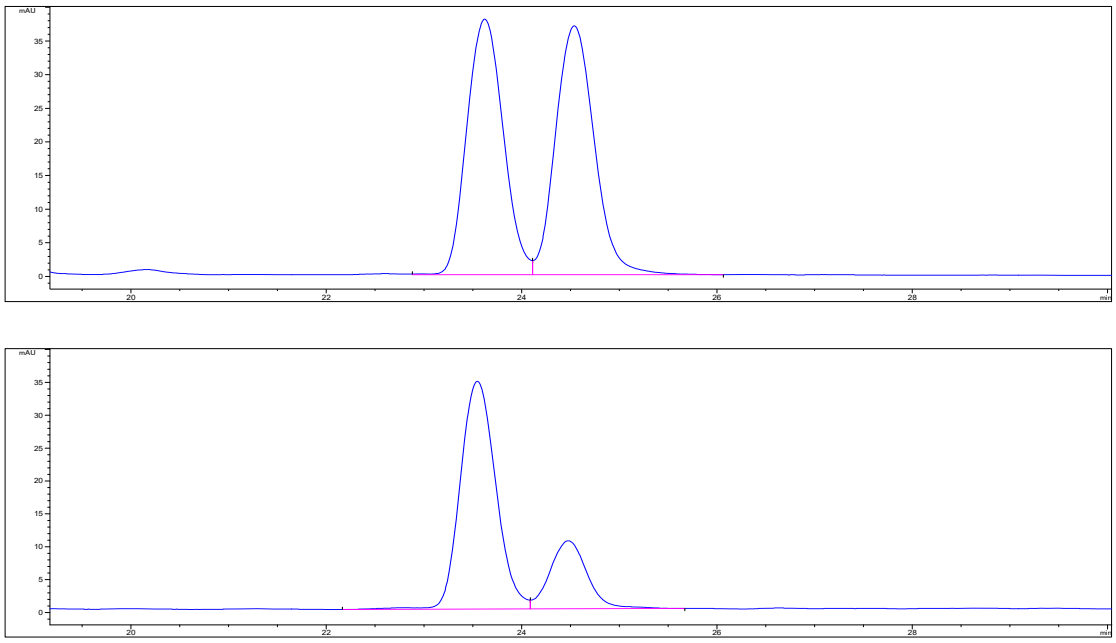

Figure S113. HPLC spectrum for **2gg**, related to **Figure 2**.

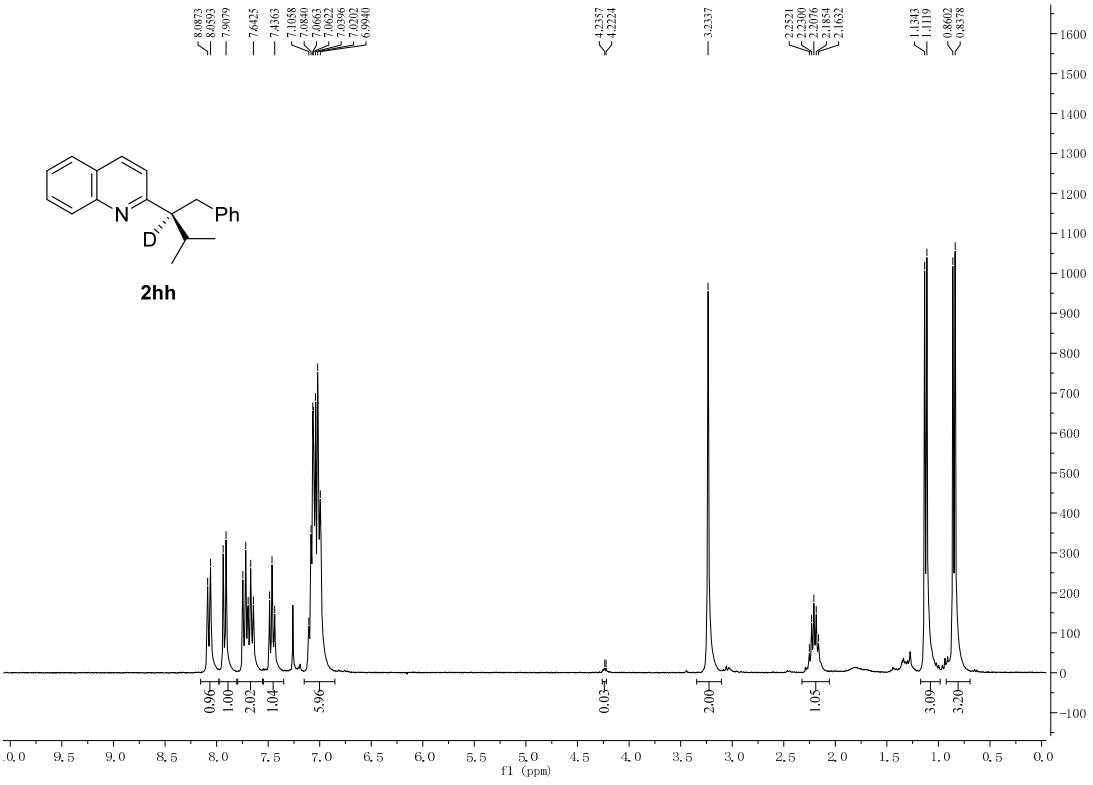

Figure S114. ^{1}H NMR spectrum for **2hh**, related to **Figure 2**.

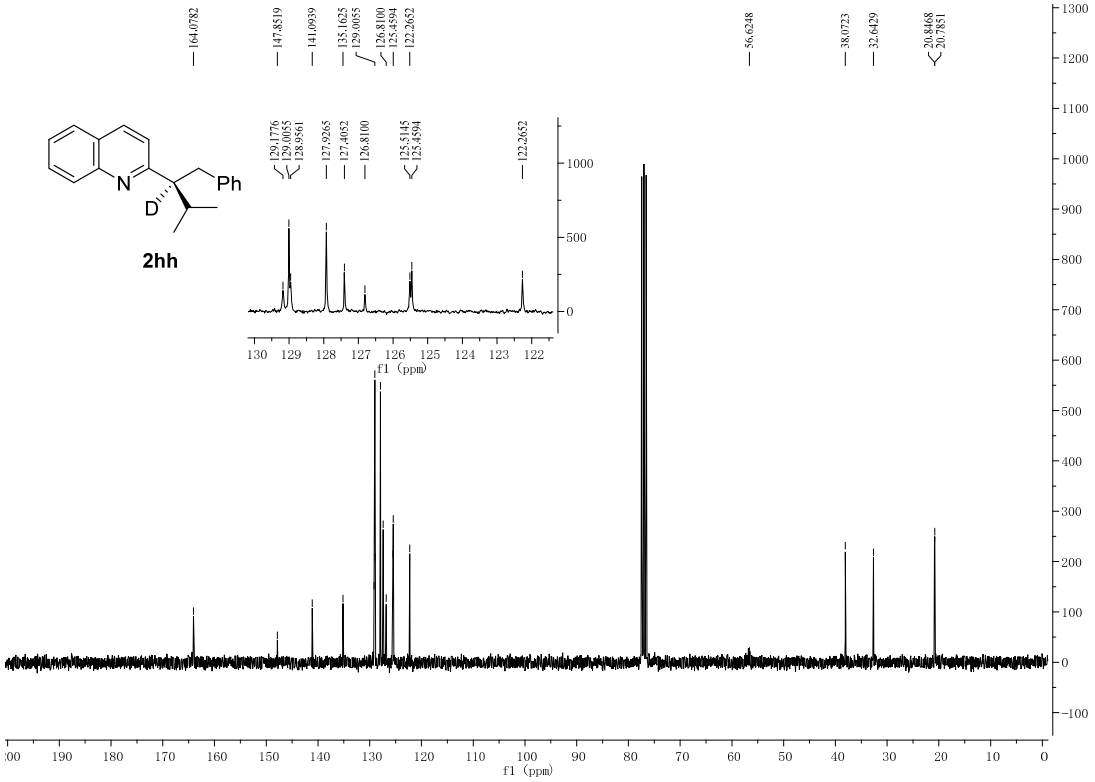

Figure S115. ^{13}C NMR spectrum for **2hh**, related to **Figure 2**.

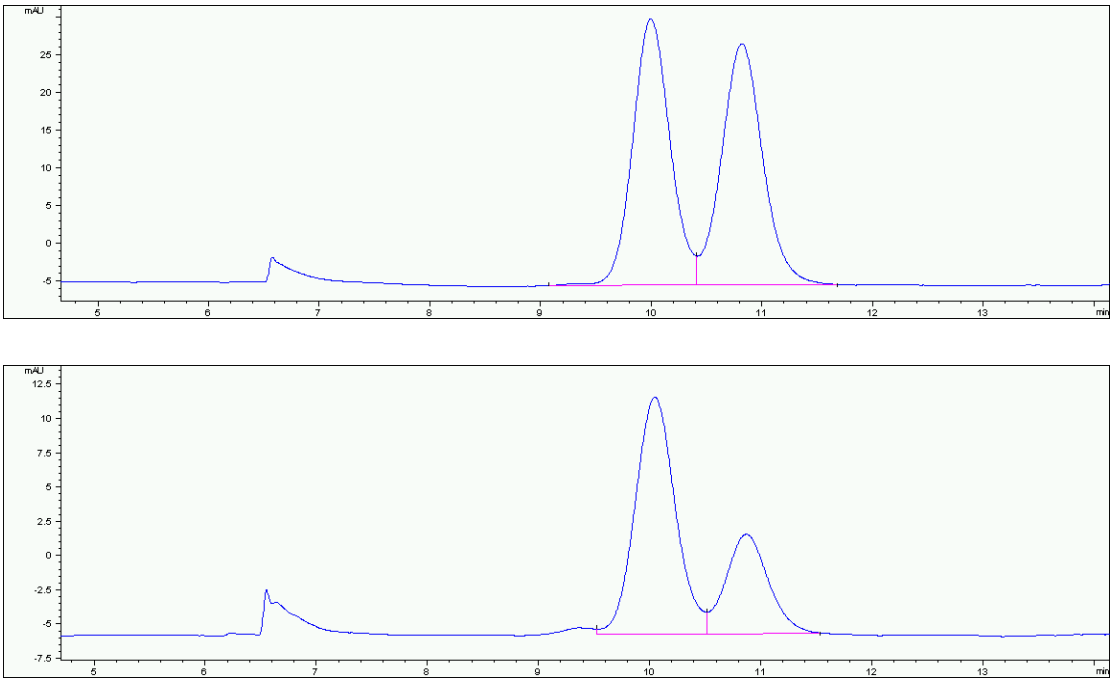

Figure S116. HPLC spectrum for **2hh**, related to **Figure 2**.

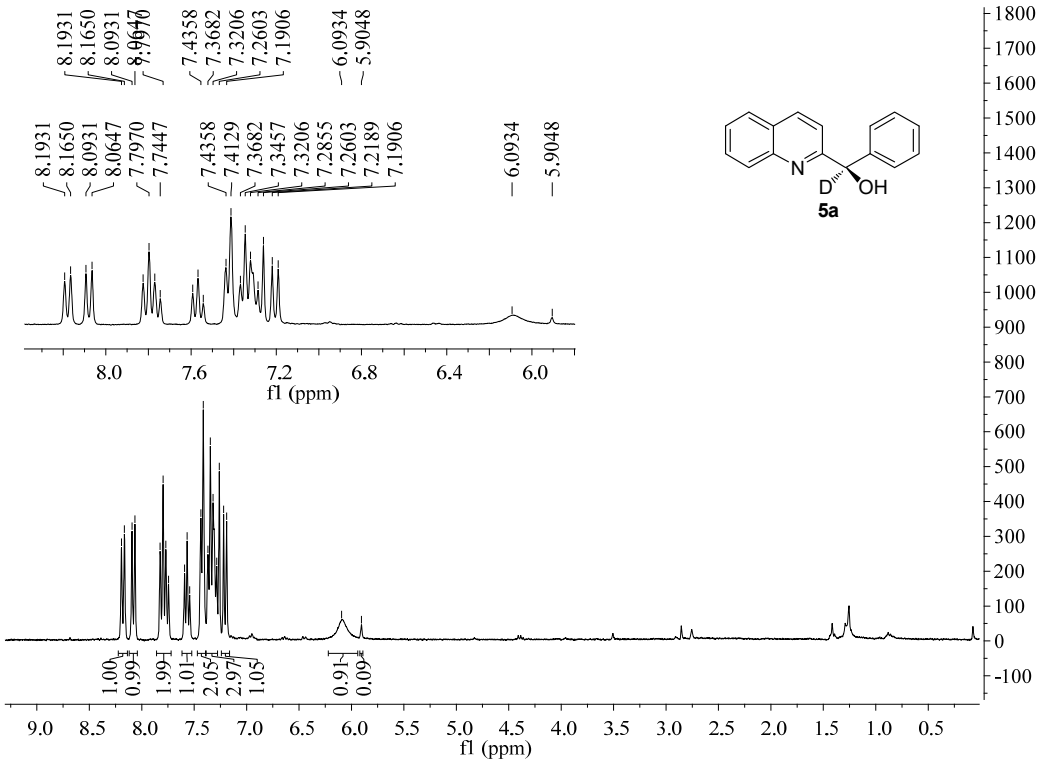

Figure S117. [1]H NMR spectrum for **5a**, related to **Figure 5**.

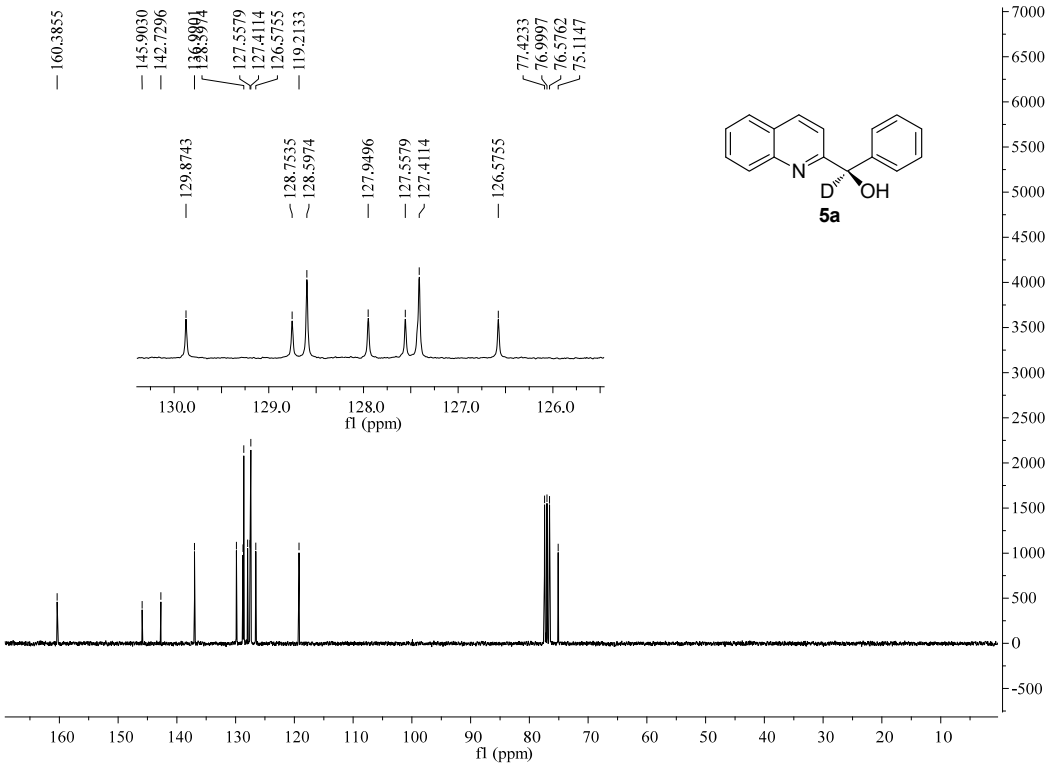

Figure S118. [13]C NMR spectrum for **5a**, related to **Figure 5**.

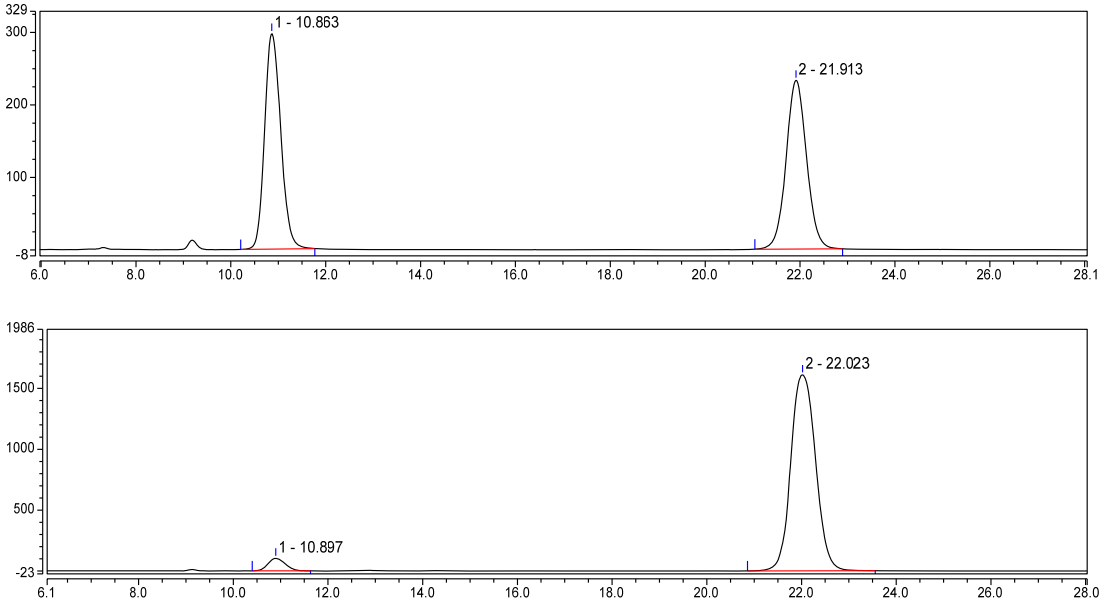

Figure S119. HPLC spectrum for **5a**, related to **Figure 5**.

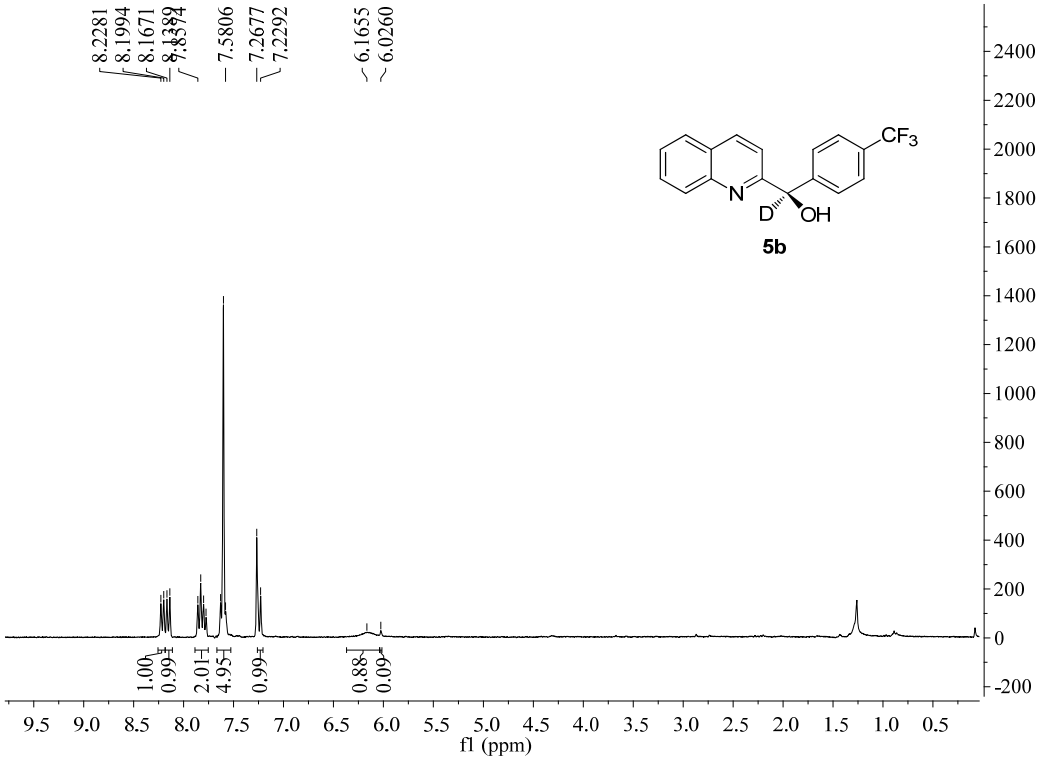

Figure S120. ^{1}H NMR spectrum for **5b**, related to **Figure 5**.

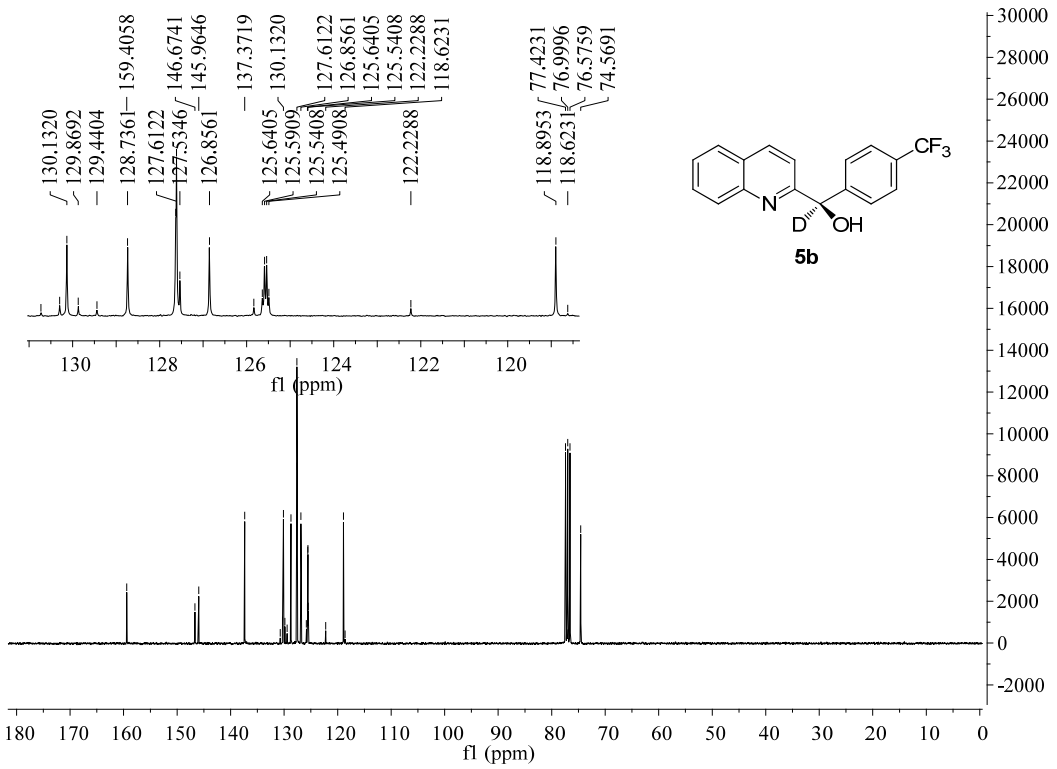

Figure S121. ^{13}C NMR spectrum for **5b**, related to **Figure 5**.

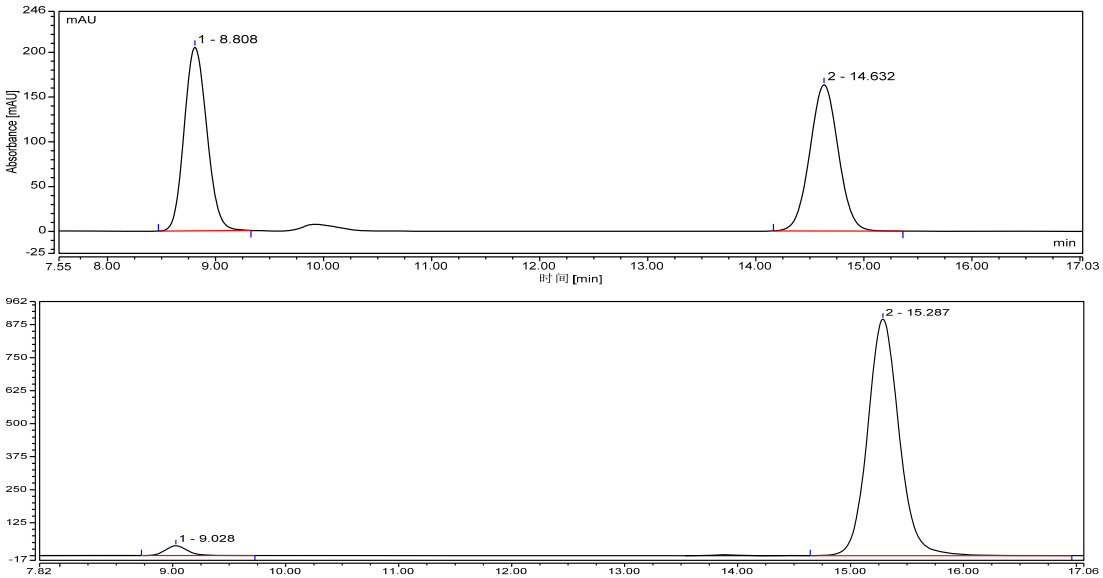

Figure S122. HPLC spectrum for **5b**, related to **Figure 5**.

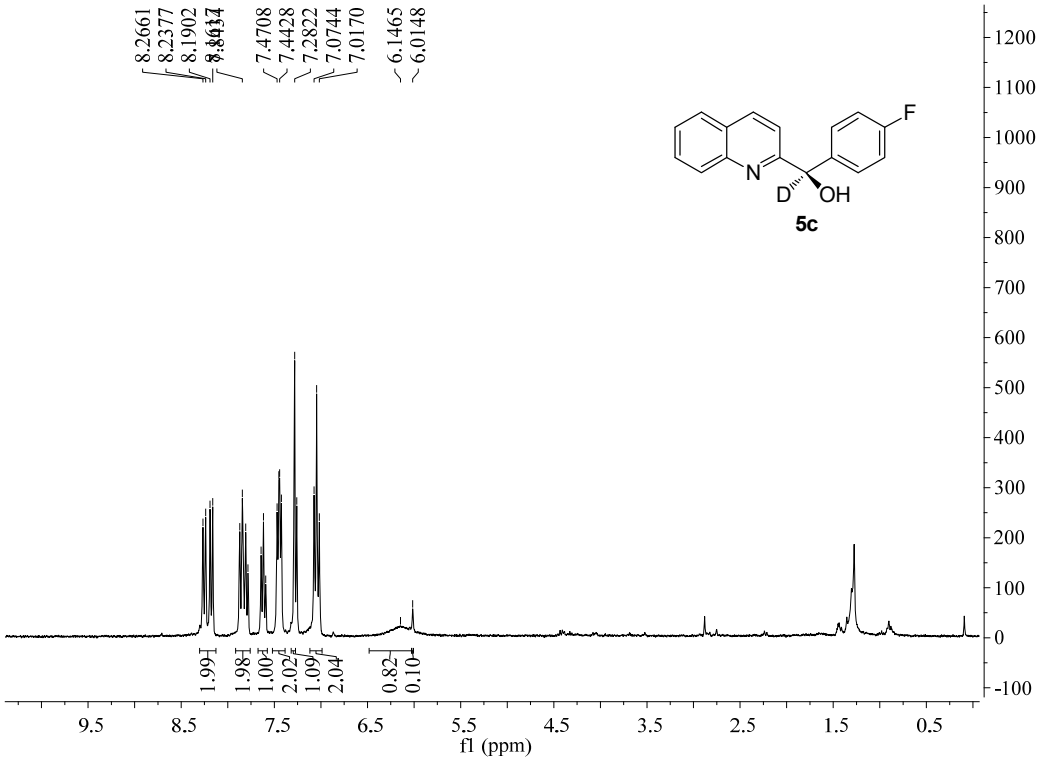

Figure S123. ^{1}H NMR spectrum for **5c**, related to **Figure 5**.

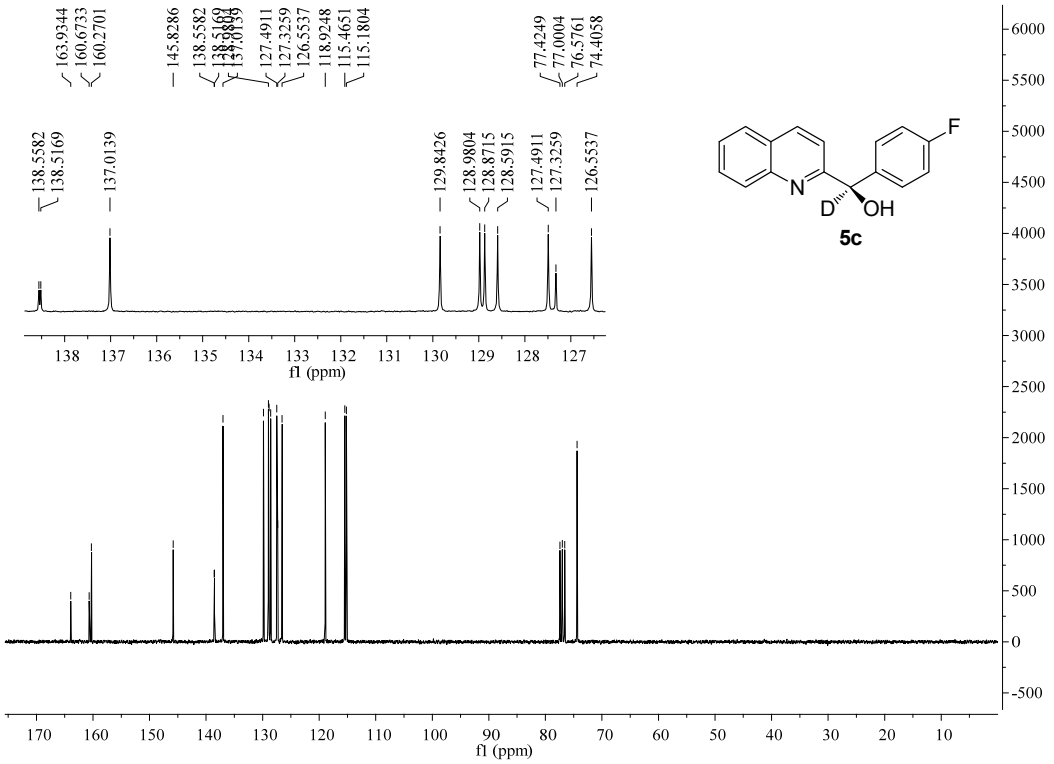

Figure S124. ^{13}C NMR spectrum for **5c**, related to **Figure 5**.

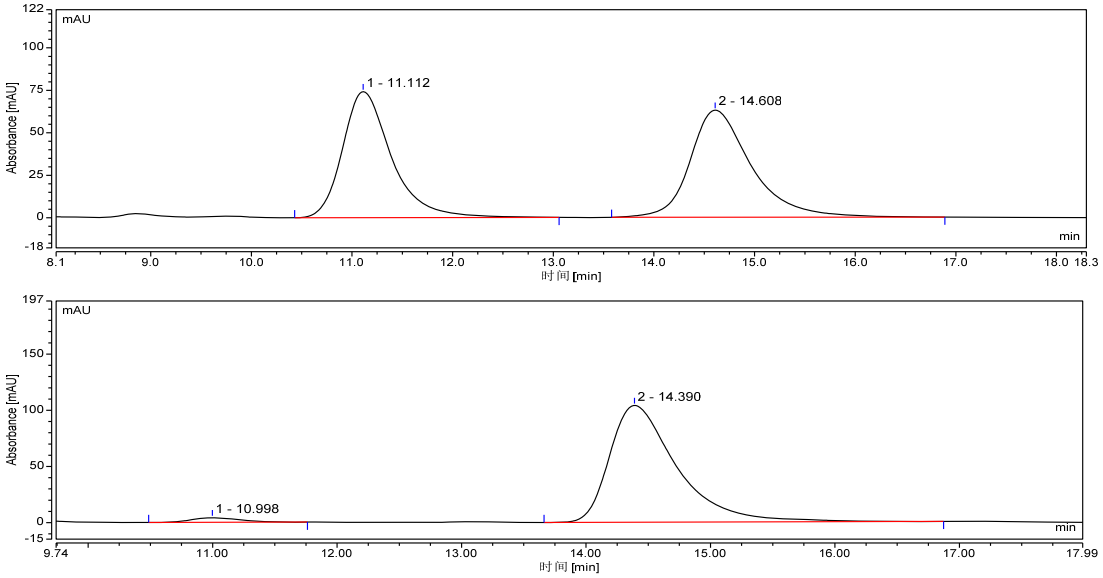

Figure S125. HPLC spectrum for **5c**, related to **Figure 5**.

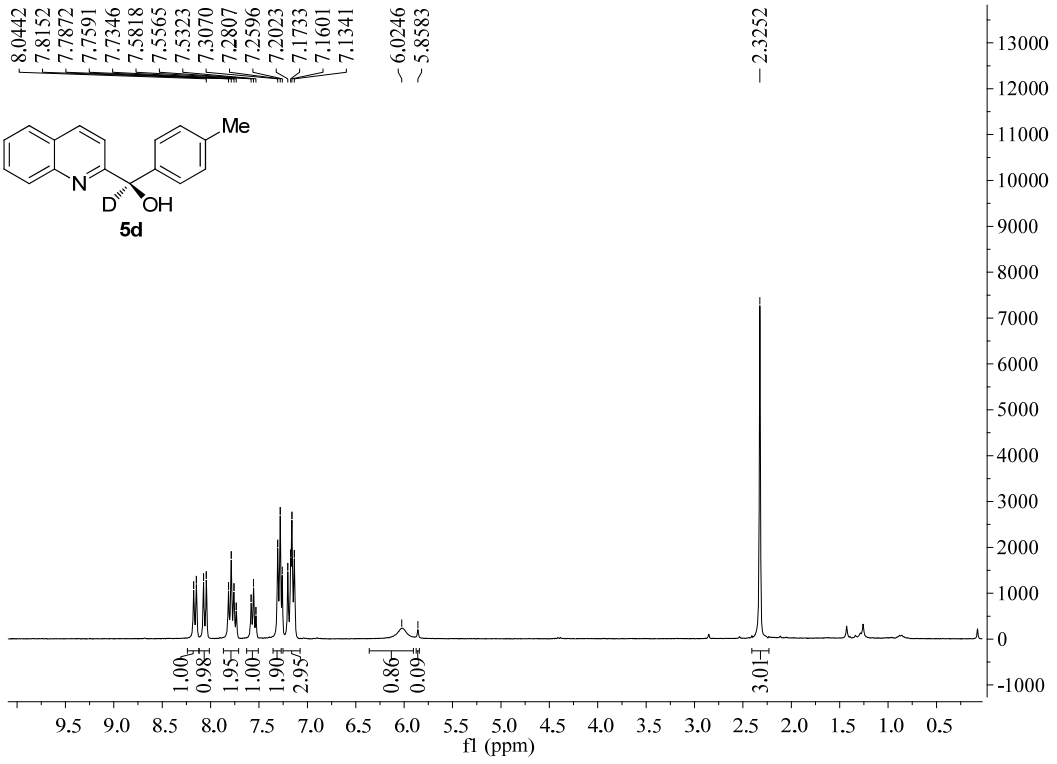

Figure S126. ^{1}H NMR spectrum for **5d**, related to **Figure 5**.

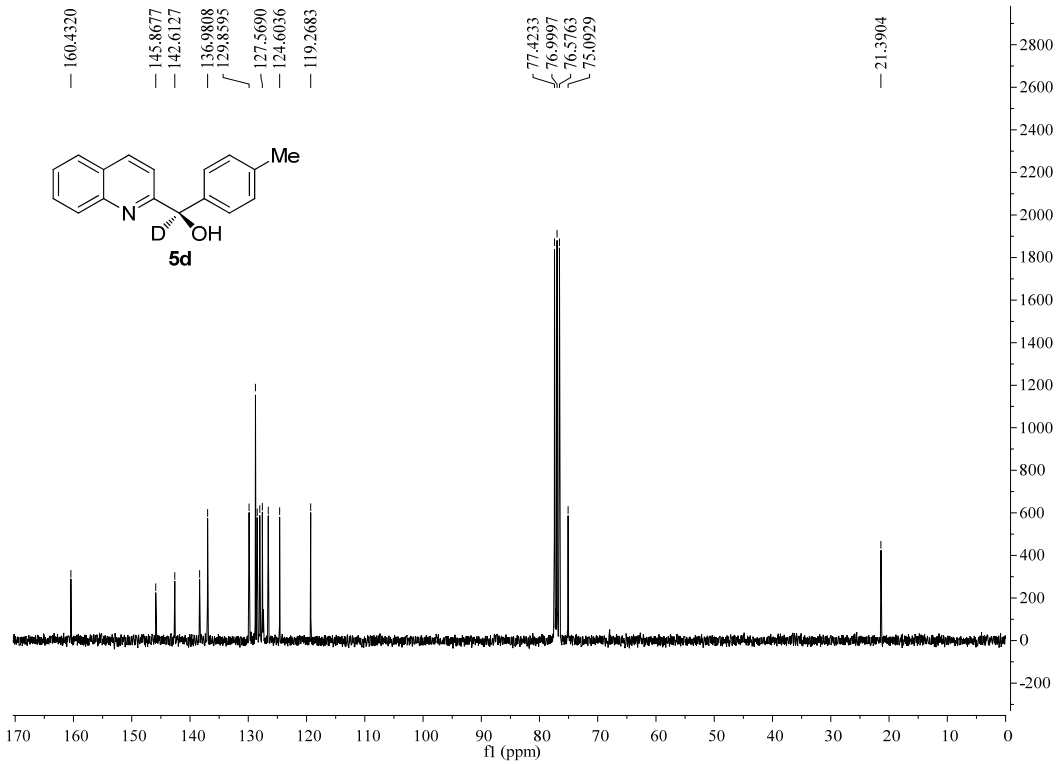

Figure S127. ^{13}C NMR spectrum for **5d**, related to **Figure 5**.

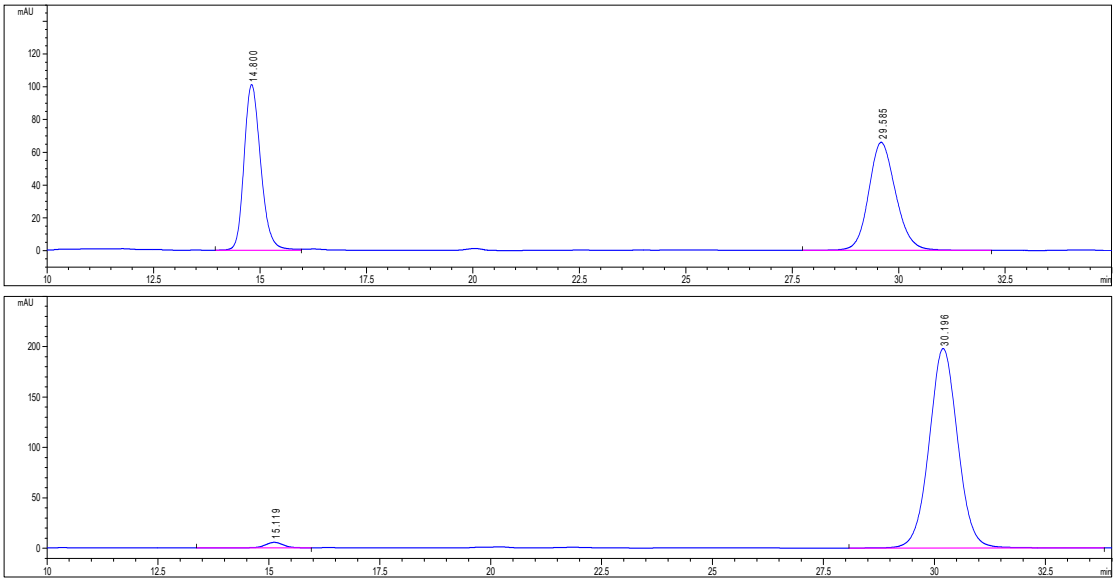

Figure S128. HPLC spectrum for **5d**, related to **Figure 5**.

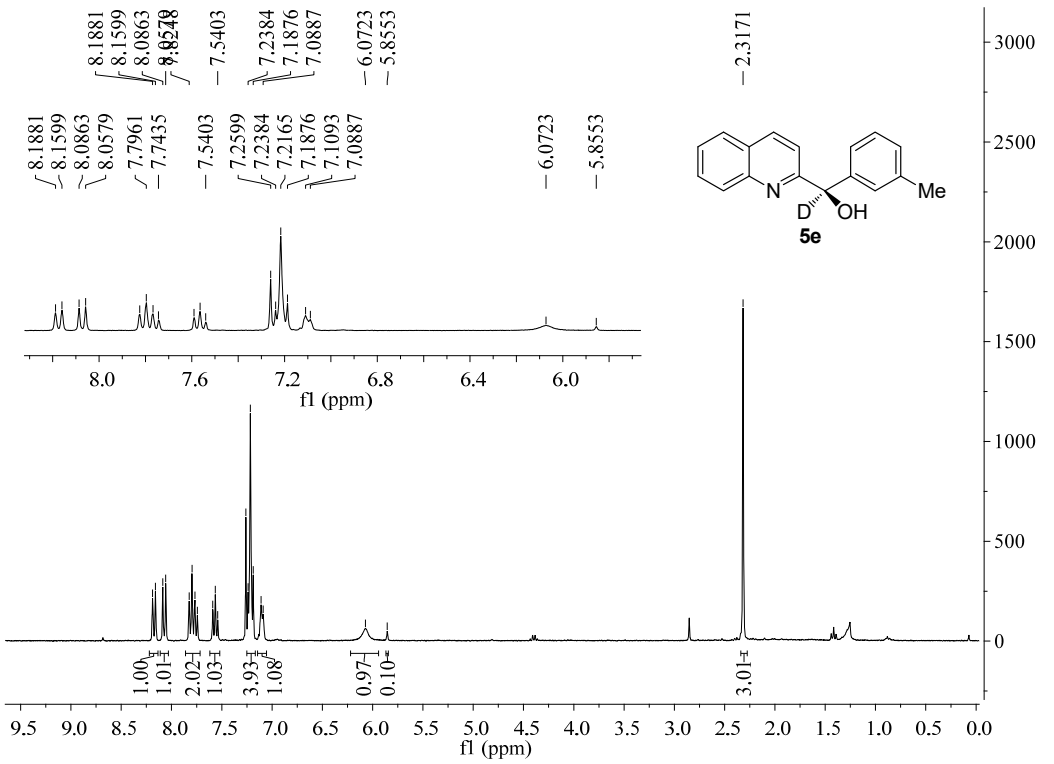

Figure S129. ^{1}H NMR spectrum for **5e**, related to **Figure 5**.

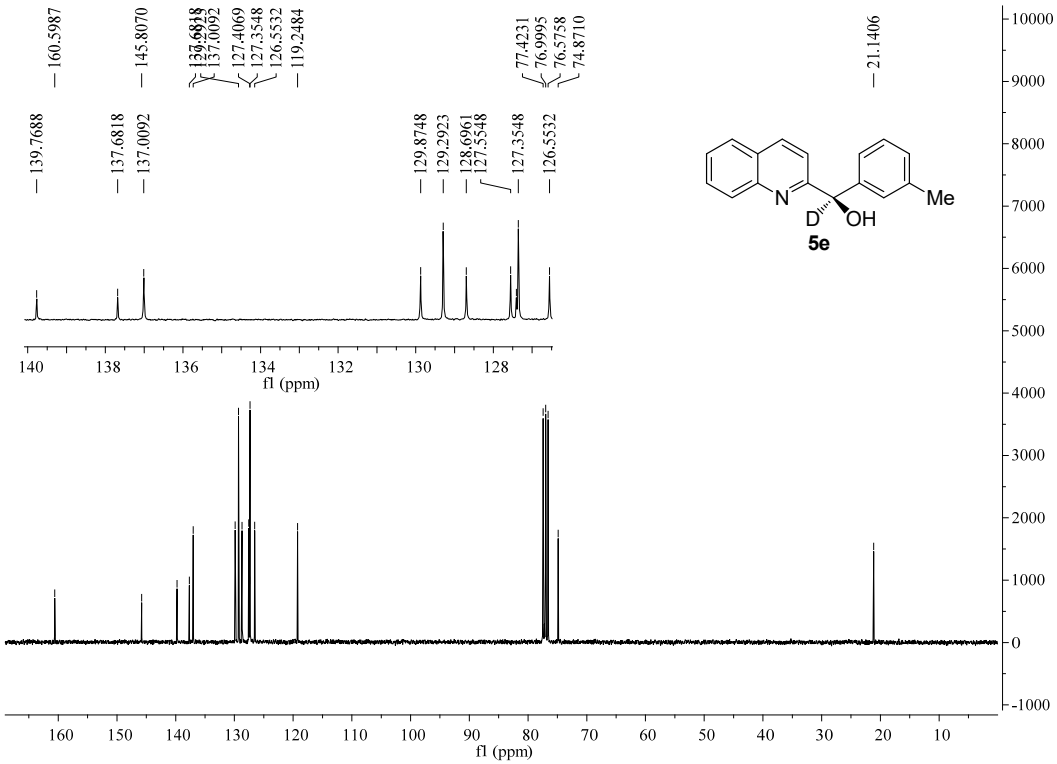

Figure S130. ^{13}C NMR spectrum for **5e**, related to **Figure 5**.

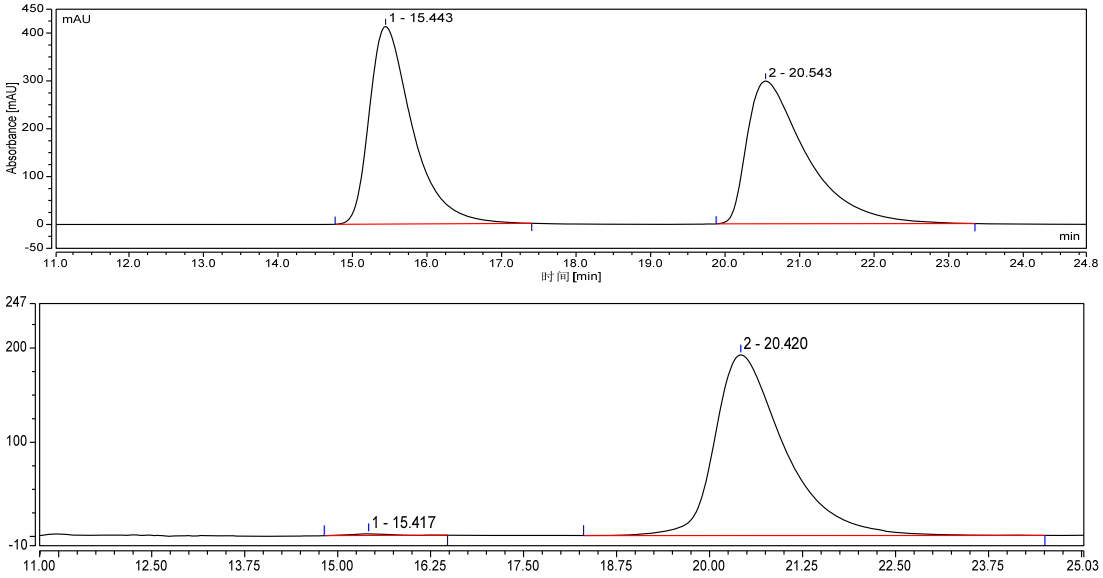

Figure S131. HPLC spectrum for **5e**, related to **Figure 5**.

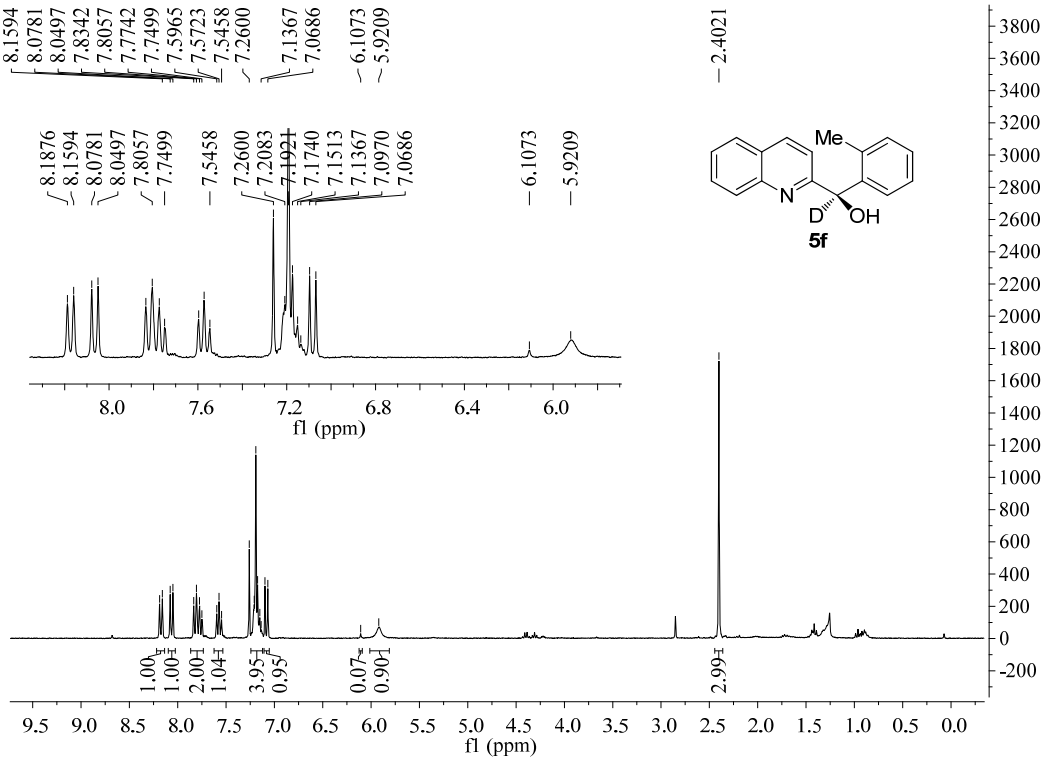

Figure S132. ^{1}H NMR spectrum for **5f**, related to **Figure 5**.

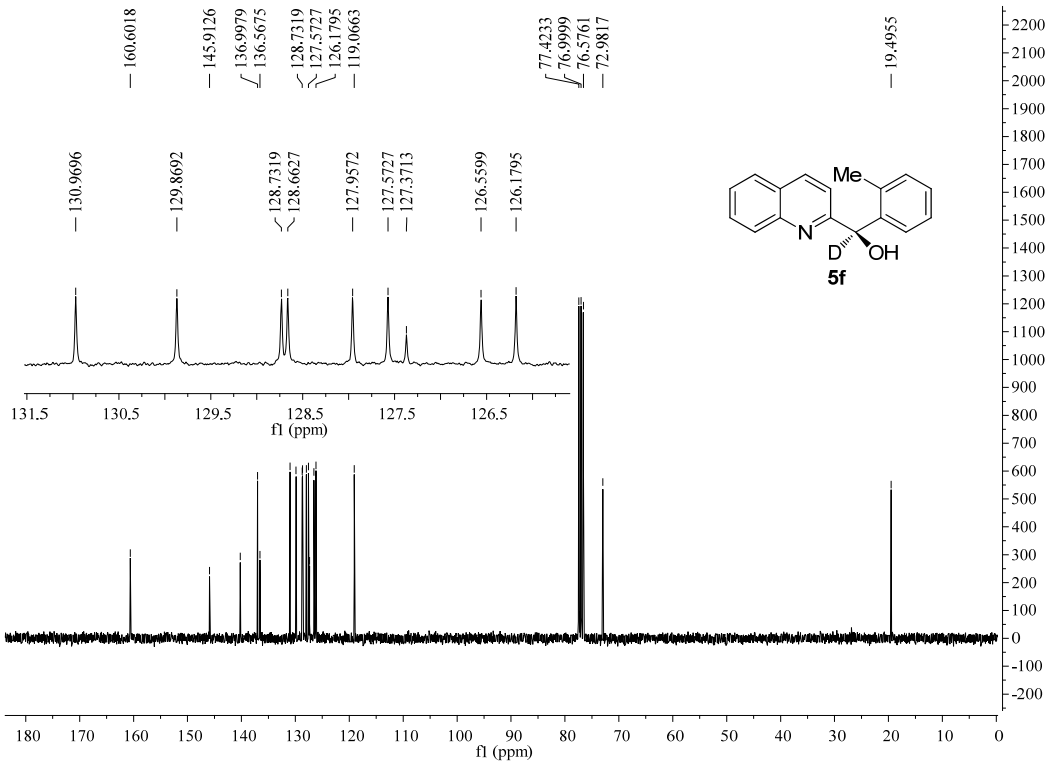

Figure S133. ^{13}C NMR spectrum for **5f**, related to **Figure 5**.

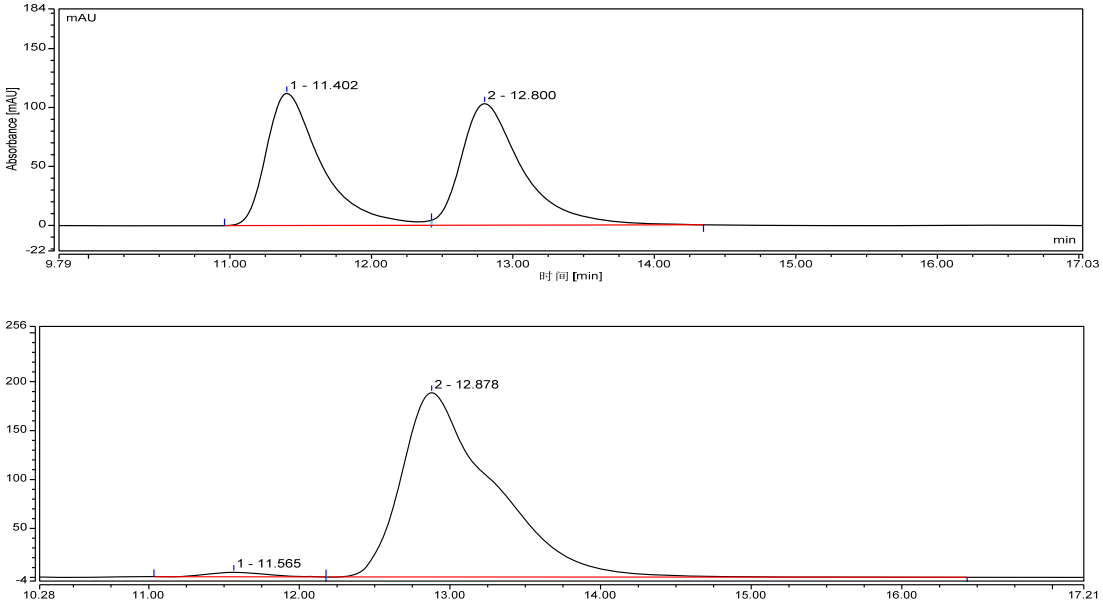

Figure S134. HPLC spectrum for **5f**, related to **Figure 5**.

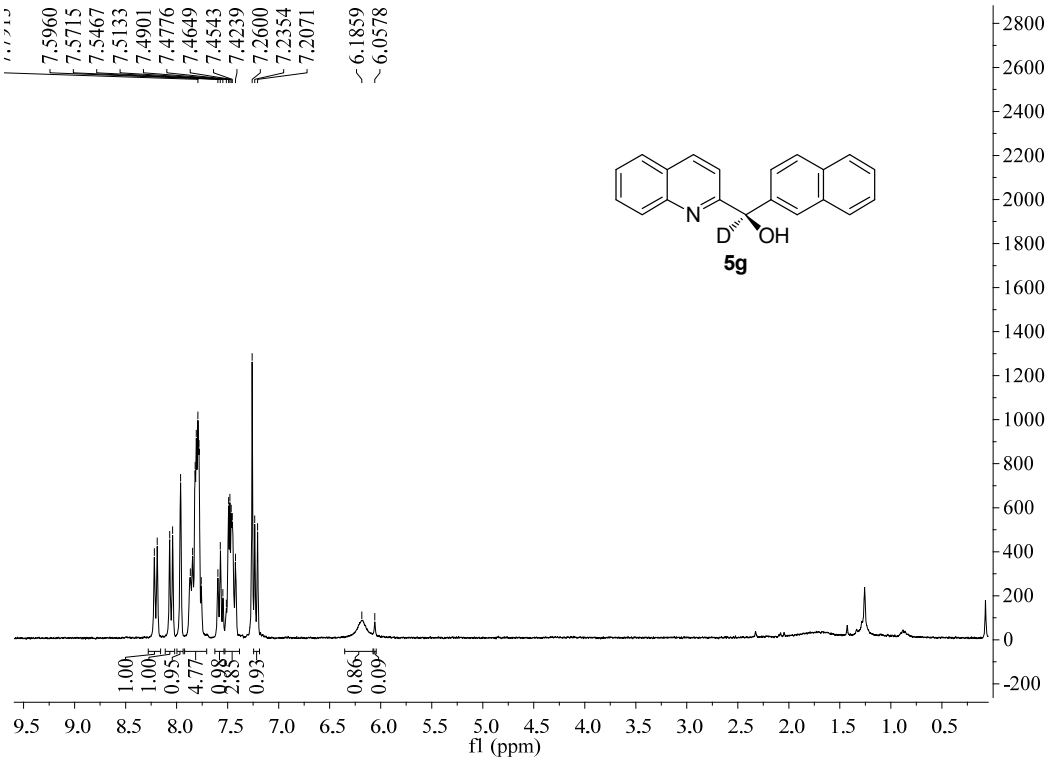

Figure S135. ^{1}H NMR spectrum for **5g**, related to **Figure 5**.

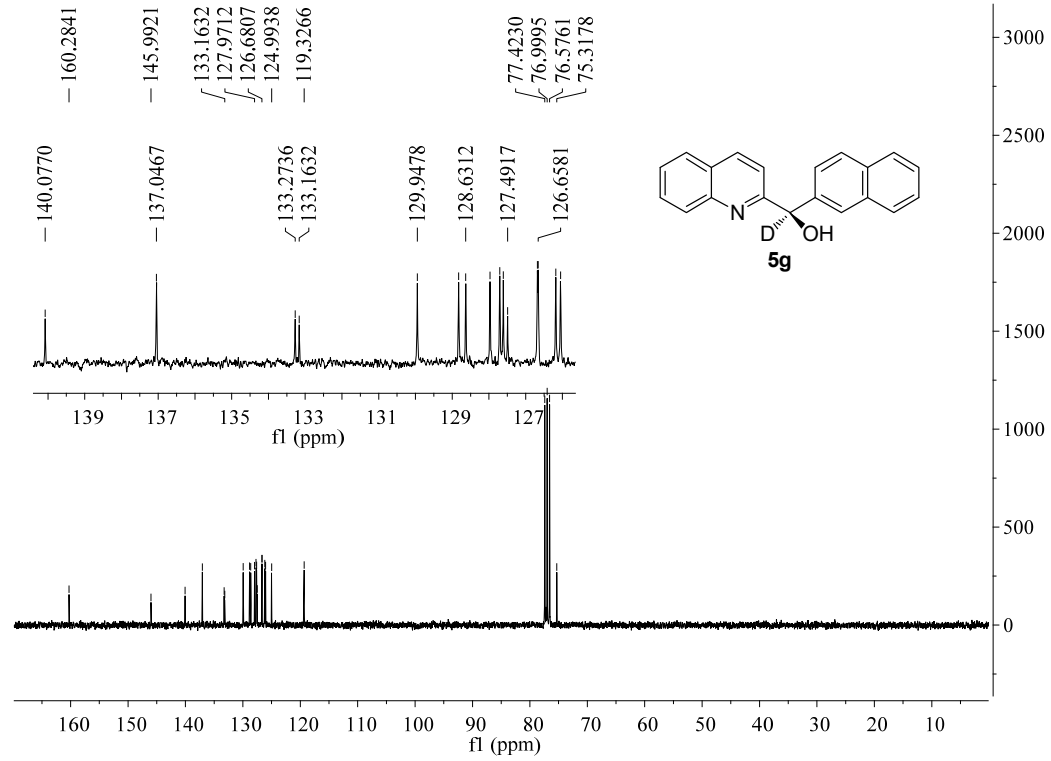

Figure S136. ^{13}C NMR spectrum for **5g**, related to **Figure 5**.

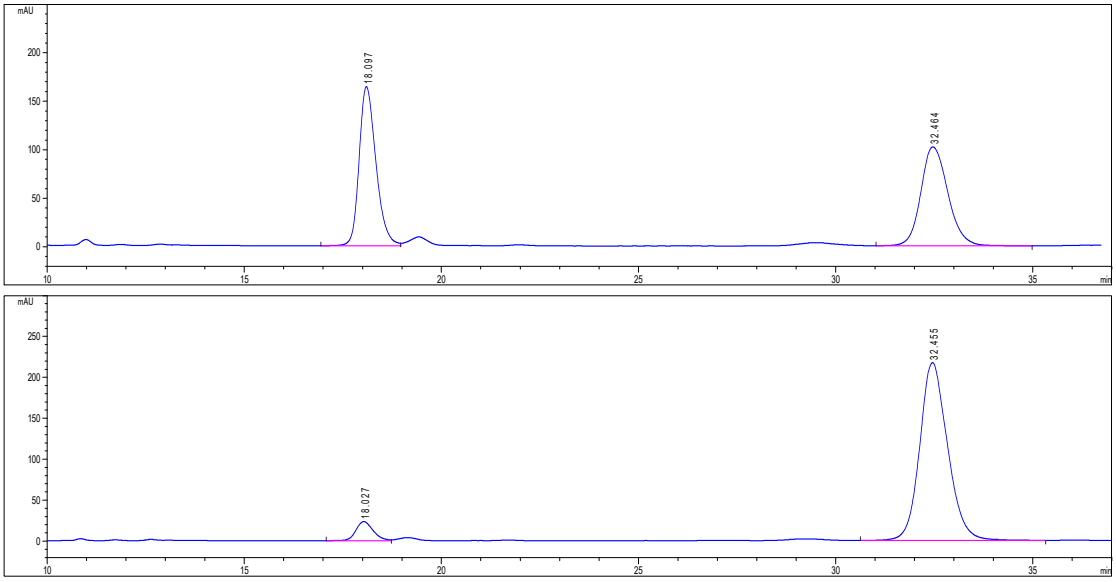

Figure S137. HPLC spectrum for **5g**, related to **Figure 5**.

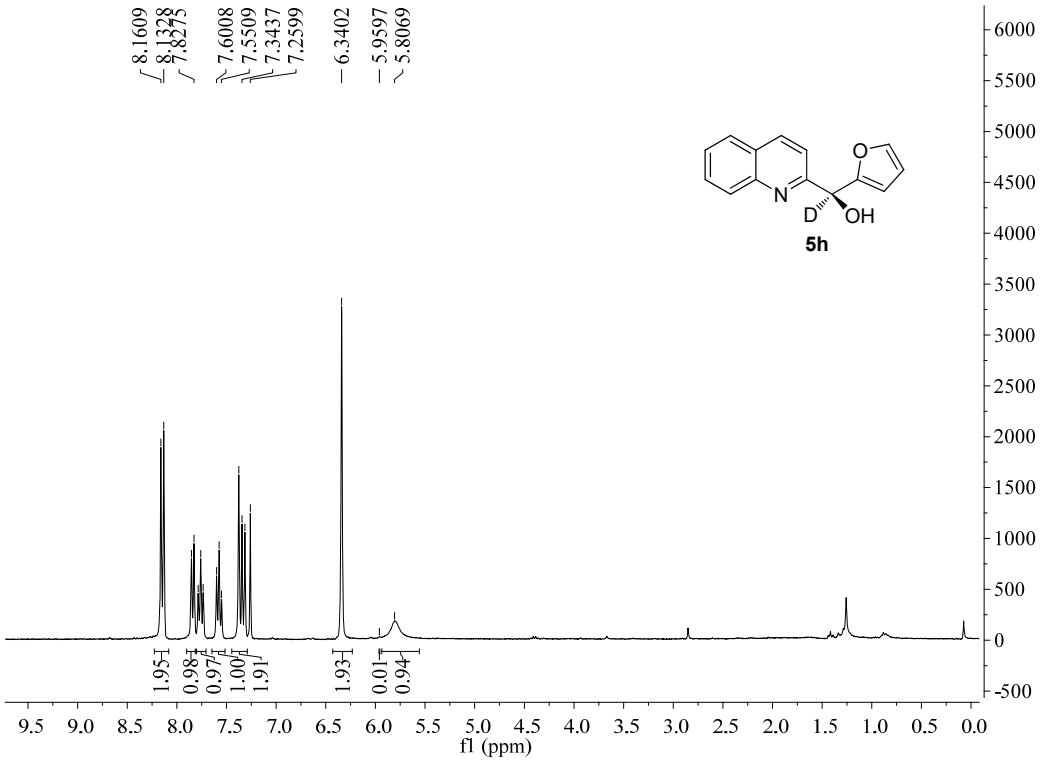

Figure S138. ^{1}H NMR spectrum for **5h**, related to **Figure 5**.

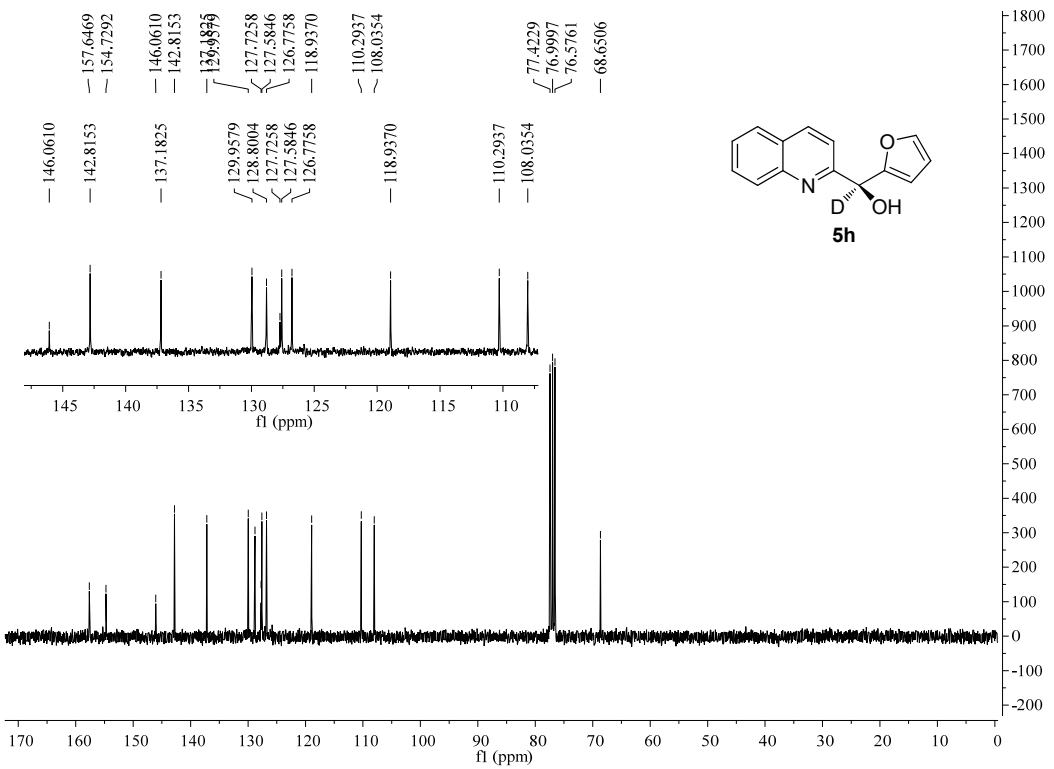

Figure S139. ^{13}C NMR spectrum for **5h**, related to **Figure 5**.

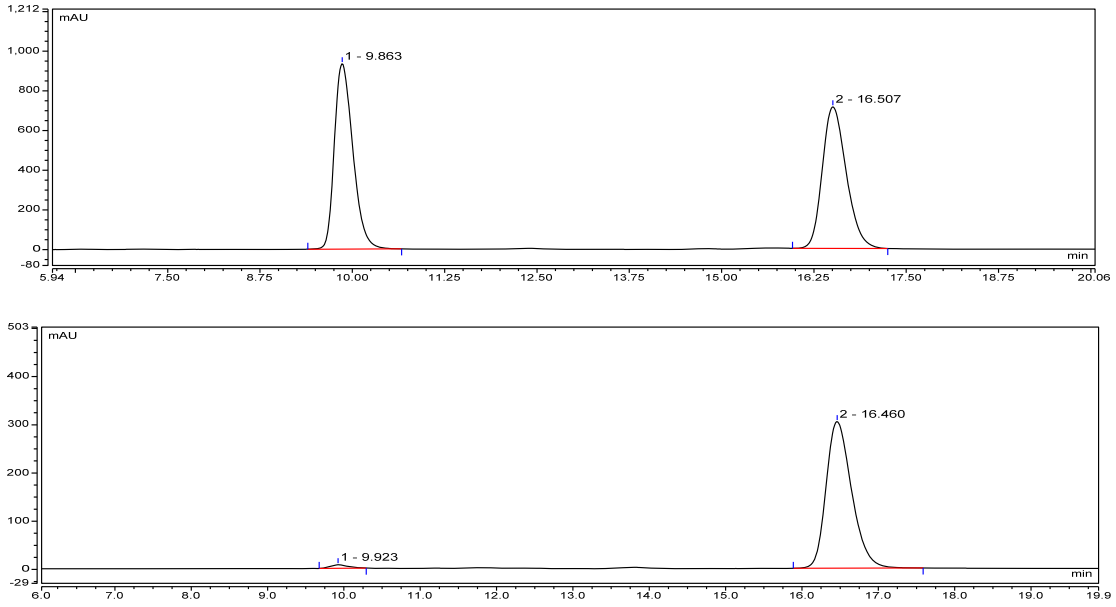

Figure S140. HPLC spectrum for **5h**, related to **Figure 5**.

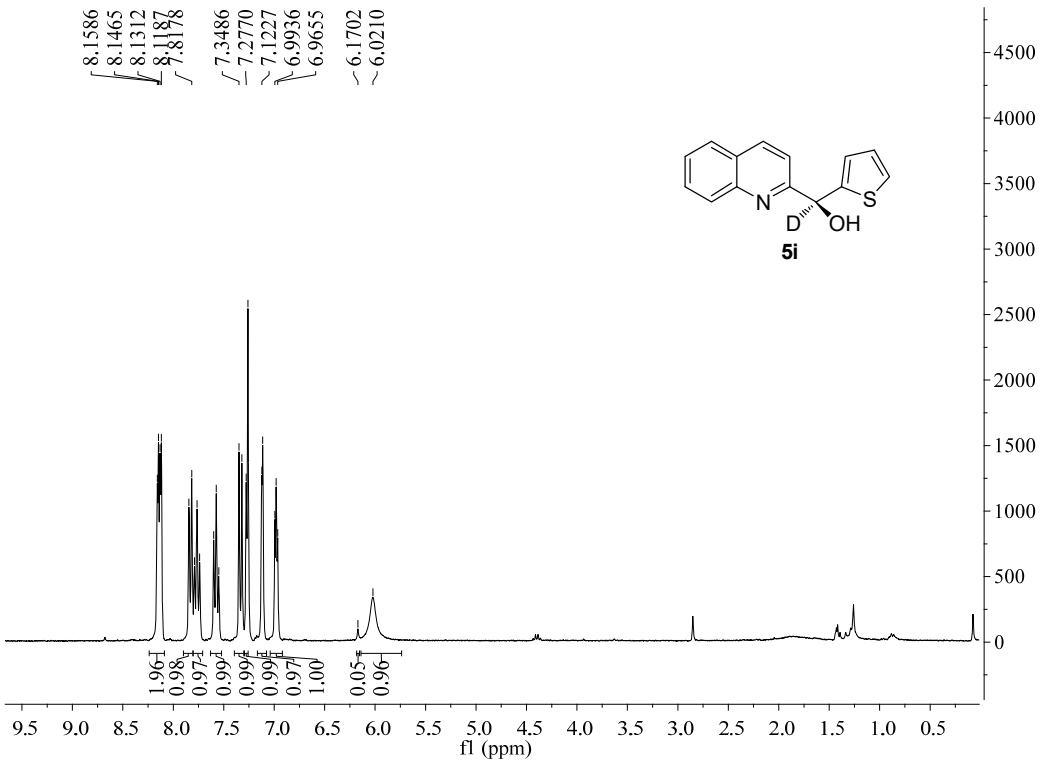

Figure S141. [1]H NMR spectrum for **5i**, related to **Figure 5**.

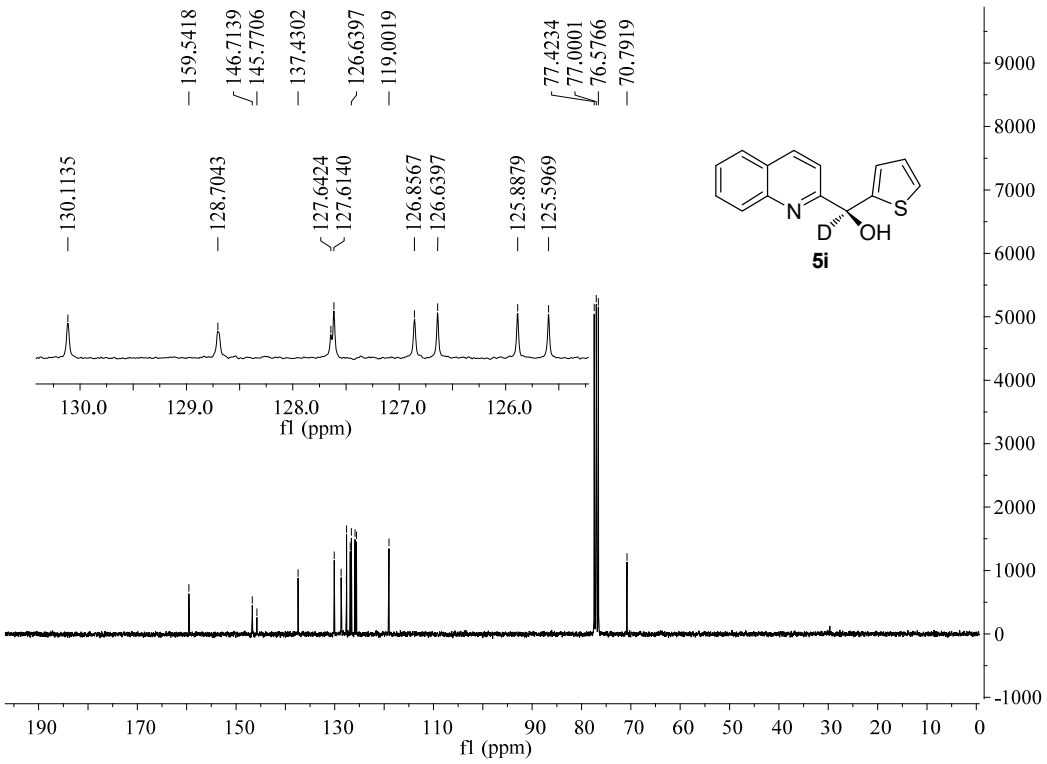

Figure S142. [13]C NMR spectrum for **5i**, related to **Figure 5**.

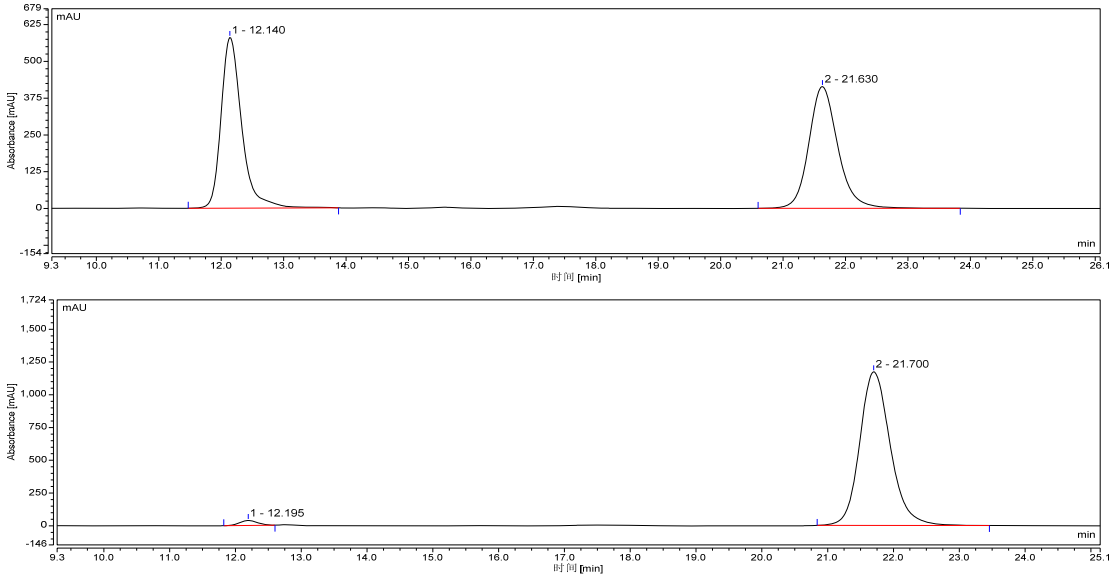

Figure S143. HPLC spectrum for **5i**, related to **Figure 5**.

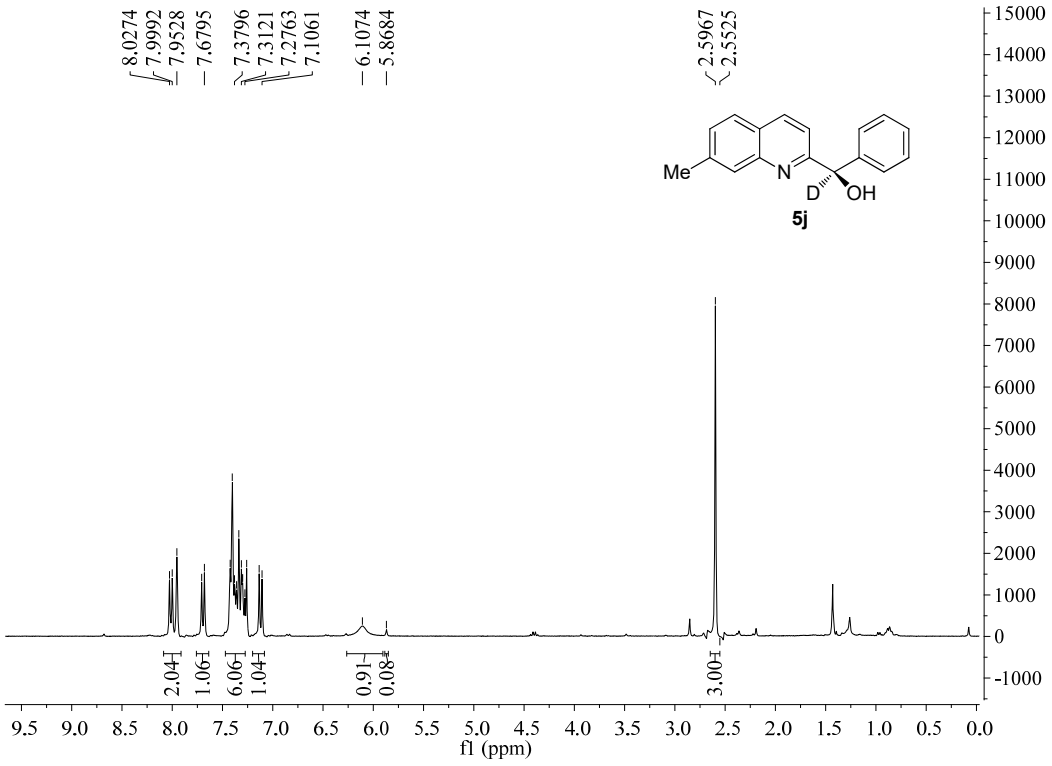

Figure S144. ^{1}H NMR spectrum for **5j**, related to **Figure 5**.

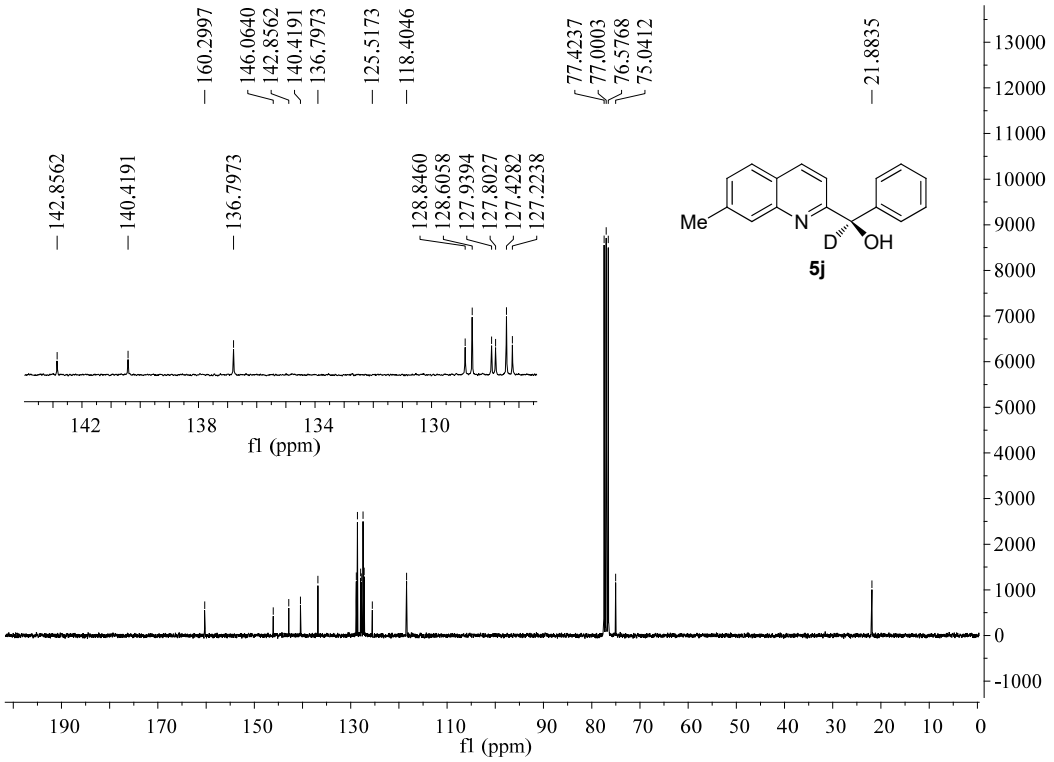

Figure S145. ^{13}C NMR spectrum for **5j**, related to **Figure 5**.

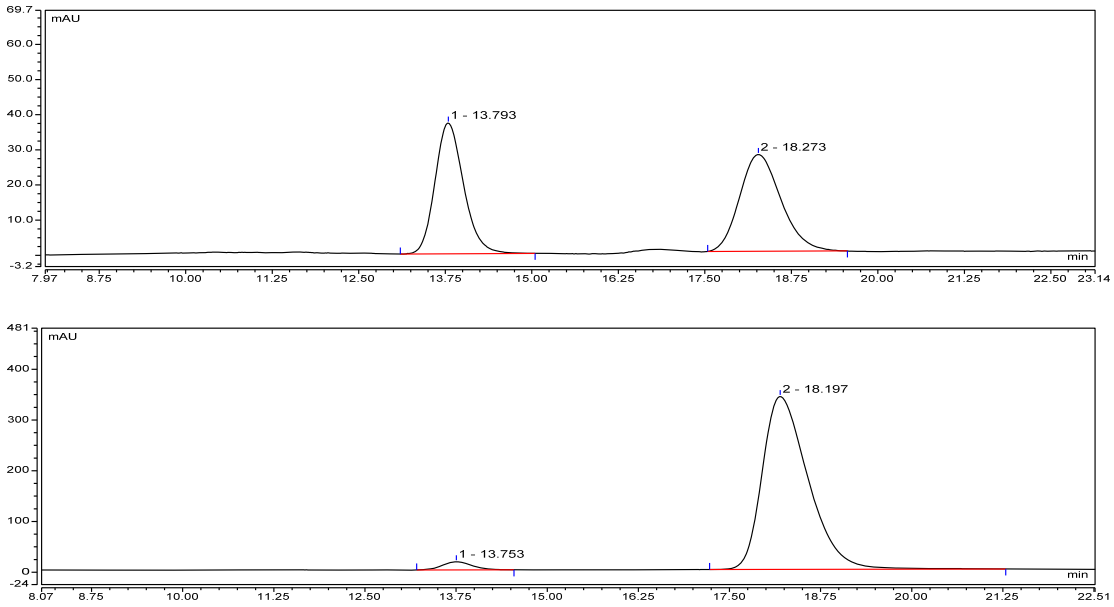

Figure S146. HPLC spectrum for **5j**, related to **Figure 5**.

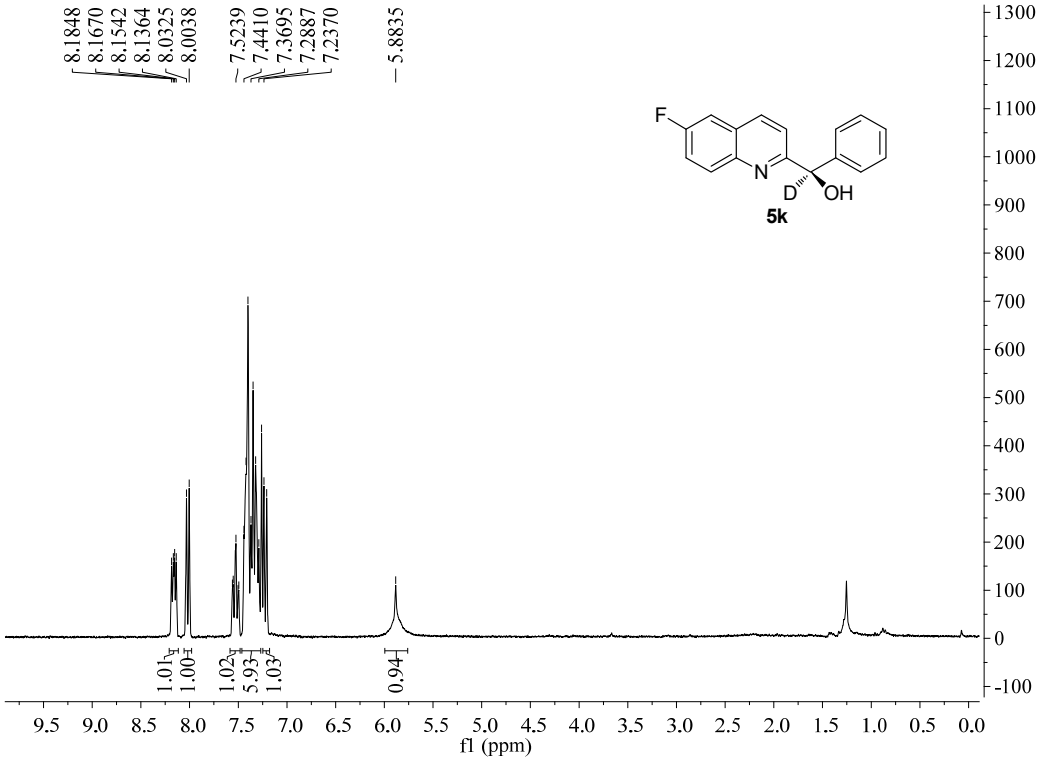

Figure S147. [1]H NMR spectrum for **5k**, related to **Figure 5**.

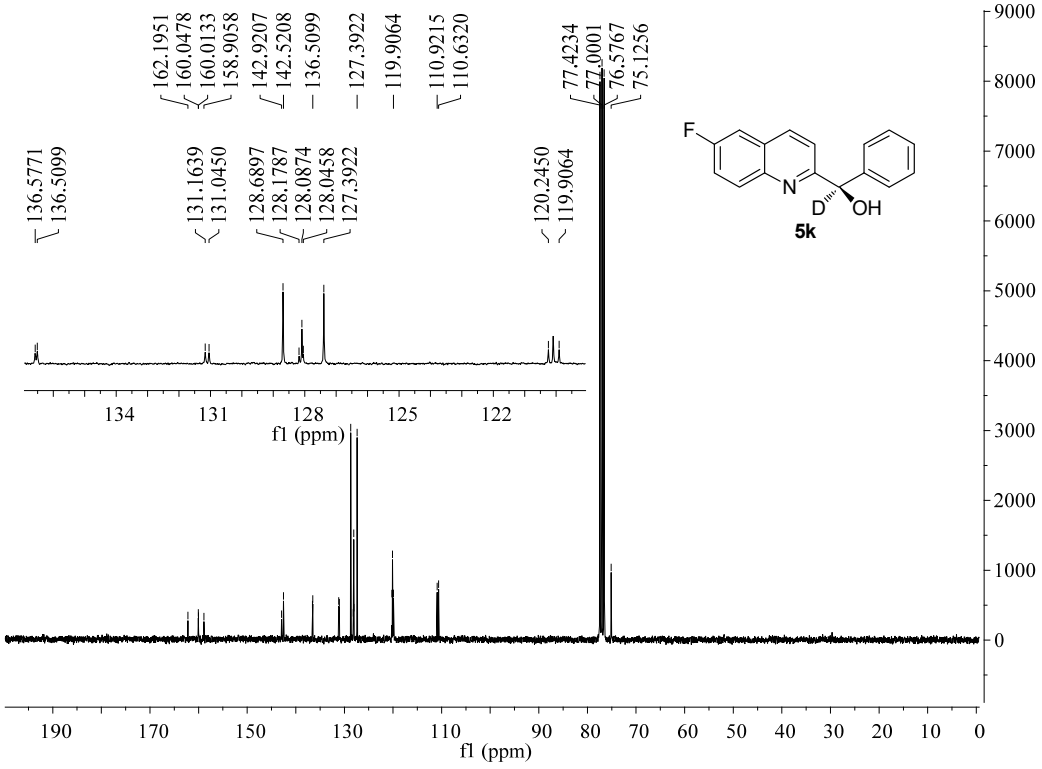

Figure S148. [13]C NMR spectrum for **5k**, related to **Figure 5**.

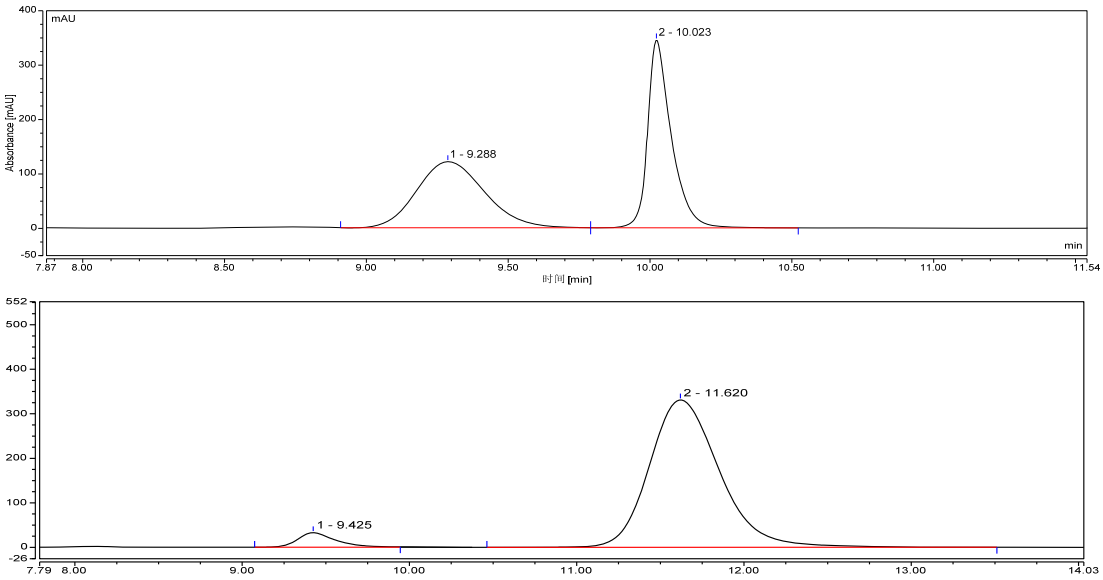

Figure S149. HPLC spectrum for **5k**, related to **Figure 5**.

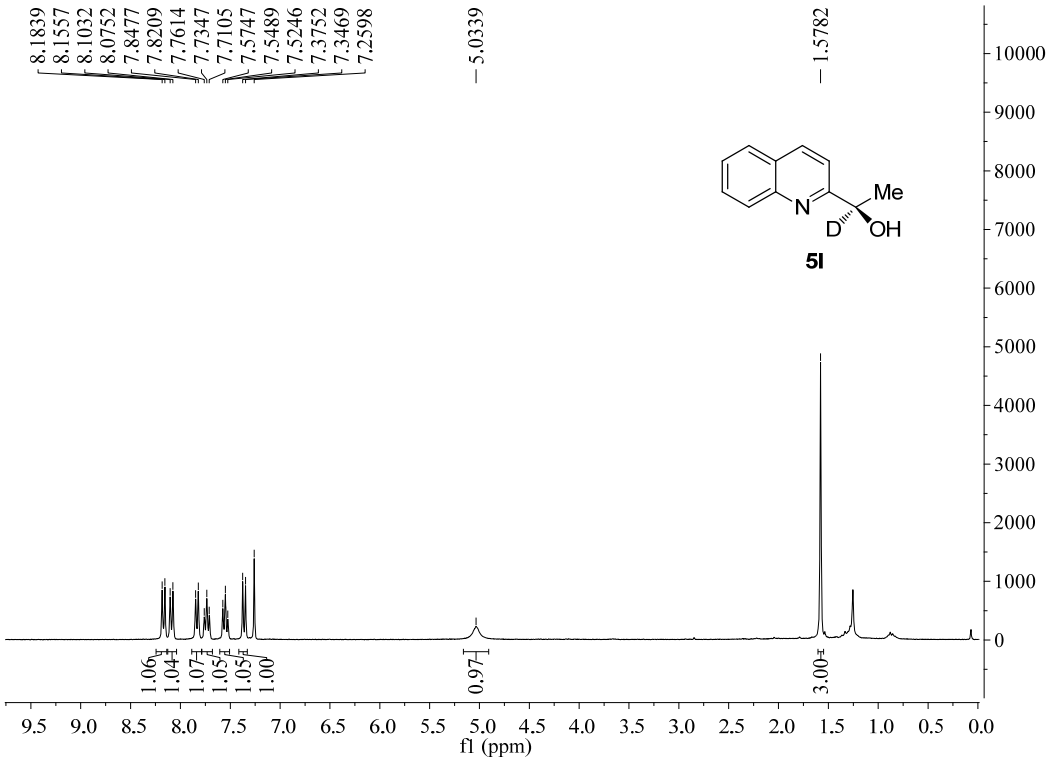

Figure S150. ^{1}H NMR spectrum for **5l**, related to **Figure 5**.

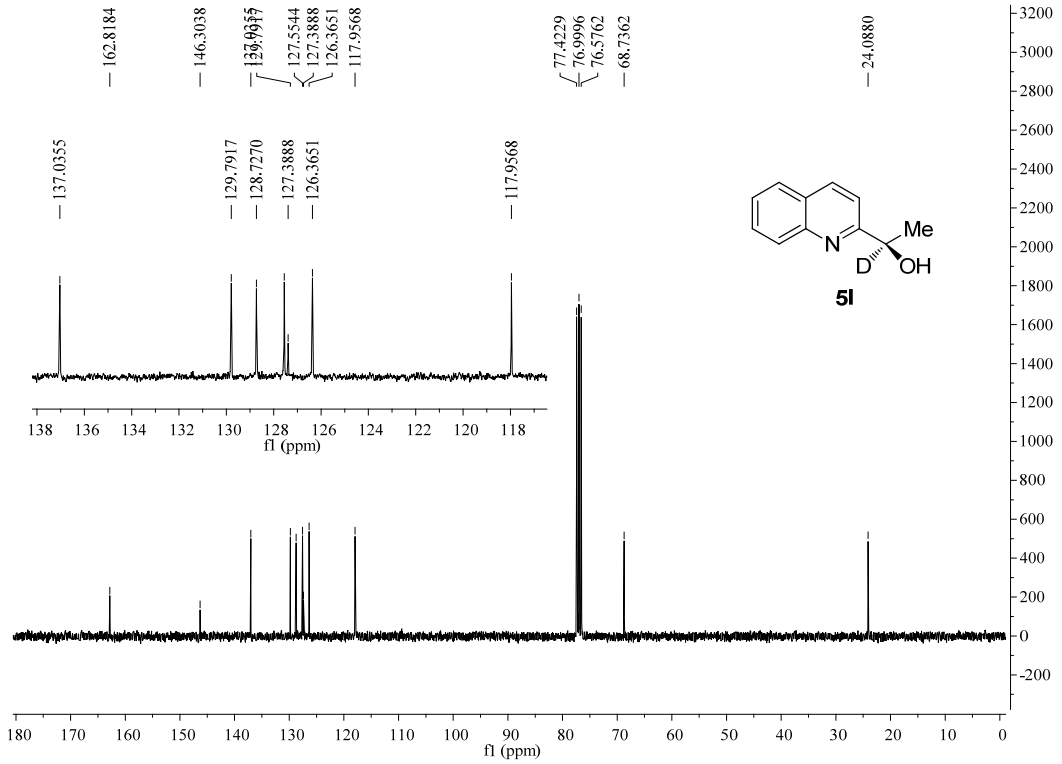

Figure S151. ^{13}C NMR spectrum for **5l**, related to **Figure 5**.

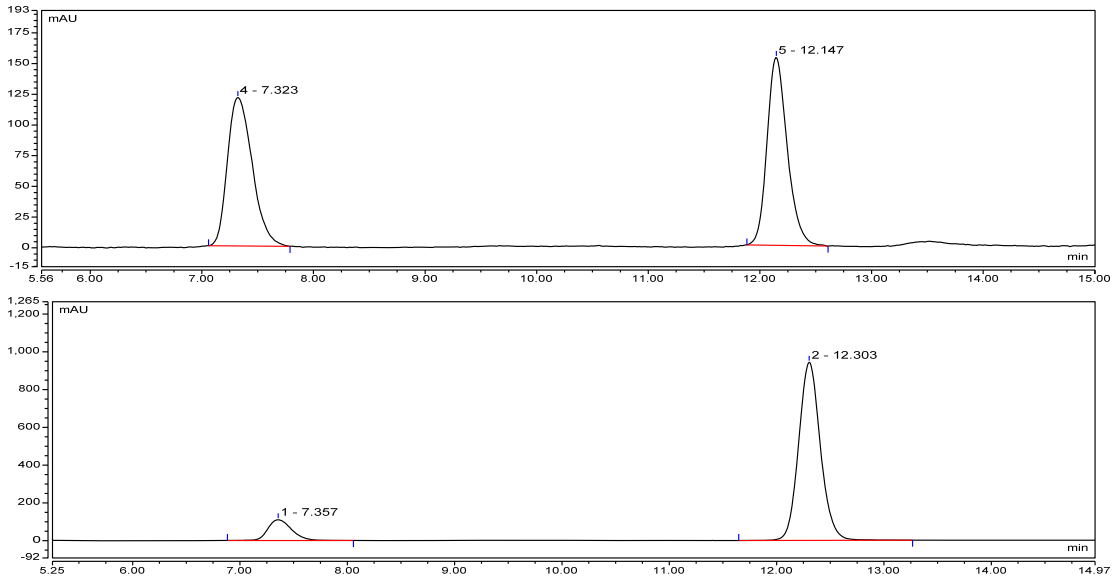

Figure S152. HPLC spectrum for **5l**, related to **Figure 5**.

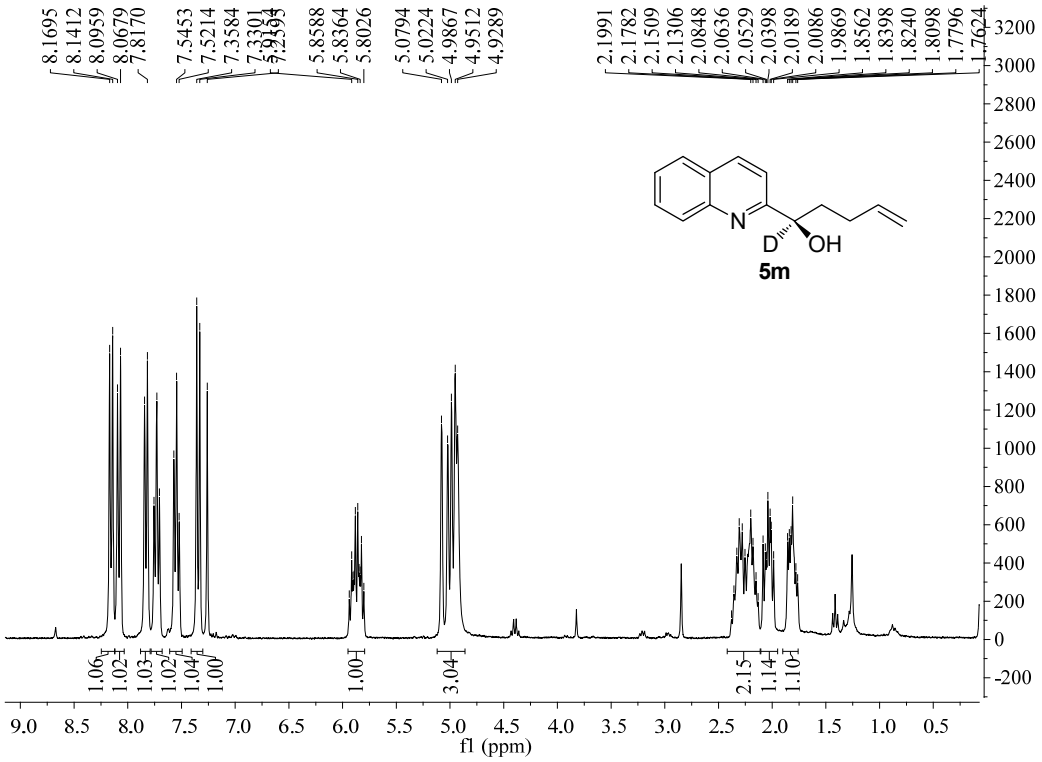

Figure S153. ^{1}H NMR spectrum for **5m**, related to **Figure 5**.

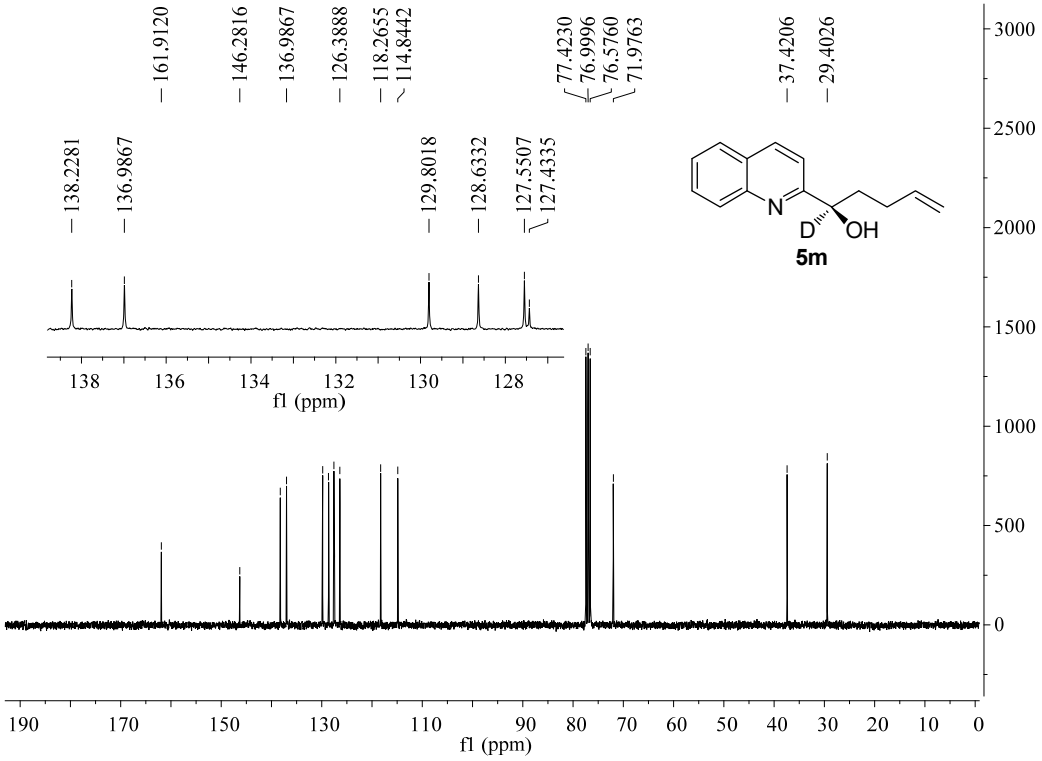

Figure S154. ^{13}C NMR spectrum for **5m**, related to **Figure 5**.

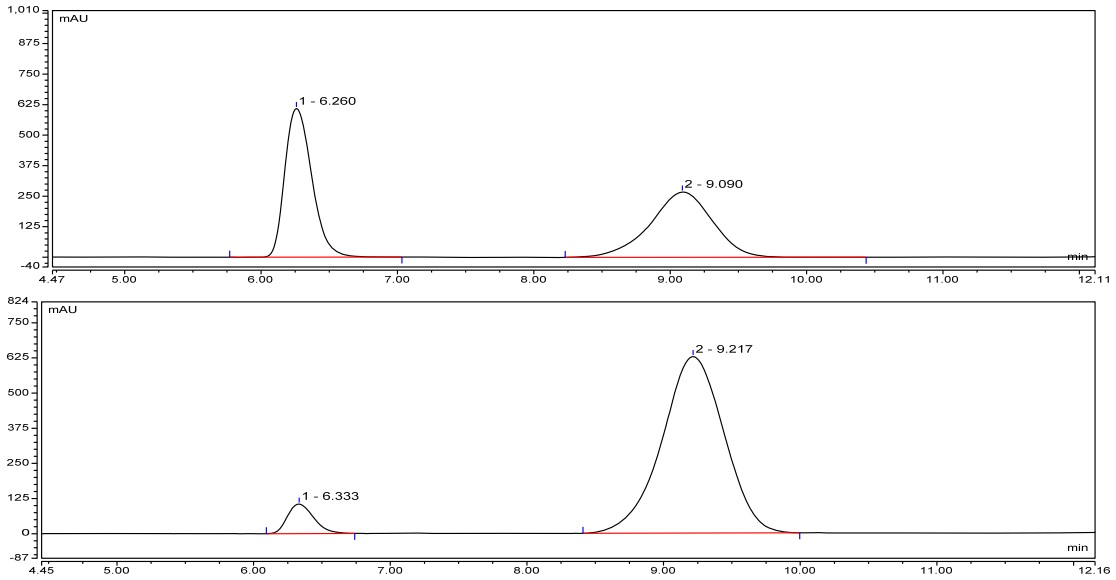

Figure S155. HPLC spectrum for **5m**, related to **Figure 5**.

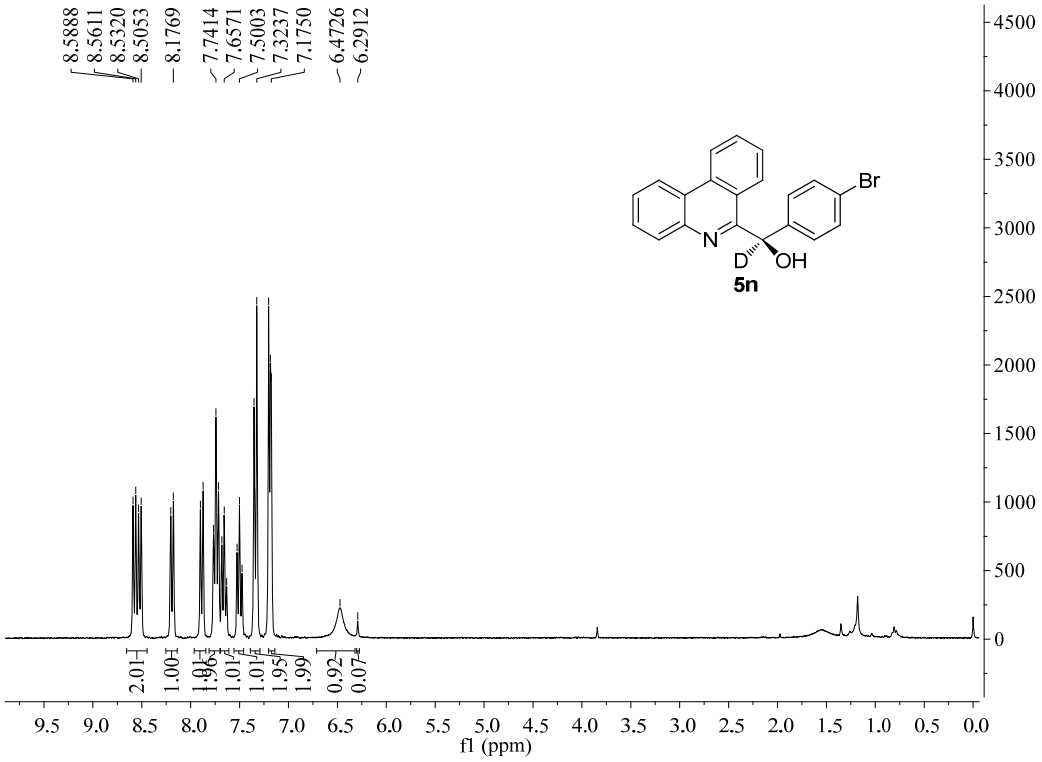

Figure S156. ^{1}H NMR spectrum for **5n**, related to **Figure 5**.

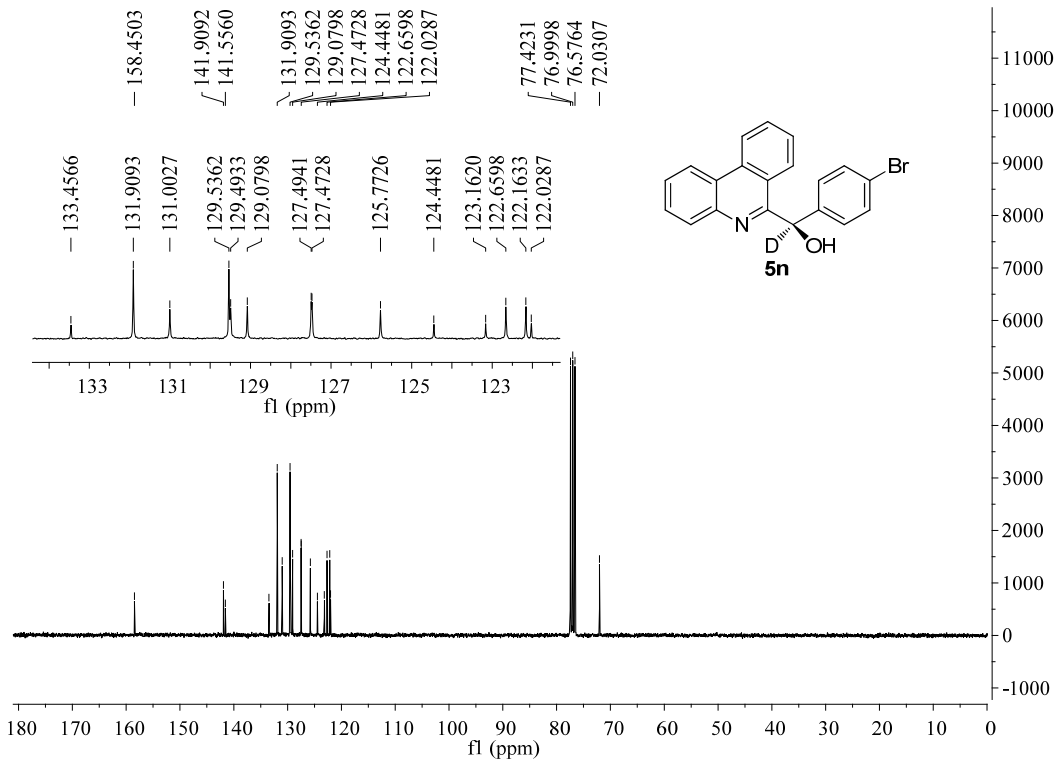

Figure S157. ^{13}C NMR spectrum for **5n**, related to **Figure 5**.

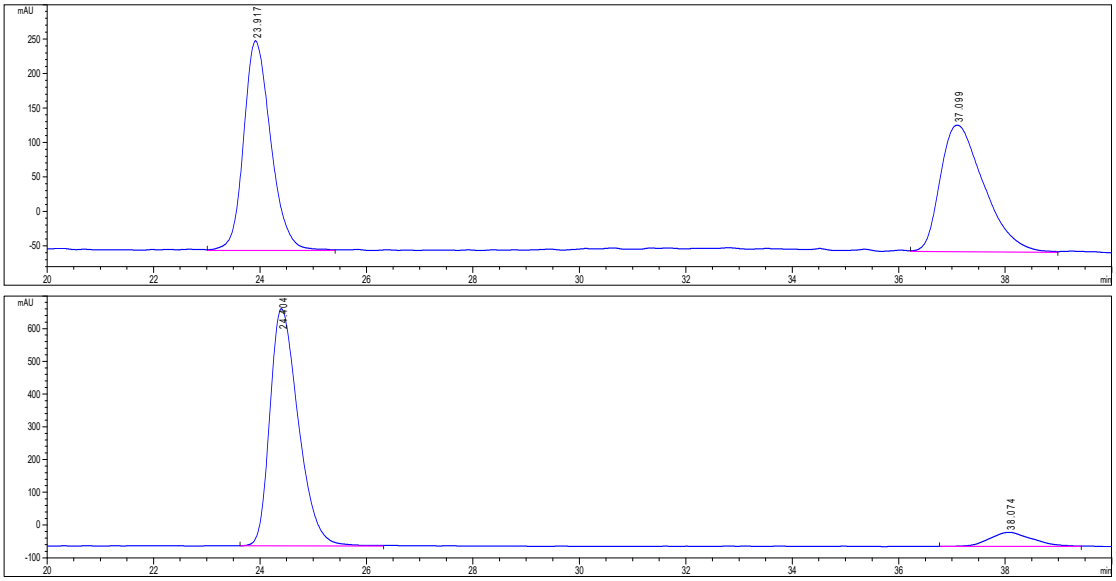

Figure S158. HPLC spectrum for **5n**, related to **Figure 5**.

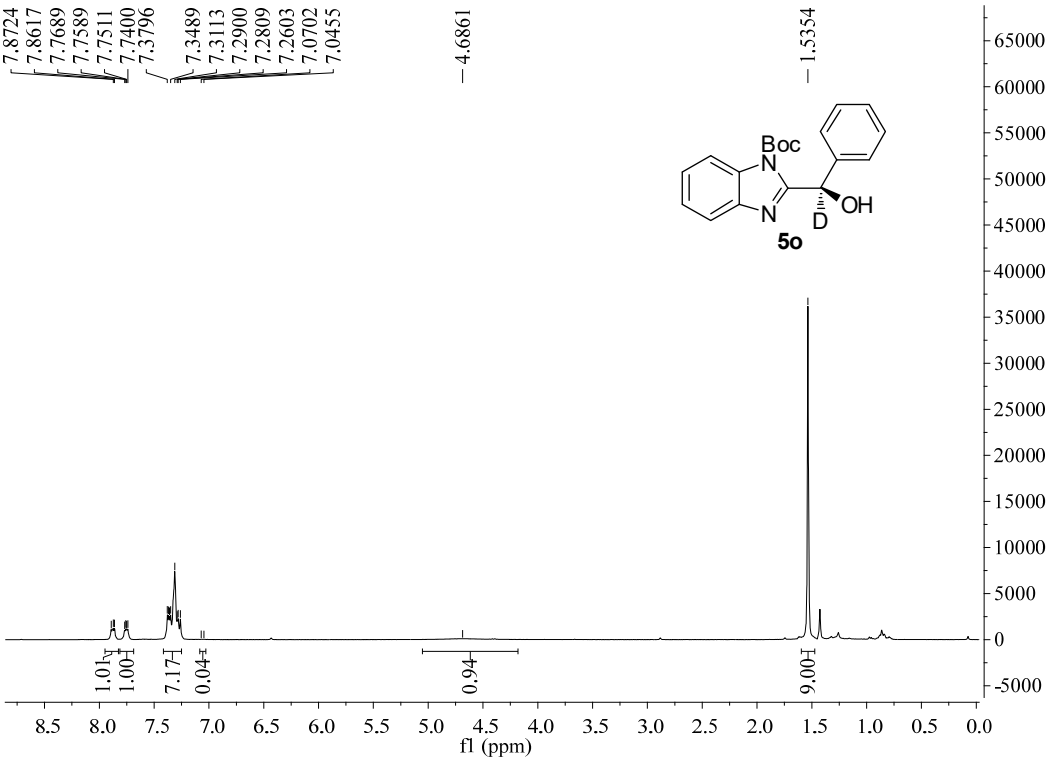

Figure S159. ^{1}H NMR spectrum for **5o**, related to **Figure 5**.

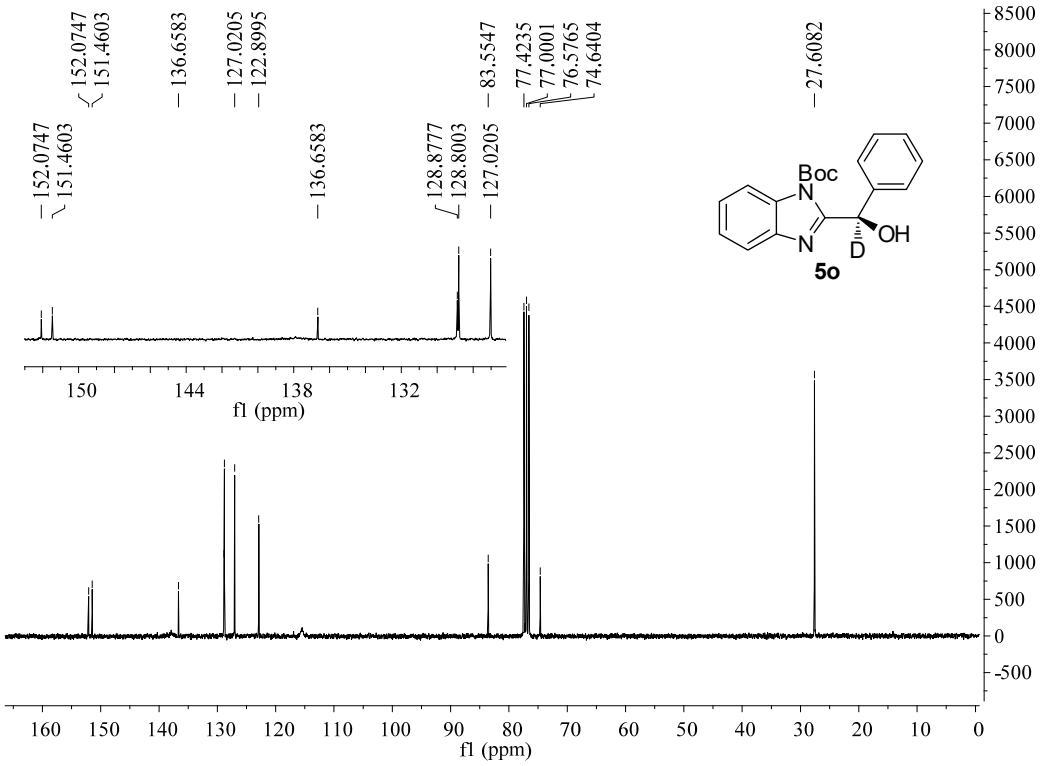

Figure S160. ^{13}C NMR spectrum for **5o**, related to **Figure 5**.

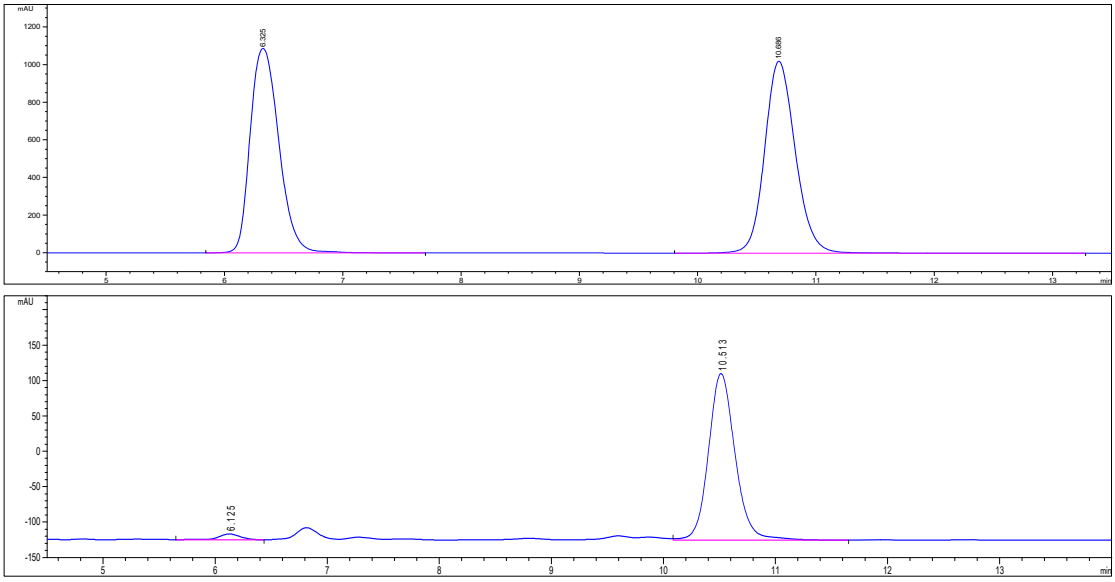

Figure S161. HPLC spectrum for **5o**, related to **Figure 5**.

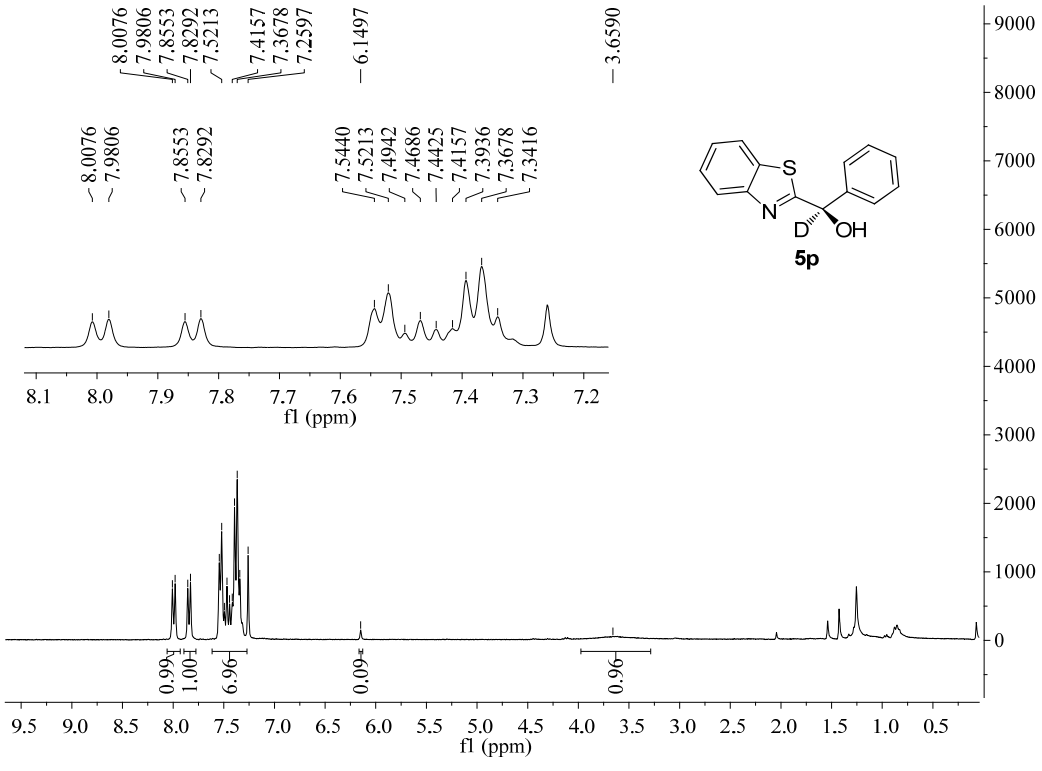

Figure S162. ^{1}H NMR spectrum for **5p**, related to **Figure 5**.

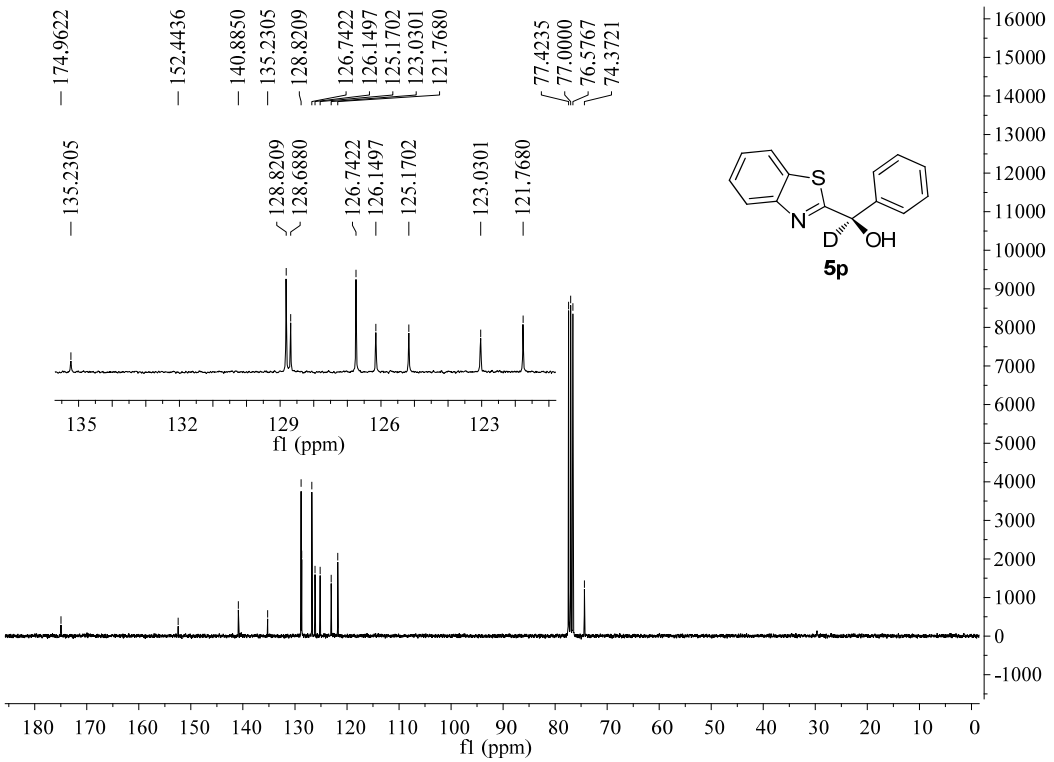

Figure S163. ^{13}C NMR spectrum for **5p**, related to **Figure 5**.

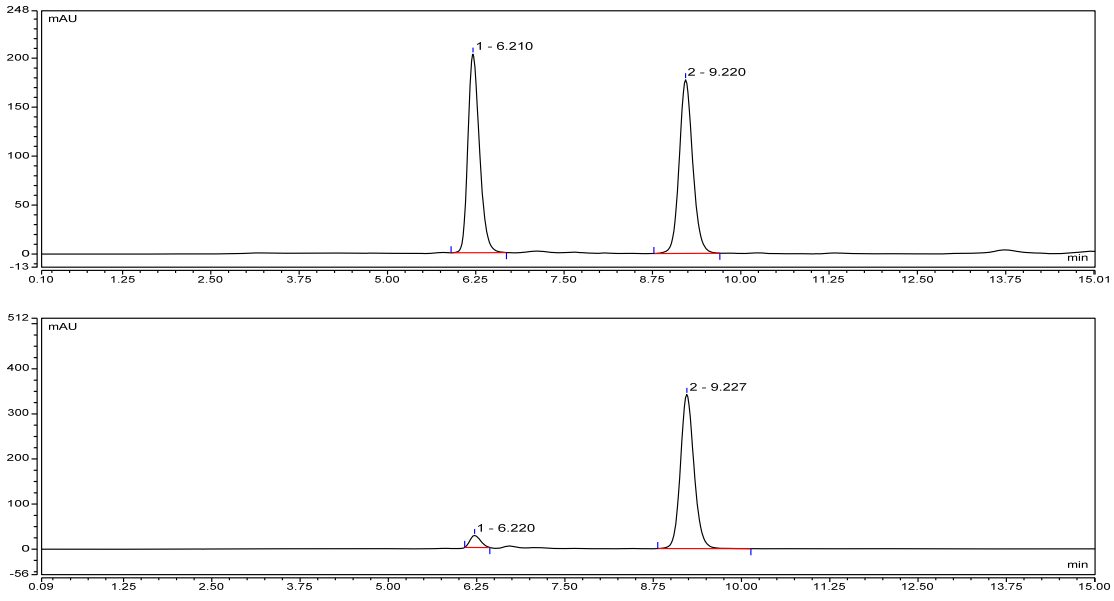

Figure S164. HPLC spectrum for **5p**, related to **Figure 5**.

Supplemental Figures for X-ray Structures of 8 and 5n

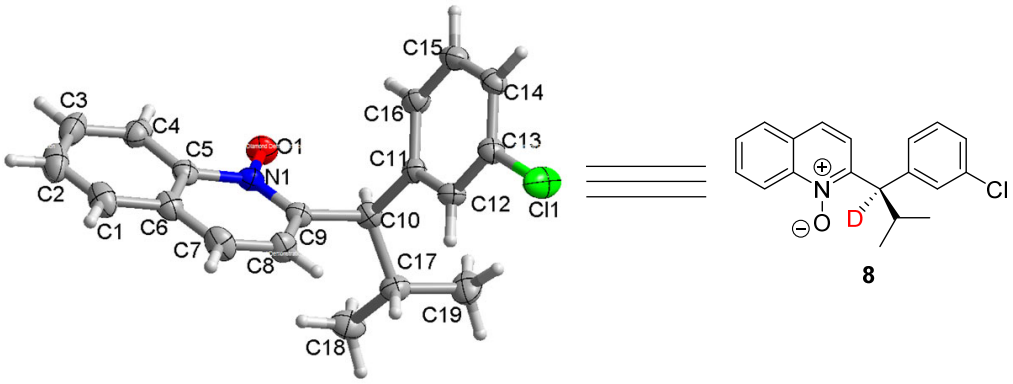

Figure S165. X-ray Structures of **8**, related to **Figure 2**.

The crystal was kept at 293(2) K during data collection. Using Olex2 (Olomanov et al., 2009), the structure was solved with the ShelXS (Sheldrick, 2008) structure solution program using Direct Methods and refined with the ShelXL (Heldrick, 2015) refinement package using Least Squares minimisation. **Crystal Data** for $C_{19}H_{18}ClNO$ (M =311.79 g/mol): orthorhombic, space group $P2_12_12_1$ (no. 19), a = 8.6267(4) Å, b = 11.8128(5) Å, c = 15.8702(8) Å, V = 1617.26(12) Å^3, Z = 4, T = 293(2) K, μ(CuKα) = 2.087 mm^{-1}, *Dcalc* = 1.281 g/cm^3, 5778 reflections measured (9.332 ≤ 2Θ ≤ 134.116), 2890 unique (R_{int} = 0.0306, R_{sigma} = 0.0395) which were used in all calculations. The final R_1 was 0.0408 (I > 2σ(I)) and wR_2 was 0.1044 (all data). CCDC 1893142 contains the supplementary crystallographic data for this paper.

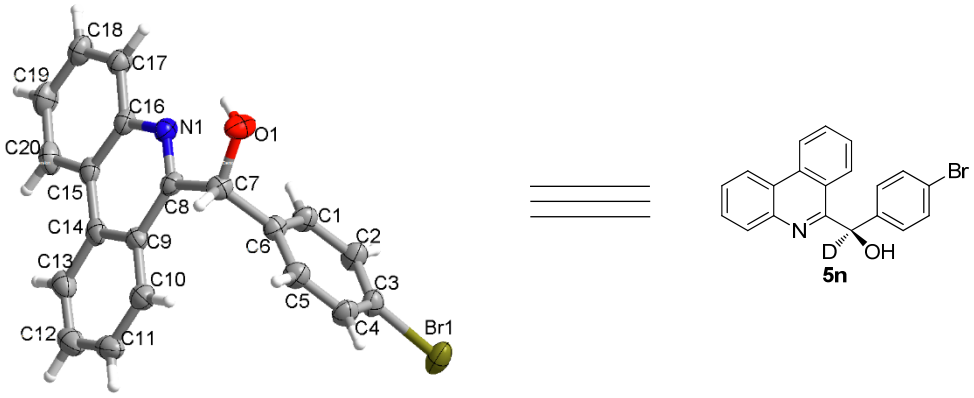

Figure S166. X-ray Structures of **5n**, related to **Figure 5**.

The crystal was kept at 293(2) K during data collection. Using Olex2, the structure was solved with the ShelXS structure solution program using Direct Methods and refined with the ShelXL refinement package using Least Squares minimisation. **Crystal Data** for $C_{20}H_{14}BrNO$ (M = 364.23 g/mol): orthorhombic, space group $P2_12_12_1$ (no. 19), a = 5.14605(13) Å, b =

11.5367(3) Å, c = 26.5758(5) Å, V = 1577.77(7) Å^3, Z = 4, T = 293(2) K, μ(CuKα) = 3.571 mm^{-1}, *Dcalc* = 1.533 g/cm^3, 5862 reflections measured (8.356° ≤ 2Θ ≤ 141.52°), 2971 unique (R_{int} = 0.0302, R_{sigma} = 0.0405) which were used in all calculations. The final R_1 was 0.0392 (I > 2σ(I)) and wR_2 was 0.1066 (all data). CCDC 1902192 contains the supplementary crystallographic data for this paper.

Supplemental Figures for Excitation and Emission spectrums of DPZ and HE-1

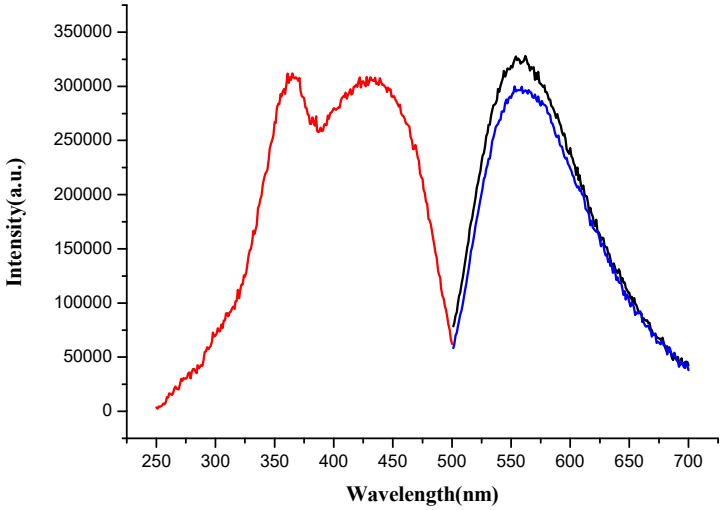

Figure S167. Excitation and emission spectrums of **DPZ**, related to **Figure 3b.**

Excitation *spectrum* was recorded on an EDINBURGH FLS 980 fluorescence spectrophotometer equipped with a monochromated 325 W Xe-arc excitation source and a visible detector (Hamamatsu R928P). Excitation spectra of **DPZ** (5.0×10^{-5} M in CH_2Cl_2) (red) and emission spectrum of **DPZ** (5.0×10^{-5} M in CH_2Cl_2) excitation wavelength as 415 nm (black) and of **DPZ** (5.0×10^{-5} M in CH_2Cl_2) excitation wavelength as 448 nm (blue) was shown in **Figure S167**.

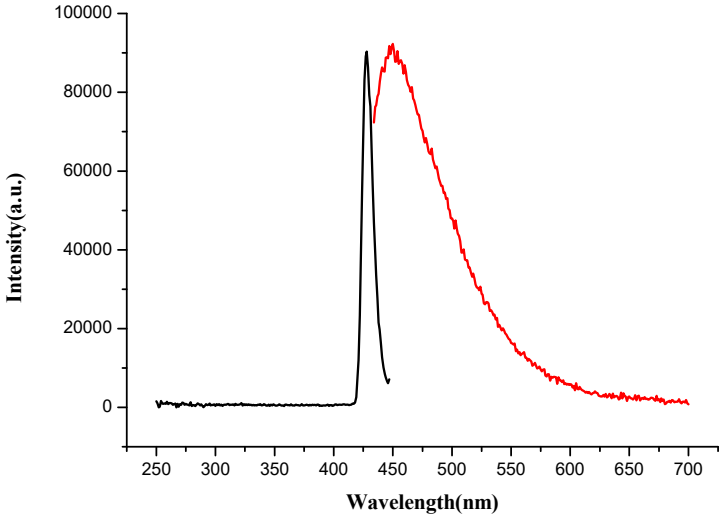

Figure S168. Excitation and emission spectrums of **HE-1**, related to **Figure 3b**.

Excitation *spectrum* was recorded on an EDINBURGH FLS 980 fluorescence spectrophotometer equipped with a monochromated 325 W Xe-arc excitation source and a visible detector (Hamamatsu R928P). The solution of **HE-1** (5.0×10^{-5} M in CH_2Cl_2) was excited at 415 nm and the emission intensity at 450 nm was observed. Based on the fluorescence spectrum of ***HE-1**, the excitation spectrum (black) and emission spectrum (red) of **HE-1** (5.0×10^{-5} M in CH_2Cl_2) was shown in **Figure S168**.

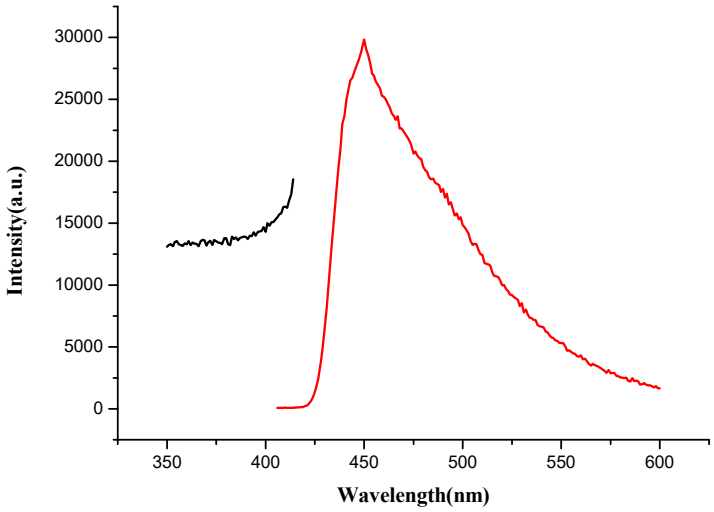

Figure S169. Excitation spectrum of **HE-1** at 380 nm, related to **Figure 3b**.

Excitation *spectrum* was recorded on an EDINBURGH FLS 980 fluorescence spectrophotometer equipped with a monochromated 325 W Xe-arc excitation source and a visible detector (Hamamatsu R928P). The solution of **HE-1** (5.0×10^{-5} M in CH_2Cl_2) was excited at 380 nm and the emission intensity at 449 nm was observed. Based on the fluorescence spectrum of ***HE-1**, the excitation spectrum (black) and emission spectrum (red) of HE-1 (5.0×10^{-5} M in CH_2Cl_2) was shown in **Figure S169**.

Supplemental Figures for the Luminescence Quenching Experiments of DPZ + HE-1, DPZ + 1a, DPZ + HE-1 + 1a, and DPZ + C21 + 1a (excitation wavelength = 448 nm)

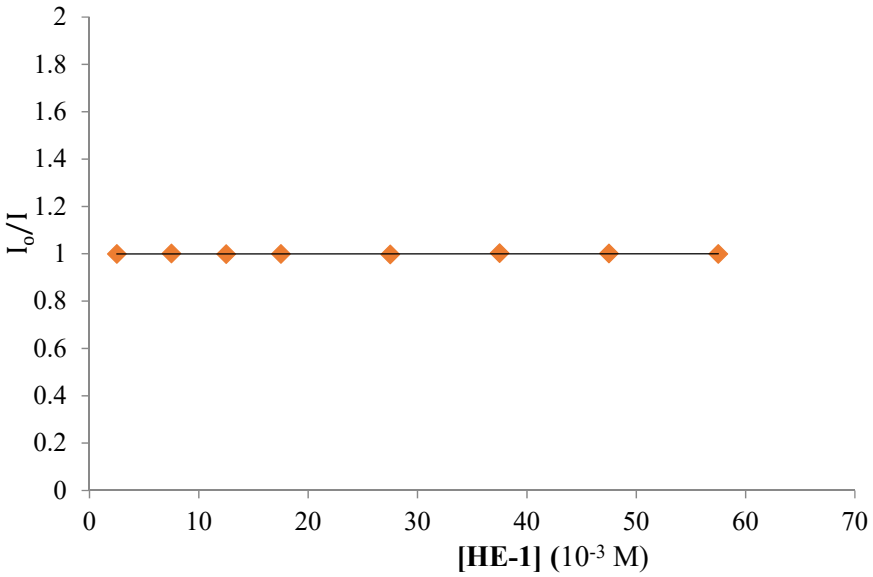

Figure S170. Stern–Volmer quenching experiment of DPZ + **HE-1** at 448 nm, related to **Figure 3b**.

Emission intensities were recorded on a spectrofluorometer. **DPZ** solution was excited at 448 nm and the emission intensity at 544 nm was observed. The appropriate amount of quencher was added to a CH_2Cl_2 solution of **DPZ** (5.0×10^{-5} M) in 3.0 mL volumetric flask under N_2. The solution was transferred to a 3.0 mL quartz cell and the emission spectrum of the sample was collected. Stern-Volmer experiment indicated that **HE-1** does not quench the luminescence of *DPZ in CH_2Cl_2 (**Figure S170**).

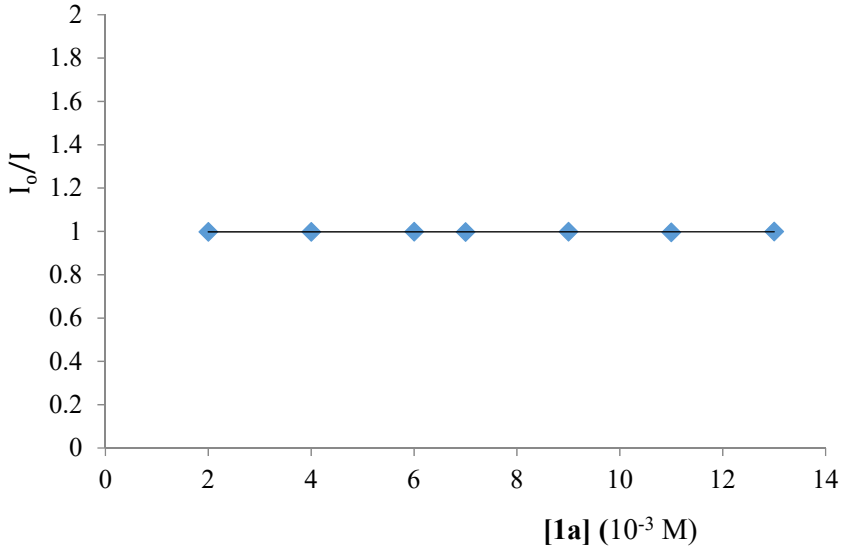

Figure S171. Stern–Volmer quenching experiment of DPZ + **1a** at 448 nm, related to **Figure 3b**.

Emission intensities were recorded on a spectrofluorometer. **DPZ** solution was excited at 448 nm and the emission intensity at 544 nm was observed. The appropriate amount of quencher was added to a CH_2Cl_2 solution of **DPZ** (5.0×10^{-5} M) in 3.0 mL volumetric flask under N_2. The solution was transferred to a 3.0 mL quartz cell and the emission spectrum of the sample was collected. Stern-Volmer experiment indicated that **1a** does not quench the luminescence of *DPZ in CH_2Cl_2 (**Figure S171**).

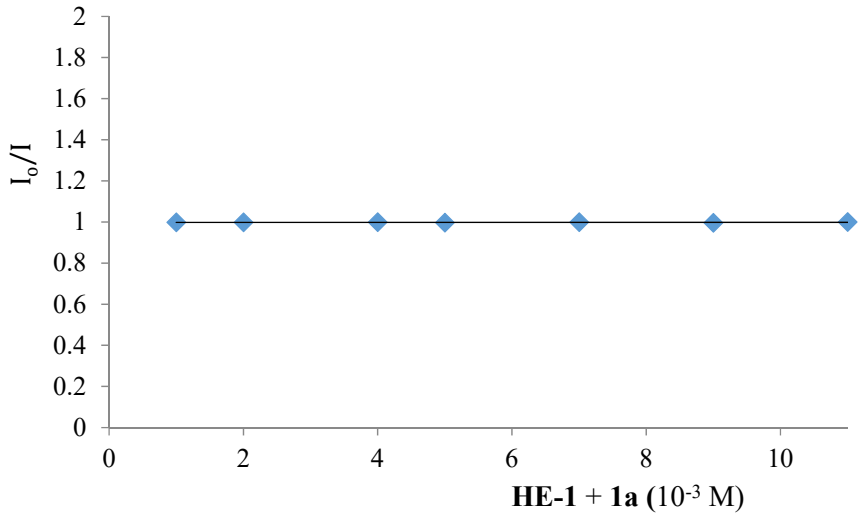

Figure S172. Stern–Volmer quenching experiment of DPZ + **HE-1**+ **1a** at 448 nm, related to **Figure 3b**.

Emission intensities were recorded on a spectrofluorometer. **DPZ** solution was excited at 448 nm and the emission intensity at 544 nm was observed. The appropriate amount of quencher was added to a CH_2Cl_2 solution of **DPZ** (5.0×10^{-5} M) in 3.0 mL volumetric flask under N_2. The solution was transferred to a 3.0 mL quartz cell and the emission spectrum of the sample was collected. Stern-Volmer experiment indicated that **HE-1**+**1a** does not quench the luminescence of *DPZ in CH_2Cl_2 (**Figure S172**).

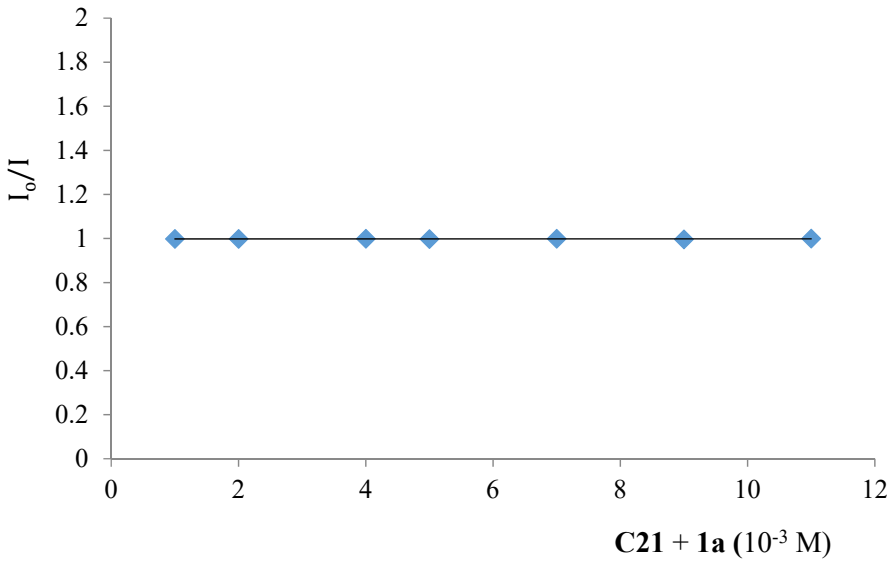

Figure S173. Stern–Volmer quenching experiment of DPZ + **C21** + **1a** at 448 nm, related to **Figure 3b**.

Emission intensities were recorded on a spectrofluorometer. **DPZ** solution was excited at 448 nm and the emission intensity at 544 nm was observed. The appropriate amount of quencher was added to a CH_2Cl_2 solution of **DPZ** (5.0×10^{-5} M) in 3.0 mL volumetric flask under N_2. The solution was transferred to a 3.0 mL quartz cell and the emission spectrum of the sample was collected. Stern-Volmer experiment indicated that **c21** + **1a** does not quench the luminescence of *DPZ in CH_2Cl_2 (**Figure S173**).

Supplemental Figures for the Luminescence Quenching Experiments of DPZ + HE-1, HE-1 + 1a, and DPZ + 1a (excitation wavelength = 415 nm)

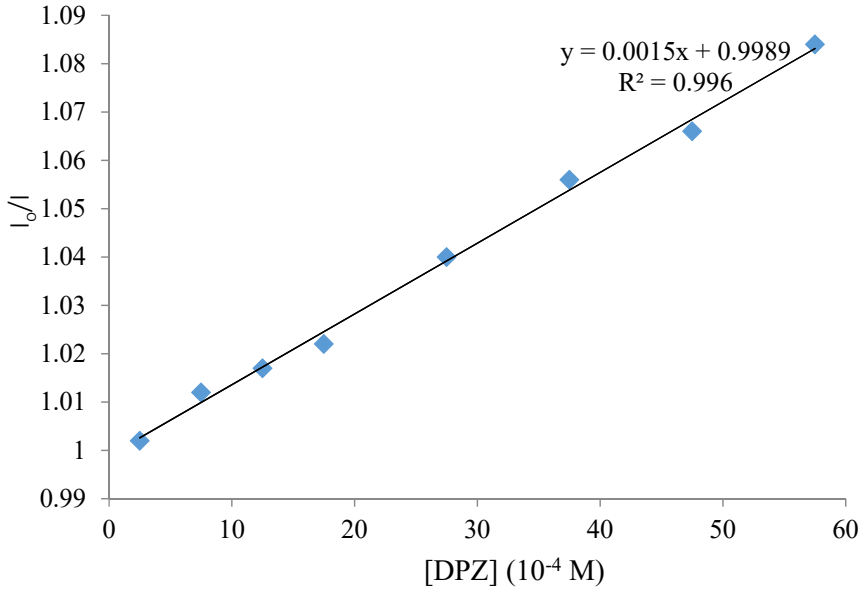

Figure S174. Stern–Volmer quenching experiment of DPZ + **HE-1** at 415 nm, related to **Figure 3b**.

Emission intensities were recorded on a spectrofluorometer. DPZ solution was excited at 415 nm and the emission intensity at 546 nm was observed. The appropriate amount of quencher was added to a CH_2Cl_2 solution of **DPZ** (5.0×10^{-5} M) in 3.0 mL volumetric flask under N_2. The solution was transferred to a 3.0 mL quartz cell and the emission spectrum of the sample was collected. Stern-Volmer experiment indicated that **HE-1** quenches the luminescence of *DPZ in CH_2Cl_2 (**Figure S174**).

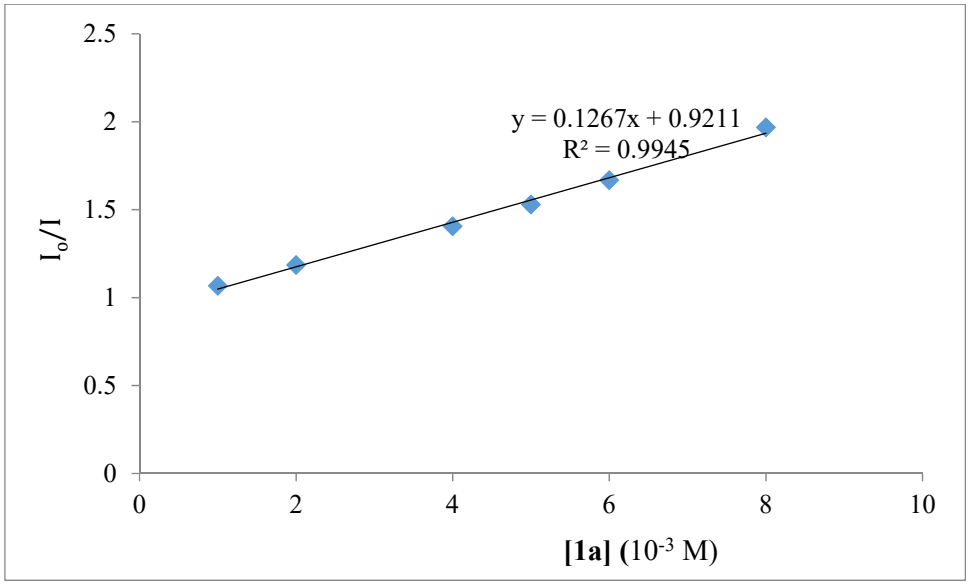

Figure S175. Stern–Volmer quenching experiment of **HE-1** + **1a** at 415 nm, related to **Figure 3b**.

Emission intensities were recorded on a spectrofluorometer. **HE-1** solution was excited at 230 nm and the emission intensity at 415 nm was observed. The appropriate amount of quencher was added to a CH_2Cl_2 solution of **HE-1** (5.0×10^{-3} M) in 3.0 mL volumetric flask under N_2. The solution was transferred to a 2.0 mL quartz cell and the emission spectrum of the sample was collected (**Figure S175**).

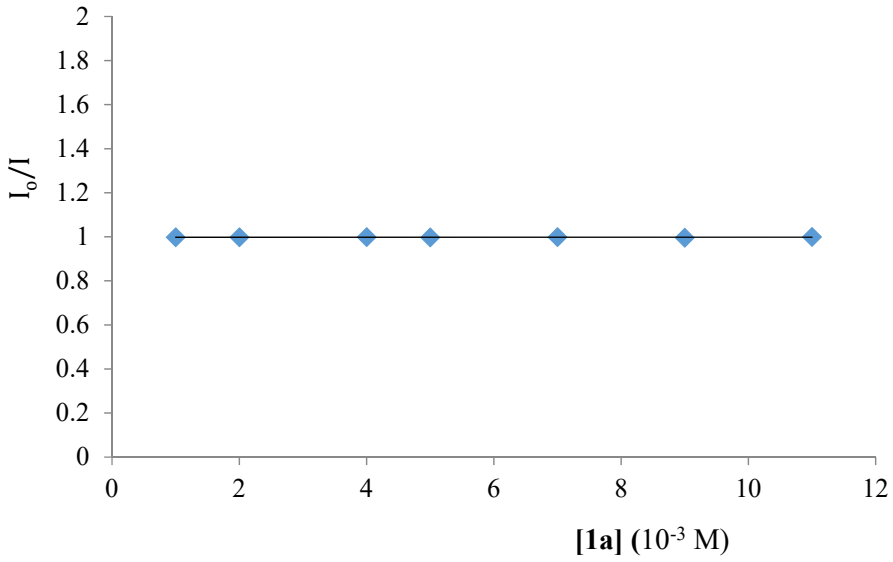

Figure S176. Stern–Volmer quenching experiment of **DPZ** + **1a** at 415 nm, related to **Figure 3b**.

Emission intensities were recorded on a spectrofluorometer. **DPZ** solution was excited at 230 nm and the emission intensity at 415 nm was observed. A solution of **1a** (5.0×10^{-3} M) in CH_2Cl_2 was added to the appropriate amount of quencher in 3.0 mL volumetric flask under N_2. The solution was transferred to a 2.0 mL quartz cell and the emission spectrum of the sample was collected (**Figure S176**).

Supplemental Figures for the Emission spectrums of the blue LED light

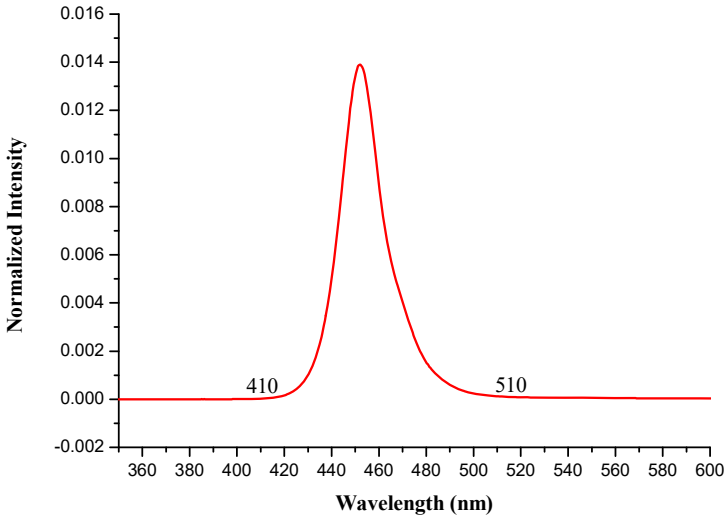

Figure S177. Emission spectrum of the used 3 W blue LED light, related to **Figure 3b**.

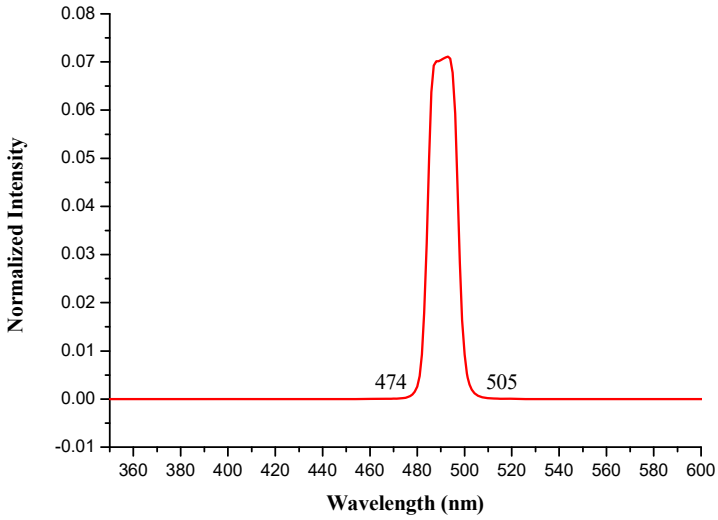

Figure S177. Emission spectrum of the LED light with the laser line filter *(CWL = 490 nm)*, related to **Figure 3b**.

Supplemental Figures for the Cyclic Voltammetry spectrums of ferrocene, 1a, 1ee, 1ff, and 4a

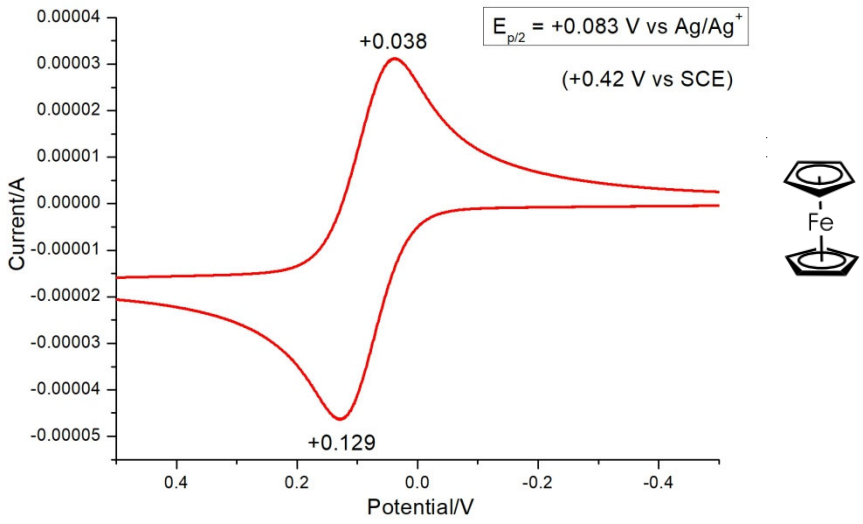

Figure S178. Cyclic voltammogram of ferrocene in MeCN referenced to $Ag/AgNO_3$, related to **Figure 3b**.

Electrochemical potentials were obtained with a standard set of conditions to main internal consistency. Cyclic voltammograms were collected with a potentiostat. Samples were prepared with 0.01 mmol of ferrocene in 10 mL anhydrous acetonitrile. Measurements employed a radium glassy carbon working electrode, platinum wire counter electrode, 0.1 M $[Bu_4N][PF_6]$ in acetonitrile, 0.01 M silver-silver nitrate reference electrode. The obtained value was converted to SCE by adding 0.337 V.

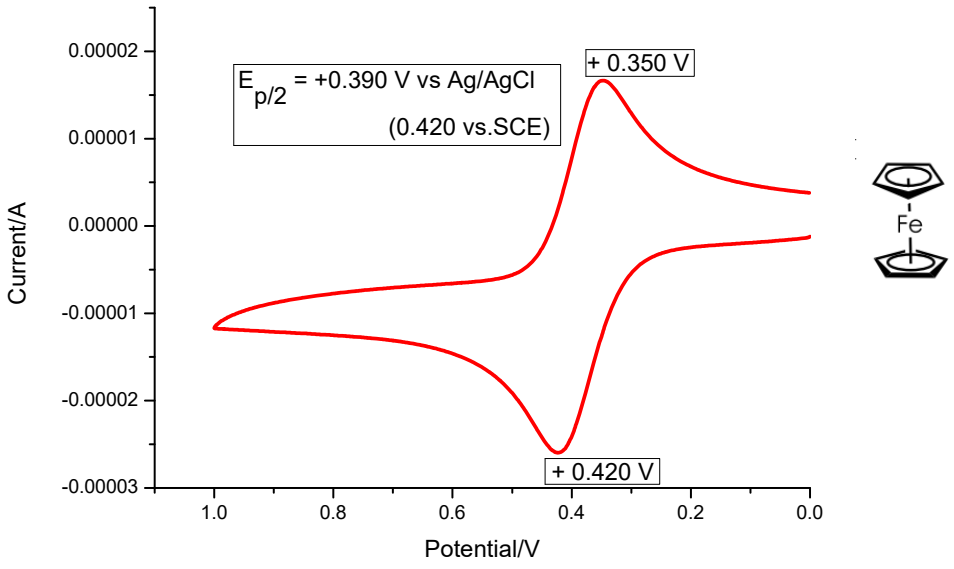

Figure S179. Cyclic voltammogram of ferrocene in MeCN referenced to Ag/AgCl, related to **Figure 3b**.

Electrochemical potentials were obtained with a standard set of conditions to main internal consistency. Cyclic voltammograms were collected with a potentiostat. Samples were prepared with 0.01 mmol of ferrocene in 10 mL anhydrous acetonitrile. Measurements employed a radium glassy carbon working electrode, platinum wire counter electrode, 0.1 M $[Bu_4N][PF_6]$ in acetonitrile, 0.01 M silver-silver chloride reference electrode. The obtained value was converted to SCE by adding 0.03 V.

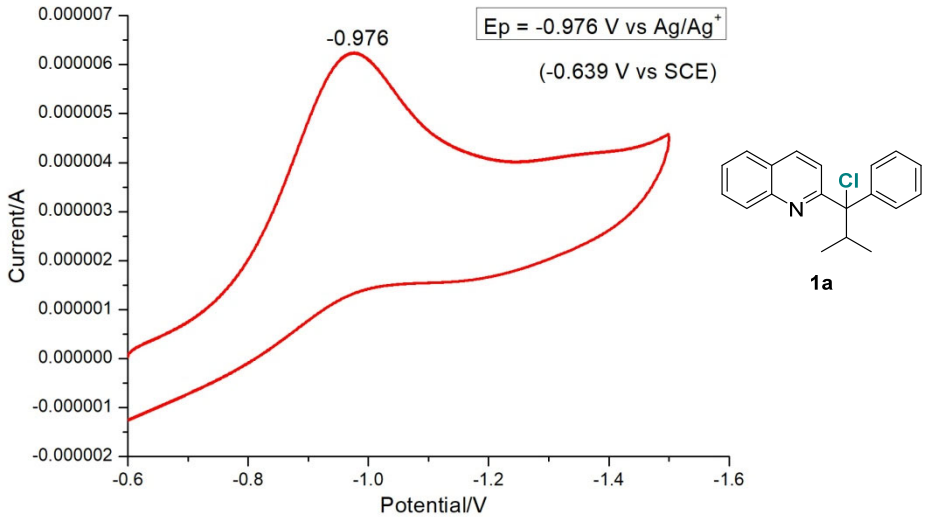

Figure S180. Cyclic voltammogram of **1a** in MeCN, related to **Figure 3b**.

Electrochemical potentials were obtained with a standard set of conditions to main internal consistency. Cyclic voltammograms were collected with a potentiostat. Samples were prepared with 0.01 mmol of **1a** in 10 mL anhydrous acetonitrile. Measurements employed a radium glassy carbon working electrode, platinum wire counter electrode, 0.1 M $[Bu_4N][PF_6]$ in acetonitrile, 0.01 M silver-silver nitrate reference electrode. The value of **1a** converted to SCE was E_p = –0.639 V vs SCE.

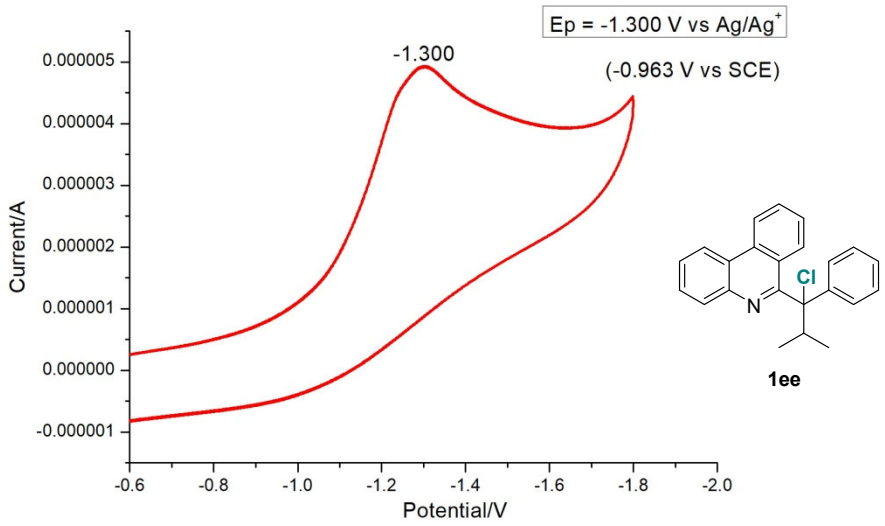

Figure S181. Cyclic voltammogram of **1ee** in MeCN, related to **Figure 3b**.

Electrochemical potentials were obtained with a standard set of conditions to main internal consistency. Cyclic voltammograms were collected with a potentiostat. Samples were prepared with 0.02 mmol of **1ee** in 10 mL anhydrous acetonitrile. Measurements employed a radium glassy carbon working electrode, platinum wire counter electrode, 0.1 M $[Bu_4N][PF_6]$ in acetonitrile, 0.01 M silver-silver nitrate reference electrode. The obtained value was referenced to $Ag/AgNO_3$. The value of **1ee** converted to SCE was E_p = –0.963 V vs SCE.

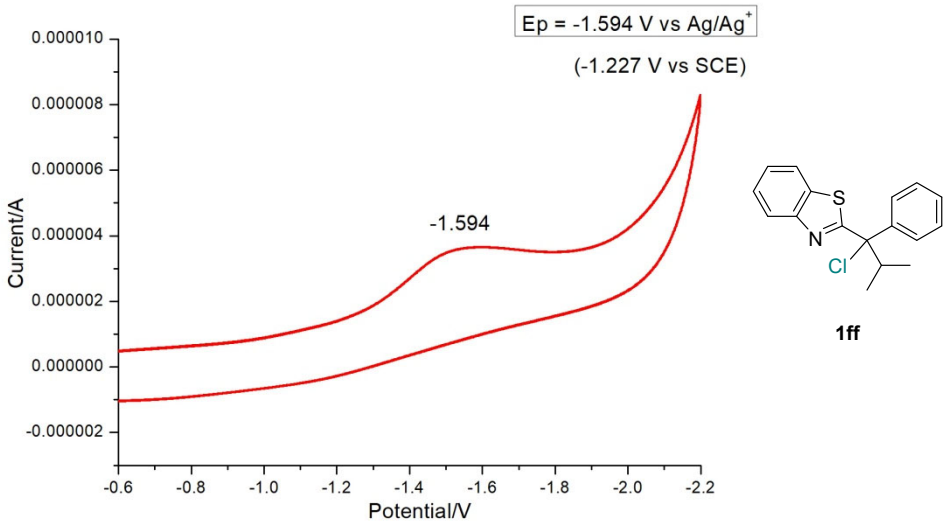

Figure S182. Cyclic voltammogram of **1ff** in MeCN, related to **Figure 3b**.

Electrochemical potentials were obtained with a standard set of conditions to main internal consistency. Cyclic voltammograms were collected with a potentiostat. Samples were prepared with 0.01 mmol of **1ff** in 10 mL anhydrous acetonitrile. Measurements employed a radium glassy carbon working electrode, platinum wire counter electrode, 0.1 M $[Bu_4N][PF_6]$ in acetonitrile, 0.01 M silver-silver nitrate reference electrode. The obtained value was referenced to $Ag/AgNO_3$. The value of **1ff** converted to SCE was $E_p = -1.227$ V vs SCE.

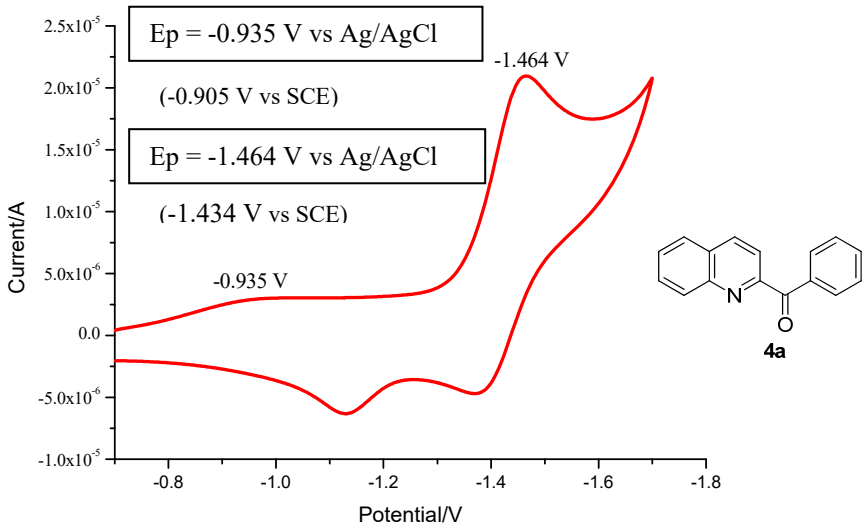

Figure S183. Cyclic voltammogram of **4a** in MeCN, related to **Figure 3b**.

Cyclic voltammetry experiments were performed on a CHI600E Workstation. Measurements were performed for anhydrous acetonitrile solutions ([**4a**] = 1.0 mM, [$(NBu_4)PF_6$] = 0.10 M) with a radium glassy carbon (working electrode) and platinum wire (counter electrode), and a Ag/AgCl reference electrode under N_2 at room temperature. The scan rate was 50 mV/s. Ferrocene (Cp_2Fe) was used as a reference. The value of **4a** converted to SCE was E_{p1} = –0.905 V vs SCE, E_{p2} = –0.935 V vs SCE.

DFT calculations

All the DFT calculations were performed with the Gaussian 09 program (Frisch et al., 1993). The geometries optimizations were performed at the B3LYP/6-31G(d) level. The vibrational frequencies were computed at the same level to check whether each optimized structure is an energy minimum or a transition state (TS) and to evaluate its thermal corrections at 298 K. The Gibbs free energies (ΔG) are used to discuss the reaction.

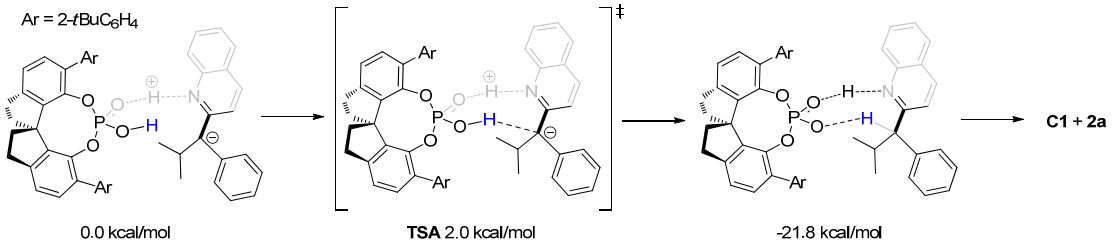

Figure S184. The calculated ΔG values (in kcal/mol) for the formation of (*R*)-**2a** through **TSA** transition state. The ΔG for the generation of **TSA** transition state are 2.0 kcal/mol and The ΔG of the formation of **C1** and **2a** are -21.8 kcal/mol, related to **Figures 3 and 4**.

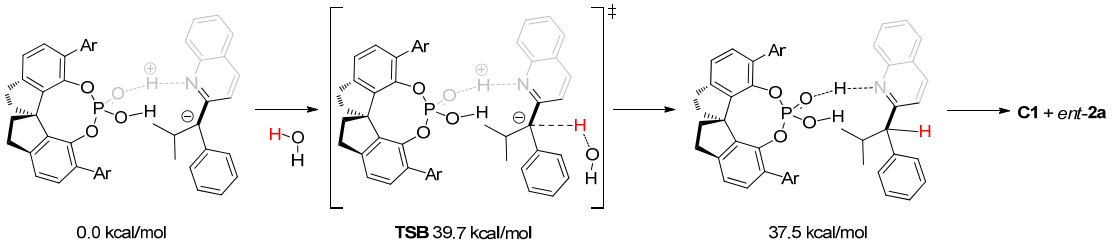

Figure S185. The calculated ΔG values (in kcal/mol) for the formation of (*ent*)-**2a** through **TSB** transition state. The ΔG for the generation of **TSB** transition state are 39.7 kcal/mol and The ΔG of the formation of **C1** and (*ent*)-**2a** are 37.5 kcal/mol, related to **Figures 3 and 4**.

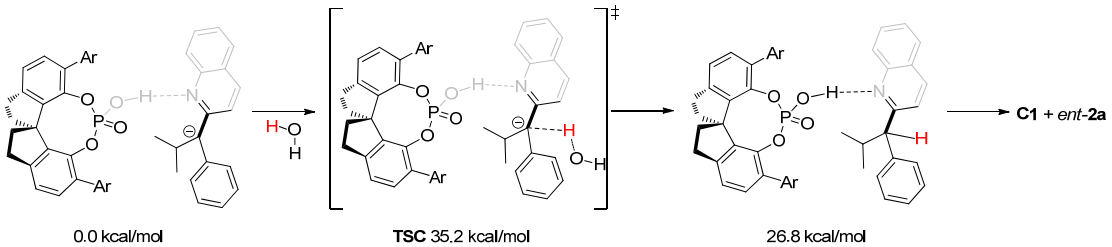

Figure S185. The calculated ΔG values (in kcal/mol) for the formation of (*ent*)-**2a** through **TSC** transition state. The ΔG for the generation of **TSC** transition state are 35.2 kcal/mol and The ΔG of the formation of **C1** and (*ent*)-**2a** are 26.8 kcal/mol, related to **Figures 3 and 4**.

Supplemental Item Legands

Table S1. **Evaluate the effect of BA, amine, base, and the solvent on the reductive dechlorination – deuteration of 1a**, related to **Table 1.**

Table S2. Evaluate the effect of PC and [D] source on the reductive dechlorination – deuteration of 1a, related to **Table 1.**

Table S3. Evaluate the effect of amine and time on the enantioselective reduction of 1a, related to **Table 1.**

Table S4. Optimization of asymmetric reduction – deuteration of 4a, related to **Figure 5**.

Table S5. Cartesian Coordinates for the formation of (*R*)-2a proceeding transferred proton of P=O–H of CPA via TSA process, related to **Figures 3 and 4.**

Table S6. Cartesian Coordinates for the formation of (*ent*)-2a proceeding transferred proton of P–O–H of CPA via TSB process, related to **Figures 3 and 4.**

Table S7. Cartesian Coordinates for the formation of (*ent*)-2a proceeding transferred proton of H_2O via TSC process, related to **Figures 3 and 4.**

Data S1. Crystal Data and structure Refinement for 8, related to **Figure 2.**

Data S2. Crystal Data and structure Refinement for 5n, related to **Figure 5.**

Transparent Methods

Proton nuclear magnetic resonance (^{1}H NMR) and carbon NMR (^{13}C NMR) were recorded in $CDCl_3$ otherwise stated. Chemical shifts are reported in parts per million (ppm), using the residual solvent signal as an internal standard: $CDCl_3$ (^{1}H NMR: δ 7.26, singlet; ^{13}C NMR: δ 77.0, triplet). Multiplicities were given as: *s* (singlet), *d* (doublet), *t* (triplet), *q* (quartet), *quintet*, *m* (multiplets), *dd* (doublet of doublets), *dt* (doublet of triplets), and *br* (broad). Coupling constants (*J*) were recorded in Hertz (Hz). The number of proton atoms (*n*) for a given resonance was indicated by *n*H. The number of carbon atoms (*n*) for a given resonance was indicated by *n*C. HRMS (Analyzer: TOF) was reported in units of mass of charge ratio (m/z). Mass samples were dissolved in CH_3CN (HPLC Grade) unless otherwise stated. Optical rotations were recorded on a polarimeter with a sodium lamp of wavelength 589 nm and reported as follows; $[\alpha]_{\lambda}^{T^{\circ}C}$ (*c* = g/100 mL, solvent). Melting points were determined on a melting point apparatus. Enantiomeric excesses were determined by chiral High Performance Liquid Chromatography (HPLC) analysis. UV detection was monitored at 254 nm and 210 nm at the same time. HPLC samples were dissolved in HPLC grade isopropanol (IPA) unless otherwise stated. All commercial reagents were purchased with the highest purity grade. They were used without further purification unless specified. All solvents used, mainly petroleum ether (PE) and ethyl acetate (EtOAc) were distilled. Anhydrous dichloromethane (DCM) was freshly distilled from CaH_2 and stored under N_2 atmosphere. Toluene and its derivatives were freshly distilled from sodium/benzophenone before use. All compounds synthesized were stored in a 0 °C freezer and light-sensitive compounds were protected with aluminium foil.

General Procedure for the Preparation of α-chloro-azaarenes

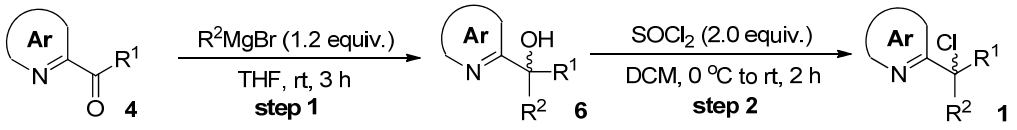

Step 1: To a flame dried flask was equipped in **4** (5.0 mmol), THF (20 mL) under N_2. To this mixture, *i*PrMgBr (6.0 mmol, 1.2 equiv.) was added with vigorous stirring at 0 °C. Subsequently, the mixture was warmed up to room temperature, and stirred for 2~5 h. Then quenched with saturated NH_4Cl solutions and extracted with Et_2O (3 x 10 mL), removed the solvent in *vacuo*, the reaction mixture was dissolved with toluene and loaded onto a short *silica gel* column, followed by gradient elution with petroleum ether/ethyl acetate (100/1 to 20/1 ratio). Removing the solvent in *vacuo*, afforded products **6** (e.g. **6a**, yield = 88%).

Step 2: To a solution of **6** (Terrasson et al., 2008) (2.0 mmol) in dry DCM (5 mL) was added $SOCl_2$ (4.0 mmol, 2.0 equiv.) at 0 °C. Subsequently, the mixture was warmed up to room temperature, and stirred for 2~10 h. TLC monitored until full conversion of **6**. Then cooled to 0 °C again, saturated $NaHCO_3$ solutions were added until no gas produced. Then extracted with DCM (3 x 10 mL), removed the solvent in *vacuo*, the reaction mixture was dissolved with toluene and loaded onto a short basified *silica gel* column, followed by gradient elution with petroleum ether. Removing the solvent in *vacuo*, afforded products **1**. (eg. **1a**, colorless oil, 65% yield; ^{1}H NMR (300 MHz, $CDCl_3$) δ 8.33 (d, J = 8.8 Hz, 1H), 8.08 (d, J = 8.8 Hz, 1H), 7.87 – 7.75 (m, 5H), 7.62 (t, J = 7.5 Hz, 1H), 7.45 – 7.30 (m, 3H), 4.06 – 3.79 (m, 1H), 1.44 (d, J = 6.3 Hz, 3H), 1.10 (d, J = 6.7 Hz, 3H); ^{13}C NMR (75 MHz, $CDCl_3$) δ 162.5, 146.2, 143.0, 136.1, 129.7, 129.3, 127.8, 127.2, 127.2, 127.1, 127.0, 126.6, 122.0, 85.8, 37.3, 19.5, 18.1).

General experimental procedures for the enantioselective reductive dechlorination – deuteration of α-chloro-azaarenes

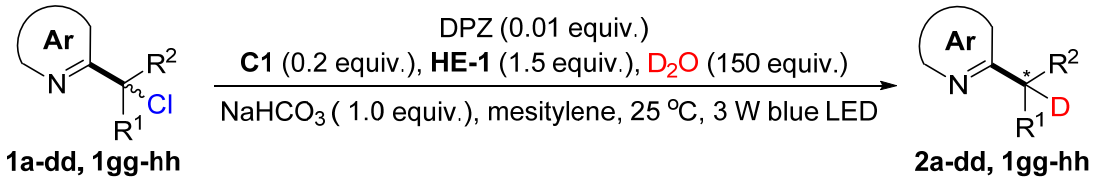

To a flame dried Schlenk tube was sequentially added **1a**−**dd** or **1gg**−**hh** (0.10 mmol, 1.0 equiv.), DPZ (0.001 mmol, 0.01 equiv.), **C1** (0.02 mmol, 0.2 equiv.), **HE-1** (0.15 mmol, 1.5 equiv.), $NaHCO_3$ (0.10 mmol, 1.0 equiv.), mesitylene (2 mL), and D_2O (15 mmol, 150 equiv.). Then degassed three times by freeze-pump-thaw method. The reaction mixture was stirred under an argon atmosphere at 25 °C (the temperature was maintained in an incubator) for 5 min without light, then irradiated by a 3 W blue LED for another 20−60 min. The reaction was monitored by TLC. After completion of the reaction, the reaction mixture was directly loaded onto a short basified *silica gel* column, followed by gradient elution with petroleum ether/ethyl acetate (100/1 ratio). Removing the solvent in *vacuo*, afforded products **2a**−**dd or 2gg**−**hh**.

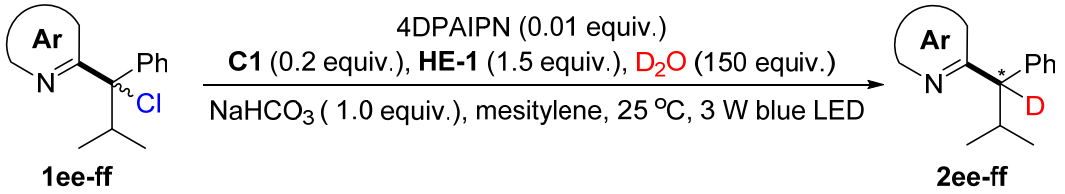

To a flame dried Schlenk tube was sequentially added **1ee**−**ff** (0.10 mmol, 1.0 equiv.), 4DPAIPN (0.001 mmol, 0.01 equiv.), **C1** (0.02 mmol, 0.2 equiv.), **HE-1** (0.15 mmol, 1.5 equiv.), $NaHCO_3$ (0.10 mmol, 1.0 equiv.), mesitylene (2 mL), and D_2O (15 mmol, 150 equiv.). Then degassed three times by freeze-pump-thaw method. The reaction mixture was stirred under an argon atmosphere at 25 °C (the temperature was maintained in an incubator) for 5 min without light, then irradiated by a 3 W blue LED for another 20−60 min. The reaction was monitored by TLC. After completion of the reaction, the reaction mixture was directly loaded onto a short basified *silica gel* column, followed by gradient elution with petroleum ether/ethyl acetate (100/1 ratio). Removing the solvent in *vacuo*, afforded products **2ee**−**ff**.

General experimental procedures for the asymmetric reduction – deuteration of azaarene-substituted ketones

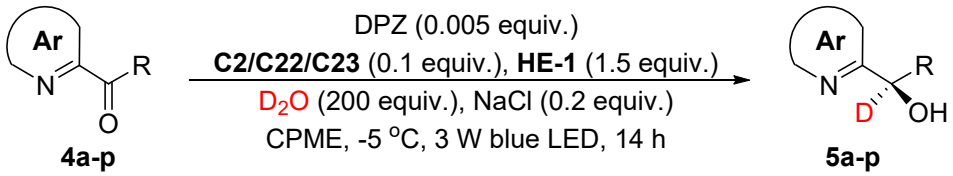

To a flame dried Schlenk tube was sequentially added **4a**−**p** (0.10 mmol, 1.0 equiv.), DPZ (0.0005 mmol, 0.005 equiv.), **C2/C22/C23** (0.01 mmol, 0.1 equiv.), **HE-1** (0.15 mmol, 1.5 equiv.), NaCl (0.02 mmol, 0.2 equiv.), CPME (2 mL), and D_2O (20 mmol, 200 equiv.). Then degassed three times by freeze-pump-thaw method. The reaction mixture was stirred under an argon atmosphere at –5/15 °C (the temperature was maintained in an incubator) for 15 min without light, then irradiated by a 3 W blue LED for another 14−24 hours. The reaction was monitored by TLC. After completion of the reaction, the reaction mixture was directly loaded onto a short basified *silica gel* column, followed by gradient elution with petroleum ether/ethyl acetate (8/1 ratio). Removing the solvent in *vacuo*, afforded products **5a**−**p**.

Procedures for the Preparation of 8

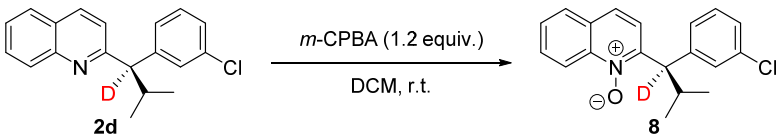

To a stirred solution of **2d** (0.1 mmol, 1.0 equiv.) in DCM 2.0 (mL) was added 3-chloroperoxy-benzoic acid (0.12 mmol, 1.2 equiv.) in portions. The mixture was stirred for 12 h at room temperature, sodium thiosulfate was added (5.0 mL) followed by saturated

sodium hydrogen carbonate (30 mL). The mixture was extracted with DCM (3 × 5.0 mL), the organic layers combined, dried with Na_2SO_4, the reaction mixture was directly loaded onto a short *silica gel* column, followed by gradient elution with petroleum ether/ethyl acetate (100/1–10/1 ratio). Removing the solvent in *vacuo*, afforded the N-O product **8** in 87% yield with 90% ee.

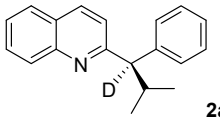

2a

White solid; Mp 104 – 106 ºC; 19.7 mg, 75% yield; >95% D, 93% ee; $[\alpha]_D^{22}$ –38.3 (*c* 1.0, $CHCl_3$); ^{1}H NMR (300 MHz, $CDCl_3$) δ 8.17 – 7.90 (m, 2H), 7.78 – 7.57 (m, 2H), 7.54 – 7.39 (m, 3H), 7.34 (d, *J* = 8.5 Hz, 1H), 7.28 – 7.18 (m, 2H), 7.17 – 7.07 (m, 1H), 2.86 – 2.67 (m, 1H), 1.00 – 0.75 (m, 6H); ^{13}C NMR (75 MHz, $CDCl_3$) δ 163.9, 142.8, 136.3, 129.2, 129.1, 128.5, 128.4, 127.4, 126.8, 126.4, 125.8, 121.1, 31.9, 21.7, 21.4; HRMS (ESI) m/z 263.1647 ($M+H^+$), calc. for $C_{19}H_{19}DN$ 263.1654. The ee was determined by HPLC analysis: CHIRALPAK IG (4.6 mm i.d. x 250 mm); hexane/2-propanol = 97/3; flow rate 1.2 mL/min; 25 ºC; 230 nm; retention time: 4.6 min (major) and 9.2 min (minor).

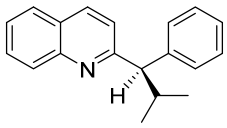

2a'

White solid; Mp 104 – 106 ºC; 18.9 mg, 73% yield; ^{1}H NMR (300 MHz, $CDCl_3$) δ 8.02 (d, *J* = 8.5 Hz, 1H), 7.90 (d, *J* = 8.5 Hz, 1H), 7.66 – 7.53 (m, 2H), 7.44 – 7.32 (m, 3H), 7.26 (d, *J* = 8.5 Hz, 1H), 7.18 (t, *J* = 7.4 Hz, 2H), 7.06 (t, *J* = 7.3 Hz, 1H), 3.75 (d, *J* = 10.9 Hz, 1H), 2.78 – 2.66 (m, 1H), 0.83 (t, *J* = 6.0 Hz, 6H); ^{13}C NMR (75 MHz, $CDCl_3$) δ 164.0, 147.8, 142.9, 136.2, 129.2, 129.2, 128.5, 128.3, 127.4, 126.8, 126.3, 125.7, 121.2, 63.2, 32.0, 21.7, 21.4.

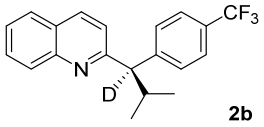

2b

Colorless oil; 19.2 mg, 58% yield; >95% D, 95% ee; $[\alpha]_D^{22}$ –111.4 (*c* 1.0, $CHCl_3$); ^{1}H NMR (300 MHz, $CDCl_3$) δ 8.28 – 7.95 (m, 2H), 7.81 – 7.59 (m, 4H), 7.51 – 7.45 (m, 3H), 7.34 (d, *J* = 8.4 Hz, 1H), 2.89 – 2.85 (m, 1H), 0.93 – 0.85 (m, 6H); ^{13}C NMR (75 MHz, $CDCl_3$) δ 162.8, 147.0, 136.5, 129.4, 129.2, 128.8, 128.4, 127.4, 126.9, 126.0, 125.3, 125.3, 125.2, 125.2, 122.4, 121.2, 32.2, 21.6, 21.3; HRMS (ESI) m/z 331.1519 ($M+H^+$), calc. for $C_{20}H_{18}DF_3N$ 331.1527. The ee was determined by HPLC analysis: CHIRALPAK ODH x 2 (4.6 mm i.d. x

250 mm); hexane/2-propanol = 98/2; flow rate 1.0 mL/min; 25 ºC; 230 nm; retention time: 9.3 min (minor) and 11.3 min (major).

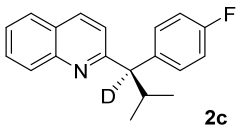

2c

White solid; Mp 92 – 94 ºC; 17.4 mg, 62% yield; 95% D, 91% ee; $[\alpha]_D^{22}$ –52.1 (*c* 1.0, $CHCl_3$); ^1H NMR (300 MHz, $CDCl_3$) δ 8.10 – 7.86 (m, 2H), 7.72 – 7.55 (m, 2H), 7.46 – 7.31 (m, 3H), 7.29 – 7.14 (m, 1H), 6.88 (t, *J* = 8.7 Hz, 2H), 3.73 (d, *J* = 10.0 Hz, 0.05H), 2.80 – 2.56 (m, 1H), 0.87 – 0.73 (m, 6H); ^{13}C NMR (75 MHz, $CDCl_3$) δ 163.6, 163.1, 159.9, 138.5, 136.6, 129.9, 129.8, 129.4, 129.0, 127.4, 126.8, 126.0, 121.1, 115.3, 115.0, 32.2, 21.6, 21.3; HRMS (ESI) m/z 281.1553 ($M+H^+$), calc. for $C_{19}H_{18}DFN$ 281.1559. The ee was determined by HPLC analysis: CHIRALPAK IG (4.6 mm i.d. x 250 mm); hexane/2-propanol = 97/3; flow rate 1.2 mL/min; 25 ºC; 230 nm; retention time: 4.5 min (major) and 6.6 min (minor).

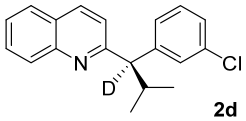

2d

White solid; Mp 91 – 93 ºC; 18.4 mg, 62% yield; >95% D, 93% ee; $[\alpha]_D^{22}$ –65.8 (*c* 1.0, $CHCl_3$); ^1H NMR (300 MHz, $CDCl_3$) δ 8.12 – 8.01 (m, 2H), 7.76 – 7.65 (m, 2H), 7.56 – 7.44 (m, 2H), 7.41 – 7.30 (m, 2H), 7.24 – 7.08 (m, 2H), 2.87 – 2.67 (m, 1H), 0.96 – 0.84 (m, 6H); ^{13}C NMR (75 MHz, $CDCl_3$) δ 163.1, 145.0, 136.4, 134.1, 129.6, 129.4, 129.2, 128.5, 127.4, 126.9, 126.8, 126.6, 126.0, 121.2, 32.1, 21.6, 21.4; HRMS (ESI) m/z 297.1257 ($M+H^+$), calc. for $C_{19}H_{18}DClN$ 297.1263. The ee was determined by HPLC analysis: CHIRALPAK IG (4.6 mm i.d. x 250 mm); hexane/2-propanol = 97/3; flow rate 1.2 mL/min; 25 ºC; 230 nm; retention time: 4.1 min (major) and 5.7 min (minor).

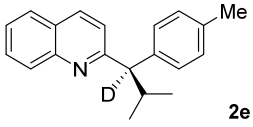

2e

Colorless oil; 21.6 mg, 78% yield; >95% D, 93% ee; $[\alpha]_D^{22}$ +17.3 (*c* 1.0, $CHCl_3$); ^1H NMR (300 MHz, $CDCl_3$) δ 8.12 (d, *J* = 8.3 Hz, 1H), 8.01 (d, *J* = 8.5 Hz, 1H), 7.81 – 7.61 (m, 2H), 7.52 – 7.42 (m, 1H), 7.42 – 7.32 (m, 3H), 7.14 – 7.03 (m, 2H), 3.84 (d, *J* = 10.1 Hz, 0.05H), 2.88 – 2.67 (m, 1H), 2.28 (s, 3H), 1.01 – 0.80 (m, 6H); ^{13}C NMR (75 MHz, $CDCl_3$) δ 164.2, 147.6, 139.8, 136.4, 135.9, 129.2, 129.1, 128.3, 127.4, 126.8, 125.8, 121.0, 31.8, 21.7, 21.4, 21.0; HRMS (ESI) m/z 277.1803 ($M+H^+$), calc. for $C_{20}H_{21}DN$ 277.1810. The ee was determined by HPLC analysis: CHIRALPAK IG (4.6 mm i.d. x 250 mm); hexane/2-propanol

= 97/3; flow rate 1.2 mL/min; 25 ºC; 230 nm; retention time: 4.9 min (major) and 8.7 min (minor).

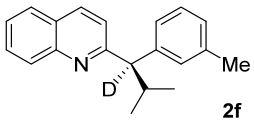

2f

White solid; Mp 89 – 91 ºC; 20.2 mg, 73% yield; 95% D, 91% ee; $[\alpha]_D^{22}$ –13.3 (*c* 1.0, $CHCl_3$); ^1H NMR (300 MHz, $CDCl_3$) δ 8.19 – 7.90 (m, 2H), 7.75 – 7.55 (m, 2H), 7.48 – 7.37 (m, 1H), 7.33 (d, *J* = 8.5 Hz, 1H), 7.23 (t, *J* = 8.5 Hz, 2H), 7.11 (t, *J* = 7.5 Hz, 1H), 6.96 – 6.85 (m, 1H), 3.78 (d, *J* = 9.0 Hz, 0.05H), 2.25 (s, 3H), 0.96 – 0.72 (m, 6H); ^{13}C NMR (75 MHz, $CDCl_3$) δ 164.0, 147.5, 142.7, 137.9, 136.3, 129.3, 129.2, 129.1, 128.2, 127.4, 127.1, 126.8, 125.8, 125.3, 121.0, 31.7, 21.7, 21.5, 21.5; HRMS (ESI) m/z 277.1804 ($M+H^+$), calc. for $C_{20}H_{21}DN$ 277.1810. The ee was determined by HPLC analysis: CHIRALPAK IG (4.6 mm i.d. x 250 mm); hexane/2-propanol = 97/3; flow rate 1.2 mL/min; 25 ºC; 230 nm; retention time: 4.0 min (major) and 6.6 min (minor).

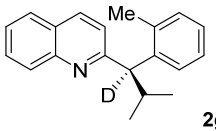

2g

White solid; Mp 89 – 91 ºC; 18.8 mg, 68% yield; 94% D, 88% ee; $[\alpha]_D^{22}$ +38.7 (*c* 1.0, $CHCl_3$); ^1H NMR (300 MHz, $CDCl_3$) δ 8.09 (d, *J* = 7.9 Hz, 1H), 7.98 (d, *J* = 8.4 Hz, 1H), 7.77 – 7.58 (m, 3H), 7.46 (t, *J* = 7.4 Hz, 1H), 7.32 (d, *J* = 8.5 Hz, 1H), 7.19 (t, *J* = 7.3 Hz, 1H), 7.12 – 7.02 (m, 2H), 4.18 – 4.15 (m, 0.06H), 2.88 – 2.75 (m, 1H), 2.49 (s, 3H), 0.96 – 0.89 (m, 6H); ^{13}C NMR (75 MHz, $CDCl_3$) δ 163.8, 147.7, 141.1, 137.0, 136.1, 130.3, 129.2, 129.1, 127.3, 127.1, 126.7, 126.1, 126.0, 125.7, 121.1, 32.1, 21.7, 21.1, 20.5; HRMS (ESI) m/z 277.1803 ($M+H^+$), calc. for $C_{20}H_{21}DN$ 277.1810. The ee was determined by HPLC analysis: CHIRALPAK IG (4.6 mm i.d. x 250 mm); hexane/2-propanol = 97/3; flow rate 1.2 mL/min; 25 ºC; 230 nm; retention time: 3.8 min (major) and 10.0 min (minor).

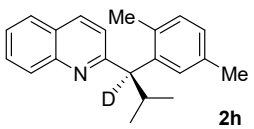

2h

Colorless oil; 19.7 mg, 68% yield; 93% D, 85% ee; $[\alpha]_D^{22}$ +138.9 (*c* 1.0, $CHCl_3$); ^1H NMR (300 MHz, $CDCl_3$) δ 8.09 (d, *J* = 8.4 Hz, 1H), 7.98 (d, *J* = 8.5 Hz, 1H), 7.74 – 7.62 (m, 2H), 7.49 – 7.40 (m, 2H), 7.31 (d, *J* = 8.5 Hz, 1H), 6.99 (d, *J* = 7.6 Hz, 1H), 6.87 (d, *J* = 7.5 Hz, 1H), 4.14 (d, *J* = 11.1 Hz, 0.07H), 2.86 – 2.76 (m, 1H), 2.45 (s, 3H), 2.31 (s, 3H), 0.96 – 0.89 (m, 6H); ^{13}C NMR (75 MHz, $CDCl_3$) δ 163.9, 147.6, 140.8, 136.1, 135.3, 133.9, 130.2, 129.2,

129.0, 127.7, 127.3, 126.7, 125.7, 121.1, 32.0, 21.7, 21.3, 21.2, 20.1; HRMS (ESI) m/z 291.1958 ($M+H^+$), calc. for $C_{21}H_{23}DN$ 291.1966. The ee was determined by HPLC analysis: CHIRALPAK IG (4.6 mm i.d. x 250 mm); hexane/2-propanol = 98/2; flow rate 1.0 mL/min; 25 ºC; 230 nm; retention time: 3.9 min (major) and 11.7 min (minor).

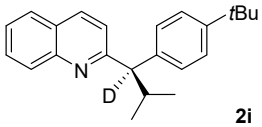

2i

White solid; Mp 94 – 97 ºC; 21.7 mg, 68% yield; 95% D, 90% ee; $[\alpha]_D^{22}$ +25.3 (*c* 1.0, $CHCl_3$); ^1H NMR (300 MHz, $CDCl_3$) δ 8.11 (d, *J* = 8.2 Hz, 1H), 8.01 (d, *J* = 8.6 Hz, 1H), 7.75 – 7.61 (m, 2H), 7.50 – 7.34 (m, 4H), 7.29 – 7.24 (m, 2H), 2.81 – 2.75 (m, 1H), 1.26 (s, 9H), 0.93 (d, *J* = 6.5 Hz, 3H), 0.89 (d, *J* = 6.5 Hz, 3H); ^{13}C NMR (75 MHz, $CDCl_3$) δ 164.3, 149.0, 147.7, 139.7, 136.2, 129.1, 128.0, 127.4, 126.8, 125.7, 125.2, 121.1, 34.3, 31.9, 31.3, 21.7, 21.5; HRMS (ESI) m/z 319.2272 ($M+H^+$), calc. for $C_{23}H_{27}DN$ 319.2279. The ee was determined by HPLC analysis: CHIRALPAK ODH x 2 (4.6 mm i.d. x 250 mm); hexane/2-propanol = 98/2; flow rate 1.2 mL/min; 25 ºC; 230 nm; retention time: 8.4 min (minor) and 9.9 min (major).

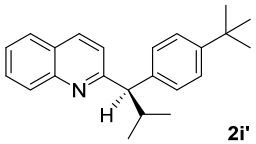

2i'

White solid; Mp 94 – 97 ºC; 22.4 mg, 70% yield; ^1H NMR (300 MHz, $CDCl_3$) δ 8.03 (d, *J* = 8.5 Hz, 1H), 7.93 (d, *J* = 8.5 Hz, 1H), 7.68 – 7.54 (m, 2H), 7.41 – 7.27 (m, 4H), 7.21 – 7.16 (m, 2H), 3.75 (d, *J* = 10.8 Hz, 1H), 2.78 – 2.60 (m, 1H), 1.18 (s, 9H), 0.86 (d, *J* = 6.6 Hz, 3H), 0.81 (d, *J* = 6.5 Hz, 3H); ^{13}C NMR (75 MHz, $CDCl_3$) δ 164.3, 149.0, 139.7, 136.3, 129.2, 129.1, 128.0, 127.4, 126.8, 125.8, 125.2, 121.1, 62.7, 34.3, 32.0, 31.3, 21.7, 21.5.

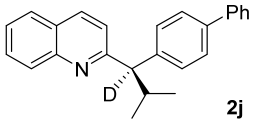

2j

Colorless oil; 26.4 mg, 78% yield; >95% D, 91% ee; $[\alpha]_D^{22}$ –7.2 (*c* 1.0, $CHCl_3$); ^1H NMR (300 MHz, $CDCl_3$) δ 8.15 – 7.98 (m, 2H), 7.77 – 7.65 (m, 2H), 7.62 – 7.27 (m, 11H), 2.94 – 2.71 (m, 1H), 0.99 – 0.90 (m, 6H); ^{13}C NMR (75 MHz, $CDCl_3$) δ 163.9, 147.8, 142.0, 140.9, 139.2, 136.3, 129.2, 128.9, 128.6, 127.4, 127.1, 127.0, 126.9, 126.8, 125.8, 121.2, 32.0, 21.7, 21.5; HRMS (ESI) m/z 339.1958 ($M+H^+$), calc. for $C_{25}H_{23}DN$ 339.1966. The ee was determined by HPLC analysis: CHIRALPAK IG (4.6 mm i.d. x 250 mm); hexane/2-propanol = 97/3; flow rate 1.2 mL/min; 25 ºC; 230 nm; retention time: 6.6 min (major) and 13.5 min (minor).

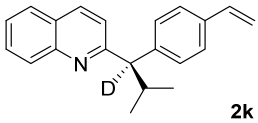

2k

Colorless oil; 23.4 mg, 81% yield; >95% D, 93% ee; $[\alpha]_D^{22}$ –23.7 (*c* 1.0, $CHCl_3$); ^1H NMR (300 MHz, $CDCl_3$) δ 8.09 (d, *J* = 8.4 Hz, 1H), 8.00 (d, *J* = 8.5 Hz, 1H), 7.79 – 7.59 (m, 2H), 7.53 – 7.40 (m, 3H), 7.36 – 7.30 (m, 3H), 6.65 (dd, *J* = 17.6, 10.9 Hz, 1H), 5.67 (d, *J* = 17.5 Hz, 1H), 5.16 (d, *J* = 11.0 Hz, 1H), 2.90 – 2.68 (m, 1H), 0.98 – 0.86 (m, 6H); ^{13}C NMR (75 MHz, $CDCl_3$) δ 163.8, 147.8, 142.6, 136.5, 136.3, 135.7, 129.2, 128.6, 127.4, 126.8, 126.2, 125.8, 121.1, 113.2, 31.9, 21.7, 21.4; HRMS (ESI) m/z 289.1802 ($M+H^+$), calc. for $C_{21}H_{21}DN$ 289.1810. The ee was determined by HPLC analysis: CHIRALPAK IG (4.6 mm i.d. x 250 mm); hexane/2-propanol = 97/3; flow rate 1.2 mL/min; 25 ºC; 230 nm; retention time: 5.4 min (major) and 9.7 min (minor).

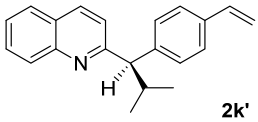

2k'

Colorless oil; 23.4 mg, 81% yield; ^1H NMR (300 MHz, $CDCl_3$) δ 8.02 (d, *J* = 8.5 Hz, 1H), 7.92 (d, *J* = 8.5 Hz, 1H), 7.67 – 7.52 (m, 2H), 7.42 – 7.35 (m, 3H), 7.30 – 7.15 (m, 3H), 6.65 – 6.50 (m, 1H), 5.64 – 5.53 (m, 1H), 5.12 – 5.06 (m, 1H), 3.75 (d, *J* = 10.9 Hz, 1H), 2.87 – 2.57 (m, 1H), 0.89 – 0.79 (m, 6H); ^{13}C NMR (75 MHz, $CDCl_3$) δ 163.8, 147.6, 142.6, 136.5, 136.4, 135.7, 129.3, 129.1, 128.6, 127.4, 126.8, 126.2, 125.8, 121.1, 113.2, 62.8, 31.9, 21.7, 21.4.

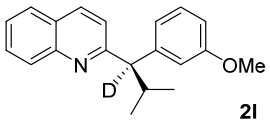

2l

Colorless oil; 20.8 mg, 71% yield; >95% D, 93% ee; $[\alpha]_D^{22}$ –24.4 (*c* 1.0, $CHCl_3$); ^1H NMR (300 MHz, $CDCl_3$) δ 8.11 (d, *J* = 8.4 Hz, 1H), 8.01 (d, *J* = 8.5 Hz, 1H), 7.77 – 7.62 (m, 2H), 7.46 (t, *J* = 7.5 Hz, 1H), 7.37 (d, *J* = 8.5 Hz, 1H), 7.19 (t, *J* = 7.8 Hz, 1H), 7.08 (d, *J* = 7.6 Hz, 2H), 6.73 – 6.67 (m, 1H) 3.78 (s, 3H), 2.90 – 2.70 (m, 1H), 0.96 – 0.86 (m, 6H); ^{13}C NMR (75 MHz, $CDCl_3$) δ 163.8, 159.5, 147.8, 144.5, 136.2, 129.2, 129.2, 127.4, 126.8, 125.7, 121.1, 120.9, 114.4, 111.4, 55.1, 31.9, 21.7, 21.4; HRMS (ESI) m/z 293.1752 ($M+H^+$), calc. for $C_{20}H_{21}DNO$ 293.1759. The ee was determined by HPLC analysis: CHIRALPAK IG (4.6 mm i.d. x 250 mm); hexane/2-propanol = 97/3; flow rate 1.2 mL/min; 25 ºC; 230 nm; retention time: 5.9 min (major) and 12.1 min (minor).

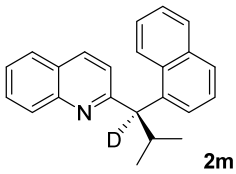

2m

Colorless oil; 20.3 mg, 65% yield; >95% D, 80% ee; $[\alpha]_D^{22}$ –165.9 (*c* 1.0, $CHCl_3$); ^1H NMR (300 MHz, $CDCl_3$) δ 8.61 (d, *J* = 8.5 Hz, 1H), 8.15 (d, *J* = 8.2 Hz, 1H), 7.92 (d, *J* = 8.5 Hz, 1H), 7.82 (t, *J* = 7.4 Hz, 2H), 7.76 – 7.60 (m, 3H), 7.57 – 7.30 (m, 5H), 3.04 – 2.96 (m, 1H), 1.02 – 0.97 (m, 6H); ^{13}C NMR (75 MHz, $CDCl_3$) δ 163.8, 138.7, 136.5, 134.0, 132.7, 129.2, 128.7, 127.4, 127.0, 126.7, 125.9, 125.8, 125., 125.3, 124.7, 124.3, 120.9, 32.0, 21.8, 21.5; HRMS (ESI) m/z 313.1802 ($M+H^+$), calc. for $C_{23}H_{21}DN$ 313.1810. The ee was determined by HPLC analysis: CHIRALPAK ODH x 2 (4.6 mm i.d. x 250 mm); hexane/2-propanol = 98/2; flow rate 1.2 mL/min; 25 °C; 230 nm; retention time: 12.6 min (minor) and 13.9 min (major).

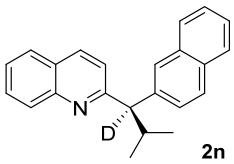

2n

Colorless oil; 22.5 mg, 72% yield; >95% D, 88% ee; $[\alpha]_D^{22}$ –182.9 (*c* 1.0, $CHCl_3$); ^1H NMR (300 MHz, $CDCl_3$) δ 8.13 (d, *J* = 8.3 Hz, 1H), 8.00 (d, *J* = 8.6 Hz, 1H), 7.91 (s, 1H), 7.84 – 7.63 (m, 6H), 7.50 – 7.33 (m, 4H), 3.00 – 2.90 (m, 1H), 0.96 (d, *J* = 6.4 Hz, 6H); ^{13}C NMR (75 MHz, $CDCl_3$) δ 163.7, 147.6, 140.4, 136.3, 133.5, 132.3, 129.3, 129.1, 128.0, 127.7, 127.5, 127.4, 127.0, 126.8, 126.8, 125.8, 125.4, 121.3, 31.7, 21.7, 21.5; HRMS (ESI) m/z 313.1802 ($M+H^+$), calc. for $C_{23}H_{21}DN$ 313.1810. The ee was determined by HPLC analysis: CHIRALPAK IG (4.6 mm i.d. x 250 mm); hexane/2-propanol = 97/3; flow rate 1.2 mL/min; 25 °C; 230 nm; retention time: 5.9 min (major) and 11.0 min (minor).

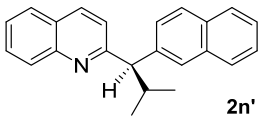

2n'

Colorless oil; 22.9 mg, 72% yield; ^1H NMR (300 MHz, $CDCl_3$) δ 8.07 (d, *J* = 8.4 Hz, 1H), 7.91 (d, *J* = 8.5 Hz, 1H), 7.82 (s, 1H), 7.75 – 7.50 (m, 6H), 7.44 – 7.26 (m, 4H), 3.94 (d, *J* = 10.8 Hz, 1H), 2.92 – 2.71 (m, 1H), 0.91 – 0.82 (m, 6H); ^{13}C NMR (75 MHz, $CDCl_3$) δ 163.8, 147.6, 140.4, 136.4, 133.5, 132.3, 129.3, 129.1, 128.0, 127.7, 127.5, 127.4, 127.0, 126.8, 125.9, 125.8, 125.4, 121.3, 63.1, 31.8, 21.7, 21.5.

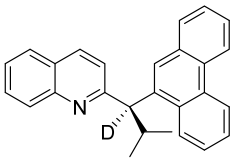

2o

White solid; Mp 160 – 162 ºC; 21.7 mg, 66% yield; >95% D, 80% ee; $[\alpha]_D^{22}$ +492.8 (*c* 1.0, $CHCl_3$); ^1H NMR (300 MHz, $CDCl_3$) δ 8.78 – 8.59 (m,3H), 8.18 (d, *J* = 8.6 Hz, 1H), 8.06 (s, 1H), 8.01 – 7.84 (m, 2H), 7.73 – 7.55 (m, 6H), 7.48 – 7.35 (m, 2H), 3.10 – 3.05 (m, 1H), 1.09 (d, *J* = 6.4 Hz, 3H), 1.02 (d, *J* = 6.5 Hz, 3H); ^{13}C NMR (75 MHz, $CDCl_3$) δ 163.7, 147.57, 136.9, 136.1, 131.9, 131.7, 130.7, 129.6, 129.2, 128.6, 127.4, 126.7, 126.6, 126.5, 126.3, 126.1, 125.8, 125.4, 125.2, 123.0, 122.4, 120.6, 31.7, 21.8, 21.7; HRMS (ESI) m/z 363.1956 ($M+H^+$), calc. for $C_{27}H_{23}DN$ 363.1966. The ee was determined by HPLC analysis: CHIRALPAK IG (4.6 mm i.d. x 250 mm); hexane/2-propanol = 97/3; flow rate 1.2 mL/min; 25 ºC; 230 nm; retention time: 6.5 min (major) and 8.2 min (minor).

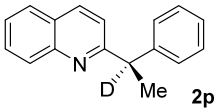

2p

Colorless oil; 19.4 mg, 83% yield; >95% D, 88% ee; $[\alpha]_D^{22}$ +15.0 (*c* 1.0, $CHCl_3$); ^1H NMR (300 MHz, $CDCl_3$) δ 8.03 (d, *J* = 8.4 Hz, 1H), 7.90 (d, *J* = 8.5 Hz, 1H), 7.68 – 7.52 (m, 2H), 7.40 (t, *J* = 7.5 Hz, 1H), 7.31 – 7.05 (m, 6H), 4.42 (q, *J* = 7.1 Hz, 0.1H), 1.71 (s, 3H); ^{13}C NMR (75 MHz, $CDCl_3$) δ 165.1, 147.5, 144.5, 136.3, 129.3, 129.1, 128.5, 127.8, 127.4, 126.8, 126.4, 125.9, 120.6, 48.0, 47.8, 47.6, 47.3, 20.3; HRMS (ESI) m/z 235.1334 ($M+H^+$), calc. for $C_{17}H_{15}DN$ 235.1340. The ee was determined by HPLC analysis: CHIRALPAK IG (4.6 mm i.d. x 250 mm); hexane/2-propanol = 97/3; flow rate 1.2 mL/min; 25 ºC; 230 nm; retention time: 6.0 min (major) and 10.3 min (minor).

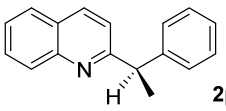

2p'

Colorless oil; 20.2 mg, 84% yield; ^1H NMR (300 MHz, $CDCl_3$) δ 8.04 (d, *J* = 8.4 Hz, 1H), 7.91 (d, *J* = 8.5 Hz, 1H), 7.68 – 7.55 (m, 2H), 7.40 (t, *J* = 7.1 Hz, 1H), 7.32 – 7.06 (m, 6H), 4.50 – 4.26 (m, 1H), 1.72 (d, *J* = 7.2 Hz, 3H); ^{13}C NMR (75 MHz, $CDCl_3$) δ 165.1, 147.6, 144.6, 136.3, 129.3, 129.2, 128.5, 127.8, 127.4, 126.8, 126.4, 125.9, 120.7, 48.0, 20.4.

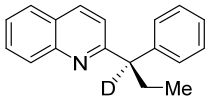

2q

Colorless oil; 21.1 mg, 85% yield; >95% D, 87% ee; $[\alpha]_D^{22}$ +31.7 (*c* 1.0, $CHCl_3$); ^1H NMR (300 MHz, $CDCl_3$) δ 8.11 (d, *J* = 8.4 Hz, 1H), 8.00 (d, *J* = 8.6 Hz, 1H), 7.79 – 7.63 (m, 2H), 7.48 (t, *J* = 7.5 Hz, 1H), 7.40 (d, *J* = 7.3 Hz, 2H), 7.34 – 7.13 (m, 4H), 4.20 – 4.18 (m, 0.05H), 2.43 – 2.32 (m, 1H), 2.27 – 2.15 (m, 1H), 0.95 (t, *J* = 7.3 Hz, 3H); ^{13}C NMR (75 MHz, $CDCl_3$) δ 164.1, 147.6, 143.2, 136.4, 129.3, 129.1, 128.4, 128.2, 127.4, 126.8, 126.4, 125.9, 120.9, 27.7, 12.6; HRMS (ESI) m/z 249.1491 ($M+H^+$), calc. for $C_{18}H_{17}DN$ 249.1497. The ee was determined by HPLC analysis: CHIRALPAK IG (4.6 mm i.d. x 250 mm); hexane/2-propanol = 97/3; flow rate 1.2 mL/min; 25 ºC; 230 nm; retention time: 5.5 min (major) and 9.9 min (minor).

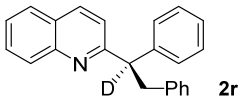

2r

White solid; Mp 54 – 56 ºC; 27.6 mg, 89% yield; >95% D, 84% ee; $[\alpha]_D^{22}$ –83.8 (*c* 1.0, $CHCl_3$); ^1H NMR (300 MHz, $CDCl_3$) δ 8.16 (d, *J* = 8.1 Hz, 1H), 7.98 (d, *J* = 8.5 Hz, 1H), 7.76 – 7.65 (m, 2H), 7.49 (t, *J* = 7.5 Hz, 1H), 7.38 – 7.33 (m, 2H), 7.29 – 7.20 (m, 3H), 7.20 – 7.06 (m, 6H), 3.86 (d, *J* = 13.7 Hz, 1H), 3.44 (d, *J* = 13.8 Hz, 1H); ^{13}C NMR (75 MHz, $CDCl_3$) δ 162.9, 142.9, 140.4, 136.4, 129.4, 129.2, 128.4, 128.3, 128.0, 127.4, 126.8, 126.5, 126.0, 125.8, 121.6, 40.9; HRMS (ESI) m/z 311.1645 ($M+H^+$), calc. for $C_{23}H_{19}DN$ 311.1653. The ee was determined by HPLC analysis: CHIRALPAK IG (4.6 mm i.d. x 250 mm); hexane/2-propanol = 97/3; flow rate 1.2 mL/min; 25 ºC; 230 nm; retention time: 7.0 min (major) and 10.0 min (minor).

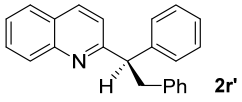

2r'

White solid; Mp 54 – 56 ºC; 26.1 mg, 85% yield; ^1H NMR (300 MHz, $CDCl_3$) δ 8.07 (d, *J* = 8.3 Hz, 1H), 7.89 (d, *J* = 8.4 Hz, 1H), 7.68 – 7.51 (m, 2H), 7.40 (t, *J* = 7.5 Hz, 1H), 7.26 (d, *J* = 7.2 Hz, 2H), 7.19 – 7.10 (m, 3H), 7.11 – 6.98 (m, 6H), 4.55 – 4.46 (m, 1H), 3.81 – 3.65 (m, 1H), 3.41 – 3.30 (m, 1H); ^{13}C NMR (75 MHz, $CDCl_3$) δ 163.0, 147.7, 143.12, 143.1, 140.5, 136.1, 129.2, 128.4, 128.3, 128.0, 127.4, 126.9, 126.5, 125.9, 125.8, 121.7, 56.0, 41.0.

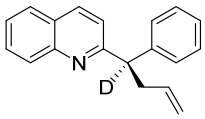

2s

Colorless oil; 18.5 mg, 71% yield; >95% D, 82% ee; $[\alpha]_D^{22}$ -45.3 (*c* 1.0, $CHCl_3$); ^1H NMR (300 MHz, $CDCl_3$) δ 8.13 (d, *J* = 8.1 Hz, 1H), 8.01 (d, *J* = 8.4 Hz, 1H), 7.74 – 7.65 (m, 2H), 7.49 (t, *J* = 7.5 Hz, 1H), 7.39 (d, *J* = 7.3 Hz, 2H), 7.35 – 7.07 (m, 4H), 5.88 – 5.71 (m, 1H), 5.10 – 5.01 (m, 1H), 4.97 – 4.90 (m, 1H), 3.17 (dd, *J* = 14.1, 6.7 Hz, 1H), 2.94 (dd, *J* = 14.2, 6.6 Hz, 1H); ^{13}C NMR (75 MHz, $CDCl_3$) δ 163.3, 147.7, 142.8, 136.7, 136.3, 129.3, 128.5, 128.2, 127.4, 126.9, 126.5, 125.9, 121.2, 116.4, 38.8; HRMS (ESI) m/z 261.1491 ($M+H^+$), calc. for $C_{19}H_{17}DN$ 261.1497. The ee was determined by HPLC analysis: CHIRALPAK IG (4.6 mm i.d. x 250 mm); hexane/2-propanol = 97/3; flow rate 1.0 mL/min; 25 ºC; 230 nm; retention time: 5.8 min (major) and 9.4 min (minor).

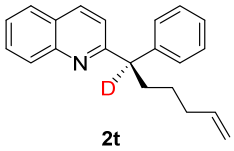

2t

Colorless oil; 19.4 mg, 71% yield; >95% D, 80% ee; $[\alpha]_D^{22}$ –73.2 (*c* 1.0, $CHCl_3$); ^1H NMR (300 MHz, $CDCl_3$) δ 8.11 (d, *J* = 8.5 Hz, 1H), 7.99 (d, *J* = 8.5 Hz, 1H), 7.74 – 7.64 (m, 2H), 7.47 (t, *J* = 7.5 Hz, 1H), 7.39 (d, *J* = 7.1 Hz, 2H), 7.33 – 7.12 (m, 4H), 5.84 – 5.68 (m, 1H), 5.01 – 4.87 (m, 2H), 2.42 – 2.01 (m, 4H), 1.51 – 1.28 (m, 2H); ^{13}C NMR (75 MHz, $CDCl_3$) δ 164.1, 147.8, 143.4, 138.7, 136.2, 129.3, 129.2, 128.5, 128.1, 127.4, 126.8, 126.4, 125.8, 120.9, 114.5, 34.1, 33.8, 27.2.HRMS (ESI) m/z 289.1804 ($M+H^+$), calc. for $C_{21}H_{21}DN$ 289.1810. The ee was determined by HPLC analysis: CHIRALPAK IG (4.6 mm i.d. x 250 mm); hexane/2-propanol = 97/3; flow rate 1.0 mL/min; 25 ºC; 230 nm; retention time: 6.1 min (major) and 9.0 min (minor).

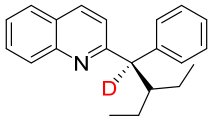

2u

Colorless oil; 21.8 mg, 75% yield; 94% D, 90% ee; $[\alpha]_D^{22}$ –58.9 (*c* 1.0, $CHCl_3$); ^1H NMR (300 MHz, $CDCl_3$) δ 8.10 (d, *J* = 7.4 Hz, 1H), 8.01 (d, *J* = 8.4 Hz, 1H), 7.75 – 7.62 (m, 2H), 7.56 – 7.34 (m, 4H), 7.29 – 7.23 (m, 2H), 7.19 – 7.11 (m, 1H), 4.15 – 4.03 (m, 0.06H), 2.59 (brs, 1H), 1.49 – 1.13 (m, 4H), 0.86 – 0.76 (m, 6H); ^{13}C NMR (75 MHz, $CDCl_3$) δ 163.9, 147.9, 142.7, 136.1, 129.3, 129.1, 128.6, 128.3, 127.3, 126.8, 126.3, 125.7, 121.2, 42.7, 22.1, 21.6, 10.1, 9.7; HRMS (ESI) m/z 291.1957 ($M+H^+$), calc. for $C_{21}H_{23}DN$ 291.1966. The ee was

determined by HPLC analysis: CHIRALPAK IG (4.6 mm i.d. x 250 mm); hexane/2-propanol = 97/3; flow rate 1.2 mL/min; 25 °C; 230 nm; retention time: 4.2 min (major) and 10.3 min (minor).

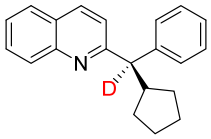

2v

White solid; Mp 103 – 105 °C; 17.9 mg, 62% yield; 92% D, 87% ee; $[\alpha]_D^{22}$ –7.2 (*c* 1.0, $CHCl_3$); ^1H NMR (300 MHz, $CDCl_3$) δ 8.09 (d, *J* = 8.5 Hz, 1H), 7.99 (d, *J* = 8.5 Hz, 1H), 7.68 (dd, *J* = 18.9, 7.9 Hz, 2H), 7.49 – 7.40 (m, 3H), 7.34 (d, *J* = 8.5 Hz, 1H), 7.29 – 7.22 (m, 2H), 7.15 (t, *J* = 7.3 Hz, 1H), 3.99 (d, *J* = 11.4 Hz, 0.08H), 3.03 – 2.93 (m, 1H), 1.78 – 1.47 (m, 6H), 1.34 – 1.09 (m, 2H); ^{13}C NMR (75 MHz, $CDCl_3$) δ 164.2, 147.8, 143.4, 136.1, 129.3, 129.1, 128.3, 127.4, 126.8, 126.3, 125.7, 121.0, 44.0, 31.9, 31.7, 25.4, 25.3; HRMS (ESI) m/z 289.1805 ($M+H^+$), calc. for $C_{21}H_{21}DN$ 289.1810. The ee was determined by HPLC analysis: CHIRALPAK IG (4.6 mm i.d. x 250 mm); hexane/2-propanol = 97/3; flow rate 1.2 mL/min; 25 °C; 230 nm; retention time: 5.4 min (major) and 13.1 min (minor).

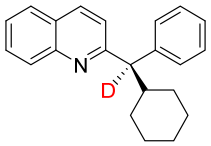

2w

White solid; Mp 98 – 100 °C; 18.7 mg, 62% yield; 95% D, 82% ee; $[\alpha]_D^{22}$ –12.8 (*c* 1.0, $CHCl_3$); ^1H NMR (300 MHz, $CDCl_3$) δ 8.09 (d, *J* = 8.2 Hz, 1H), 8.00 (d, *J* = 8.6 Hz, 1H), 7.77 – 7.61 (m, 2H), 7.51 – 7.41 (m, 3H), 7.36 (d, *J* = 8.5 Hz, 1H), 7.32 – 7.21 (m, 2H), 7.15 (t, *J* = 7.3 Hz, 1H), 3.93 – 3.87 (m, 0.05H), 2.49 – 2.40 m, 1H), 1.78 – 1.44 (m, 5H), 1.32 – 1.11 (m, 3H), 1.01 – 0.87 (m, 2H); ^{13}C NMR (75 MHz, $CDCl_3$) δ 163.7, 147.8, 142.4, 136.2, 136.2, 129.2, 128.6, 128.3, 127.4, 126.8, 126.3, 125.7, 121.2, 41.2, 32.0, 31.6, 26.5, 26.3, 26.2; HRMS (ESI) m/z 303.1958 ($M+H^+$), calc. for $C_{22}H_{23}DN$ 303.1966. The ee was determined by HPLC analysis: CHIRALPAK IG (4.6 mm i.d. x 250 mm); hexane/2-propanol = 97/3; flow rate 1.2 mL/min; 25 °C; 230 nm; retention time: 5.0 min (major) and 11.6 min (minor).

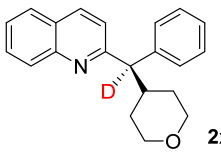

2x

Colorless oil; 21.9 mg, 72% yield; >95% D, 85% ee; $[\alpha]_D^{22}$ –84.2 (*c* 1.0, $CHCl_3$); ^1H NMR (300 MHz, $CDCl_3$) δ 8.04 (d, *J* = 7.9 Hz, 1H), 7.94 (d, *J* = 8.4 Hz, 1H), 7.67 – 7.60 (m, 2H), 7.42 – 7.38 (m, 3H), 7.29 – 7.06 (m, 4H), 4.35 – 4.29 (m, 0.03H), 3.84 (t, *J* = 11.9 Hz, 2H),

3.35 (t, J = 11.5 Hz, 2H), 2.72 – 2.65 (m, 1H), 1.48 – 1.18 (m, 4H); ^{13}C NMR (75 MHz, $CDCl_3$) δ 162.4, 147.8, 141.4, 141.4, 136.3, 129.3, 128.6, 128.5, 127.4, 126.8, 126.6, 125.9, 121.7, 68.1, 67.9, 38.7, 32.0, 31.6; HRMS (ESI) m/z 305.1752 ($M+H^+$), calc. for $C_{21}H_{21}DNO$ 305.1759. The ee was determined by HPLC analysis: CHIRALPAK IG (4.6 mm i.d. x 250 mm); hexane/2-propanol = 80/20; flow rate 1.0 mL/min; 25 ºC; 230 nm; retention time: 14.3 min (major) and 15.8 min (minor).

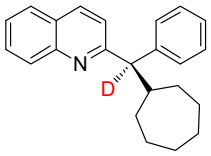

2y

Colorless oil; 20.3 mg, 64% yield; 94% D, 81% ee; $[\alpha]_D^{22}$ –8.7 (*c* 1.0, $CHCl_3$); ^{1}H NMR (300 MHz, $CDCl_3$) δ 8.08 (d, J = 8.4 Hz, 1H), 7.99 (d, J = 8.5 Hz, 1H), 7.75 – 7.63 (m, 2H), 7.49 – 7.42 (m, 3H), 7.36 (d, J = 8.5 Hz, 1H), 7.30 – 7.22 (m, 2H), 7.15 (t, J = 7.1 Hz, 1H), 4.00 (d, J = 11.5 Hz, 0.06H), 2.75 – 2.72 (m, 1H), 1.71 – 1.35 (m, 10H), 1.33 – 1.00 (m, 2H); ^{13}C NMR (75 MHz, $CDCl_3$) δ 164.1, 147.7, 143.0, 136.2, 129.2, 128.6, 128.4, 127.3, 126.7, 126.3, 125.7, 121.1, 42.1, 33.0, 32.3, 28.5, 28.5, 26.5, 26.5; HRMS (ESI) m/z 317.2114 ($M+H^+$), calc. for $C_{23}H_{25}DN$ 317.2123. The ee was determined by HPLC analysis: CHIRALPAK IG (4.6 mm i.d. x 250 mm); hexane/2-propanol = 97/3; flow rate 1.2 mL/min; 25 ºC; 230 nm; retention time: 5.6 min (major) and 14.8 min (minor).

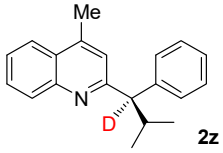

2z

White solid; Mp 66 – 68 ºC; 19.6 mg, 71% yield; >95% D, 92% ee; $[\alpha]_D^{22}$ –37.0 (*c* 1.0, $CHCl_3$); ^{1}H NMR (300 MHz, $CDCl_3$) δ 8.11 (d, J = 7.7 Hz, 1H), 7.90 (d, J = 8.4 Hz, 1H), 7.67 (t, J = 7.6 Hz, 1H), 7.50 – 7.44 (m, 3H), 7.31 – 7.10 (m, 4H), 3.76 (brs, 0.02 H), 2.86 – 2.75 (m, 1H), 2.62 (s, 3H), 0.93 – 0.88 (m, 6H); ^{13}C NMR (75 MHz, $CDCl_3$) δ 163.5, 147.6, 144.2, 143.0, 129.7, 128.9, 128.5, 128.3, 126.9, 126.3, 125.5, 123.5, 121.8, 31.8, 21.7, 21.4, 18.8; HRMS (ESI) m/z 277.1803 ($M+H^+$), calc. for $C_{20}H_{21}DN$ 277.1810. The ee was determined by HPLC analysis: CHIRALPAK IG x 2 (4.6 mm i.d. x 250 mm); hexane/2-propanol = 98/2; flow rate 1.0 mL/min; 25 ºC; 230 nm; retention time: 10.4 min (major) and 11.6 min (minor).

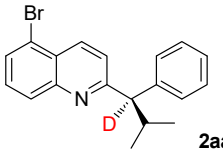

2aa

Colorless oil; 22.2 mg, 65% yield; 95% D, 90% ee; $[\alpha]_D^{22}$ –95.0 (*c* 1.0, $CHCl_3$); ^1H NMR (300 MHz, $CDCl_3$) δ 8.36 (d, *J* = 8.8 Hz, 1H), 8.06 (d, *J* = 8.4 Hz, 1H), 7.72 (d, *J* = 7.2 Hz, 1H), 7.53 – 7.41 (m, 4H), 7.28 – 7.22 (m, 2H), 7.15 (t, *J* = 7.3 Hz, 1H), 3.83 (d, *J* = 10.8 Hz, 0.05H), 2.87 – 2.75 (m, 1H), 0.93 – 0.86 (m, 6H); ^{13}C NMR (75 MHz, $CDCl_3$) δ 164.8, 148.6, 142.5, 135.6, 129.5, 129.4, 129.2, 128.4, 128.4, 126.5, 126.2, 122.5, 121.7, 31.9, 21.7, 21.4; HRMS (ESI) m/z 341.0750 ($M+H^+$), calc. for $C_{19}H_{18}DBrN$ 341.0758. The ee was determined by HPLC analysis: CHIRALPAK IG x 2 (4.6 mm i.d. x 250 mm); hexane/2-propanol = 98/2; flow rate 1.0 mL/min; 25 °C; 230 nm; retention time: 12.4 min (major) and 14.3 min (minor).

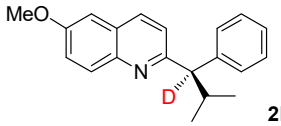

2bb

Colorless oil; 21.9 mg, 75% yield; >95% D, 90% ee; $[\alpha]_D^{22}$ –69.7 (*c* 1.0, $CHCl_3$); ^1H NMR (300 MHz, $CDCl_3$) δ 7.98 (d, *J* = 9.2 Hz, 1H), 7.89 (d, *J* = 8.5 Hz, 1H), 7.48 (d, *J* = 7.3 Hz, 2H), 7.35 – 7.20 (m, 4H), 7.15 (t, *J* = 7.3 Hz, 1H), 6.98 (d, *J* = 2.6 Hz, 1H), 3.88 (s, 3H), 2.87 – 2.65 (m, 1H), 0.93 – 0.86 (m, 6H); ^{13}C NMR (75 MHz, $CDCl_3$) δ 161.5, 157.2, 143.8, 143.2, 135.0, 130.6, 128.4, 128.3, 127.6, 126.2, 121.6 , 121.3, 105.0, 55.5, 32.0, 21.7, 21.4; HRMS (ESI) m/z 293.1752 ($M+H^+$), calc. for $C_{20}H_{21}DNO$ 293.1759. The ee was determined by HPLC analysis: CHIRALPAK ODH x 2 (4.6 mm i.d. x 250 mm); hexane/2-propanol = 98/2; flow rate 1.2 mL/min; 25 °C; 230 nm; retention time: 6.6 min (minor) and 8.2 min (major).

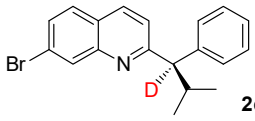

2cc

White solid; Mp 76 – 78 °C; 21.5 mg, 63% yield; 94% D, 92% ee; $[\alpha]_D^{22}$ –114.1 (*c* 1.0, $CHCl_3$); ^1H NMR (300 MHz, $CDCl_3$) δ 8.23 (s, 1H), 7.88 (d, *J* = 8.5 Hz, 1H), 7.52 – 7.44 (m, 2H), 7.39 (d, *J* = 7.3 Hz, 2H), 7.27 (d, *J* = 8.5 Hz, 1H), 7.20 – 7.15 (m, 2H), 7.11 – 7.05 (m, 1H), 3.70 (d, *J* = 10.4 Hz, 0.06H), 2.79 – 2.70 (m, 1H), 0.84 – 0.80 (m, 6H); ^{13}C NMR (75 MHz, $CDCl_3$) δ 165.0, 148.4, 142.6, 136.0, 131.7, 131.6, 129.3, 128.6, 128.5, 128.4, 126.5, 125.4, 121.8, 31.94, 21.7, 21.3; HRMS (ESI) m/z 341.0751 ($M+H^+$), calc. for $C_{19}H_{18}DBrN$ 341.0758. The ee was determined by HPLC analysis: CHIRALPAK IG x 2 (4.6 mm i.d. x 250

mm); hexane/2-propanol = 98/2; flow rate 1.0 mL/min; 25 ºC; 230 nm; retention time: 10.3 min (major) and 11.6 min (minor).

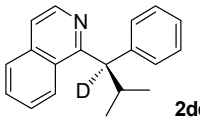

2dd

White solid; Mp 45 – 47 ºC; 20.5 mg, 78% yield; 93% D, 82% ee; $[\alpha]_D^{22}$ +27.6 (*c* 1.0, $CHCl_3$); ^1H NMR (300 MHz, $CDCl_3$) δ 8.59 (d, *J* = 5.6 Hz, 1H), 8.36 (d, *J* = 8.1 Hz, 1H), 7.77 (d, *J* = 7.8 Hz, 1H), 7.64 – 7.45 (m, 5H), 7.29 – 7.18 (m, 2H), 7.15 – 7.08 (m, 1H), 4.45 (d, *J* = 10.9 Hz, 0.08H), 3.14 – 2.84 (m, 1H), 0.93 – 0.85 (m, 6H); ^{13}C NMR (75 MHz, $CDCl_3$) δ 162.6, 142.9, 141.8, 136.4, 129.5, 128.6, 128.2, 127.5, 127.5, 127.0, 126.2, 124.8, 119.0, 32.7, 22.0, 21.5; HRMS (ESI) m/z 263.1646 ($M+H^+$), calc. for $C_{19}H_{19}DN$ 263.1653. The ee was determined by HPLC analysis: CHIRALPAK INB + ODH + ODH (4.6 mm i.d. x 250 mm); hexane/2-propanol = 98/2; flow rate 1.0 mL/min; 25 ºC; 230 nm; retention time: 16.1 min (major) and 17.1 min (minor).

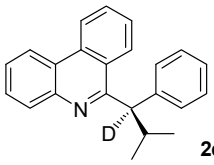

2ee

White solid; Mp 135 – 137 ºC; 25.3 mg, 81% yield; 90% D, 83% ee; $[\alpha]_D^{22}$ –380.5 (*c* 1.0, $CHCl_3$); ^1H NMR (300 MHz, $CDCl_3$) δ 8.61 (d, *J* = 8.2 Hz, 1H), 8.53 (d, *J* = 8.1 Hz, 1H), 8.43 (d, *J* = 8.2 Hz, 1H), 8.25 (d, *J* = 8.1 Hz, 1H), 7.81 – 7.70 (m, 2H), 7.67 – 7.54 (m, 4H), 7.28 – 7.19 (m, 2H), 7.12 (t, *J* = 7.3 Hz, 1H), 4.50 (d, *J* = 10.1 Hz, 0.15H), 3.25 – 3.14 (m, 1H), 0.98 (d, *J* = 6.4 Hz, 3H), 0.92 (d, *J* = 6.7 Hz, 3H); ^{13}C NMR (75 MHz, $CDCl_3$) δ 162.0, 143.8, 142.8, 133.0, 130.2, 129.8, 128.8, 128.3, 128.1, 127.1, 126.3, 126.2, 125.9, 125.7, 123.3, 122.4, 121.8, 56.7, 32.6, 22.2, 21.4; HRMS (ESI) m/z 313.1801 ($M+H^+$), calc. for $C_{23}H_{21}DN$ 313.1810. The ee was determined by HPLC analysis: CHIRALPAK ODH (4.6 mm i.d. x 250 mm); hexane/2-propanol = 98/2; flow rate 1.0 mL/min; 25 ºC; 230 nm; retention time: 6.2 min (minor) and 11.7 min (major).

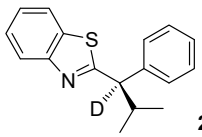

2ff

White solid; Mp 62 – 64 ºC; 19.1 mg, 71% yield; 93% D, 80% ee; $[\alpha]_D^{22}$ –47.0 (*c* 1.0, $CHCl_3$); ^1H NMR (300 MHz, $CDCl_3$) δ 7.93 (d, *J* = 8.1 Hz, 1H), 7.72 (d, *J* = 7.8 Hz, 1H), 7.41 – 7.31

(m, 3H), 7.28 – 7.07 (m, 4H), 3.92 (d, J = 10.5 Hz, 0.07H), 2.68 – 2.54 (m, 1H), 0.97 (d, J = 6.5 Hz, 3H), 0.82 (d, J = 6.6 Hz, 3H); ^{13}C NMR (75 MHz, $CDCl_3$) δ 174.5, 153.0, 141.0, 135.0, 128.6, 128.5, 127.1, 125.8, 124.6, 122.8, 121.4, 33.6, 21.6, 21.2; HRMS (ESI) m/z 269.1211 ($M+H^+$), calc. for $C_{17}H_{17}DNS$ 269.1217. The ee was determined by HPLC analysis: CHIRALPAK IG (4.6 mm i.d. x 250 mm); hexane/2-propanol = 80/20; flow rate 1.0 mL/min; 25 ºC; 230 nm; retention time: 5.6 min (major) and 11.3 min (minor).

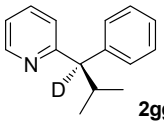

2gg

Colorless oil; 13.8 mg, 65% yield; 85% D, 53% ee; ^{1}H NMR (300 MHz, $CDCl_3$) δ 8.48 (d, J = 4.3 Hz, 1H), 7.46 (m, 7.51 – 7.40, 1H), 7.38 – 7.30 (m, 2H), 7.21 – 7.03 (m, 4H), 7.01 – 6.95 (m, 1H), 3.49 (d, J = 10.8 Hz, 0.15H), 2.62 – 2.57 (m, 1H), 0.78 (d, J = 6.5 Hz, 1H); ^{13}C NMR (75 MHz, $CDCl_3$) δ 163.7, 149.2, 143.4, 143.4, 136.2, 128.3, 126.2, 123.1, 123.1, 121.1, 62.7, 62.5, 62.2, 32.2, 32.1, 21.7, 21.4. The ee was determined by HPLC analysis: CHIRALPAK ODH x 3 (4.6 mm i.d. x 250 mm); hexane/2-propanol = 96/4; flow rate 0.7 mL/min; 25 ºC; 230 nm; retention time: 23.5 min (major) and 24.5 min (minor).

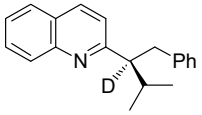

2hh

Colorless oil; 13.8 mg, 65% yield; >95% D, 38% ee; ^{1}H NMR (300 MHz, $CDCl_3$) δ 8.07 (d, J = 8.4 Hz, 1H), 7.92 (d, J = 8.4 Hz, 1H), 7.79 – 7.60 (m, 2H), 7.46 (t, J = 7.5 Hz, 1H), 7.12 – 6.89 (m, 6H), 4.24 – 4.21 (M, 0.03H), 3.23 (s, 2H), 2.31 – 2.05 (m, 1H), 1.12 (d, J = 6.7 Hz, 3H), 0.85 (d, J = 6.7 Hz, 3H); ^{13}C NMR (75 MHz, $CDCl_3$) δ 164.1, 147.8, 141.1, 135.2, 129.2, 129.0, 129.0, 127.9, 127.4, 126.8, 125.5, 125.5, 122.3, 38.1, 32.6, 20.8, 20.8. The ee was determined by HPLC analysis: Lux 5u Cellulose-3 & Chiral MJ (2) (4.6 mm i.d. x 250 mm); hexane/2-propanol = 98/2; flow rate 1.0 mL/min; 25 ºC; 254 nm; retention time: 10.0 min (major) and 10.9 min (minor).

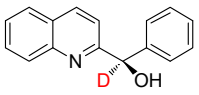

5a: white solid, Mp 50 – 52 ºC, 22.7 mg, 96% yield, 91% D, 91% ee, $[\alpha]_D^{22}$ –88.6 (*c* 1.0, $CHCl_3$); ^{1}H NMR (300 MHz, $CDCl_3$) δ 8.18 (d, J = 8.4 Hz, 1H), 8.08 (d, J = 8.5 Hz, 1H), 7.78 (dd, J = 16.1, 8.0 Hz, 2H), 7.57 (t, J = 7.5 Hz, 1H), 7.42 (d, J = 6.9 Hz, 2H), 7.33 (dd, J = 16.2, 8.7 Hz, 3H), 7.20 (d, J = 8.5 Hz, 1H), 6.09 (s, 1H), 5.90 (s, 0.09H); ^{13}C NMR (75

MHz, $CDCl_3$) δ 160.4, 145.9, 142.7, 137.0, 129.9, 128.8, 128.6, 128.0, 127.6, 127.4, 126.6, 119.2, 75.1; HRMS (ESI) m/z 237.1131 ($M+H^+$), calc. for $C_{16}H_{13}DNO$ 237.1133. The ee was determined by HPLC analysis: CHIRALPAK INB (4.6 mm i.d. x 250 mm); Hexane/2-propanol = 90/10; flow rate 1.0 mL/min; 25 ºC; 230 nm; retention time: 10.9 min (minor) and 22.0 min (major).

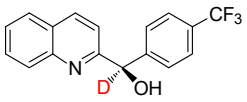

5b: white solid, Mp 120 – 122 ºC, 24.9 mg, 82% yield, 91% D, 94% ee, $[\alpha]_D^{22}$ −143.8 (*c* 1.0, $CHCl_3$); ^1H NMR (300 MHz, $CDCl_3$) δ 8.21 (d, *J* = 8.6 Hz, 1H), 8.15 (d, *J* = 8.5 Hz, 1H), 7.82 (dd, *J* = 16.6, 8.0 Hz, 2H), 7.60 (m, 5H), 7.23 (s, 1H), 6.17 (s, 1H), 6.03 (s, 0.09 H); ^{13}C NMR (75 MHz, $CDCl_3$) δ 159.4, 146.7, 146.0, 137.4, 130.1, 130.1 (q, *J* = 32.4 Hz), 128.7, 127.6, 127.6, 127.5, 126.9, 125.6 (q, *J* = 3.8 Hz), 124.0 (q, *J* = 272.1 Hz), 118.9, 74.6; ^{19}F NMR (376 MHz, $CDCl_3$) δ -63.07; HRMS (ESI) m/z 305.0997 ($M+H^+$), calc. for $C_{17}H_{12}DF_3NO$ 305.1007. The ee was determined by HPLC analysis: CHIRALPAK INB (4.6 mm i.d. x 250 mm); Hexane/2-propanol = 90/10; flow rate 1.0 mL/min; 25 ºC; 230 nm; retention time: 9.0 min (minor) and 15.3 min (major).

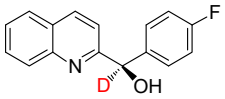

5c: white solid, Mp 74 – 75 ºC, 24.1 mg, 95% yield, 90% D, 92% ee, $[\alpha]_D^{22}$ −27.5 (*c* 1.0, $CHCl_3$); ^1H NMR (300 MHz, $CDCl_3$) δ 8.21 (dd, *J* = 22.8, 8.5 Hz, 2H), 7.83 (dd, *J* = 18.7, 7.9 Hz, 2H), 7.62 (t, *J* = 7.6 Hz, 1H), 7.45 (dd, *J* = 8.4, 5.5 Hz, 2H), 7.28 (s, 1H), 7.05 (t, *J* = 8.6 Hz, 2H), 6.15 (s, 1H), 6.01 (s, 0.1 H); ^{19}F NMR (376 MHz, $CDCl_3$) δ -105.11; ^{13}C NMR (75 MHz, $CDCl_3$) δ 162.3 (d, *J* = 246.1 Hz), 160.3, 145.8, 138.5 (d, *J* = 3.1 Hz), 137.0, 129.8, 128.9 (d, *J* = 8.2 Hz), 128.6, 127.5, 127.3, 126.6, 118.9, 115.3 (d, *J* = 21.5 Hz), 74.4; HRMS (ESI) m/z 255.1032 ($M+H^+$), calc. for $C_{16}H_{12}DFNO$ 255.1038. The ee was determined by HPLC analysis: CHIRALPAK OZ–H (4.6 mm i.d. x 250 mm); Hexane/2-propanol = 94/6; flow rate 1.0 mL/min; 25 ºC; 254 nm; retention time: 11.3 min (minor) and 14.7 min (major).

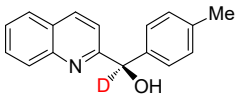

5d: white solid, Mp 67 – 69 ºC, 24.8 mg, 99% yield, 91% D, 97% ee, $[\alpha]_D^{22}$ −156.9 (*c* 1.0, $CHCl_3$); ^1H NMR (300 MHz, $CDCl_3$) δ 8.16 (d, *J* = 8.4 Hz, 1H), 8.06 (d, *J* = 8.5 Hz, 1H), 7.77 (dd, *J* = 16.3, 7.9 Hz, 2H), 7.56 (t, *J* = 7.4 Hz, 1H), 7.29 (d, *J* = 7.9 Hz, 2H), 7.17 (dd, *J* = 12.2, 8.2 Hz, 3H), 6.02 (s, 1H), 5.86 (s, 0.09H), 2.33 (s, 3H); ^{13}C NMR (75 MHz, $CDCl_3$) δ 160.4, 145.9, 142.6, 138.3, 137.0, 129.9, 128.8, 128.5, 128.0, 127.6, 126.6, 124.6, 119.3, 75.1, 21.4; HRMS (ESI) m/z 251.1293 ($M+H^+$), calc. for $C_{17}H_{15}DNO$ 251.1289. The ee was determined by HPLC analysis: CHIRALPAK INB (4.6 mm i.d. x 250 mm); Hexane/2-propanol = 94/6; flow rate 1.0 mL/min; 25 ºC; 254 nm; retention time: 15.1 min (minor) and 30.2 min (major).

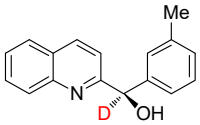

5e: white solid, Mp 79 – 81 ºC, 22.8 mg, 91% yield, 90% D, 99% ee, $[\alpha]_D^{22}$ −76.1 (*c* 1.0, $CHCl_3$); ^1H NMR (300 MHz, $CDCl_3$) δ 8.17 (d, *J* = 8.4 Hz, 1H), 8.07 (d, *J* = 8.5 Hz, 1H), 7.78 (dd, *J* = 16.5, 7.9 Hz, 2H), 7.57 (t, *J* = 7.5 Hz, 1H), 7.21 (m, 4H), 7.10 (d, *J* = 6.2 Hz, 1H), 6.07 (s, 1H), 5.86 (s, 0.1 H), 2.32 (s, 3H); ^{13}C NMR (75 MHz, $CDCl_3$) δ 160.6, 145.8, 139.8, 137.7, 137.0, 129.9, 129.3, 128.7, 127.6, 127.4, 127.4, 126.6, 119.3, 74.9, 21.1; HRMS (ESI) m/z 251.1284 ($M+H^+$), calc. for $C_{17}H_{15}DNO$ 251.1289. The ee was determined by HPLC analysis: CHIRALPAK OZ–H (4.6 mm i.d. x 250 mm); Hexane/2-propanol = 94/6; flow rate 1.0 mL/min; 25 ºC; 254 nm; retention time: 15.4 min (minor) and 20.4 min (major).

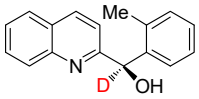

5f: white solid, Mp 82 – 84 ºC, 20.7 mg, 83% yield, 93% D, 97% ee, $[\alpha]_D^{22}$ –171.8 (*c* 1.0, $CHCl_3$); ^1H NMR (300 MHz, $CDCl_3$) δ 8.17 (d, *J* = 8.5 Hz, 1H), 8.06 (d, *J* = 8.5 Hz, 1H), 7.79 (dd, *J* = 17.4, 7.9 Hz, 2H), 7.57 (t, *J* = 7.6 Hz, 1H), 7.17 (m, 4H), 7.08 (d, *J* = 8.5 Hz, 1H), 6.11 (s, 0.07 H), 5.92 (s, 1H), 2.40 (s, 3H); ^{13}C NMR (75 MHz, $CDCl_3$) δ 160.4 (d, *J* = 246.2 Hz), 159.7, 145.9, 137.4, 130.0, 129.8, δ 129.4 (d, *J* = 8.3 Hz), 128.8 (d, *J* = 4.0 Hz),

128.7, 127.6, 127.6, 126.7, 124.5 (d, J = 3.5 Hz), 118.9 (d, J = 3.1 Hz), 115.5 (d, J = 21.9 Hz), 68.1 (d, J = 4.0 Hz); HRMS (ESI) m/z 251.1288 ($M+H^+$), calc. for $C_{17}H_{15}DNO$ 251.1289. The ee was determined by HPLC analysis: CHIRALPAK OZ–H (4.6 mm i.d. x 250 mm); Hexane/2-propanol = 94/6; flow rate 1.0 mL/min; 25 ºC; 254 nm; retention time: 11.6 min (minor) and 12.9 min (major).

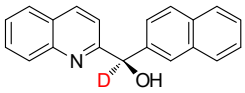

5g: white solid, Mp 132 – 133 ºC, 24.6 mg, 86% yield, 91% D, 90% ee, $[\alpha]_D^{22}$ −91.3 (*c* 1.0, $CHCl_3$); ^1H NMR (300 MHz, $CDCl_3$) δ 8.20 (d, J = 8.5 Hz, 1H), 8.05 (d, J = 8.5 Hz, 1H), 7.96 (s, 1H), 7.81 (m, 5H), 7.57 (t, J = 7.4 Hz, 1H), 7.47 (dt, J = 12.3, 8.0 Hz, 3H), 7.22 (d, J = 8.5 Hz, 1H), 6.19 (s, 1H), 6.06 (s, 0.09H); ^{13}C NMR (75 MHz, $CDCl_3$) δ 160.3, 146.0, 140.1, 137.0, 133.3, 133.2, 130.0, 128.8, 128.6, 128.0, 127.7, 127.6, 127.5, 126.7, 126.7, 126.2, 126.0, 125.0, 119.3, 75.3; HRMS (ESI) m/z 287.1286 ($M+H^+$), calc. for $C_{20}H_{15}DNO$ 287.1289. The ee was determined by HPLC analysis: CHIRALPAK INB (4.6 mm i.d. x 250 mm); Hexane/2-propanol = 94/6; flow rate 1.0 mL/min; 25 ºC; 254 nm; retention time: 12.2 min (minor) and 15.2 min (major).

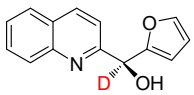

5h: white solid, Mp 120 – 122 ºC, 16.3 mg, 72% yield, >95% D, 97% ee, $[\alpha]_D^{22}$ +78.8 (*c* 1.0, $CHCl_3$); ^1H NMR (300 MHz, $CDCl_3$) δ 8.15 (d, J = 8.4 Hz, 2H), 7.84 (d, J = 8.0 Hz, 1H), 7.76 (t, J = 7.6 Hz, 1H), 7.58 (t, J = 7.5 Hz, 1H), 7.35 (m, 2H), 6.34 (s, 2H), 5.96 (s, 0.01H), 5.81 (s, 1H); ^{13}C NMR (75 MHz, $CDCl_3$) δ 157.6, 154.7, 146.1, 142.8, 137.2, 130.0, 128.8, 127.7, 127.6, 126.8, 118.9, 110.3, 108.0, 68.6; HRMS (ESI) m/z 227.0927 ($M+H^+$), calc. for $C_{14}H_{11}DNO_2$ 227.0926. The ee was determined by HPLC analysis: CHIRALPAK INB (4.6 mm i.d. x 250 mm); Hexane/2-propanol = 90/10; flow rate 1.0 mL/min; 25 ºC; 254 nm; retention time: 9.9 min (minor) and 16.5 min (major).

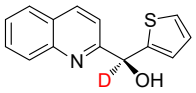

5i: white solid, Mp 118 – 119 ºC, 24.1 mg, 99% yield, 95% D, 96% ee, $[\alpha]_D^{22}$ −121.3 (*c* 1.0, $CHCl_3$); ^1H NMR (300 MHz, $CDCl_3$) δ 8.14 (dd, *J* = 8.3, 3.7 Hz, 2H), 7.83 (d, *J* = 8.1 Hz, 1H), 7.77 (t, *J* = 7.6 Hz, 1H), 7.57 (t, *J* = 7.4 Hz, 1H), 7.33 (d, *J* = 8.5 Hz, 1H), 7.27 (d, *J* = 5.0 Hz, 1H), 7.12 (d, *J* = 2.6 Hz, 1H), 6.98 (m, 1H), 6.17 (s, 0.05H), 6.02 (s, 1H); ^{13}C NMR (75 MHz, $CDCl_3$) δ 159.5, 146.7, 145.8, 137.4, 130.1, 128.7, 127.6, 127.6, 126.9, 126.6, 125.9, 125.6, 119.0, 70.8; HRMS (ESI) m/z 243.0695 ($M+H^+$), calc. for $C_{14}H_{11}DNOS$ 243.0697. The ee was determined by HPLC analysis: CHIRALPAK INB (4.6 mm i.d. x 250 mm); Hexane/2-propanol = 90/10; flow rate 1.0 mL/min; 25 ºC; 210 nm; retention time: 12.2 min (minor) and 21.7 min (major).

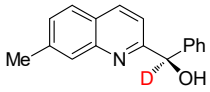

5j: white solid, Mp 120 – 122 ºC, 20.5 mg, 82% yield, 92% D, 94% ee, $[\alpha]_D^{22}$ −173.8 (*c* 1.0, $CHCl_3$); ^1H NMR (300 MHz, $CDCl_3$) δ 7.99 (m, 2H), 7.69 (d, *J* = 8.3 Hz, 1H), 7.34 (m, 2H), 7.12 (d, *J* = 8.4 Hz, 1H), 6.11 (s, 0.08H), 5.87 (s, 1H), 2.57 (d, *J* = 13.3 Hz, 3H); ^{13}C NMR (75 MHz, $CDCl_3$) δ 160.9, 144.4, 142.4, 136.1, 132.4, 130.8, 130.4, 128.7, 128.1, 128.1, 127.4, 126.3, 120.2, 75.2; HRMS (ESI) m/z 251.1291 ($M+H^+$), calc. for $C_{17}H_{15}DNO$ 251.1289. The ee was determined by HPLC analysis: CHIRALPAK INB (4.6 mm i.d. x 250 mm); Hexane/2-propanol = 85/15; flow rate 1.0 mL/min; 25 ºC; 230 nm; retention time: 13.8 min (minor) and 18.2 min (major).

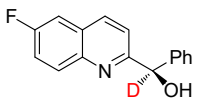

5k: white solid, Mp 126 – 127 ºC, 16.5 mg, 65% yield, 92% D, 90% ee, $[\alpha]_D^{22}$ −113.3 (*c* 1.0, $CHCl_3$); ^1H NMR (300 MHz, $CDCl_3$) δ 8.16 (dd, *J* = 9.2, 5.3 Hz, 1H), 8.02 (d, *J* = 8.6 Hz, 1H), 7.53 (m, 1H), 7.37 (m, 6H), 7.22 (d, *J* = 8.6 Hz, 1H), 5.88 (s, 1H), 5.88 (s, 0.08 H); ^{19}F NMR (376 MHz, $CDCl_3$) δ -112.87. ^{13}C NMR (75 MHz, $CDCl_3$) δ 159.4, 146.7, 146.0, 137.4, 130.1, 130.1 (q, *J* = 32.4 Hz), 128.7, 127.6, 127.6, 127.5, 126.9, 125.6 (q, *J* = 3.8 Hz), 124.0

(q, J = 272.1 Hz), 118.9, 74.6; ^{19}F NMR (376 MHz, $CDCl_3$) δ -112.87; HRMS (ESI) m/z 255.1035 ($M+H^+$), calc. for $C_{16}H_{12}DFNO$ 255.1038. The ee was determined by HPLC analysis: CHIRALPAK INB (4.6 mm i.d. x 250 mm); Hexane/2-propanol = 90/10; flow rate 1.0 mL/min; 25 ºC; 254 nm; retention time: 9.4 min (minor) and 11.6 min (major).

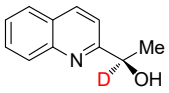

5l: yellow solid, Mp 84 – 85 ºC, 15.8 mg, 91% yield, > 95% D, 80% ee, $[\alpha]_D^{22}$ +18.1 (*c* 1.0, $CHCl_3$); ^{1}H NMR (300 MHz, $CDCl_3$) δ 8.17 (d, J = 8.5 Hz, 1H), 8.09 (d, J = 8.4 Hz, 1H), 7.83 (d, J = 8.1 Hz, 1H), 7.74 (t, J = 7.6 Hz, 1H), 7.55 (t, J = 7.5 Hz, 1H), 7.36 (d, J = 8.5 Hz, 1H), 5.03 (s, 1H), 1.58 (s, 3H); ^{13}C NMR (75 MHz, $CDCl_3$) δ 162.8, 146.3, 137.0, 129.8, 128.7, 127.6, 127.4, 126.4, 118.0, 68.7, 24.1; HRMS (ESI) m/z 175.0980 ($M+H^+$), calc. for $C_{11}H_{11}DNO$ 175.0976. The ee was determined by HPLC analysis: CHIRAL INB (4.6 mm i.d. x 250 mm); Hexane/2-propanol = 90/10; flow rate 1.0 mL/min; 25 ºC; 230 nm; retention time: 7.4 min (minor) and 12.3 min (major).

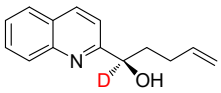

5m: white solid, Mp 120 – 122 ºC, 21.2 mg, 99% yield, >95% D, 88% ee, $[\alpha]_D^{22}$ −26.3 (*c* 1.0, $CHCl_3$); ^{1}H NMR (300 MHz, $CDCl_3$) δ 8.16 (d, J = 8.5 Hz, 1H), 8.08 (d, J = 8.4 Hz, 1H), 7.83 (d, J = 8.0 Hz, 1H), 7.73 (t, J = 7.6 Hz, 1H), 7.55 (t, J = 7.5 Hz, 1H), 7.34 (d, J = 8.5 Hz, 1H), 5.87 (ddt, J = 16.9, 10.2, 6.6 Hz, 1H), 4.99 (m, 3H), 2.26 (m, 2H), 2.04 (ddd, J = 15.9, 9.6, 6.4 Hz, 1H), 1.81 (m, 1H); ^{13}C NMR (75 MHz, $CDCl_3$) δ 161.9, 146.3, 138.2, 137.0, 129.8, 128.6, 127.6, 127.4, 126.4, 118.3, 114.8, 72.0, 37.4, 29.4; HRMS (ESI) m/z 214.1291 ($M+H^+$), calc. for $C_{14}H_{15}DNO$ 215.1289. The ee was determined by HPLC analysis: CHIRALPAK INB (4.6 mm i.d. x 250 mm); Hexane/2-propanol = 90/10; flow rate 1.0 mL/min; 25 ºC; 210 nm; retention time: 6.3 min (minor) and 9.2 min (major).

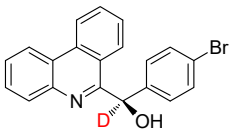

5n: white solid, Mp 160 – 161 ºC, 35.9 mg, 99% yield, 93% D, 88% ee, $[\alpha]_D^{22}$ −118.9 (*c* 1.0, $CHCl_3$); ^1H NMR (300 MHz, $CDCl_3$) δ 8.55 (dd, *J* = 16.9, 8.2 Hz, 2H), 8.19 (d, *J* = 7.9 Hz, 1H), 7.89 (d, *J* = 8.3 Hz, 1H), 7.74 (t, *J* = 7.6 Hz, 2H), 7.66 (t, *J* = 7.5 Hz, 1H), 7.50 (t, *J* = 7.7 Hz, 1H), 7.34 (d, *J* = 8.3 Hz, 2H), 7.19 (m, 2H), 6.47 (s, 1H), 6.29 (s, 0.07H); ^{13}C NMR (75 MHz, $CDCl_3$) δ 158.4, 141.9, 141.6, 133.5, 131.9, 131.0, 129.5, 129.5, 129.1, 127.5, 127.5, 125.8, 124.4, 123.2, 122.7, 122.2, 122.0, 72.0; HRMS (ESI) m/z 386.0392 ($M+H^+$), calc. for $C_{20}H_{14}DBrNO$ 365.0395. The ee was determined by HPLC analysis: CHIRALPAK IE (4.6 mm i.d. x 250 mm); Hexane/2-propanol = 90/10; flow rate 1.0 mL/min; 25 ºC; 210 nm; retention time: 24.4 min (major) and 38.1 min (minor).

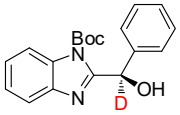

5o: white solid, Mp 120 – 122 ºC, 22.0 mg, 83% yield, >95% D, 95% ee, $[\alpha]_D^{22}$ +23.4 (*c* 1.0, $CHCl_3$); ^1H NMR (300 MHz, $CDCl_3$) δ 7.88 (m, 1H), 7.75 (dd, *J* = 5.5, 3.2 Hz, 1H), 7.33 (ddd, *J* = 15.3, 7.4, 4.7 Hz, 7H), 7.06 (s, 0.04H), 4.69 (s, 1H), 1.54 (s, 9H); ^{13}C NMR (75 MHz, $CDCl_3$) δ 152.1, 151.5, 136.7, 128.9, 128.8, 127.0, 122.9, 83.6, 74.6, 27.6; HRMS (ESI) m/z 326.1612 ($M+H^+$), calc. for $C_{19}H_{20}DN_2O_3$ 326.1610. The ee was determined by HPLC analysis: cell-4 (4.6 mm i.d. x 250 mm); Hexane/2-propanol = 60/40; flow rate 1.0 mL/min; 25 ºC; 254 nm; retention time: 6.1 min (minor) and 10.5 min (major).

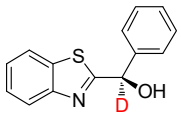

5p: yellow oil, 22.5 mg, 93% yield, 91% D, 89% ee, $[\alpha]_D^{22}$ −13.1 (*c* 1.0, $CHCl_3$); ^1H NMR (300 MHz, $CDCl_3$) δ 7.99 (d, *J* = 8.1 Hz, 1H), 7.84 (d, *J* = 7.8 Hz, 1H), 7.44 (m, 7H), 6.15 (s, 0.09H), 3.66 (s, 1H); ^{13}C NMR (75 MHz, $CDCl_3$) δ 175.0, 152.4, 140.9, 135.2, 128.8, 128.7, 126.7, 126.2, 125.2, 123.0, 121.8, 74.4; HRMS (ESI) m/z 243.0688 ($M+H^+$), calc. for $C_{14}H_{15}DNOS$ 243.0697.

The ee was determined by HPLC analysis: CHIRAL INB (4.6 mm i.d. x 250 mm); Hexane/2-propanol = 80/20; flow rate 1.0 mL/min; 25 ºC; 230 nm; retention time: 6.2 min (minor) and 9.2 min (major).

Supplemental References:

Olomanov, O. V., Bourhis, L. J., Gildea, R. J., Howard, J. A., and Puschmann, H. (2009). OLEX2: a complete structure solution, refinement and analysis program. J. Appl. Cryst. *42*, 339–341.

Sheldrick, G. M. (2008). A short history of SHELX. Acta Cryst. A: Foundations of Crystallography *64*, 112–122.

Heldrick, G. M. (2015). Crystal structure refinement with SHELXL. Acta Cryst. C: Structural Chemistry *71*, 3–8.

Frisch, M., Trucks, G., Schlegel, H., Scuseria, G., Robb, M., Cheeseman, J., Scalmani, G., Barone, V., Mennucci, B., and Petersson, G. (1993). Gaussian 09, Revision D. 01, Gaussian, Inc., Wallingford CT, 2013 Search PubMed; (b) AD Becke. J Chem Phys *98*, 785–789.

Terrasson, V., Planas, J. G., Prim, D., Vinas, C., Teixidor, F., Light, M. E., and Hursthouse, M. B. (2008). Cooperative Effect of Carborane and Pyridine in the Reaction of Carboranyl Alcohols with Thionyl Chloride: Halogenation versus Oxidation. J. Org. Chem. *73*, 9140–9143.